

Rheology & Solid State Properties of
Polyethylene/CNT Nanocomposites:
Impact of CNT Characteristics and Surface
Modification.

BY

Sarfraz Haider Abbasi

A Dissertation Presented to the
FACULTY OF THE COLLEGE OF GRADUATE STUDIES
KING FAHD UNIVERSITY OF PETROLEUM & MINERALS
DHAHRAN, SAUDI ARABIA

In Partial Fulfillment of the
Requirements for the Degree of

DOCTOR OF PHILOSOPHY

In

CHEMICAL ENGINEERING

OCTOBER 2010

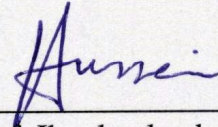
KING FAHD UNIVERSITY OF PETROLEUM & MINERALS

DHAHRAN- 31261, SAUDI ARABIA


DEANSHIP OF GRADUATE STUDIES

This dissertation, written by **SARFRAZ HAIDER ABBASI** under the direction of his dissertation adviser and approved by his dissertation committee, has been presented and accepted by the Dean of Graduate Studies, in partial fulfillment of the requirements for the degree of **DOCTOR OF PHILOSOPHY IN CHEMICAL ENGINEERING**.

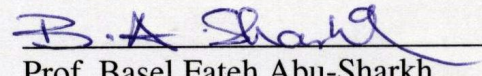
Dissertation Committee



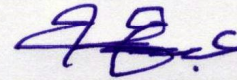
Prof. Ibnelwaleed Ali Hussein
(Dissertation Advisor)



Prof. Adnan M. Al-Amer
(Member)



Prof. Basel Fateh Abu-Sharkh
(Member)



Dr. Abdulhadi Al-Juhani
(Member)



Dr. Anwar Ul-Hamid
(Member)



Dr. Usamah A. Al-Mubaiyedh
(Department Chairman)



Dr. Salam A. Zummo
(Dean of Graduate Studies)



Date 25/10/10

DEDICATION

This work is dedicated to my wife & children.

ACKNOWLEDGEMENT

In the name of ALLAH, the most Beneficient, the most Merciful.

All praise be to Allah and may the peace and blessing of Allah be upon his prophet, Muhammad (S.A.W). First, I would like to thank King Fahd University of Petroleum & Minerals for providing the assistantship and the Department of Chemical Engineering for their continuous support throughout my Ph.D. tenure. Also I am thankful to the Center of Research Excellence in Petroleum Refining & Petrochemicals (CoRE-PRP), established by the Ministry of Higher Education, for providing the funding for this research.

I wish to express my sincere gratitude to many people whose help, directly or indirectly, made this dissertation possible. I am grateful, with deep sense of debt, to my Dissertation advisor, Dr. Ibnelwaleed A. Hussein for continuous help during my dissertation work. He is a great teacher, adviser, motivator and role model whom I greatly admire. For me he reinvented the meaning of hard work, not by words, but by his actions. I would like to thank all my committee members, Dr. Adnan M. Al-Amer, Dr. Basel F. Abu-Sharkh, Dr. Abdulhadi Al-Juhani & Dr. Anwar Ul-Hamid for their contribution and critical review of the dissertation. Special thanks to Dr. Anwar Ul-Hamid for his help with the SEM part of this research.

I would like to offer my sincere thanks to former and present Chairman of Chemical Engineering Department, Dr. Adnan M. Al-Amer & Dr. Usamah A. Al-Mubaiyedh respectively for prompt and swift action on logistical problems during the dissertation work. I am also thankful to all the Chemical Engineering Faculty and Staff for their cooperation. Special thanks to Mr. Anwar Parvez and Mr. Mofizul Islam and other technicians who helped me during my work.

I would like to thank all my friends and colleagues for all their support during this work. Finally I offer my sincere thanks to my parents, wife and other family members for their encouragement, support and prayers.

TABLE OF CONTENTS

LIST OF TABLES.....	viii
LIST OF FIGURES	ix
ABSTRACT	xiv
ABSTRACT (Arabic).....	Error! Bookmark not defined.
CHAPTER ONE.....	1
INTRODUCTION	1
CHAPTER TWO.....	6
LITERATURE SURVEY.....	6
CHAPTER THREE	32
OBJECTIVES	32
CHAPTER FOUR	34
RESULTS & DISCUSSION.....	34
4.1. Impact of Aspect ratio and Chemical modification of Carbon Nanotubes on the shear and extensional Rheology of Polyethylene Nanocomposites.	34
4.1.1. Abstract.....	34
4.1.2. Introduction.....	35
4.1.3. Experimental	39
4.1.4. Results & Discussion.....	40
4.1.4.1. Morphology.....	40
4.1.4.2. Impact of Aspect ratio and MWNCT loading on viscous properties ...	47
4.1.4.3. Impact of Aspect ratio and loading on Elastic properties	61
4.1.4.4. Extensional Rheology	73
4.1.5. Conclusion	82
4.1.6. Acknowledgement.....	83
4.1.7. References.....	84
4.2. Effect of aspect ratio, surface modification & compatibilizer on the mechanical & thermal properties of LDPE-MWCNT nanocomposites.....	88
4.2.1. Abstract.....	88
4.2.2. Introduction.....	89
4.2.3. Experimental Section.....	95

4.2.3.1. Materials and Sample Preparation.....	95
4.2.3.2. Scanning Electron Microscopy	98
4.2.3.3. Mechanical Testing.....	98
4.2.3.4. Differential Scanning Calorimetry	98
4.2.4. Results & Discussion.....	99
4.2.4.1. Morphology of the LDPE/MWCNT composites	99
4.2.4.2. Mechanical Testing.....	111
4.2.4.3. DSC Analysis	129
4.2.5. Conclusion	134
4.2.6. Acknowledgement.....	136
4.2.7. References.....	136
4.3. Rheology, mechanical and thermal properties of LDPE-C ₁₈ -CNT nanocomposites.	141
4.3.1. Abstract.....	141
4.3.2. Introduction.....	142
4.3.3. Experimental	145
4.3.3.1. Mechanical Testing.....	148
4.3.3.2. Differential Scanning Calorimetry	148
4.3.3.3. Rheology	149
4.3.4. Results & Discussion.....	149
4.3.4.1. Morphology of the LDPE/C ₁₈ -CNT composites	149
4.3.4.2. Mechanical Testing.....	153
4.3.4.3. Thermal Characterization.....	160
4.3.4.4. Rheological Characterization	162
4.3.5. Conclusion	172
4.3.6. Acknowledgment	173
4.3.7. References.....	173
4.4 Non-isothermal crystallization kinetics study of LDPE / MWCNT nanocomposites: Effect of Aspect ratio and surface modification.	179
4.4.1. Abstract	179
4.4.2. Introduction	180
4.4.3. Experimental.....	182

4.4.3.1. Materials and Sample Preparation	182
4.4.3.2 Differential Scanning Calorimetry (DSC).....	185
4.4.4. Theory & Calculation	185
4.4.4.1. Non-isothermal crystallization kinetics.....	185
4.4.5. Results & Discussion	189
4.4.6. Conclusion.....	215
4.4.7. Acknowledgement	216
4.4.8. References	216
CHAPTER FIVE.....	219
CONCLUSIONS	219
CHAPTER SIX	223
RECOMMENDATIONS	223
NOMENCLATURE	224
REFERENCES	225
VITA.....	232

LIST OF TABLES

Table 4.1.1. Time at break and critical extensional stress for the various composites and 0.5 and 1.5 henky rate.	81
Table 4.2.1. Elementary compositions of MWCNT used in this study.	97
Table 4.2.2. Dimensions of the multi-walled carbon nano tubes (MWCNT).	97
Table 4.2.3. Various thermal properties of Pure LDPE and its composites at various loadings.	133
Table 4.3.1. Mechanical properties of LDPE and its nanocomposites.	156
Table 4.3.2. Thermal properties of C ₁₈ -CNT/LDPE nanocomposites at various loadings.	161
Table 4.4.1. Energy dispersive X-ray spectroscopy of MWCNTs.	184
Table 4.4.2. Dimensions of the multi-walled carbon nano tubes (MWCNT).	184
Table 4.4.3. Peak and onset crystallization temperatures for different nanocomposites.	193
Table 4.4.4. Avrami Parameters for LDPE / MWCNT nanocomposites.	203
Table 4.4.5. Avrami Parameters for LDPE / MWCNT nanocomposites at 40 and 95 % crystallinity.	204
Table 4.4.6. Values of the Mo Parameters, α and F(T), at a fixed value of the Relative Degree of Crystallinity [X(t)] for All of the LDPE/Nanocomposites.	209
Table 4.4.7. Parameter values for the proposed model.	214

LIST OF FIGURES

Figure 4.1.1.a. FE-SEM image of LCNT-LDPE nanocomposite with 5.0% loading.	41
Figure 4.1.1.b. FE-SEM image of LCNT-LDPE nanocomposite with 5.0% loading.	42
Figure 4.1.1.c. FE-SEM image of LCNT-LDPE nanocomposite with 5.0% loading.	43
Figure 4.1.2.a. Cole Cole plot of LCNT / LDPE.	45
Figure 4.1.2.b. Cole Cole plot of SCNT / LDPE.	46
Figure 4.1.3.a. Dynamic viscosity versus frequency plots for LCNT/LDPE nanocomposites.	49
Figure 4.1.3.b. Dynamic viscosity versus frequency plots for MCNT/LDPE nanocomposites.	50
Figure 4.1.3.c. Dynamic viscosity versus frequency plots for SCNT/LDPE nanocomposites.	53
Figure 4.1.3.d. Dynamic viscosity versus frequency plots for various MWCNT/LDPE nanocomposites with 5.0% loading.....	54
Figure 4.1.3.e. Tan (δ) versus frequency plots for LCNT/LDPE nanocomposites at various loadings.....	55
Figure 4.1.4.a. Steady shear viscosity vs shear rate for LCNT / LDPE.	57
Figure 4.1.4.b. Steady shear viscosity vs shear rate for MCNT / LDPE.	58
Figure 4.1.4.c. Steady shear viscosity vs shear rate for SCNT / LDPE.	59
Figure 4.1.4.d. Steady shear viscosity vs shear rate for various LDPE nanocomposites at 5.0% loading.	60
Figure 4.1.5.a. Storage modulus versus frequency plot for LCNT/LDPE nanocomposites.	63
Figure 4.1.5.b. Storage modulus versus frequency plot for MCNT/LDPE nanocomposites.	64
Figure 4.1.5.c. Storage modulus versus frequency plot for SCNT/LDPE nanocomposites.	65
Figure 4.1.5.d. Storage modulus versus frequency plot various MWCNT/LDPE nanocomposites.	66
Figure 4.1.6.a. Normal force vs rate for LCNT / LDPE nanocomposites.	69
Figure 4.1.6.b. Normal force vs rate for MCNT / LDPE nanocomposites.	70

Figure 4.1.6.c. Normal force vs rate for SCNT / LDPE nanocomposites.	71
Figure 4.1.6.d. Normal force vs rate for various LDPE composites at 5.0 wt% loading nanocomposites.....	72
Figure 4.1.7.a. Extensional viscosity (η_e) vs time (s) for LCNT 5.0%-LDPE ($T_{mix} = 190^\circ\text{C}$, $T_{test} = 120^\circ\text{C}$).....	75
Figure 4.1.7.b. Extensional viscosity (η_e) vs time (s) for MCNT 5.0%-LDPE ($T_{mix} = 190^\circ\text{C}$, $T_{test} = 120^\circ\text{C}$).....	76
Figure 4.1.7.c. Extensional viscosity (η_e) vs time (s) for SCNT 5.0%-LDPE ($T_{mix} = 190^\circ\text{C}$, $T_{test} = 120^\circ\text{C}$).....	77
Figure 4.1.8.a. Extensional viscosity (η_e) vs time (s) for pure LDPE, Short CNT 0.5% - LDPE, Long CNT 0.5% - LDPE, Modified CNT 0.5% - LDPE ($T_{mix} = 190^\circ\text{C}$, Henky rate 1.5, $T_{test} = 120^\circ\text{C}$).....	78
Figure 4.1.8.b. Extensional viscosity (η_e) vs time (s) for pure LDPE, Short CNT 5% - LDPE, Long CNT 5% - LDPE, Modified CNT 5%-LDPE ($T_{mix} = 190^\circ\text{C}$, Henky rate 1.5, $T_{test} = 120^\circ\text{C}$).....	79
Figure 4.2.1.a. FE-SEM image of SCNT-LDPE nanocomposite with 0.5% loading.	101
Figure 4.2.1.b. FE-SEM image of SCNT-LDPE nanocomposite with 5.0% loading.	102
Figure 4.2.1.c. FE-SEM image of LCNT-LDPE nanocomposite with 0.5% loading.	103
Figure 4.2.1.d. FE-SEM image of LCNT-LDPE nanocomposite with 0.5% loading.	104
Figure 4.2.1.e. FE-SEM image of LCNT-LDPE nanocomposite with 5.0% loading.	105
Figure 4.2.1.f. FE-SEM image of LCNT-LDPE nanocomposite with 5.0% loading.	106
Figure 4.2.2.a. FE-SEM image of LCNT-LDPE nanocomposite with 5.0% loading coupled with 2.0% MAPE.	107
Figure 4.2.2.b. FE-SEM image of LCNT-LDPE nanocomposite with 5.0% loading coupled with 2.0% MAPE.....	108
Figure 4.2.2.c. FE-SEM image of MCNT-LDPE nanocomposite with 5.0% loading coupled with 2.0% MAPE.....	109
Figure 4.2.2.d. FE-SEM image of MCNT-LDPE nanocomposite with 5.0% loading coupled with 2.0% MAPE.....	110
Figure 4.2.3. Tensile stress-strain diagram for Pure LDPE & various loadings of MCNT.....	112

Figure 4.2.4.a. Yield strength at various loading for LDPE and its composites.	115
Figure 4.2.4.b. Yield strength at various loading for LDPE and its LCNT, MCNT composites with and without 2.0% MAPE.	116
Figure 4.2.5.a. Ultimate strength for pure LDPE and its various composites.	118
Figure 4.2.5.b. Ultimate strength for pure LDPE and various loading for LDPE and its LCNT, MCNT composites with and without 2.0% MAPE.	119
Figure 4.2.6.a. Young's Modulus for pure LDPE and its composites at various loadings.	122
Figure 4.2.6.b. Young's Modulus for pure LDPE and its composites for LCNT, MCNT at various loadings with 2% MAPE.	123
Figure 4.2.7.a. Percent elongation of pure LDPE and its composites at various loadings.	124
Figure 4.2.7.b. Percent elongation of pure LDPE and its composites of LCNT, MCNT at various loadings with 2.0% of MAPE.	125
Figure 4.2.8.a. Toughness of pure LDPE and its composites at various loadings.	127
Figure 4.2.8.b. Toughness of pure LDPE and its composites at various loadings of LCNT, MCNT with and without 2.0% MAPE.	128
Figure 4.2.9.a. Melting curves for pure LDPE and its composites at various loadings.	131
Figure 4.2.9.b. Crystallization curves for pure LDPE and its composites at various loadings.	132
Figure 4.3.1. FTIR of C ₁₈ -CNT showing the evidence of long carbon alkyl chain on the MWCNT.	147
Figure 4.3.2.a. FE-SEM image of C ₁₈ -CNT/LDPE nanocomposite with 5.0% loading and 2.0% MAPE.	150
Figure 4.3.2.b. FE-SEM image of C ₁₈ -CNT/LDPE nanocomposite with 0.5% loading.	151
Figure 4.3.2.c. FE-SEM image of LCNT-LDPE nanocomposite with 0.5% loading.	152
Figure 4.3.3.a Percent increase in yield strength, ultimate strength and Young's modulus for various C ₁₈ CNT/LDPE nanocomposites.	157
Figure 4.3.3.b Percent decrease in elongation and toughness for various C ₁₈ CNT/LDPE nanocomposites.	158
Figure 4.3.3.c. Tensile stress-strain representative curves for Pure LDPE & various loadings of C ₁₈ .CNT.	159
Figure 4.3.4.a. Dynamic viscosity & Storage modulus versus frequency plots for C ₁₈ -CNT/LDPE nanocomposites.	164

Figure 4.3.4.b. Dynamic viscosity & Storage modulus versus frequency plots for C ₁₈ -CNT/LDPE nanocomposites with MAPE.....	165
Figure 4.3.4.c. Dynamic viscosity & Storage modulus versus frequency plots for C ₁₈ -CNT/LDPE nanocomposites with MAPE.....	166
Figure 4.3.4.d. Dynamic viscosity & Storage modulus versus frequency plots for C ₁₈ -CNT/LDPE nanocomposites with MAPE.....	167
Figure 4.3.4.e. Tan (δ) versus frequency plots for C ₁₈ -CNT/LDPE nanocomposites with and without MAPE.....	168
Figure 4.3.5.a. Extensional viscosity (η_E) vs time (s) for C ₁₈ -CNT/LDPE nanocomposites at 0.5 s ⁻¹ henky rate.....	170
Figure 4.3.5.b. Extensional viscosity (η_E) vs time (s) for C ₁₈ -CNT/LDPE nanocomposites at 1.5 s ⁻¹ henky rate.....	171
Figure 4.4.1.a. Non-isothermal crystallization exotherms of LDPE / MWCNT nanocomposites with R of 2 °C/min.....	190
Figure 4.4.1.b. Non-isothermal crystallization exotherms of LDPE / MWCNT nanocomposites with R 6 °C/min.....	191
Figure 4.4.1.c. Non-isothermal crystallization exotherms of LDPE / MWCNT nanocomposites with R of 10 °C/min.....	192
Figure 4.4.2.a. X _T vs. T _c for LDPE/MWCNT nanocomposites at cooling rate of 2 °C/min.....	196
Figure 4.4.2.b. X _T vs. T _c for LDPE/MWCNT nanocomposites at cooling rate of 6 °C/min.....	197
Figure 4.4.2.c. X _T vs. T _c for LDPE/MWCNT nanocomposites at cooling rate of 6 °C/min.....	198
Figure 4.4.3.a. X _t vs t for LDPE/MWCNT nanocomposites at cooling rate of 2 °C/min.....	199
Figure 4.4.3.b. X _t vs t for LDPE/MWCNT nanocomposites at cooling rate of 6 °C/min.....	200
Figure 4.4.3.c. X _t vs t for LDPE/MWCNT nanocomposites at cooling rate of 10 °C/min.....	201
Figure 4.4.4. Avrami plot for LDPE/MWCNT nanocomposites obtained at 2°C/min.....	202
Figure 4.4.5.a. ln R versus ln t at each given relative crystallization for LCNT 5.0%.....	206
Figure 4.4.5.b. ln R versus ln t at each given relative crystallization for SCNT 5.0%.....	207

Figure 4.4.5.c. $\ln R$ versus $\ln t$ at each given relative crystallization for MCNT 5.0%.....	208
Figure 4.4.6.a. Activation energy versus crystallization temperature for LDPE with varying loadings of SCNT. Continuous lines show predictions of the proposed model.	211
Figure 4.4.6.b. Activation energy versus crystallization temperature for LDPE with different MWCNT at 5 wt%. Continuous lines show predictions of the proposed model.	212

ABSTRACT

NAME OF STUDENT: SARFRAZ HAIDER ABBASI
TITLE OF STUDY: RHEOLOGY AND SOLID-STATE PROPERTIES OF
POLYETHYLENE/CNT NANOCOMPOSITES: IMPACT
OF CNT CHARACTERISTICS AND SURFACE
MODIFICATION.
MAJOR FIELD : CHEMICAL ENGINEERING
DATE OF DEGREE: OCTOBER 2010

Nanocomposites of low density polyethylene (LDPE)/multiwall carbon nanotubes (MWCNTs) were prepared by melt blending. Different MWCNT [Long MWCNT (LCNT), Modified MWCNT (MCNT) & Short MWCNT (SCNT)] were used. The effect of surface modification and aspect ratio on dynamic, steady shear and extensional rheology were studied. In general, the rheological tools used in this study reveal a possible plasticization effect for MWCNT with high aspect ratio at low loadings (<1.0 wt%) and a filler effect at higher loadings (>1.0 wt%). The effect of COOH modification was more apparent in extensional viscosity and in N_1 to some extent. Aspect ratio has influenced both viscous and elastic shear properties as well as strain hardening. Also, analysis of mechanical properties revealed that yield strength and modulus increased with increased loading of various MWCNTs. However, ultimate strength, percent elongation and toughness were reduced for 2% MWCNT loading and higher. Addition of compatibilizer improved most of the mechanical properties. However, percent elongation and toughness did not show any improvement. Thereafter, MCNT was further modified to produce C_{18} -CNT. The addition of C_{18} -CNT to LDPE matrix improved most mechanical properties. The use of C_{18} reduced dynamic viscosity and storage modulus at all loadings covered in this study. Results of phase angle suggest no presence of network. Addition of C_{18} -CNT did not increase strain hardening, maintained extensional viscosity and time of break. On the other hand, the effect of CNT loading surface modification and aspect ratio on non isothermal crystallization kinetics reveal that presence of long MWCNT promotes initial crystallization and it impacts both the onset as well as peak crystallization temperatures. The Hoffman-Lauritzen theory showed a decrease in the activation energy with the increase in MWCNT concentration which supports the observed promotion of the initial crystallization. In summary, both the aspect ratio and C_{18} surface modification of CNT proved to enhance both the mechanical and rheological properties of LDPE/MWCNT nanocomposites. The selection of the proper surface modifier and its compatibility with the matrix is the key in enhancing the properties of the nanocomposites.

ملخص الرسالة

الإسم:	سرفراز حيدر عباسي
عنوان الرسالة:	خصائص التدفق وخصائص الحالة الصلبة لمركب البولي ايثيلين مع أنابيب الكربون، النانو: تأثير صفات والتحسين السطحي لأنابيب الكربون
الدرجة:	دكتوراه الفلسفه
التخصص:	الهندسة الكيميائية
تاريخ التخرج:	اكتوبر 2010م

تم تجهيز مركبات نانو مكونة من البولي ايثيلين المنخفض الكثافة مع أنابيب النانو الكربونية بواسطة طريقة الخلط الحراري. استخدمت أنابيب نانو مختلفة (طويلة، قصيرة، وطويلة محسنة سطحياً). تمت دراسة التحسين السطحي وطول الأنابيب على اختبارات التدفق. بشكل عام تشير النتائج إلى أن أنابيب الكربون الطويلة تقوم بدور المضافات المليئة عندما تكون نسبتها في البوليمر أقل من 1%، وتقوم بدور المضافات المقوية عندما تكون نسبتها أكثر من 1%. الاختبارات الميكانيكية أثبتت زيادة معامل المرونة مع زيادة نسبة أنابيب الكربون في البوليمر، ولكن نسبة التمدد تناقصت عندما تكون نسبة الأنابيب 2% أو أكثر. إضافة المادة الرابطة إلى المركب لم تؤدي إلى تحسين نسبة التمدد لذلك، تم تحسين سطح أنابيب الكربون أكثر من أجل إنتاج أنابيب كربون مضاف إليها جزيئ C18 أثبتت اختبارات التدفق عدم تكون شبكة متصلة من الأنابيب داخل البوليمر. أثبتت النتائج بشكل عام أن استخدام الأنابيب الطويلة المحسنة بجزيئ C18 أعطت أفضل النتائج في تحسين الخصائص الميكانيكية والتدفقية معاً لمركبات البولي ايثيلين مع أنابيب الكربون.

CHAPTER ONE

INTRODUCTION

Since the landmark paper by Iijima in 1991, CNTs have generated huge activity in most areas of science and engineering due to their remarkable properties. Since then the nano-science has drastically altered the landscape of scientific research and technology development. Nano reinforcement of engineering materials can impart dramatic structural (e.g., stiffness) and physical property benefits without adding significant weight (Deng et al., 2007; Yoon et al., 2002). For example, nanolayered reinforcement can impart greater thermal stability (Mishra et al., 2005; Gilman et al., 2000).

Ideally, the nanolayer reinforcement distributes internal stresses more uniformly allowing greater dimensional latitude in forming and shaping processes compared to conventional macroscale reinforcement. The unparalleled characteristics of clay nanolayers to boost mechanical properties of an engineering polymer (Nylon-6) were first demonstrated by Toyota researchers (Kojima et al., 1993). With only 4.2 wt.% of clay nanolayers, the modulus doubled and heat distortion temperature increased by 80°C compared to the pristine polymer, along with a reduction in water permeability and an increase in flame retardant properties. These dramatic improvements in properties made it possible to extend the use of low-cost polymers in under-the-hood applications.

Although several studies have been focused on producing nano-composites, many practical challenges concerning their fabrication still remain, compromising the full

realization of their enormous potential. Dispersing nanotubes individually and uniformly into the polymer matrix seems to be fundamental when producing composites with enhanced and reproducible properties. The reinforcement efficiency of nanocomposites with 2 to 6% of anisotropic nanoparticles can in some situations match that of conventional composites with 40–50% of loading with classical fillers. Various nano reinforcements are currently being developed; however, layered silicate clay minerals are the most popular due to their availability (natural source), low cost and more importantly environmentally friendly (Sinha Ray and Okamoto, 2003; Grim, 1953).

Various nano reinforcements currently being developed are nanoclay layered silicates (Giannelis, 1996; Chen et al., 2005; Biswas and Sinha Ray, 2001; Giannelis et al., 1999; Le Baron et al., 1999), cellulose nanowhiskers (Mohanty et al., 2003 a & b), ultra fine layered titanate (Hiroi et al., 2004), and carbon nanotubes (Mitchell et al., 2002; Pötschke et al., 2003; Andrews and Wisenberger, 2004). Of particular interest organically modified layered silicate (OMLS) polymer nanocomposites. OMLS showed significant enhancement of a large number of physical properties, including gas barrier properties, flammability resistance, thermal and environmental stability of polymers (Sinha Ray and Okamoto, 2003, Sinha-Ray and Bousmina, 2005).

These improvements were generally attained at lower silicate content (≤ 6 wt%) compared to that of conventionally filled systems. For these reasons, polymer/OMLS nanocomposites are far lighter in weight than conventional composites, which make them competitive with other materials for specific applications such as packaging and automotive parts. Furthermore, the nanoscale morphology affords the opportunity to

develop model systems consisting entirely of interfaces using conventional bulk characterization techniques such as differential scanning calorimetry (DSC), rheology, NMR, and various kinds of spectroscopy (Hackett et al., 1998; Hackett et al., 2000; Vander Hart et al., 2001; Loo and Gleason, 2003). The main reason for these improved properties in polymer/layered silicate nanocomposites is the high surface area of the OMLS particles as opposed to conventional fillers (Chen et al., 2002). Layered silicates generally have layer thickness in the order of 1 nm and very high aspect ratios (10–1000).

The conductivity (Andrews et al., 2002), strength, toughness (Dufres et al., 2002), and flammability properties (Kashiwagi et al., 2002) of polymers may all be substantially improved by the addition of CNTs. However, the effective utilization of CNTs in nanocomposite applications may depend on the ability to homogeneously disperse them into the polymer matrix (Baughman et al., 2002). Furthermore, extensive interfacial interaction is required to achieve load transfer (Schadler et al., 1998) across the CNT-polymer interface, to prevent re-aggregation during subsequent processing, and to enable other enhanced properties in the nanocomposite. Nanotubes preferentially aggregate into bundles, where adjacent tubes are held together by strong van der Waals' attractions (Thess et al., 1996).

Considerable research has been focused on CNTs to improve their compatibility with monomers and polymers (Hirsh et al., 2002; Cui et al., 2003). Compatibilization can be achieved through functionalization, such as through covalently bonding organic groups directly to the CNTs (Hirsh et al., 2002; Bahr et al., 2002). Mitchell and co-workers reacted organic diazonium compounds with single-walled nanotubes (SWNTs) to

facilitate incorporation into polystyrene (PS) by solution mixing in toluene (Mitchell et al., 2002); Hill et al. functionalized SWNTs and multiwalled carbon nanotubes (MWNTs) with a PS co-polymer, by esterification of carboxylic acid-functionalized nanotubes (Hill et al., 2002); while Smith and co-workers reacted the carboxyl and hydroxyl groups on oxidized SWNTs with alkoxy silane-terminated amide acid polymers (Smith et al., 2004). In some cases, covalent functionalization of the CNT sidewalls occurs to some extent. This process may disrupt the extended p-networks on CNT surfaces, diminishing both their mechanical and electronic properties. This is more of a concern for SWNTs, since MWNTs have interior tubes which would presumably remain intact. To avoid this potential effect, several groups have focused on finding non-covalent approaches to compatibilization. This can be accomplished through van der Waals' interactions between the alkyl chain of a surfactant and the aromatic surface of the CNT (Hirsh et al., 2002). The non-covalent compatibilization may be a more facile and practical processing method.

It is believed that the dispersion of the CNT in the polymer matrix is strongly affected by the polymer-CNT surface interactions, and hence the melt and solid state properties of the nanocomposite are affected. Initially the impact of aspect ratio and chemical modification of carbon nanotubes on the shear and extensional rheology of polyethylene nanocomposites were studied. The effect of aspect ratio, surface modification & compatibilizer on the mechanical & thermal properties of LDPE-MWCNT nanocomposites were then studied. MCNT was then modified with C₁₈ chain and rheology, mechanical and thermal properties of LDPE/C₁₈-CNT nanocomposites were

studied. The non-isothermal crystallization kinetics study of LDPE / MWCNT nanocomposites was also carried out.

CHAPTER TWO

LITERATURE SURVEY

The following literature review will mainly search the melt rheology, mechanical properties, increased interfacial interaction between fiber and matrix and improvement of the dispersion of nano material into the matrix of polymer nanocomposites in general and PEs in particular.

Small amplitude oscillatory shear measurements of polymeric materials (in strain controlled rheometers) are generally performed by applying a time dependent strain of $\gamma(t) = \gamma^0 \sin(\omega t)$ and measuring the resultant shear stress $\tau(t) = \tau^0 [G' \sin(\omega t) + G'' \cos(\omega t)]$, where G' and G'' are the storage and loss moduli, respectively. Generally, the dynamic rheology of polymer melts depends strongly on the temperature and frequency at which the measurement is carried out. In the case of polymer melts, it is expected that polymers should exhibit characteristic of homopolymer-like terminal flow behavior, expressed by the power-laws $G' \sim \omega^2$ and $G'' \sim \omega$ at high temperatures/low frequencies. For polymer nanocomposites, such a behavior changes from liquid-like to solid-like ($G' \gg G''$ with $G'' \sim 0$) with increasing clay content.

In contrast to pure polymers, intercalated nanocomposites exhibit strong time dependent behavior (Sinha Ray and Bousmina, 2005). With increasing shear rates, the shear-viscosity attains a plateau after a certain time, and the time required to attain this plateau decreases with increasing shear rates. The possible reason for this type of behavior may

be due to the planer alignment of the silicate particles towards the flow direction under shear. Polymer nanocomposites show a very strong shear-thinning behavior at high shear rates. These observations suggest that the silicate layers are strongly oriented towards the flow direction (may be perpendicular alignment of the silicate layers toward the stretching direction) at high shear rates and that of pure polymer dominates shear-thinning behavior.

Galgali et al. (2001) performed an experimental investigation on the creep behavior of molten polypropylene organically modified clay nanocomposites. The nanocomposite hybrids were prepared by melt intercalation in an extruder in the presence or absence of a compatibilizer. They were subsequently annealed and simultaneously characterized using high-temperature wide-angle X-ray diffraction (WAXD) and controlled stress rheometry. The creep resistance of compatibilized hybrids was significantly higher than that of uncompatibilized hybrids and increased with annealing time. The microstructure of the nanocomposites was investigated by transmission electron microscopy (TEM) and high-temperature WAXD showed the presence of clay crystallites dispersed within the polymer matrix. The creep data together with the microstructural investigation are probably indicative of a small amount of exfoliation from the edges of the clay crystallites during extrusion and annealing.

The zero shear viscosity of the compatibilized nanocomposites with more than 3 wt % clay was at least 3 orders of magnitude higher than that of matrix resin and the uncompatibilized hybrids. Importantly, the large increase in zero shear viscosity was not accompanied by any increase in the flow activation energy compared to the matrix

polymer. The compatibilized hybrids also showed an apparent “yield” behavior. The solid-like rheological response of the molten nanocomposite was suggested to originate from large frictional interactions of the clay crystallites. Compatibilizer has a significant influence in modifying the rheological behavior.

Lee and Han (2003) investigated the linear dynamic viscoelastic properties and non-linear transient rheology of polycarbonate (PC) /clay nanocomposites at temperatures ranging from 240° to 280°C. Nanocomposites of PC and natural montmorillonite (Cloisite Na) or chemically modified clay (Cloisite 30B) were prepared by melt blending in a twin-screw extruder. Cloisite 30B is a natural montmorillonite modified with methyl, tallow, bis-2-hydroxyethyl, quaternary ammonium chloride (MT₂EtOH). In both PC/Cloisite Na and PC/Cloisite 30B nanocomposites the concentration of clay was varied from 2.3 to 4.3 wt%. In situ Fourier transform infrared (FTIR) spectroscopy results showed that at temperatures ranging from 30 to 280°C the carbonyl groups in PC and the hydroxyl groups in MT₂EtOH of Cloisite 30B in PC/Cloisite 30B nanocomposites formed hydrogen bonds, while no evidence of hydrogen bonding was observed in the PC/Cloisite nanocomposites. TEM images showed that organoclay platelets were well dispersed in PC/Cloisite 30B nanocomposites, while the untreated clay platelets are poorly dispersed in PC/Cloisite Na nanocomposites. The results of rheological measurements (linear dynamic viscoelasticity, non-linear transient shear flow, and steady-state shear flow) supported the results of XRD FTIR and TEM.

Ren and Krishnamoorti (2003b) reported the nonlinear viscoelastic properties for a series of intercalated nanocomposites of organically modified clay and a disordered styrene-

isoprene di-block copolymer. The linear-to-nonlinear transition for stress relaxation measurements was also examined. The nanocomposites exhibit strong shear thinning behavior thought to result from orientation of the layers in response to the applied shear deformation. The empirical Cox-Merz rule was found to be inapplicable for such nanocomposites and that steady and dynamic oscillatory flow are not equivalent for such materials.

Lim and Park (2000) investigated the rheological behavior of intercalated polystyrene/layered silicate nanocomposites. Both storage and loss moduli increased with silicate loading at all frequencies and showed non-terminal behavior at low frequencies which is a typical behavior of non-homogeneous systems with ordered microstructures. The rheological behavior in intercalated polystyrene/layered silicate nanocomposite was suggested to depend not only on the intercalation of polymers, but also on the alignment of silicate layers. Furthermore, the real time intercalation dynamics of polystyrene into the layered silicate was monitored by rheological measurements. As polymer intercalates into the silicate layers, long range order of alternating polymer/layered silicate was suggested to preserve.

Solomon et al (2001) examined the melt-state linear and nonlinear shear rheological properties of hybrid materials of polypropylene (PP) and amine-exchanged montmorillonite. The materials were prepared by melt mixing with maleic anhydride functionalized polypropylene as the compatibilizer. The clay interlayer spacing (as determined by WAXD) increased upon melt mixing; however, the short range ordering of the clay layers was preserved. Above clay loadings of 2.0 wt % the hybrid materials

exhibited apparent low-frequency plateaus in the linear viscoelastic moduli. The hybrid storage modulus was sensitive to the chemistry of the amine exchanged into the clay. The amount of stress overshoot observed in flow reversal experiments was found to be a function of the rest time allowed between the reversals. The transient stress in start-up of steady shear scaled with the applied strain. These observations allow features of the PP/montmorillonite hybrid structure to be deduced. The transient nonlinear rheology suggests an anisometric, non-Brownian structure that is thermodynamically unstable. The authors demonstrated the sensitivity of melt-state rheological measurements to inter particle structure and chemistry of the hybrid materials.

Ren et al. (2003a) studied the kinetics of disorientation of polymer layered silicate nanocomposites following alignment of the silicate layers by prolonged large amplitude oscillatory shear using linear viscoelastic measurements. Nanometer thick disks with diameters of 30 nm, 0.3-0.6 μ m, and 5 μ m dispersed in polymer matrices exhibited disorientation kinetics that was non-Brownian. The disorientation process exhibits signatures of aging observed in soft-colloidal glasses and is shown to be independent of temperature, nano particle size, and chemical details, viscoelasticity and molecular weight of the polymeric matrix.

Lele et al. (2002) examined the experimental results for both the rheology and flow-induced orientation of a series of intercalated syndiotactic polypropylene nanocomposites which were prepared by melt intercalation in the presence or absence of an i-PP/maleic anhydride copolymer. The nanocomposites showed typical rheological signatures of well-dispersed intercalated nanocomposites such as a low frequency plateau in dynamic

moduli and an apparent yield transition from very high viscosity at low shear stresses to low viscosity above a yield stress. In situ XRD measurements during shear provided direct evidence of rheology-microstructure links in these materials. It was found that the clay could be easily oriented by shear and that a high degree of orientation can be achieved after the yield transition. Further, the rheo-XRD apparatus allowed measurements of the relaxation of orientation upon the cessation of flow. The orientation relaxation time matched the characteristic relaxation times estimated from independent rheological measurements well. Also, Lim and Park (2001) studied the phase morphology and rheological behavior of polymer/layered silicate nanocomposites.

Mousa and Karger (2001) examined rheological and thermodynamical behavior of styrene/butadiene rubber-organoclay nanocomposites. Organophilic layered silicate (montmorillonite type) was added up to 10 phr to a cured styrene/butadiene rubber (SBR). The compounds were characterized in respect to their curing, rheological and mechanical properties. Viscosity decreased as a function of shear rate and high elongation at break of the compounds caused by the incorporation of organoclay were observed.

Hyun et al. (2001) investigated the rheology of polyethylene oxide (PEO)/organoclay nanocomposites. Using three different organoclays modified with the alkyl ammonium salts, the effect of surfactants on organoclay surfaces in polymer/organoclay nanocomposites was investigated by focusing on two major aspects: internal structure analysis and rheological measurement of the nanocomposites. Rheological properties of these nanocomposites exhibited different behavior with different modifier concentrations

and surfactant sizes (chain lengths). Viscosity data showed that steady shear viscosity and power-law behavior increase with organoclay content. Hysteresis phenomenon was also enhanced with organoclay content. The increase in the storage/loss moduli, thermal stability and interactions among organoclay platelets were observed to increase with increasing organoclay content.

Krishnamoorti et al. (2001) investigated the linear and nonlinear melt state viscoelastic properties for a series of layered silicate based intercalated polymer nanocomposites. The study elucidated the role of highly anisotropic nanometer thick layers in altering the flow properties of such hybrids. The steady shear viscosities for the nanocomposites exhibited enhanced shear-thinning at all shear rates. The viscosity at high shear rates was almost independent of silicate loading and comparable to that of the unfilled polymer. Further, the elasticity, as measured by the first normal stress difference, when compared at constant shear stress is surprisingly independent of the silicate loading and identical to that of the unfilled polymer. This unique combination of unfilled polymer like viscosity and elasticity for these filled nanocomposites was attributed to the ability of the highly-anisotropic layered silicates to be oriented in the flow direction and results in a minimal contribution by the silicate layers to both the viscosity and the elasticity of the hybrids.

Wu et al. (2005a) investigated the linear rheological behavior and thermal stability of poly(butylene terephthalate)/epoxy/clay ternary nanocomposites. Epoxy resin was used as a compatibilizer to prepare poly(butylene terephthalate)/clay nanocomposites (PCN) via melt intercalation. Their results revealed that with the addition of epoxy, the silicates were easily intercalated and present a nice dispersion in the matrix. The ternary hybrids

showed a stronger solid-like response at terminal zone than that of the sample without epoxy. Thermogravimetric analysis showed that only the hybrids with lower epoxy loading (2-4 wt%) showed a higher thermal stability than that of the sample without epoxy, while with increase in epoxy content, the thermal stability of the ternary nanocomposites declined somewhat. The compatibilizer loadings did have an influence on the performance of nanocomposites and, the best compatibilizer dosage, 4 wt%, was decided by a new 'crossover point' rheological method.

Wu et al. (2004a) investigated the influence of chlorinated polyethylene (CPE) on mechanical properties, morphology, and rheology of nanocomposites of poly(vinyl chloride, PVC) and nanometric calcium carbonate particles. Nanocomposites of PVC and nano-calcium carbonate (CaCO_3) particles were prepared via melt blending, and CPE as an interfacial modifier was also introduced into the nanocomposites. The mechanical properties, morphology, and rheology were studied. The elongation at break and Young's modulus also increased with increasing the nano CaCO_3 concentration. Also, the notched Izod impact strength achieved a significant improvement by incorporating CPE into the nanocomposites, and obtained a value of 745 J/m. Morphology investigation indicated that the nano CaCO_3 particles in the PVC matrix were encapsulated with a CPE layer. The evaluation of rheological properties revealed that the introduction of nano- CaCO_3 particles into PVC resulted in a remarkable increase in the melt viscosity. However, the viscosity decreased with addition of CPE, especially at high shear rates; thus, the processability of the ternary nanocomposites was suggested to improve.

Lee and Han (2003b) studied the effects of polymer matrix/organoclay compatibility and the gallery distance of organoclay on rheology of organoclay nanocomposites. The organoclay nanocomposites were prepared with poly(ethylene-*ran*-vinyl acetate) (EVA), poly(ethylene-*ran*-vinyl alcohol) having 53 mol % vinyl alcohol (EVOH), or poly(ethylene-*ran*-vinyl acetate-*ran*-vinyl alcohol) having 5 mol % vinyl alcohol (EVAOH) were investigated. Two organoclays from Southern Clay Products were used: (i) Cloisite 30B treated with a surfactant containing tallow, quaternary ammonium chloride, and hydroxyl groups and (ii) Cloisite 15A treated with a surfactant containing hydrogenated tallow, quaternary ammonium chloride but no hydroxyl group. Thus, a total of six nanocomposites were prepared by melt blending using a Brabender mixer. Before taking rheological measurements, the nanocomposites were characterized by XRD and TEM.

The linear dynamic viscoelastic measurements indicated that the dynamic storage modulus of the (EVAOH)/Cloisite 30B and EVA/Cloisite 15A nanocomposites increased as the temperature increased from 120° to 180°C, while the dynamic storage modulus of the (EVAOH)/Cloisite 15A and EVA/Cloisite 30B nanocomposites decreased with increasing temperature. The intermittent shear flow experiments indicated that structural reorganization occurred, during the rest period upon cessation of the initial transient, in the (EVAOH)/Cloisite 30B and EVA/Cloisite 15A nanocomposites, while there was very little evidence of such behavior in the (EVAOH)/Cloisite 15A and EVA/Cloisite 30B nanocomposites. Their rheological observations were explained in terms of the compatibility between the polymer matrix and organoclay and the gallery distance of

organoclay. In-situ FTIR indicated that EVAOH and Cloisite 30B, which both have hydroxyl groups, formed hydrogen bonds even at 180°C, the highest experimental temperature employed, while little evidence was found indicating the formation of hydrogen bonds between EVAOH and Cloisite 15A.

Lee et al (2004) studied the time and shear dependent rheology of maleated polyethylene and its nanocomposites. Dipole–dipole and/or hydrogen-bonding interactions between the pendant functional groups within maleated HDPE (PE-g-MAN) establish a physical polymer network, whose formation kinetics and shear-sensitivity are revealed by dynamic oscillatory testing. The pronounced time and shear dependent viscoelastic properties of PE-g-MAN were not observed for a corresponding imide derivative, PE-g-imide, presumably due to weakened functional group associations in the latter material.

Dynamic mechanical analysis (DMA) measures the response of a given material to an oscillatory deformation as a function of temperature or frequency. DMA results are composed of three parameters: (a) the storage modulus (G' or E'), (b) the loss modulus (G'' or E''), and (c) $\tan \delta$, the ratio (G''/G' or E''/E'), useful for determining the occurrence of molecular mobility transition, such as the glass transition temperature (T_g). DMA has been used to study temperature dependence of G' of polymers upon nanocomposite formation under different experimental conditions. (Sinha Ray et al., 2003). The enhancement of G' at high temperature was observed by Maiti et al. (2002) and suggested to be due to mechanical reinforcement by the silicate layers as well as extended intercalation at high temperature. Above T_g , when materials become soft, the

reinforcement effect of the silicate layers becomes prominent due to the restricted movement of the polymer chains.

The tensile modulus of a polymeric material has been shown to be remarkably improved when nanocomposites are formed with layered silicates (Sinha Ray and Okamoto, 2003). The dramatic enhancement of the modulus for such extremely low clay concentrations cannot be attributed simply to the introduction of the higher modulus inorganic filler layers. A theoretical approach is assuming a layer of affected polymer on the filler surface, with a much higher modulus than the bulk equivalent polymer (Shia et al., 1998). This affected polymer can be thought of as the region of the polymer matrix that is physisorbed on the silicate surface, and is thus stiffened through its affinity. Obviously, for such high aspect ratio fillers as silicate layers, the surface area is exposed to the polymer

The thermal stability of polymeric materials is usually studied by thermogravimetric analysis (TGA). The weight loss due to the formation of volatile products after degradation at high temperature is monitored as a function of temperature. When the heating occurs under an inert gas flow, a non-oxidative degradation occurs, while the use of air or oxygen allows oxidative degradation of the samples. Generally, the incorporation of clay into the polymer matrix was found to enhance thermal stability by acting as a superior insulator and mass transport barrier to the volatile products generated during decomposition.

Bandyopadhyay et al. (1999) reported the first improved thermal stability of polymer nanocomposites that included clay. These nanocomposites were prepared by melt intercalation. Authors argue that the silicate layers act as a barrier for both the incoming gas and also the gaseous by-products, which in one hand increases the degradation onset temperature and also widens the degradation process. The addition of clay enhances the performance of the char formed, by acting as a superior insulator and mass transport barrier to the volatile products generated during decomposition. Recently, there have been many reports concerned with the improved thermal stability of polymer nanocomposites prepared with various kinds of organically modified layered silicate (Chang et al., 2003 b & c; Paul et al., 2003).

Liu and Wu (2002) investigated polyamide 66/Clay nanocomposites via melt intercalation. Polyamide 66/clay nanocomposites (PA66CN) were prepared via a melt compounding method using a new kind of organophilic clay, which was obtained through co-intercalation of epoxy resin and quaternary ammonium into Na modified clay. The dispersion effect of silicate layers in the matrix was studied by means of XRD and TEM. The silicate layers were dispersed homogeneously and nearly exfoliated in the matrix as a result of the strong interaction between epoxy groups and PA66. The mechanical properties and heat distortion temperature of PA66CN increased dramatically. The notched Izod impact strength of PA66CN was 50% higher than that of PA66 when the clay loading was 5 wt%. Even at 10 wt% clay content, the impact strength was still higher than that of PA66. The finely dispersed silicate layers and the strong interaction between silicate layers and the matrix reduced the water absorption, at 10 wt% clay

content; PA66CN only absorbs 60% water compared with PA66. The addition of silicate layers changed the crystal structure in PA66CN.

Ma et al. (2005) examined the preparation, morphology, and mechanical, electrical, and thermal properties of polystyrene nanocomposite materials. Polystyrene (PS) resin nanocomposites were prepared with antistatic properties by melt blending PS with nanoscale zinc oxide (ZnO). The effects of nanoscale ZnO on the electrical and physical characteristics of the PS nanocomposites were investigated. Two kinds of nanoscale powders, spherical ZnO (s-ZnO) and zinc oxide whisker (w-ZnO), were selected. The coupling agents, vinyltriethoxysilane (VTES) and phenyltriethoxysilane (PTES) were used to improve the compatibility between the nano powders and PS resin. The addition of s-ZnO and w-ZnO improved the antistatic characteristics of the materials. The surface resistivities of the s-ZnO and w-ZnO nanocomposites were significantly reduced by modification with VTES and PTES. The addition of ZnO nano powder increased the flexural modulus and reduced the flexural strength. The silane coupling agents improved the flexural properties of the nanocomposites. The glass-transition temperatures and thermal degradation temperatures of the ZnO/PS nanocomposites increased with ZnO content. Treatment with silane increased the glass-transition temperatures and thermal degradation temperatures of the composites.

Zhang and Fang (2005) investigated the enhancement of radiation-resistant effect in EVA copolymers by the formation of EVA copolymers/clay nanocomposites. EVA copolymers/clay nanocomposites, prepared by using non-reactive organophilic clay and reactive organophilic clay, were characterized by XRD and by high-resolution TEM. The

influence of gamma irradiation on the structure and properties of the pure EVA and EVA/clay nanocomposites was systematically investigated. In the presence of gamma radiation, the clay was observed to restrain the increase of the storage modulus of EVA/clay nanocomposites, which was supported by DMA. Gamma irradiation was suggested to have almost no effect on the thermal properties of EVA/clay nanocomposites. However, the use of reactive organophilic clay improved the thermal stability of EVA/clay nanocomposites by using.

Ni et al. (2005) reported results on preparation and characterization of a novel polyether polyurethane/clay nanocomposites synthesized with organically modified clay MMT as chain extenders. The mechanical analysis indicated that, when the organically modified clay was used as a chain extender to replace a part of the 1,2-diaminopropane to form PU/clay nanocomposites. The strength and strain at break of the polymer was enhanced when increasing the content of nanoclay in the matrix. When the nanoclay content reached about 5%, the tensile strength and elongation at break were over 2 times that of the pure PU. The thermal stability and the glass transition of the modified clay/PU nanocomposites also increased with increasing clay content.

Zhang et al. (2005) investigated PE and PP nanocomposites based upon oligomerically modified clay (lauryl clay). Nanoclay was modified with an oligomeric surfactant, which was then melt blended with PE and PP in a Brabender mixer. The morphology was characterized by XRD and TEM, while thermal stability was evaluated from TGA and the fire properties by cone calorimetry. The nanocomposites were best described as

mixed immiscible/intercalated/delaminated systems and the reduction in peak heat release rate is about 40% at 5% inorganic clay loading.

Shin et al. (2003) investigated in situ polymerization using bi-functional organic modifiers of PE–clay hybrid nanocomposites. A hybrid PE–clay nanocomposite was prepared using in situ polymerization with bi-functional organic modifiers. Morphological characterization of the product showed that a fraction of the PE chains was chemically linked to the silicate surface. The chemical modification and intercalation of nanoclay was carried out with alkylaluminum and vinyl alcohol. The vinyl groups chemically linked to the silicate surface were copolymerized with ethylene inside the clay galleries using a coordination catalyst. The polymerization led not only to effective exfoliation of the layered silicate but also to PE chains that were chemically bonded to silicate surface.

Tjong and Meng (2003) reported their results on preparation and characterization of melt-compounded polyethylene/vermiculite nanocomposites. PE-layered vermiculite (VMT) nanocomposites were fabricated via direct melt compounding in a twin-screw extruder followed by injection molding. Exfoliated PE/VMT nanocomposites were readily prepared via *in situ* melt mixing of maleic anhydride modified VMT with PE. Maleic anhydride acts as either the intercalation agent for VMT or as a compatibilizer for the PE and VMT phases. XRD and TEM observations revealed the formation of exfoliated PE/VMT nanocomposites. The experimental results showed that the storage modulus and strength of nanocomposites tend to increase with increasing VMT content. Nearly 25% increment in the tensile strength and 50% increment in the storage modulus were

achieved by incorporating 4 wt % VMT into PE. The thermal properties of the nanocomposites were investigated by DMA and DSC. The glass-transition temperature of PE/VMT nanocomposites appeared to increase upon the introduction of VMT into the PE matrix.

Zhang and Wilkie (2005) examined the preparation and flammability properties of PE and modified clay nanocomposites. PE–clay nanocomposites were prepared using melt blending in a Brabender mixer. XRD and TEM were used to characterize the nanostructure of these composites while the thermal stability was evaluated from TGA and the flammability parameters using cone calorimetry. It was found that the PE–clay nanocomposites had a mixed immiscible-intercalated structure and there is better intercalation when maleic anhydride is combined with the polymer and clay to be melt blended. The reduction in peak heat release rate is 30–40%.

Hasegawa et al. (2004) prepared and characterized ethylene propylene rubber (EPR)–clay nanocomposites based on maleic anhydride-modified EPR and organophilic clay. EPR–clay nanocomposites (EPR–CNs) were prepared by melt-compounding maleic anhydride modified EPR (EPR-MA) with organophilic clay, and their properties were examined. Silicate layers of organophilic clay were found to exfoliate and homogeneously disperse into the nanometer level in the nanocomposites by TEM observation. EPR–CNs exhibited higher tensile moduli compared to EPR-MA and composites containing conventional fillers such as carbon black talc. The storage moduli of EPR–CNs were also higher than those of EPR-MA and the conventional composites. Creep resistances of EPR–CNs were much improved compared for EPR-MA. Also, Lin et al. (2005) presented a novel method

to prepare chitosan/clay nanocomposites. Chitosan is a partially deacetylated derivative of chitin, the most abundant natural polymer next to cellulose. The exfoliated nanoclay layers were found to flatten out in parallel with the surface, which not only increased the tensile strength of the chitosan film but also hindered degradation.

Osman and Rupp (2005) studied the interfacial interactions and properties of PE-layered silicate nanocomposites. Organically modified nanoclay, carrying alkyl chains, phenyl groups, or a combination of both, were prepared and compounded with PE. The oxygen permeability coefficients and tensile properties of the nanocomposites were correlated to the exfoliation of the organically modified nanoclay. Partial exfoliation was achieved, although no intercalation was observed. Aromatic moieties attached to the clay surface led to a stronger interaction between the OMMT layers and reduced exfoliation.

Mishra and Shimpi (2005) reported the mechanical and flame-retarding properties of SBR filled with nano-CaCO₃ as a filler and linseed oil as an extender. A nano size CaCO₃ filler was synthesized by an in situ deposition technique, and its size was confirmed by XRD. Because of the reduction in the nano size of CaCO₃, drastic improvements in the mechanical properties were found (Mishra and Shimpi, 2005). The size of 9 nm showed the highest increase in the tensile strength (3.89 MPa) in comparison with commercial CaCO₃ and the two other sizes of nano- CaCO₃ up to an 8 wt % loading in SBR. The elongation at break also increased up to 824% for the 9-nm size in comparison with commercial CaCO₃ and the two other sizes (15 and 20 nm) of nano- CaCO₃. Also, these results were compared with nano-CaCO₃-filled SBR without linseed oil as an extender. The modulus at 300% elongation, hardness, specific gravity, and flame-retarding

properties increased with a reduction in the nano size with linseed oil as an extender, which helped with the uniform dispersion of nano- CaCO_3 in the rubber matrix.

Al-Kandary et al. (2005) investigated the morphology and thermomechanical properties of compatibilized polyimide-silica nanocomposites. Polyimide-silica nanocomposites were prepared from an aromatic polyamic acid derived from pyromellitic dianhydride and oxydianiline and a silica network using the sol-gel reaction. Compatibilization of the two components was achieved by modifying the silica network with imide linkages. Morphology, thermal, and mechanical properties of these composite materials were studied as a function of silica content. Results were compared with unmodified silica network. The $\tan \delta$ spectra obtained from DMA showed a large increase in the glass transition temperature with increasing silica content for the compatibilized system in contrast to the un-compatibilized one. Mechanical properties of the polyimide composites improved due to better interaction between the organic and inorganic phases.

Hotta and Paul (2004) analyzed the nanocomposites formed from LLDPE and organoclays. PE-clay nanocomposites were prepared by melt compounding various combinations of a maleic anhydride grafted LLDPE (LLDPE-g-MA), a LLDPE, and two organoclays. The two types of organoclays were selected to show the effect of the number of alkyl groups attached to the nitrogen of the organic modifier on exfoliation and improvement of mechanical properties. Nanocomposites derived from the organoclay having two alkyl tails, exhibited better dispersion and improvement of mechanical properties than nanocomposites based on the organoclay having one alkyl tail. This result was the opposite of what was observed for nylon-6 nanocomposites. In addition, the

rheological properties and gas permeability of the nanocomposites derived from the organoclay having two alkyl tails were investigated. Both melt viscosity and melt strength increased with increased content of clay (MMT) and LLDPE-g-MA. Gas permeability was decreased by the addition of MMT.

Chen et al. (2005) attempted a new method to improve the interaction between poly(butylene succinate) (PBS) and a commercially available organoclay, Cloisite 25A (C25A), by the addition of epoxy groups to the clay. Epoxy groups were grafted to C25A by a treatment with (glycidoxypropyl) trimethoxy silane to produce twice functionalized organoclay (TFC). The morphological structure of the composites was analyzed with XRD and TEM. The higher degree of exfoliation of the silicate layers in PBS/TFC and the improved mechanical properties, in comparison with those of PBS/C25A, were attributed to the increased interfacial interaction between PBS and TFC. TFC accelerated the crystallization of PBS more effectively than C25A, and this indicated that TFC was more efficient for the nucleation than C25A.

Wu and Chu (2005b) described the preparation and characterization of thermoplastic vulcanizate/silica nanocomposites. The nanocomposites were prepared by the melt blending of TPV and maleic anhydride grafted PP (mPP) into organically modified SiO₂ (m-SiO₂), treated with *n*-hexadecyl trimethylammonium bromide as a grafting agent for TPV during the melt mixing. The thermal stability and storage modulus of the 1 wt % m-SiO₂ containing TPV/mPP/m-SiO₂ nanocomposite were higher than those of pristine TPV. DMA revealed that the glass-transition temperature of the PP phase of the nanocomposites increased (in comparison with that of virgin TPV), whereas the

ethylene–propylene–diene monomer phase remained almost the same. The adhesion strength between the TPV/mPP/m-SiO₂ nanocomposites and steel also increased with increasing m-SiO₂ content.

Yang et al. (2003) prepared PE/ Montmorillonite nanocomposites by in situ coordination polymerization using a nanoclay/MgCl₂/TiCl₄ catalyst activated by Al(Et)₃. The catalyst was prepared by first diffusing MgCl₂ into the swollen MMT layers, followed by loading TiCl₄ on the inner/outer layer surfaces of MMT where MgCl₂ was already deposited. The intercalation of nanoclay layers by MgCl₂ and TiCl₄ was demonstrated by the enlarged interlayer spacing determined by WAXD. The nanoscale dispersion of nanoclay layers in the PE matrix was characterized by WAXD and TEM. As a consequence, the crystallinity of the nanocomposite decreased sharply, whereas the tensile strength was significantly improved compared to that of virgin PE of comparable molecular weight. The confinement of the nanodispersed clay layers to molecular chain and the strong interaction between the nanoscale nanoclay layers and the resin matrix were thought to account for the decrease of crystallinity and the remarkable enhancement of strength.

Van Zyl et al. (2002) synthesized a hybrid inorganic-polymer composite through nanosize silica filler particles (<30 nm) that were incorporated inside a nylon-6 matrix. Compared to pure nylon-6, mechanical tests on the hybrid composite showed an increase in impact toughness, an increase in modulus as a function of filler percentage, and a strain-at-break of more than 50%.

Lee et al. (2005) synthesized and characterized PE-based ionomer nanocomposites. The introduction of ionic functionality resulted in substantial increase in melt elasticity and viscosity, as well as improved ability to exfoliate onium ion-exchanged nanoclay (NR4C-MM) and to disperse nanosilica (SiO₂). Physical and rheological analysis of these nanocomposites suggest that in spite of its relatively small surface area and its capacity to engage only in ion-dipole interactions with PE-g-PA, nanosilica provided a better balance of viscoelastic and mechanical properties when compared with onium-ion exchanged nanoclay.

Kim et al. (2004) studied the synthesis and material properties of syndiotactic polystyrene/organophilic clay nanocomposites. Syndiotactic polystyrene (sPS)/organophilic clay nanocomposites were fabricated by direct-melt intercalation method. To overcome the thermal instability of organophilic clay at high-melt processing temperatures of sPS, organophilic clay modified by alkyl phosphonium was adopted, which is known to be thermally stable. The microstructures of nanocomposites were confirmed by XRD and TEM. The crystallization rate of nanocomposites investigated by DSC does not increase despite the presence of clay, which was suggested by the authors to be a result of physical hindrance of organic modifiers in the clay dispersion. Nanocomposites exhibited enhanced mechanical properties such as strength and stiffness relative to the virgin polymer. In addition, thermal stability was confirmed to be improved by TGA.

Gopakumar et al. (2002) investigated the influence of clay exfoliation on the physical properties of nanoclay/polyethylene composites. Melt compounding was used to prepare

conventional composites of Montmorillonite clay and PE as well as nanocomposites of exfoliated nanoclay platelets dispersed in a maleated polyethylene (PE-g-MAn) matrix. The extent of clay platelet exfoliation in the PE-g-MAn nanocomposites was confirmed by XRD and resulted in a significant reduction of the degree of crystallinity and increased polymer crystallization rates. Studies of non-isothermal crystallization kinetics suggested that the exfoliated clay promotes heterogeneous nucleation and two-dimensional crystallite growth. PE/clay composites behaved in a similar manner as conventional macro composites, exhibiting modest increases in their rheological properties and Young's modulus. Conversely, the nanoscale dimensions of the dispersed clay platelets in the nanocomposites led to significantly increased viscous and elastic properties and improved stiffness. This was attributed to the high surface area between the polymer matrix and the exfoliated clay, which resulted in enhanced phase adhesion.

Wu et al. (2004b) investigated the effects of characteristics of rubber, mixing and vulcanization on the structure and properties of rubber/clay nanocomposites by melt blending. Three rubber-based nanocomposites, natural rubber (NR), SBR and ethylenepropylene-diene rubber (EPDM) matrices, were prepared with octadecylamine modified fluorohectorite (OC) by melt blending. XRD revealed that the SBR/OC and EPDM/OC nanocomposites exhibited a well-ordered intercalated structure and a disordered intercalated structure, respectively. In the case of the NR/OC nanocomposite, it exhibited an intermediate intercalated and even exfoliated structure. These results were in good agreement with TEM observations.

Furthermore, in the NR/OC and SBR/OC systems, the mixing process was suggested to play a predominant role in the formation of nanometer-scale dispersion structure, whereas the intercalated structure of EPDM/OC formed mainly during the vulcanization process. The tensile strength of SBR/OC and EPDM/OC nanocomposites loading 10 phr OC was observed to be 4–5 times higher than the value obtained for the corresponding pure rubber vulcanizate. The authors suggest that the slippage of the rubber molecules and the orientation of the intercalated OC is likely the reason for the enhancement of tensile strength. For the strain-induced crystallization, the exfoliated OC improved the modulus of the NR/OC nanocomposite relative to the pure NR. However, the decrease in tensile strength of NR/OC was believed to be a consequence of hindrance of strain hardening on NR crystallization during the tensile process.

Ramanathan et al. (2005) produced polymer nanocomposites of poly- (methyl methacrylate) (PMMA) and amide-functionalized single walled carbon nanotubes (SWNTs). They demonstrated that even at very low loadings, 1 wt % (0.5 vol %), the mechanical and electrical properties were significantly improved. The improvement over PMMA properties exceeds the theoretical bounds for composites with the same volume fraction loading of randomly oriented, straight, individually dispersed nanotubes. There experimental results thus suggested that the nanotube bundles were well dispersed in the polymer matrix, that the functionalization significantly improves interaction with polymer, and that the interphase formed has improved mechanical properties over that of the matrix material. Loss modulus results indicate a significant difference between functionalized and non-functionalized tubes in the composite. Functionalized tubes

resulted in a composite in which relaxation mechanisms were shifted by 30°C from that of the matrix material, indicating extensive interphase regions and absence of PMMA with bulk properties. Unfunctionalized composites demonstrated a broadening of relaxation modes, but still retain the signature of bulk PMMA properties. These data suggest a morphological difference with a discrete interphase layer in unfunctionalized composites and a fully transformed matrix in the case of functionalization. This difference is consistent with electrical and mechanical property data.

Buffa et al. (2005) functionalized Single wall Carbon nanotube with 4-hydroxymethylaniline (HMA) via the diazonium salt. Thermal analysis indicated 1 out of every 33 C atoms remained functionalized. Raman, FTIR, and optical absorption spectroscopy confirmed the side-wall functionalization and show that it can be reversed by thermolysis. The OH group that was generated from the functionalization could be used to start the ring-opening polymerization of ϵ -caprolactone. The polymer produced remained grafted to the nanotube and was demonstrated by FTIR.

Bellayer et al. (2005) produced multiwalled carbon nanotubes (MWNT)/polystyrene nanocomposites via melt extrusion. They used trialkylimidazolium tetrafluoroborate-compatible MWNTs that were well dispersed in the matrix. They used DSC, X-ray diffraction to show st-cation, nanotube-imidazolium interaction and the conversion from an interdigitated bilayer, for the imidazolium salt, to an ordered lamellar structure, for the imidazolium on the surface of the MWNTs.

Al-Ostaz et al. (2007) used molecular dynamic simulation to study single-wall carbon nanotube (SWCNT) embedded in polyethylene matrix. They also compared the elastic properties of bundles with 7, 9, and 19 SWCNTs. The results they obtained were in good agreement with experimental data. They found out that interface is an important constituent of CNT-PE composites. They were able to model it with reasonable success.

Kanagaraj et al. (2007) produced CNT/ high density polyethylene (HDPE) nanocomposites. The nanocomposites were produced by injection molding of high density polyethylene (HDPE) reinforced with specific volume fraction of CNTs. CNT-HDPE composites showed a good enhancement of mechanical properties with an increase of CNT concentration, even though it is not very significant. Halpin-Tsai model and modified series model give a close agreement to calculate Young's modulus of CNT-HDPE composites. The measure of reinforcement increases with an increase of CNT because of good load transfer effect and interface link between CNT and polymer.

Mierczynska et al. (2006) developed a method for preparation conductive composites of ultrahigh-molecular weight polyethylene with different carbon nanotubes (CNTs) as conductive fillers. The composites were prepared through the covering of the surface of polyethylene granules with CNTs and sintering under optimized conditions. They investigated electrical and mechanical properties of the composites as functions of the CNT concentration and CNT dispersion process for several kinds of single-walled carbon nanotubes (SWCNTs) and multiwalled carbon nanotubes (MWCNTs). The CNTs were not uniformly dispersed in the composites but were prelocalized on the granule boundaries, very efficiently forming conductive networks. It was, however, critically

important to ensure the good dispersion of the nanotubes in the microscale, and this was performed by sonication in solvents before dry mixing. The mechanical properties of the composites were also strongly modified by the presence of CNTs. The modulus and ultimate strength increased by about 100% with 2% CNTs. The elongation at break decreased but was still about 500–1000%. Near the electrical percolation threshold, the mechanical properties were not significantly modified.

Kuan et al. (2007) developed a novel method to prepare the carbon nanotube (MWCNT)/linear low density polyethylene (LLDPE) composite. The method is a combination of free radical reaction and water-crosslinking reaction. The composite produced was characterized by Raman and FT-IR. Mechanical properties and thermal stability of the composite were significantly improved after silane modification and water-crosslinking reaction.

The above literature review shows that the focus of previous research is on nanoclays rather than CNT. In addition, the work on surface modification is very limited. Further, the dispersion and orientation of the CNT in the polymer matrix is strongly affected by the polymer-CNT surface interactions, and this will have a direct correlation of the rheological and mechanical property of the nanocomposite. However, this issue was not studied thoroughly in the literature. Therefore, this study is expected to shed light on how the specific CNT characteristics such as aspect ratio and its surface properties will influence the final properties of nanocomposites. A detailed investigation of aspect ratio and surface modification of the CNT and its ultimate impact on the rheological and mechanical properties of s-CNT-PE nanocomposite was carried out.

CHAPTER THREE

OBJECTIVES

This research work done herewith will assess the possibility of improving the mechanical properties of local PE resins using CNT. CNT will be modified in the university laboratory as well as purchased from the market and would be used in combination with resins to develop new polymer nanocomposites that will add high value to the polyolefins produced in the Kingdom. Then, a detailed investigation of the impact of CNT addition on PE's properties will be carried out. This includes rheological testing, mechanical properties, and thermal properties. Specific attention will be given for the effect aspect ratio and surface modification of the CNT and its ultimate impact on the mechanical and rheological properties in s-CNT-PE nanocomposites.

This research proposal has the following detailed objectives:

1. Determine the impact of CNT loading that leads to enhanced mechanical and melt properties using SEM analysis and rheological testing.
2. Specify the melt conditions of temperature and shear that leads to enhanced mechanical properties of the CNT-PE nanocomposites.
3. Modify the CNT surface to improve their dispersion in the PE matrix and see its effect of the overall mechanical properties of CNT-PE nanocomposite.
4. Incorporate suitable compatibilizer to improve the interfacial interaction between CNT and the PE matrix, ultimately enhancing the mechanical properties.

The results of this research are expected to develop local expertise in surface modification and polymer nanocomposites.

CHAPTER FOUR

RESULTS & DISCUSSION

4.1. Impact of Aspect ratio and Chemical modification of Carbon Nanotubes on the shear and extensional Rheology of Polyethylene Nanocomposites.

4.1.1. Abstract

In this paper, the effect of aspect ratio and chemical modification of multiwall carbon nanotubes (MWCNT) on the rheological behavior of low density polyethylene (LDPE) nanocomposites were studied. Fifteen different samples were prepared by melt blending using different MWCNT to study both effects. Agglomerations were observed in the produced nanocomposite as shown by FE-SEM. The shear rheology suggested no network formation was present in nanocomposites with low or high aspect ratio CNTs. Both dynamic (η') and steady shear viscosities (η) increased with increased CNT and aspect ratio. However, at low loadings of up to 1 wt% and for CNT with high aspect ratio η' , η , and G' for the nanocomposites were below the corresponding values for the matrix. The Cox-Merz rule did not hold for the different nanocomposites. No negative normal forces were observed for CNT loadings up to 5 wt% and aspect ratio of 375. Results of extensional viscosity show that nanocomposites with high aspect ratio (LCNT) exhibit the highest strain hardening followed by chemically modified CNT (MCNT) and then short CNT (SCNT). For all types of nanocomposites, the time of break decreases with the increase in aspect ratio and henky rate. The value of critical extensional stress increased

with the increase in loading and henky rate for both LCNT and MCNT. Different rheological properties such as η' , η , G' and N_1 agree that CNTs with high aspect ratio can lead to viscous and elastic properties of nanocomposites that are lower than the matrix. MWCNT are suggested to play a role of plasticizer as well as filler depending on their aspect ratio and loading.

4.1.2. Introduction

Since 1991 [1], the nano-science has revolutionized the landscape of modern scientific research and technology development. It has been observed time and again that nano reinforcement of engineering material can cause dramatic structural (e.g., stiffness) and physical property benefits without adding significant weight [2]. For example, nano layered reinforcement can induce greater thermal stability [3-4]. It is believed that the dispersion and orientation of the CNT in the polymer matrix is strongly affected by the polymer-CNT surface interactions, and hence the ultimate properties of the nano-composite. However, it is also observed that a lot of effort and research has been diverted towards improvement of mechanical, thermal and conductive properties, plus improvement of the dispersion of nano materials. The dispersion of nanomatierals has a major impact on the rheological properties of nanocomposites and hence their processing.

Generally, the dynamic shear rheology of polymer melts depends strongly on the temperature and frequency at which the measurement is carried out. In the case of unstructured polymer melts, it is expected that polymers exhibit characteristic of homopolymer-like terminal flow behavior, expressed by the power-laws $G' \sim \omega^2$ and $G'' \sim \omega$ at high temperatures/low frequencies. For polymer nanocomposites, even if the

nanomaterial is not carbon nanotubes (CNTs), such a behavior changes from liquid-like to solid-like ($G' \gg G''$) with increasing nanomaterial content [5-8]. Galgali et al. [5] showed that zero-shear viscosity of the compatibilized nanocomposites with more than 3 wt % nanoclay was at least 3 orders of magnitude higher than that of matrix resin and the uncompatibilized hybrids. Lim and Park [6] showed that storage and loss moduli increased with nanomaterial loading at all frequencies and showed non-terminal behavior at low frequencies. Wu et al. [8] investigated the rheology of nanocomposites of poly(vinyl chloride) and nanometric calcium carbonate particles. The evaluation revealed a remarkable increase in the melt viscosity with the addition of nanomaterial. However, the viscosity decreased at high shear rates. This drop in viscosity for nanocomposite at high shear rate has been reported in other literature as well [9-10]. Krishnamoorti et al [10] attributed, this drop in viscosity at high shear rates and becoming almost equal to unfilled polymer, to layered silicates being oriented in the flow direction and resulting in minimum contribution to viscosity at high shear rates.

In contrast to pure polymers, intercalated nanocomposites exhibit strong time dependent behavior [11-13]. With increasing shear rates, the shear-viscosity attains a plateau after a certain time, and the time required to attain this plateau decreases with increasing shear rates. Polymer nanocomposites show a very strong shear-thinning behavior at high shear rates. Ren and Krishnamoorti [14] reported strong shear thinning behavior of the nanocomposites thought to have resulted from orientation of the layers in response to the applied shear deformation. The empirical Cox-Merz rule was found to be inapplicable for such nanocomposites and that steady and dynamic oscillatory flow are not equivalent for

such materials. Carbon nanofibers (CNFs) have also been used with polymers as well [15-17]. Lozano et al. studied rheological properties of CNF / polymer nanocomposite. They used PE [16] and PP [17]. In both studies they used upto 30 wt% loading. Viscosity and storage modulus enhancement with increased CNF loading was reported. Shear thinning behavior at higher frequencies was also observed, more prominent at high CNF loadings.

Apart from nanoclay and CNFs, CNTs were used with polymer matrix [18-22]. Lee et al [18] used chemically functionalized MWCNTs and PP was used as matrix. Complex viscosity, η^* , was found to reduce with increasing frequency in dynamic shear tests. Storage modulus increased with increasing frequency. Similar trend for η^* was observed by Potschke et al. [19] with MWCNT / polycarbonate composite. However, concentrations above 2 wt% of MWCNT in the matrix tend to show a plateau behavior at low frequency. Moniruzzaman et al [20] discuss a detailed review of polymer nanocomposite containing carbon nanotubes.

A typical behavior of a polyolefin/MWCNT nanocomposite is detailed in the work by McNally et al [24]. MWCNTs composites with weight fractions that ranged from 0.1 to 10% were prepared by melt blending in a mini-twin screw extruder. It was observed that η^* increases with the increase of the concentration of MWCNT. The magnitude of increase is more pronounced at low ω . However, η^* decreases with increasing ω for all nanocomposites and pure PE. It was also observed that G' for the nanocomposites show a monotonic increase with increasing MWCNT content at all ω . The G' versus ω curve for nanocomposites with 8.5 and 10 wt% MWCNTs approached a plateau at lower ω . This

low ω response is indicative of 'pseudo-solid-like' behavior, and has been seen for a conventionally filled polymer with strong interactions between filler and polymer.

Kharchenko et al [25] reported a peculiar behavior for MWCNT/PP nanocomposite. Negative normal stresses were observed, which until their work were only sometimes seen in liquid crystalline polymers. The aspect ratio of their CNT was in the range 300-400. Xu et al [26] studied the normal stresses and used CNT with aspect ratio in the range of 22-45, but did not observe any negative normal forces. On the other hand, Kim et al. [27] studied extensional viscosity of CNT/epoxy composites. The produced composites showed strong strain hardening behavior. Extensional viscosity increased with addition of CNTs that were modified with surface treatments. Authors attributed this increase in extensional viscosity to improved polymer/CNT interfacial bonding and better dispersion due to surface treatment. Lee et al. [18] also studied the elongational flow properties PP / MWCNT nanocomposite. It was observed that acid treated and heat treated MWCNT / PP nanocomposites show higher elongational viscosity than pure PP. Amine treated MWCNT / PP showed weak strain hardening. Also, MA-g-PP has negative effects on strain hardening due to low molecular weight.

In general, the literature on the shear and extensional rheology of polyolefin / CNT is limited. Literature on the rheology of modified CNT / polyolefin is even less. In our present study, the principal focus is to analyze the rheology of nanocomposites of MWCNT and LDPE. Melt blending was used to produce the nanocomposites. The effects of aspect ratio, chemical modification and loading of the MWCNTs on dynamic, steady

shear and extensional rheology are studied in detail. Film grade LDPE is used to assess the possibility of producing thinner and stronger films by adding CNTs.

4.1.3. Experimental

MWCNTs with different aspect ratios and surface modification were supplied by Cheap Tubes Inc, USA. All three types of MWNCTs used had outer diameter of 30-50 nm and inner diameter of 5-15 nm. Length for Long MWCNT (LCNT), Short MWCNT (SCNT) and COOH-MWCNT (MCNT) were 10-20 μm , 0.5-2.0 μm and 10-20 μm , respectively. Therefore, the aspect ratio (length / outer diameter) for LCNT, SCNT and MCNT was 375, 31 and 375, respectively. As stated by the producing company, COOH-MWCNT contains 0.7% -COOH groups. On the other hand, The LDPE was supplied by Nova Chemicals, Canada. It has a weight average molecular weight of 99.5 kg/mol and a MWD of 6.5 and a melt index of 0.75 g/10 min and a total short branch content of 22 branches/1000 C as determined by GPC and NMR, respectively [28]. The as received LDPE resin and MWCNT/LDPE nanocomposites were conditioned (or blended) in a Haake PolyDrive melt blender. The temperature used was 190°C at 50 rpm and time of blending was 10 minutes.

Melt blended samples were dipped in liquid nitrogen for approximately 5 minutes to render them brittle and then shattered to reveal the cryo-fractured surfaces. A thin layer of gold was evaporated on the exposed fracture surfaces to make them electrically conducting to avoid charge build-up during examination within SEM. Field emission scanning electron microscope (FE-SEM) Model FEI Nova Nano SEM 230 having a probe resolution of 1.0 nm (at 15 keV) and accelerating voltage range of 50 V to 30 keV

was used to observe the surface morphology of samples. Backscattered electron images were obtained using a low voltage high contrast detector.

Carver press was used to prepare samples for rheological testing. Measurements were carried out in an ARES constant strain rheometer. Dynamic shear tests were performed using cone and plate of 25 mm diameter, cone angle of 0.1 radians. The strain used was 15% in the linear viscoelastic range; temperature was 190°C and the frequency was varied from 100 rad/s to 0.01 rad/s. Steady shear testing was done using cone and plate setup. Tests were conducted in the range 0.05 s⁻¹ to 10 s⁻¹. The first normal stress difference, N₁, was obtained during a step-rate test followed by relaxation. For extensional rheology, SER Extensional viscosity fixture was used. Test temperature was 120°C. Sample dimension were length: 17-19 mm, width: 6.5-6.7 mm and thickness: 0.48-0.62 mm. Henky rates used were 0.5 s⁻¹, 1.0 s⁻¹ and 1.5 s⁻¹.

4.1.4. Results & Discussion

4.1.4.1. Morphology

FE-SEM images of LCNT-LDPE nanocomposites with 5.0% loading are shown in Figures 4.1.1.a-c. Agglomeration of the LCNT in the LDPE matrix was observed (Figure 4.1.1.a). Higher magnification image clearly shows that the agglomerated region is composed of MWCNTs (Figure 4.1.1.b). However, this agglomeration was not localized to a particular region, but was distributed in the LDPE matrix (Figure 4.1.1.c). Although, not shown here, but a similar trend was observed for SCNT and MCNT at various loadings.

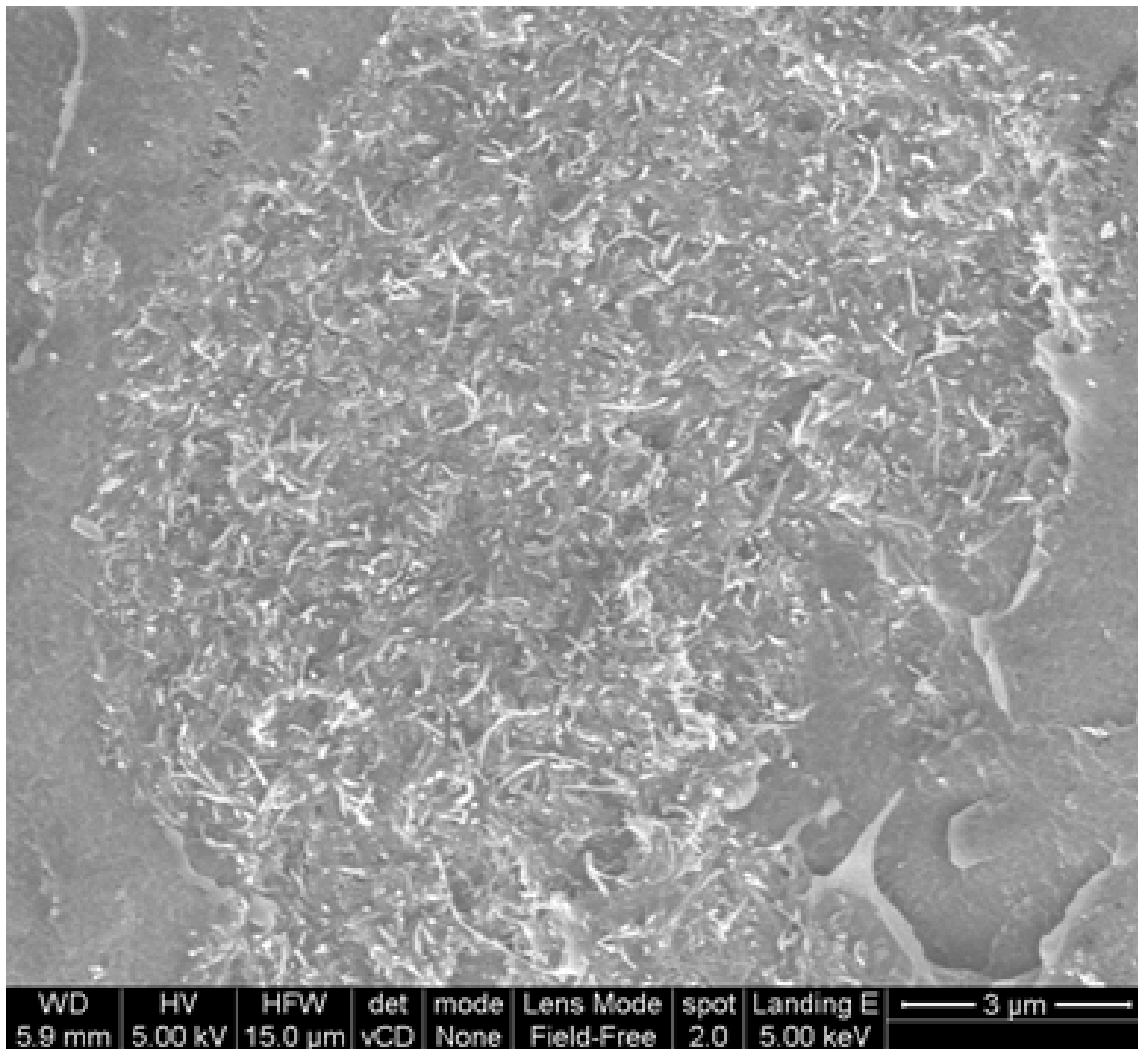


Figure 4.1.1.a. FE-SEM image of LCNT-LDPE nanocomposite with 5.0% loading.

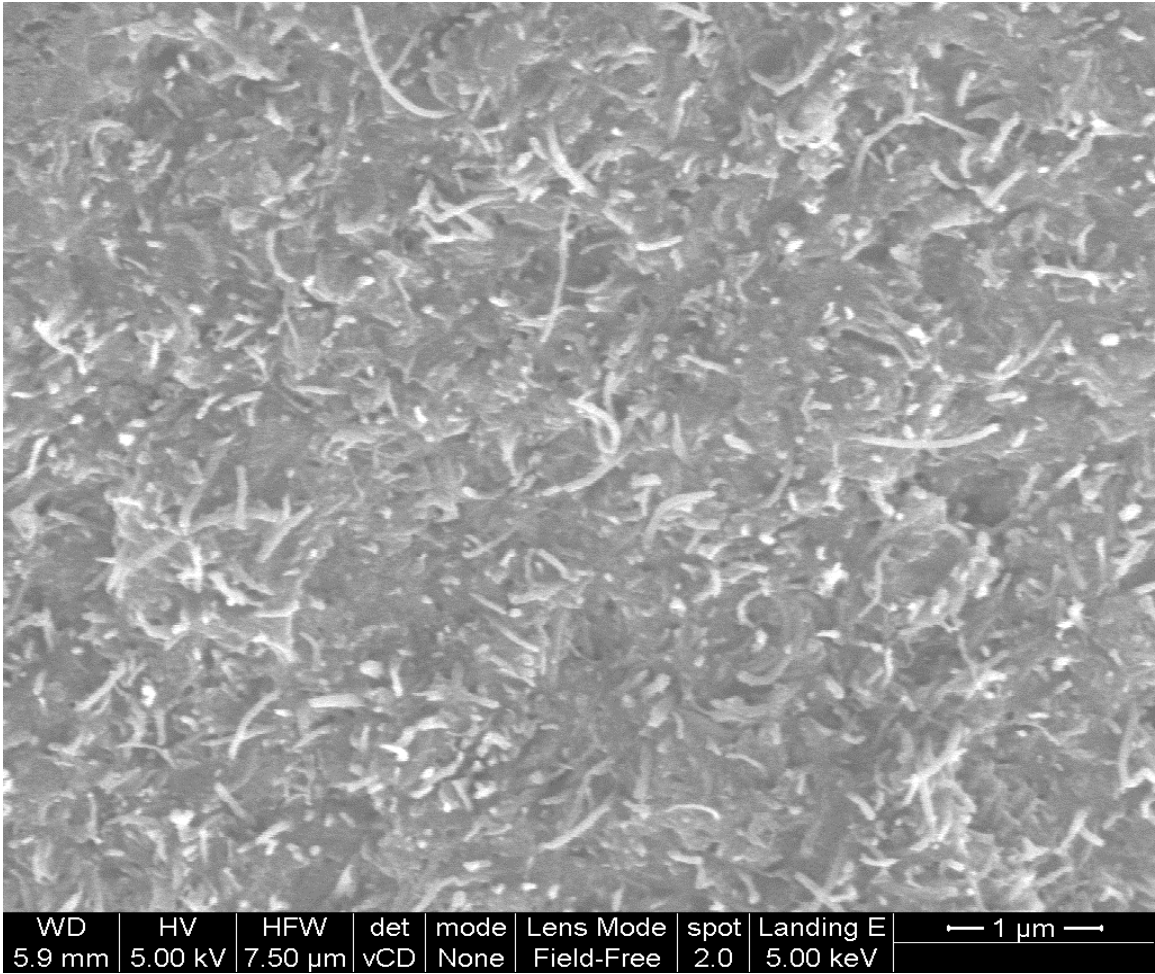


Figure 4.1.1.b. FE-SEM image of LCNT-LDPE nanocomposite with 5.0% loading.

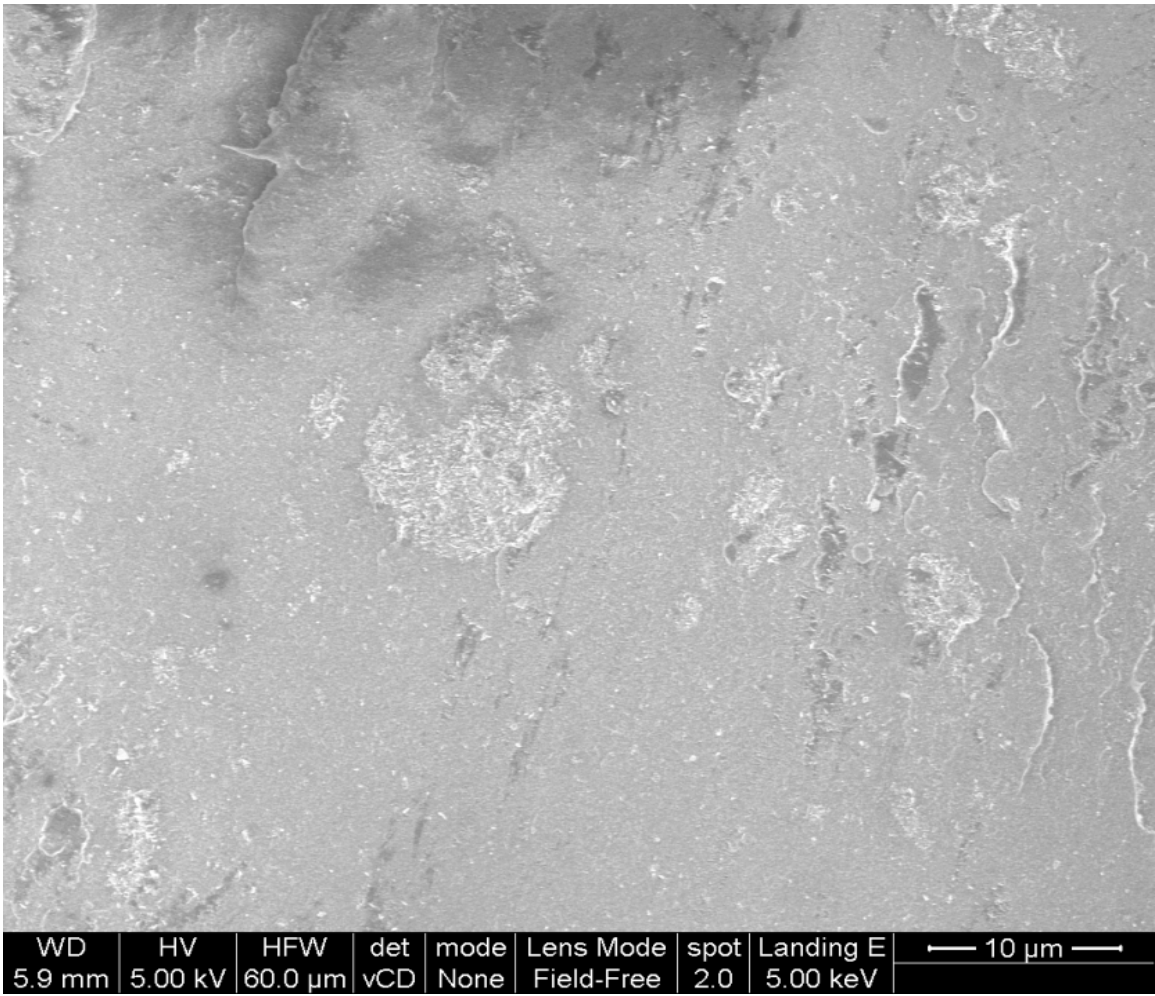


Figure 4.1.1.c. FE-SEM image of LCNT-LDPE nanocomposite with 5.0% loading.

Figures 4.1.2.a and b show the Cole-Cole plot for LCNT and SCNT composites with varying amounts of CNT. These plots are usually used to infer the degree of dispersion in the matrix of the bulk polymer [24, 29]. The LCNT loading (0.25 wt% - 5.0 wt%) does not seem to affect the degree of dispersion in the composite material. A similar trend was observed for MCNT composites. The results of FE-SEM and Cole-Cole plot suggest that various nanocomposites produced using the melt blending process have agglomeration. These agglomerations are distributed in the LDPE matrix. The degrees of dispersion for the produced nanocomposites are similar, irrespective of the aspect ratio, loading and chemical modification.

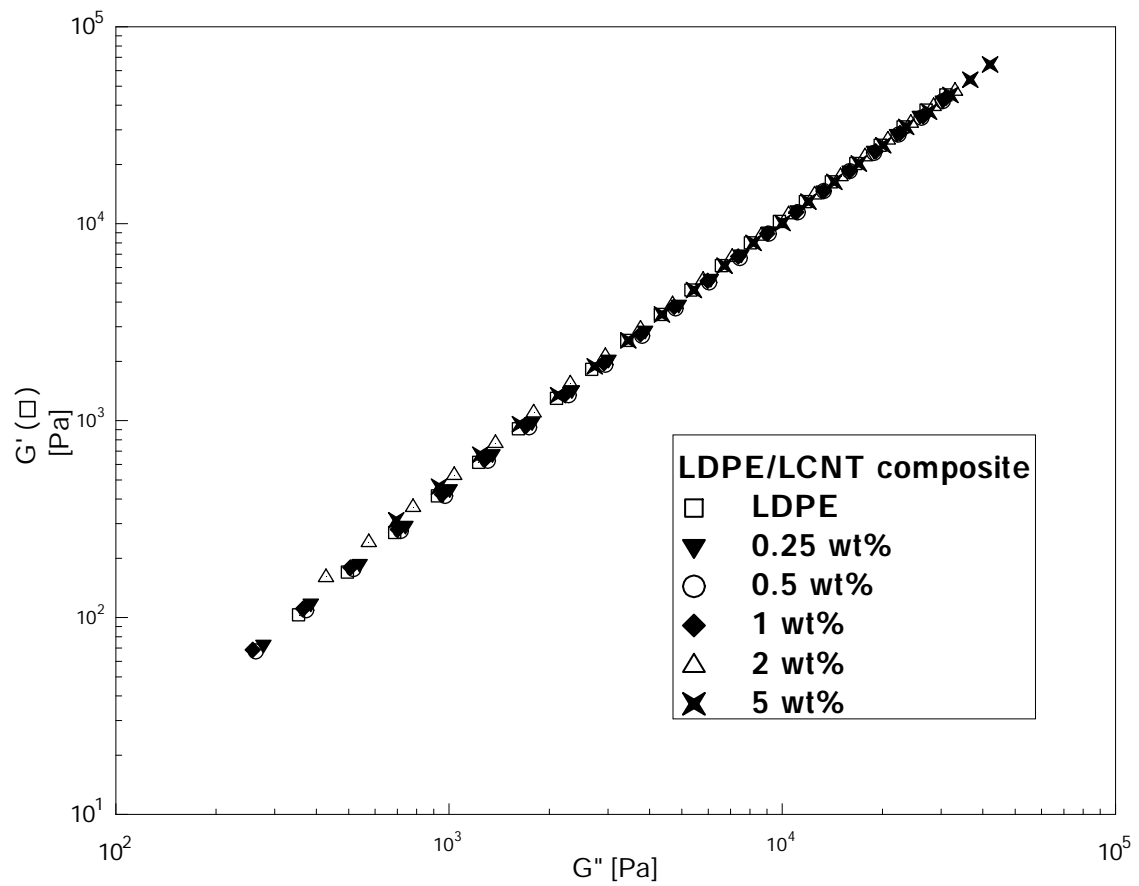


Figure 4.1.2.a. Cole Cole plot of LCNT / LDPE.

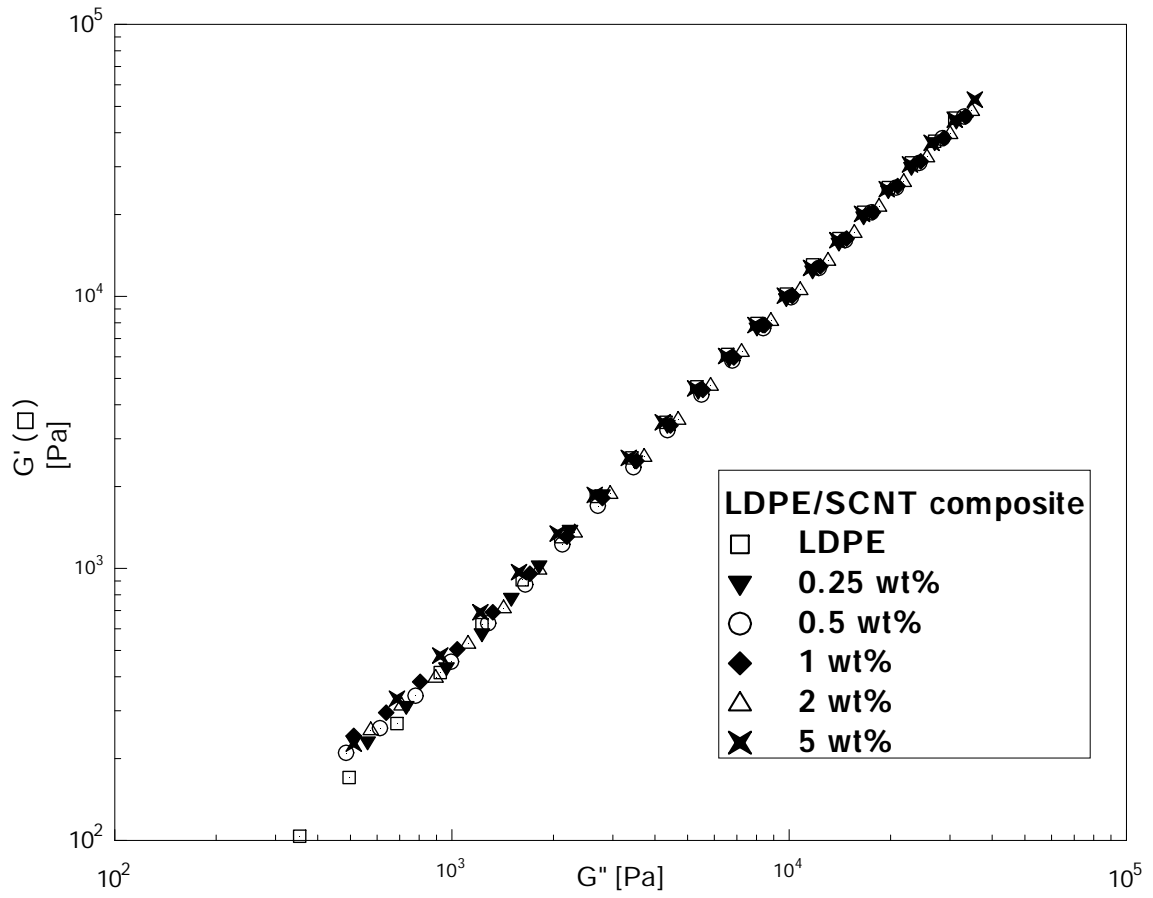


Figure 4.1.2.b. Cole Cole plot of SCNT / LDPE.

4.1.4.2. Impact of Aspect ratio and MWNCT loading on viscous properties

In this section, we will focus on the viscosity obtained from dynamic and steady shear measurements. Figure 4.1.3.a displays the dynamic viscosity (η') vs frequency (ω) for LCNT/LDPE nanocomposites. The first observation is that η' increases with the increase of the amount of LCNT. This is more prominent at lower ω (10^{-2} rad/s). This observation is in agreement with previous literature reports [24, 30-32]. But it is interesting to note that at low concentrations of LCNT, of ~ 0.25 to 1.0%, η' for the nanocomposite was lower than that of the matrix, again this is more prominent at low ω (10^{-2} rad/s). Previous work of McNally et al. [24] observed significant increase in η' only at MWCNT loading higher than 2%. In addition, we observe a general shear thinning effect with increasing ω , this is true for all the loadings covered in this study, and hence no plateau was observed in the frequency range 0.01-100 rad/s.

η' vs ω for the nanocomposites of MCNT and LDPE are shown in Figure 4.1.3.b. Also, as the amount of loading is increased then η' increases. But what is important here is that at low loadings of MCNT (0.25-1.0 wt%), η' is lower than that of pure LDPE. This initial drop in η' has been observed before by many authors [33-35]. Qinghua et al [33] produced nanocomposites of UHMWPE (Ultra high molecular weight polyethylene) and SWNT (single walled carbon nanotubes). They observed an initial drop in η' up to 0.25% of SWNT loading. Jain et al. [34] also reported a decrease in viscosity when silica nanoparticles were used as filler, whereas Mackey et al. [35] observed a similar drop in viscosity using polystyrene filled with cross-linked polystyrenes. In nanocomposites filled with silica, the explanation provided for the drop in viscosity was the selective

physicoadsorption of polymer chains onto the surface of nanoparticles. When the CNT content was increased beyond 0.2 wt %, the nanotube network was formed. Even though our results are in agreement with their findings [33-35]; however, our interpretation is different. We suggest that at low loadings the MWCNT acts as plasticizer, while at loadings above 1.0 wt%, they act as filler. The plasticizer usually increases chain mobility and the free volume; hence it increases the fluidity of the nanocomposite. This increase in the fluidity of the nanocomposite can explain the observed decrease in viscosity.

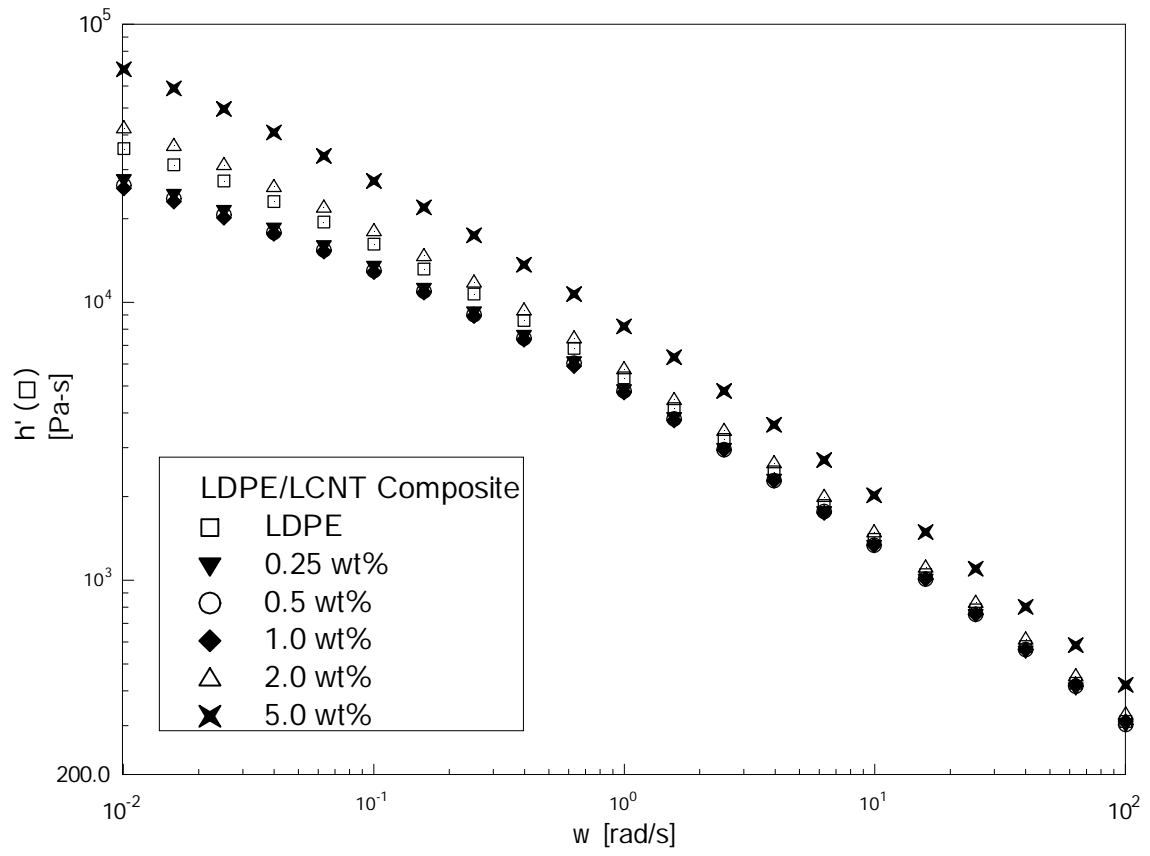


Figure 4.1.3.a. Dynamic viscosity versus frequency plots for LCNT/LDPE nanocomposites.

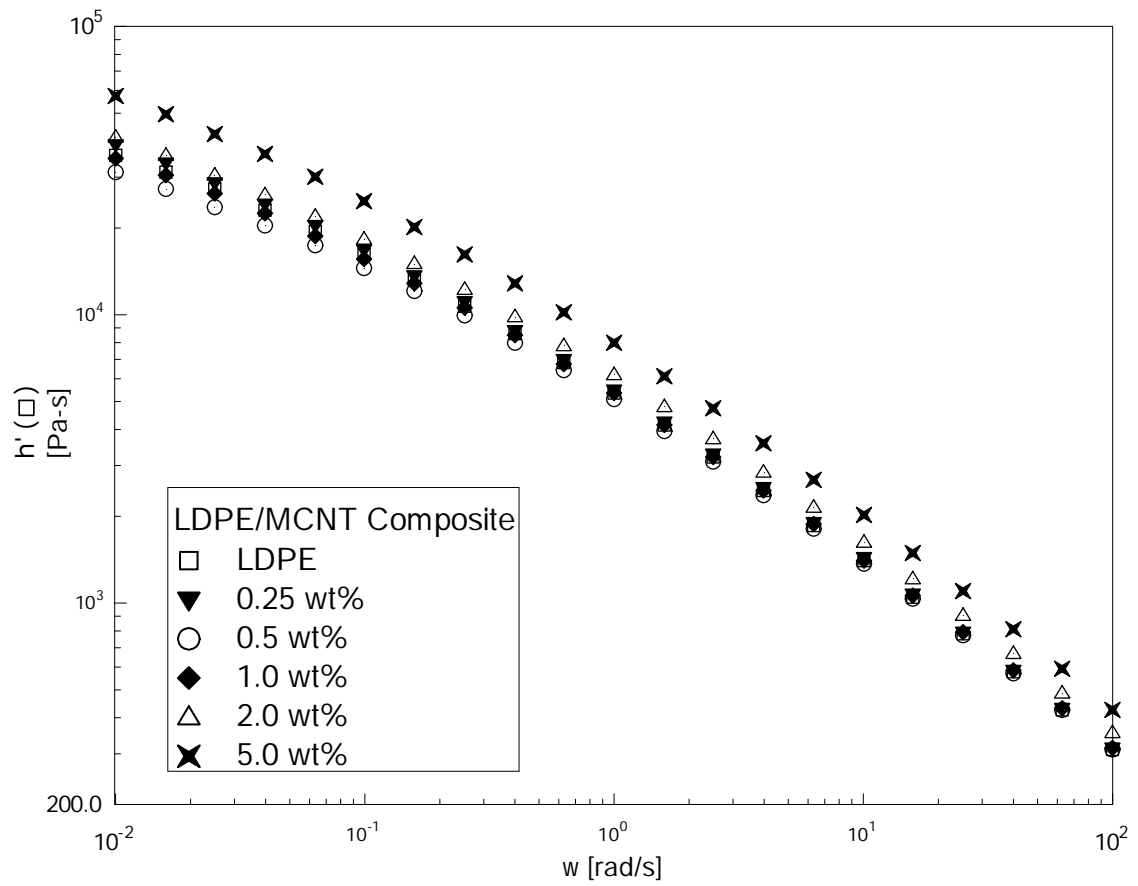


Figure 4.1.3.b. Dynamic viscosity versus frequency plots for MCNT/LDPE nanocomposites.

Figure 4.1.3.c shows η' vs ω for nanocomposites of SCNT with LDPE. Though the trend is similar to that of LCNT & MCNT the increase in η' is not as prominent as for MCNT and LCNT. Here, it is worth noting that SCNT has a lower aspect ratio compared to MCNT and LCNT. Also, at lower loadings of 0.25 and 0.5%, the η' is higher than pure LDPE. It should be noted that SCNT has lower aspect ratio as compared to LCNT and MCNT. It is likely that the decrease in η' of nanocomposites below that of the matrix takes place at values lower than 0.25 wt% due to low aspect ratio of SCNT. So, the role of MWCNT as plasticizer is strongly influenced by its aspect ratio.

Figure 4.1.3.d shows the η' vs ω for MWCNT /LDPE nanocomposite. At low ω and at 5 wt% MWCNT loading, LCNT is showing the highest η' , followed by MCNT, while SCNT is showing the lowest values of η' . Surface modification is suggested to be the reason for the slight reduction of η' since LCNT and MCNT have the same aspect ratio. Furthermore, SCNT has a lower aspect ratio, which tends to reduce η' , especially at low ω . For all the MWCNT nanocomposites and with MWCNT loadings of 0.25-2.0 wt% the power law index was in the range 0.36-0.38. At 5.0 wt% loading, the index is in the range 0.33-0.34 while that of pure polymer is 0.35. Therefore, the power law index or shear thinning is not a strong function of CNT loading.

Plots of phase angle (δ) versus ω are used to expose the transitions of the nanocomposites from liquid-like to solid-like behavior. $\tan(\delta)$ is highest at low ω and decreases with increasing ω . $\tan(\delta)$ becomes independent of ω once interconnected network is formed [29]. For nanocomposites of LDPE/LCNT (Figure 4.1.3.e) we observe a decrease in $\tan(\delta)$ with increasing ω . None of the loadings show network formation behavior since \tan

$(\delta) > 1$ even at ω as high as 10, which suggests the dominance of liquid-like behavior. A similar result was obtained for LDPE/MCNT & LDPE/SCNT nanocomposites. It can be concluded from the above discussion that no network was formed at low or high aspect ratio of the MWCNTs used in this study. Also, at high aspect ratio, MWCNT with low loadings act as plasticizer in the matrix and MWCNT loadings and above 1.0% MWCNT plays the role of fillers.

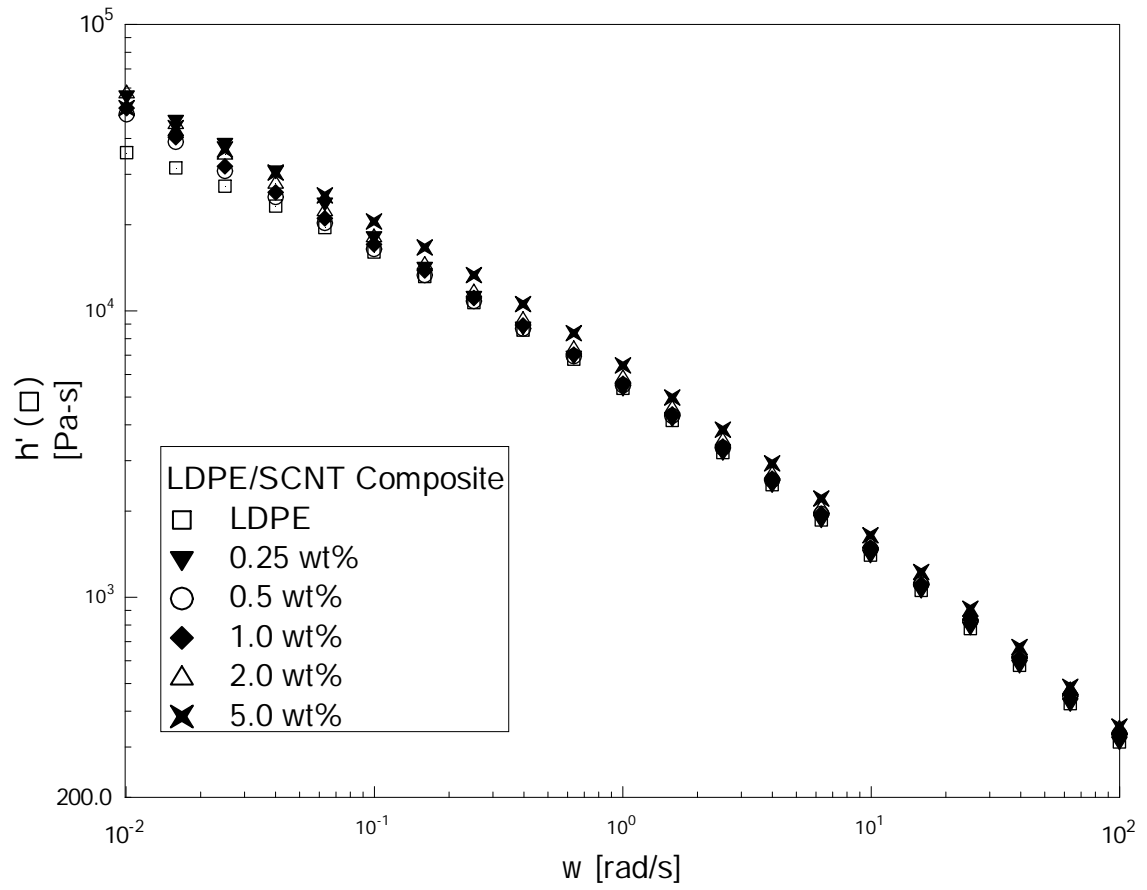


Figure 4.1.3.c. Dynamic viscosity versus frequency plots for SCNT/LDPE nanocomposites.

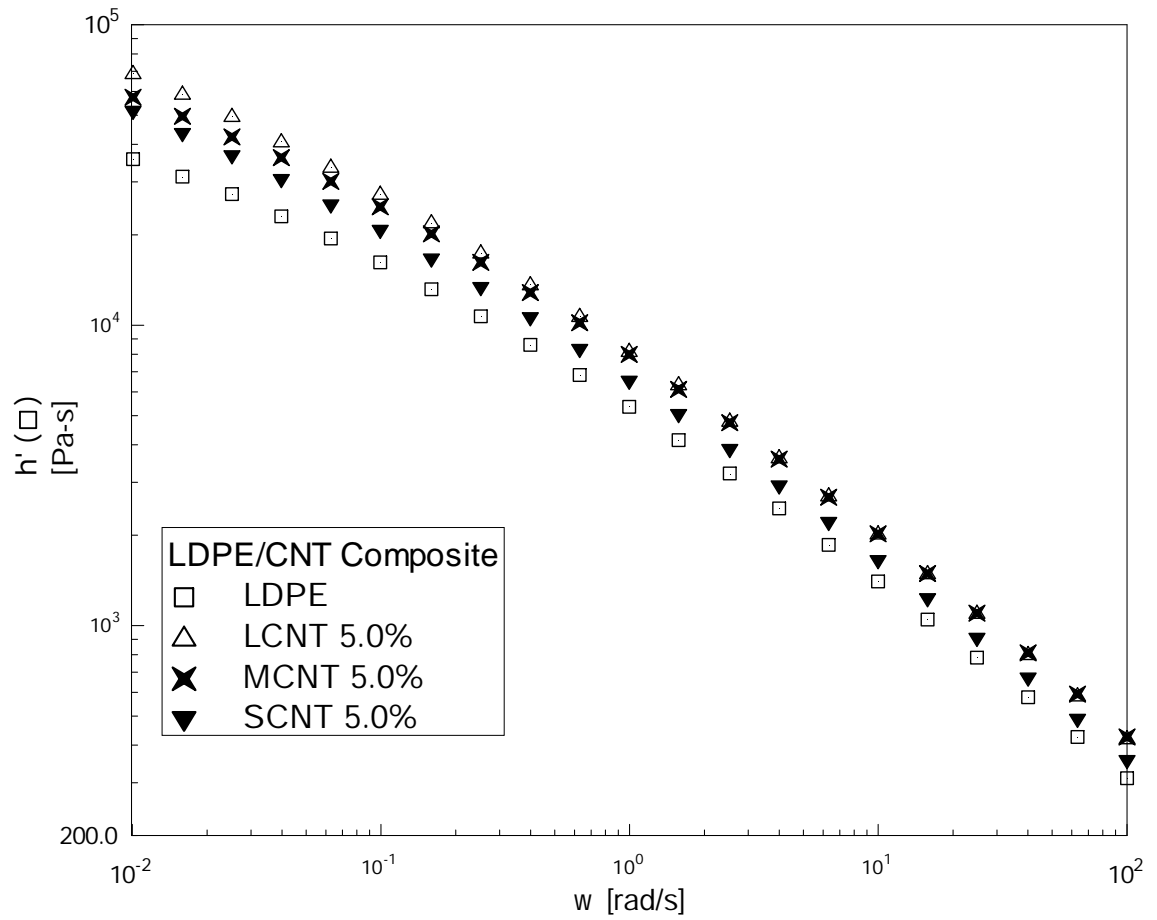


Figure 4.1.3.d. Dynamic viscosity versus frequency plots for various MWCNT/LDPE nanocomposites with 5.0% loading.

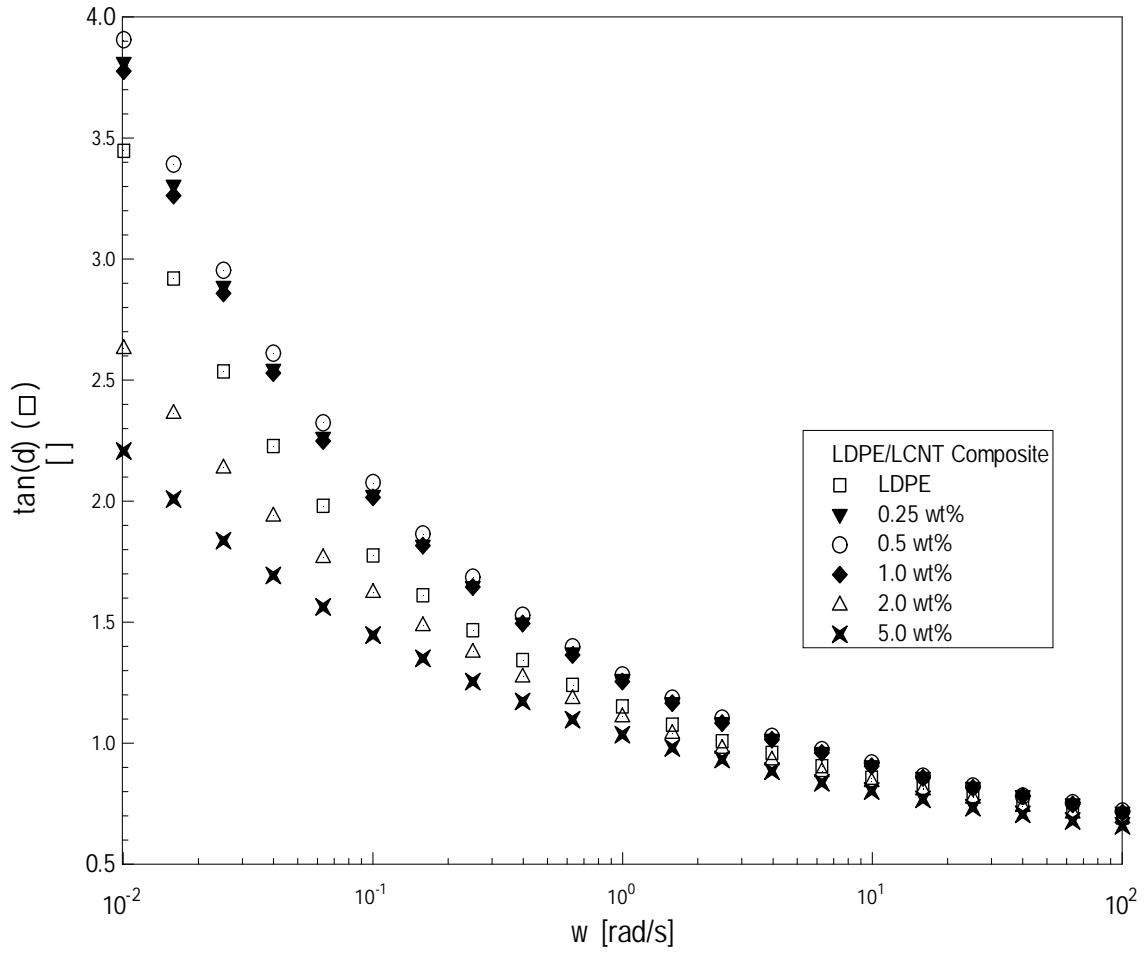


Figure 4.1.3.e. Tan (δ) versus frequency plots for LCNT/LDPE nanocomposites at various loadings.

Further, steady shear measurements were performed. Results of steady shear viscosity (η) vs shear rate ($\dot{\gamma}$) are given in Figures 4.1.4.(a-d). The behavior of η is very similar to that of η' , it increases with the increase of the amount of MWCNT. However, at low MWCNT loadings the viscosity drop at low $\dot{\gamma}$ is not just for LCNT and MCNT but also for SCNT nanocomposites. Our explanation for the drop in η at low CNT loading is discussed earlier for η' . As $\dot{\gamma}$ is increased the nanocomposites show shear thinning behavior, also seen for pure LDPE. High shear leads to disentanglement and orientation of the chains. This would decrease local frictions hence facilitates the movement in the direction of flow [38]. The shear thinning behavior is observed at all loadings. This behavior is similar to that of reinforced polymers or layered polymer blends which show drop in viscosity with increasing shear rate [36-38]. It was also noticed that Cox-Merz rule that generally holds for homopolymers, did not hold for the different nanocomposites. A similar result was reported for polymer / clay nanocomposites [9, 39].

It can be concluded that η' and η increase with increased loading of MWCNT for low and high aspect ratio CNT. No network was formed for three types of MWCNT nanocomposites at loadings up to 5.0 wt%. At high aspect ratio, a plasticization effect of MWCNT was observed both in η' , η measurements up to 1.0 wt% loading. Loadings above 2.0 wt% increase η' and η above pure LDPE, more pronounced at low ω and $\dot{\gamma}$, respectively. Increasing ω and $\dot{\gamma}$ shows shear thinning in both η' and η for low and high aspect ratio MWCNT and at all loadings. Cox-Merz rule did not hold for the produced nanocomposites.

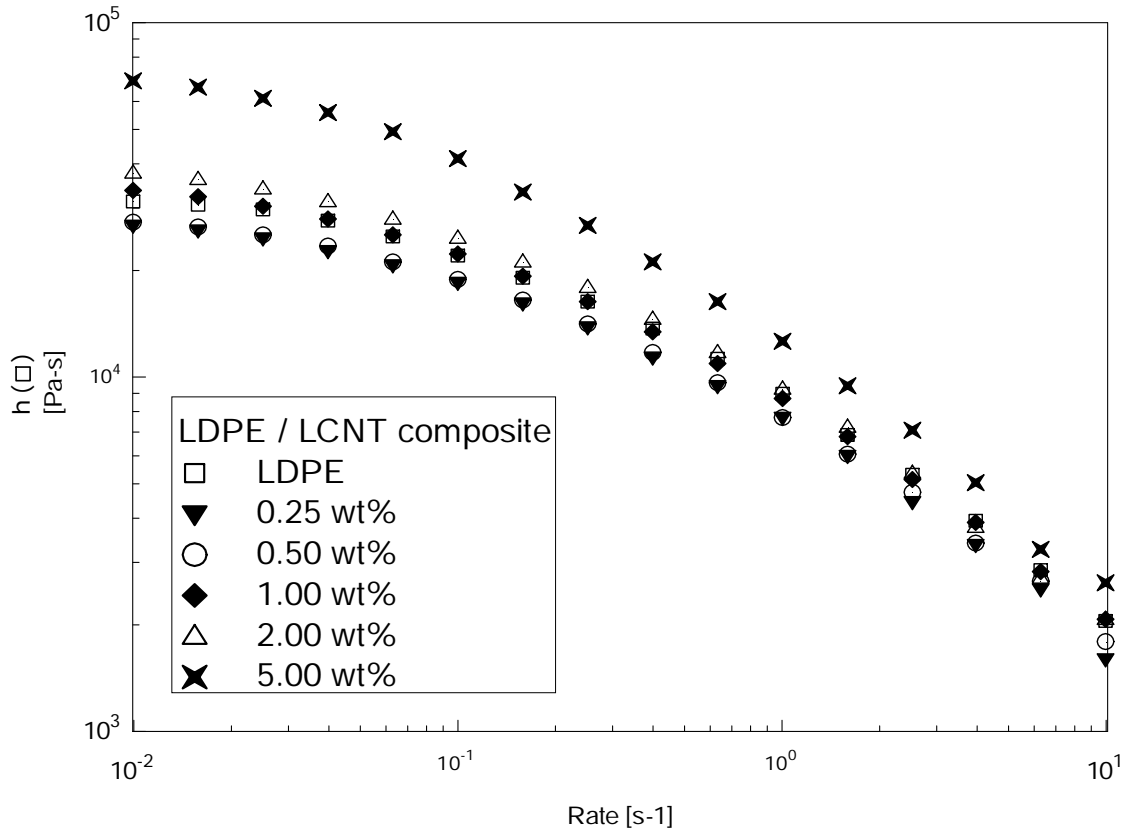


Figure 4.1.4.a. Steady shear viscosity vs shear rate for LCNT / LDPE.

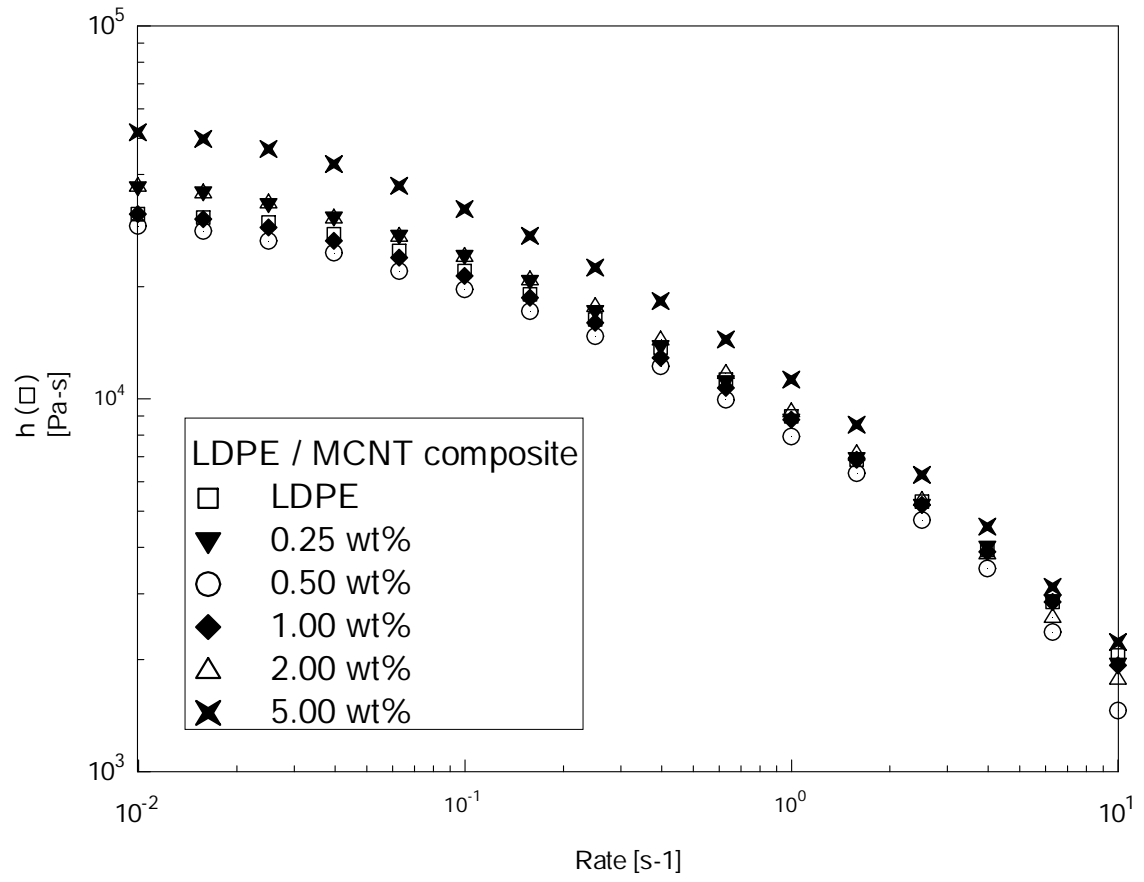


Figure 4.1.4.b. Steady shear viscosity vs shear rate for MCNT / LDPE.

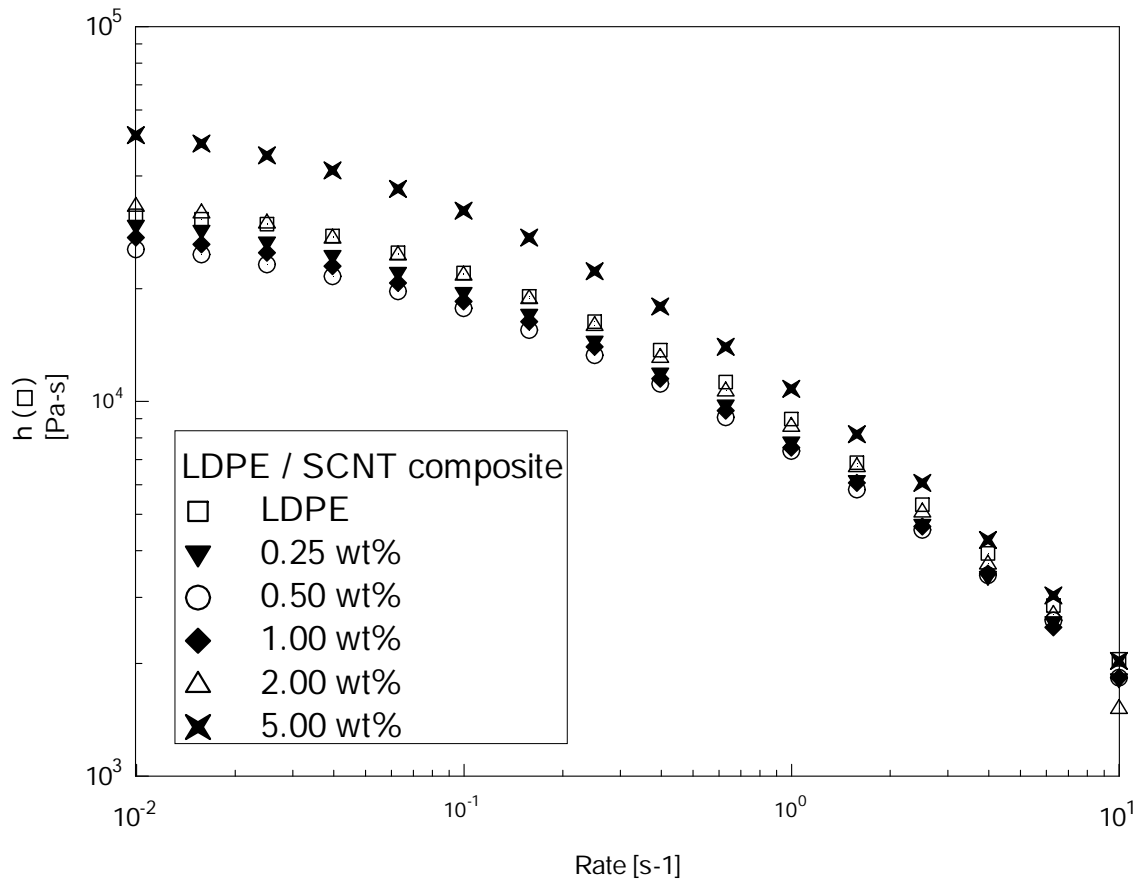


Figure 4.1.4.c. Steady shear viscosity vs shear rate for SCNT / LDPE.

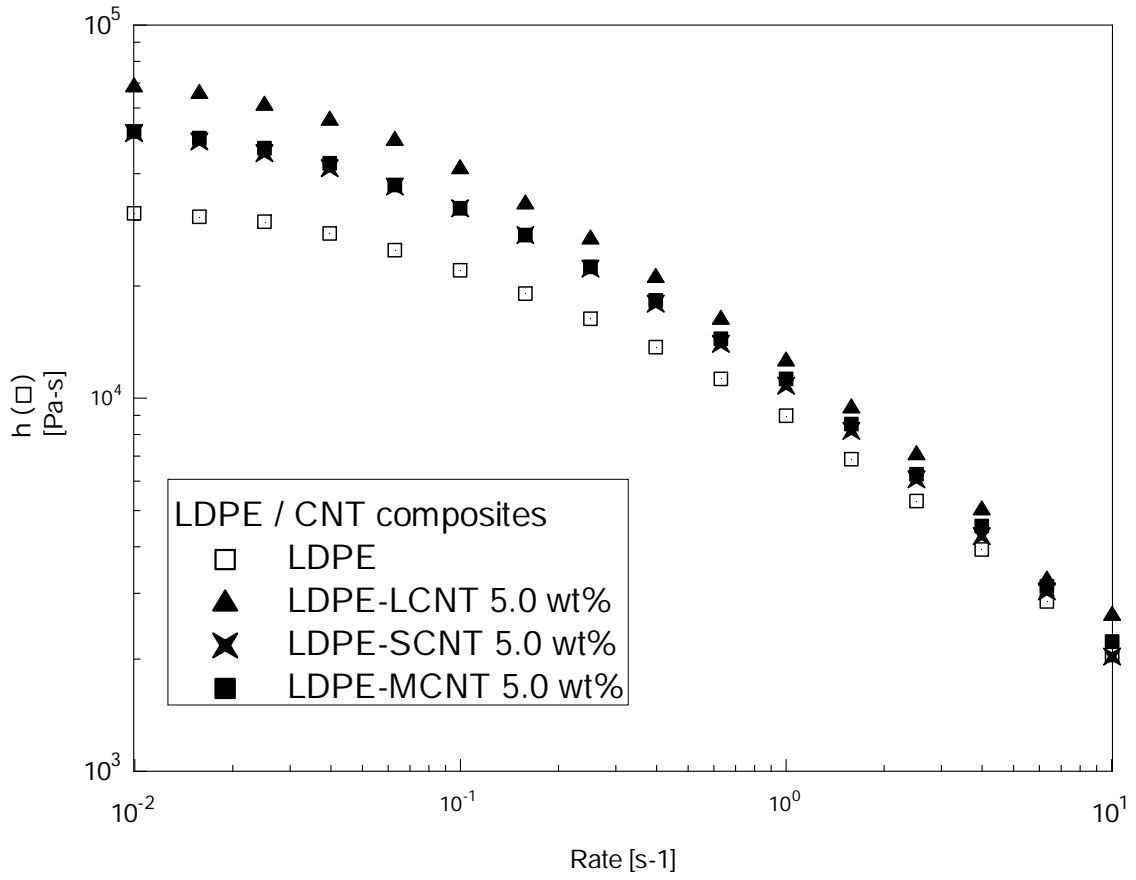


Figure 4.1.4.d. Steady shear viscosity vs shear rate for various LDPE nanocomposites at 5.0% loading.

4.1.4.3. Impact of Aspect ratio and loading on Elastic properties

Results for storage modulus (G') versus frequency (ω) for LCNT/LDPE composites are displayed in Figure 4.1.5.a. We observe that for MWCNT loadings of 2 and 5%, the G' increases with increasing loading at a fixed ω , more prominent at low ω . However, at lower MWCNT loadings of 0.25 -1.0 wt% G' for nanocomposites was lower than that of the matrix. At higher ω the differences tend to reduce significantly, a trend that was observed by other researchers too [24]. Also, McNally et al [24] observed a plateau at low frequencies for MWCNT loadings higher than 8.5%. No such plateau was observed in our different nanocomposites upto 5.0 wt% MWCNT loading. This observation again points toward our previous suggestion that there is no network formation for the nanocomposites covered in this study.

Figure 4.1.5.b shows G' versus ω plot for MCNT/LDPE composites. Their behavior is similar to that of LCNT / LDPE nanocomposite since the aspect ratio for both is the same. Figure 4.1.5.c shows the G' versus ω plot for SCNT/LDPE nanocomposites. At low ω , there is a marked difference between pure LDPE and the composite at all loading. Also, as observed for η' , G' for SCNT at all ω and at all loadings is higher than pure LDPE, a trend that is different from LCNT and MCNT. On the other hand, at high ω the difference is reduced. Figure 4.1.5.d displays G' versus ω for various MWCNT/LDPE nanocomposites with 5 wt% loading. At low ω , LCNT composites are showing slightly higher values of G' , and composites of MCNT and SCNT are showing similar G' that are still higher than G' for the matrix. As usual, at high frequency no effect for aspect ratio can be detected. It is interesting to note that at high ω , LCNT and MCNT show the same

storage modulus. Therefore, at such high MWCNT loadings (5%) the impact of MWCNT loading dominates over that of aspect ratio or chemical modification. Nevertheless, the results of G' support the previous results of η' . G' for the nanocomposites with low loadings (0.25-1.0%) are lower than the matrix. This observation is limited to nanocomposites with high aspect ratio (LCNT & MCNT). Our tentative explanation for this observation on η' and G' is that the role of MWCNT in transition from plasticization to filler morphology and the threshold is aspect ratio dependent.

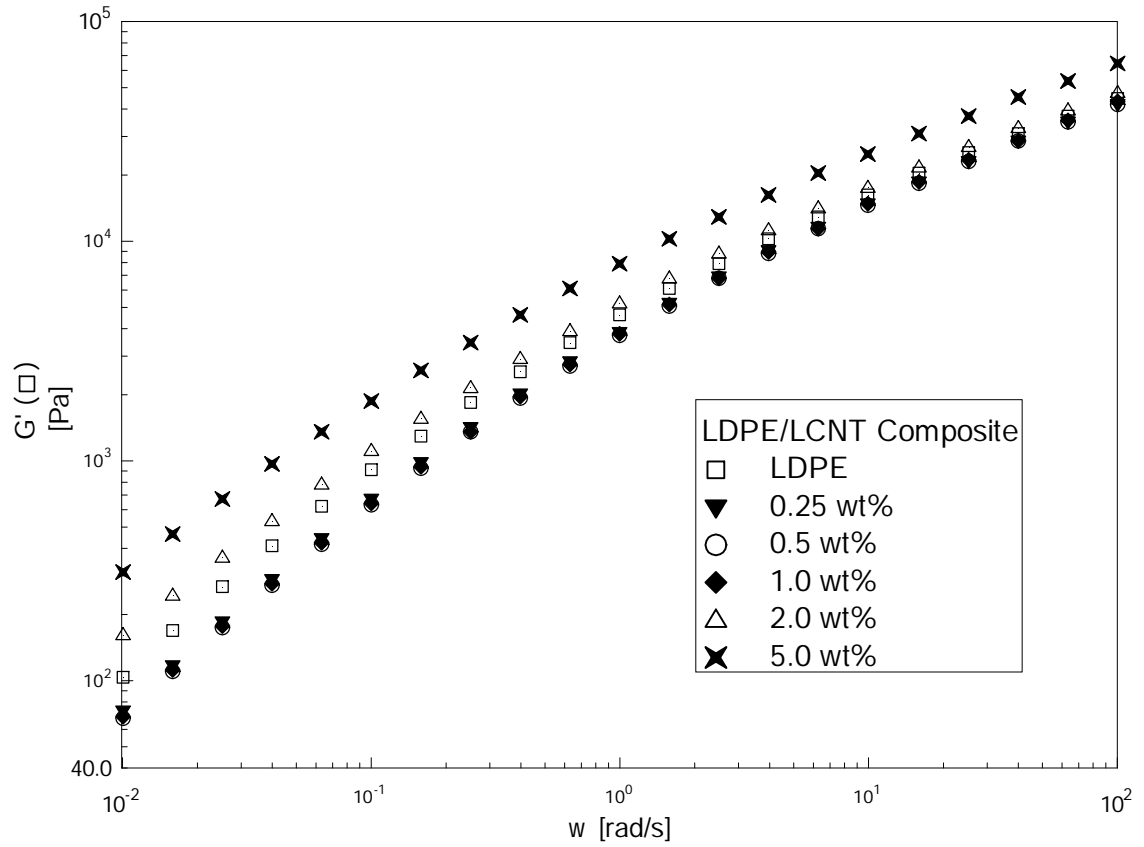


Figure 4.1.5.a. Storage modulus versus frequency plot for LCNT/LDPE nanocomposites.

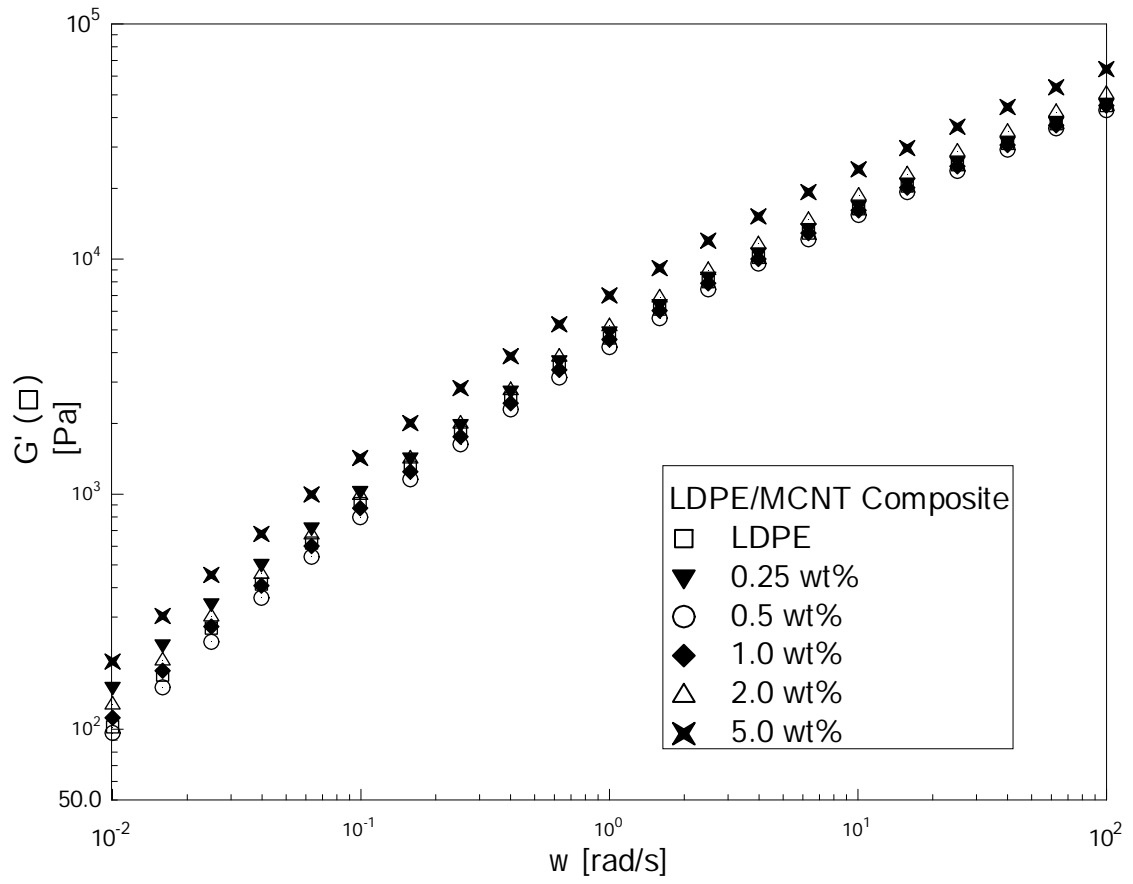


Figure 4.1.5.b. Storage modulus versus frequency plot for MCNT/LDPE nanocomposites.

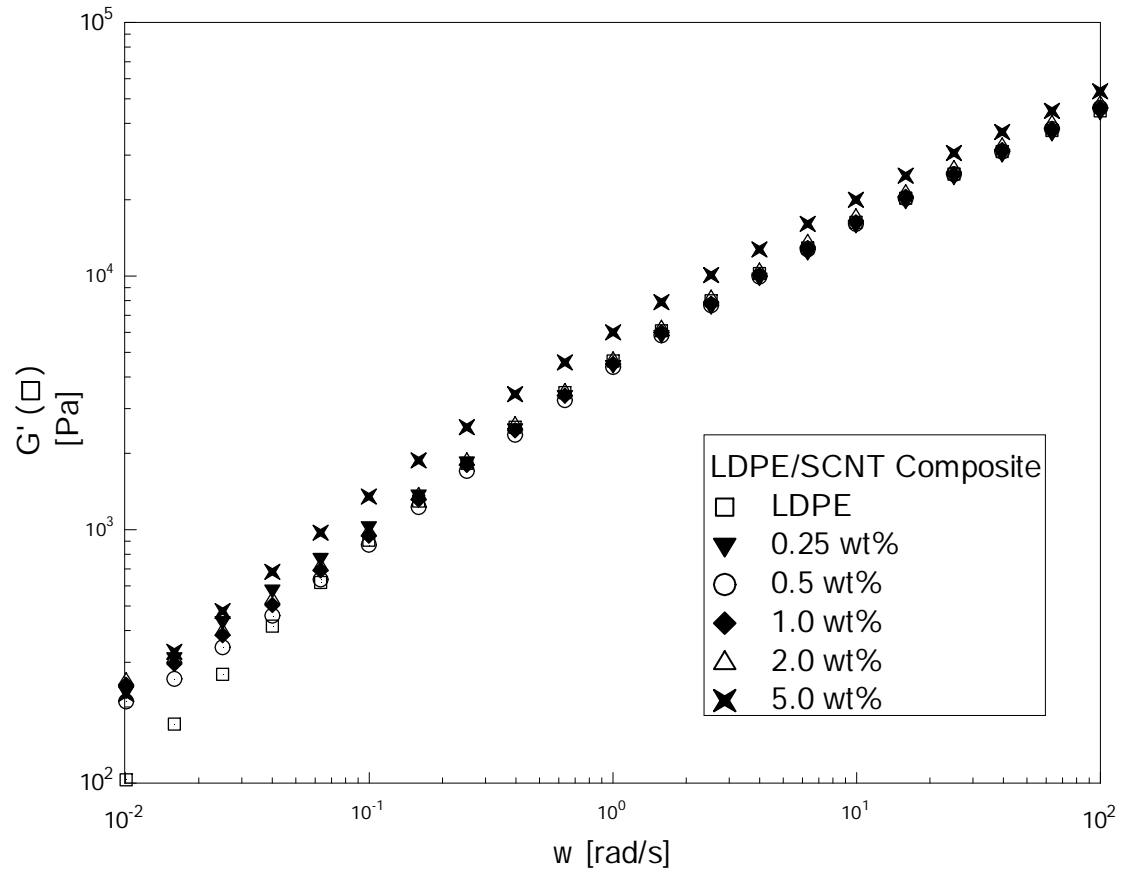


Figure 4.1.5.c. Storage modulus versus frequency plot for SCNT/LDPE nanocomposites.

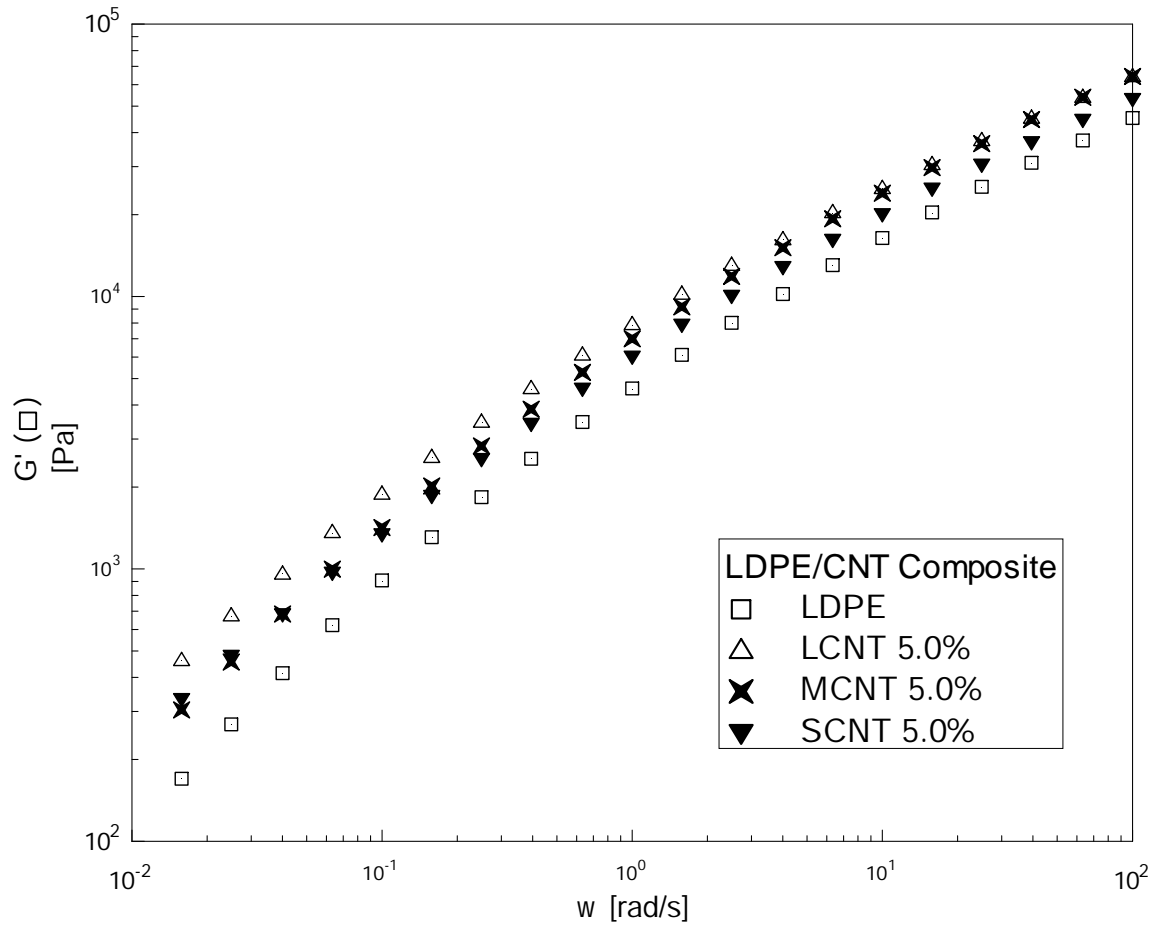


Figure 4.1.5.d. Storage modulus versus frequency plot for various MWCNT/LDPE nanocomposites.

On the other hand, MWCNT with aspect ratio of 31 and 375 were tested, and no negative normal stresses were observed. First thing to note is the reduction of normal force, N_1 at low $\dot{\gamma}$ for low MWCNT loadings of 0.25 to 1.0 % of nanocomposites (Figure 4.1.6.a). Also, N_1 increases with the increase of MWCNT loading. As the shear rate is increased, we see that N_1 for loadings in the range 0.25% to 2.0% go below the value of N_1 for the matrix. In addition, this observation supports the previous η , η' and G' findings and our explanations are discussed above. It is likely that the increase in $\dot{\gamma}$ is destroying polymer entanglements and the MWCNT agglomeration. For the MCNT / LDPE (Figure 4.1.6.b) nanocomposite, the 5.0% MWCNT nanocomposite loading shows the highest values of N_1 at low shear rates. Results of SCNT / LDPE nanocomposite (Figure 4.1.6.c) show a very similar behavior to that of LCNT / LDPE nanocomposite. Figure 4.1.6.d shows LDPE with 5.0 wt% loading of different MWCNTs. It is observed that at low shear rate, LCNT shows the highest N_1 , followed by MCNT and SCNT nanocomposites. As the shear rate is increased, LCNT and SCNT maintain N_1 values above that of the matrix. However, MCNT nanocomposites show slightly lower values of normal force. It is likely due to the chemical modification of the MWCNT. Nevertheless, the detailed mechanism for lowering the normal force is not clear.

It can be concluded that at low shear rate, the normal force increases with increasing loading of the CNT material for all aspect ratios. At low shear rate, low loadings of 0.25 to 1.0 wt% actually reduced the N_1 for LCNT and MCNT to be less than that for pure LDPE. But at high loadings of 2 and 5 wt% N_1 values were higher than pure LDPE. This observation is in agreement with our previous observation from dynamic shear testing

that showed lowering in G' . As the shear rate is increased, N_1 increases but become less than pure LDPE for loading of 0.25 to 2 for LCNT and SCNT nanocomposite. However, polymer entanglements and MWCNT agglomerations in MCNT dissipate much faster than LCNT and SCNT due to surface modification of MCNT, even though modification is small but it still has influenced N_1 . N_1 was able to reveal some impact for SCNT on the rheology of the composite at low MWCNT loadings which was not exposed by η' or G' .

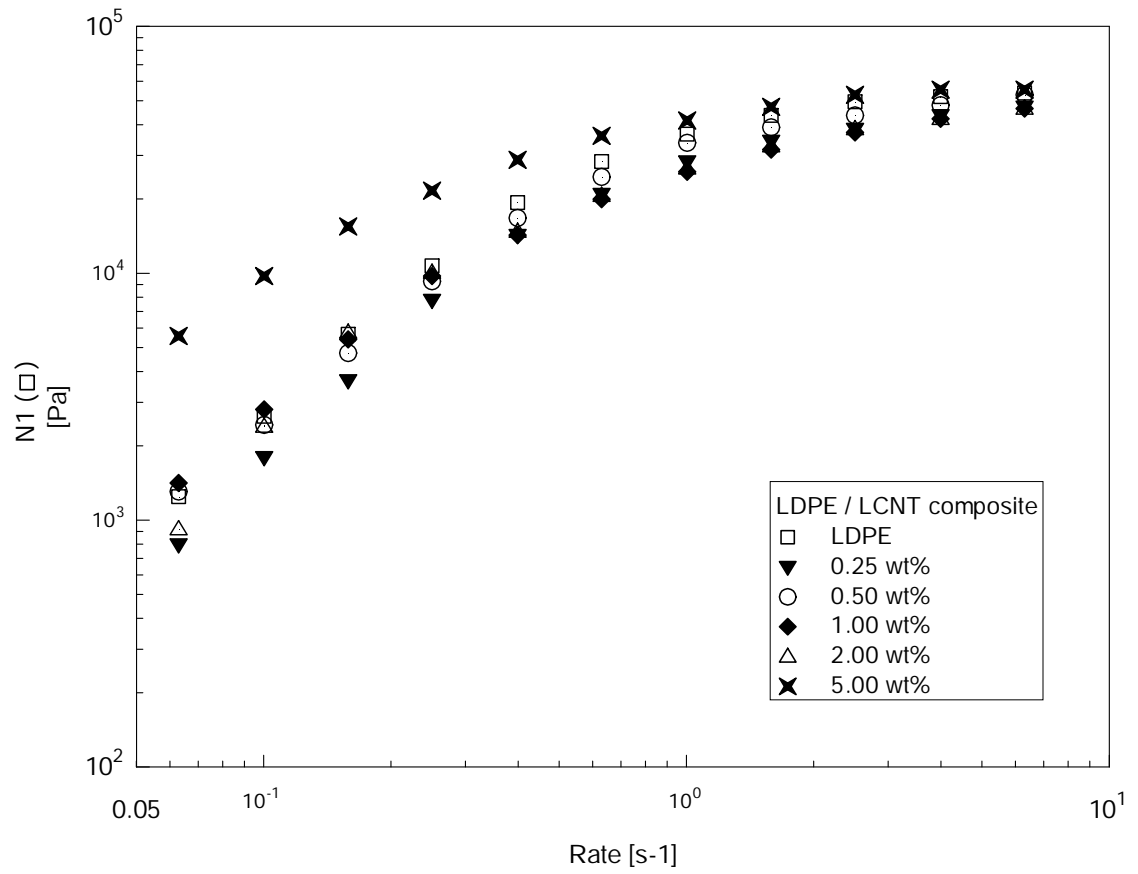


Figure 4.1.6.a. Normal force vs rate for LCNT / LDPE nanocomposites.

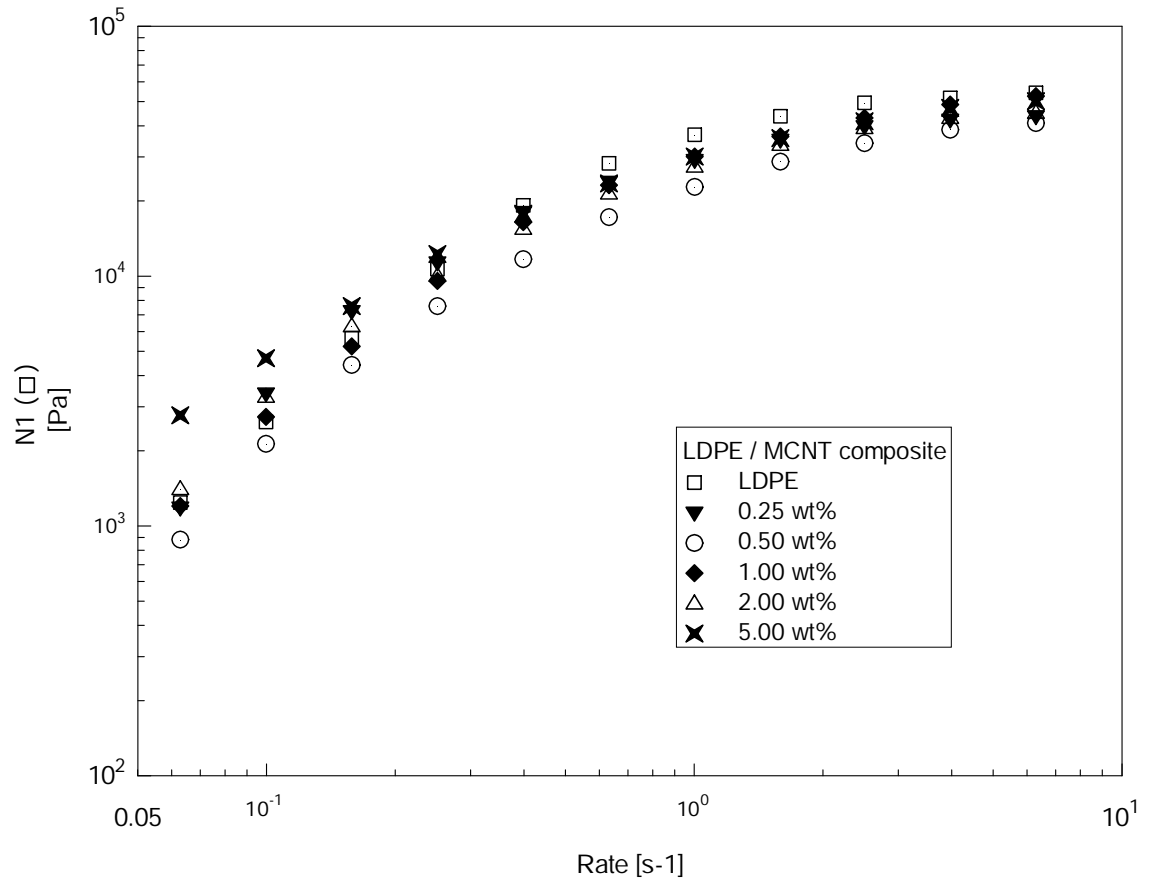


Figure 4.1.6.b. Normal force vs rate for MCNT / LDPE nanocomposites.

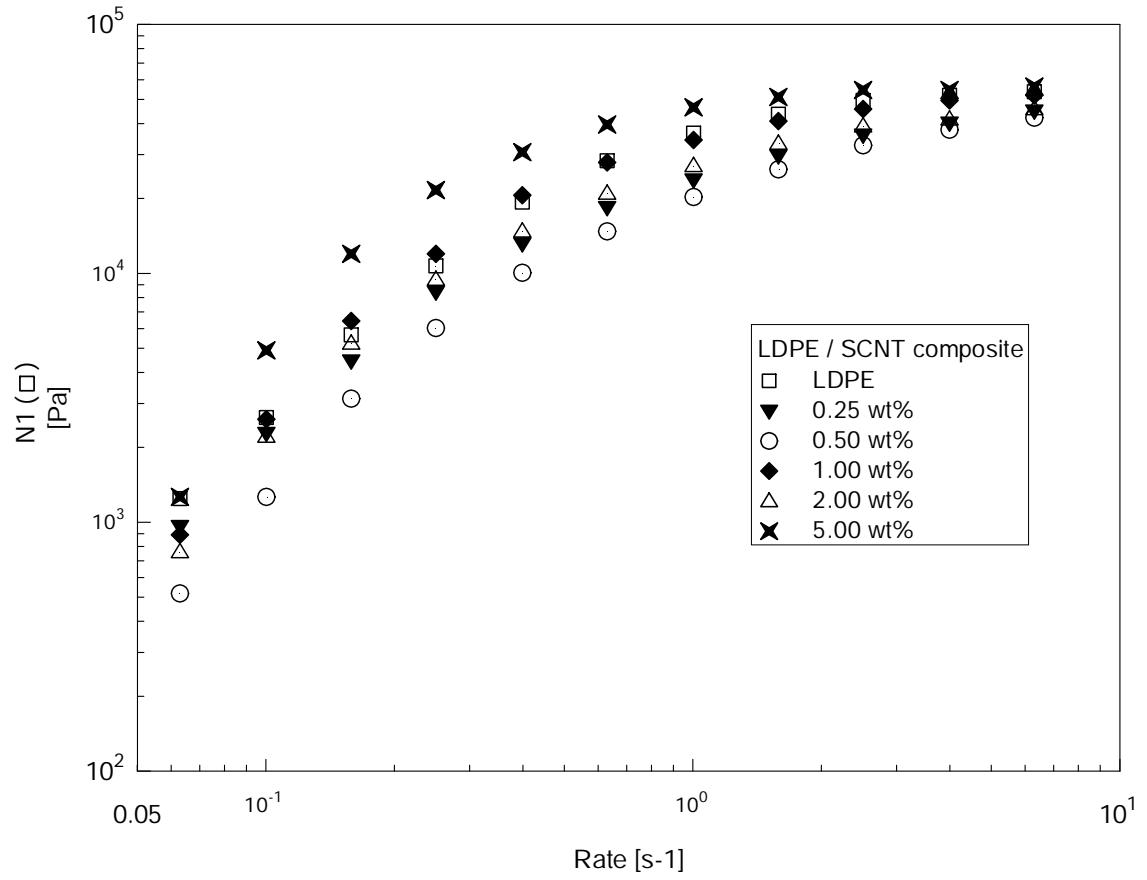


Figure 4.1.6.c. Normal force vs rate for SCNT / LDPE nanocomposites.

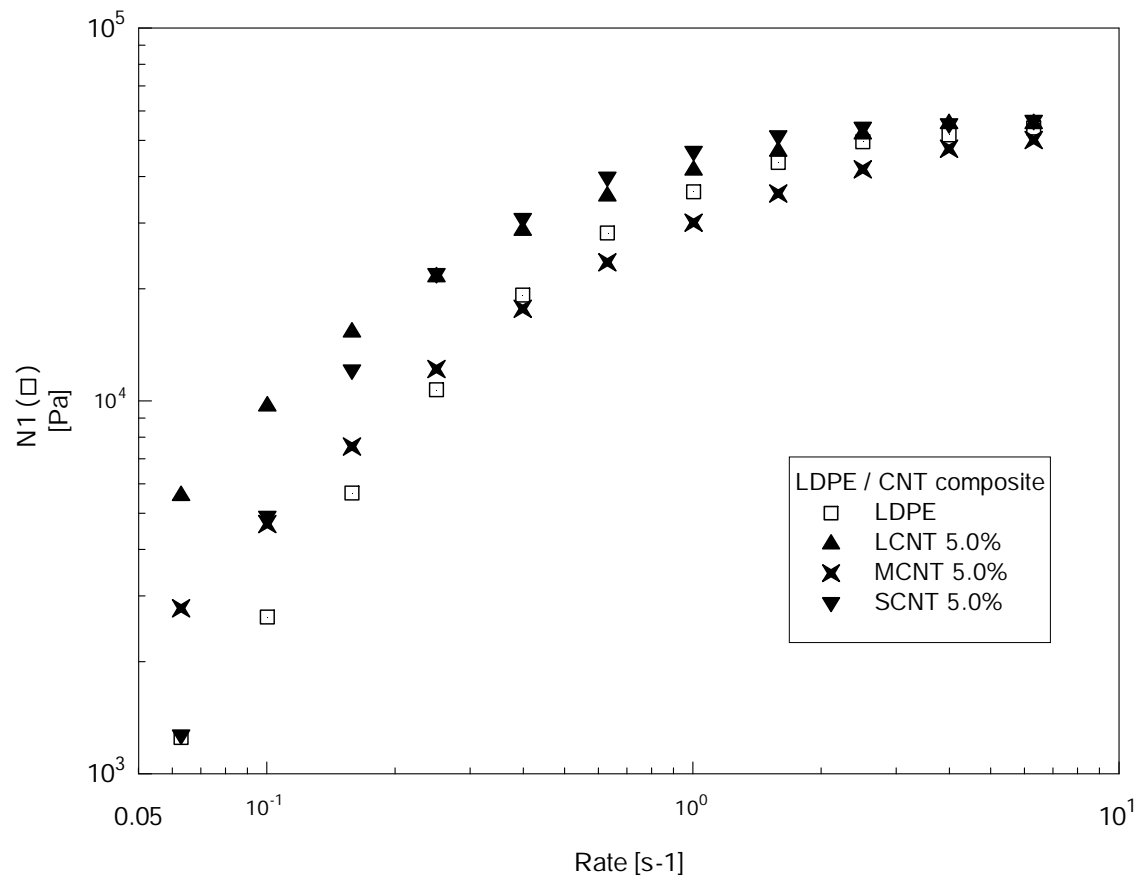


Figure 4.1.6.d. Normal force vs rate for various LDPE composites at 5.0 wt% loading nanocomposites.

4.1.4.4. Extensional Rheology

Figure 4.1.7.a shows the extensional viscosity, η_E^+ , vs time (s) for LDPE/LCNT composite with 5.0 wt % loading. The henky rate was varied from 0.5 to 1.5 s^{-1} . It is observed that as the henky rate is increased from 0.5 to 1.5 s^{-1} , the composite tend to show more strain hardening and also the time of break reduces considerably as well. A similar trend is observed for MCNT and SCNT in Figures 4.1.7.b and 4.1.7.c. η_E^+ vs time for various composites of LCNT, MCNT and SCNT with 0.5 (Figure 4.1.8.a) and 5.0 (Figure 4.1.8.b) wt% loading at fixed 1.5 henky rate show that as the loading is increased from 0.5 to 5.0 wt% the composite tend to show more strain hardening and time of break also is reduced. It makes sense since 0.5 wt% loading is more liquid-like than the 5.0 wt% loading. The SCNT, with the lowest aspect ratio, shows the least strain hardening. It is also observed (Figure 4.1.8.b) that LCNT is showing the maximum strain hardening, followed by MCNT and then SCNT. For MCNT the extensional viscosity at break is lower than that of LCNT. Although, not shown here, results for 0.5 s^{-1} and 1.0 s^{-1} henky rate showed exactly the same trend for all the produced composites at 5.0 wt% loading.

Even though LCNT and MCNT have the same aspect ratio; however it seems that slight modification of the MCNT tend to reduce its strain hardening effect compared to LCNT composites. A tentative explanation for this observation is as follows: MCNT has a –COOH modification, although it is very small, the effect of this modification is more or less similar to that of short branching on linear polymers. Hence, it is expected that this modification will increase the free volume which eases the flow and reduces or delays the strain hardening. However the impact of COOH modification is weak. The LCNT and

MCNT have the same high aspect ratio, which enhances the orientation of polymer chains in comparison to SCNT based composite. The enhancement in orientation in high aspect ratio MWCNT nanocomposites is likely responsible for the strain hardening.

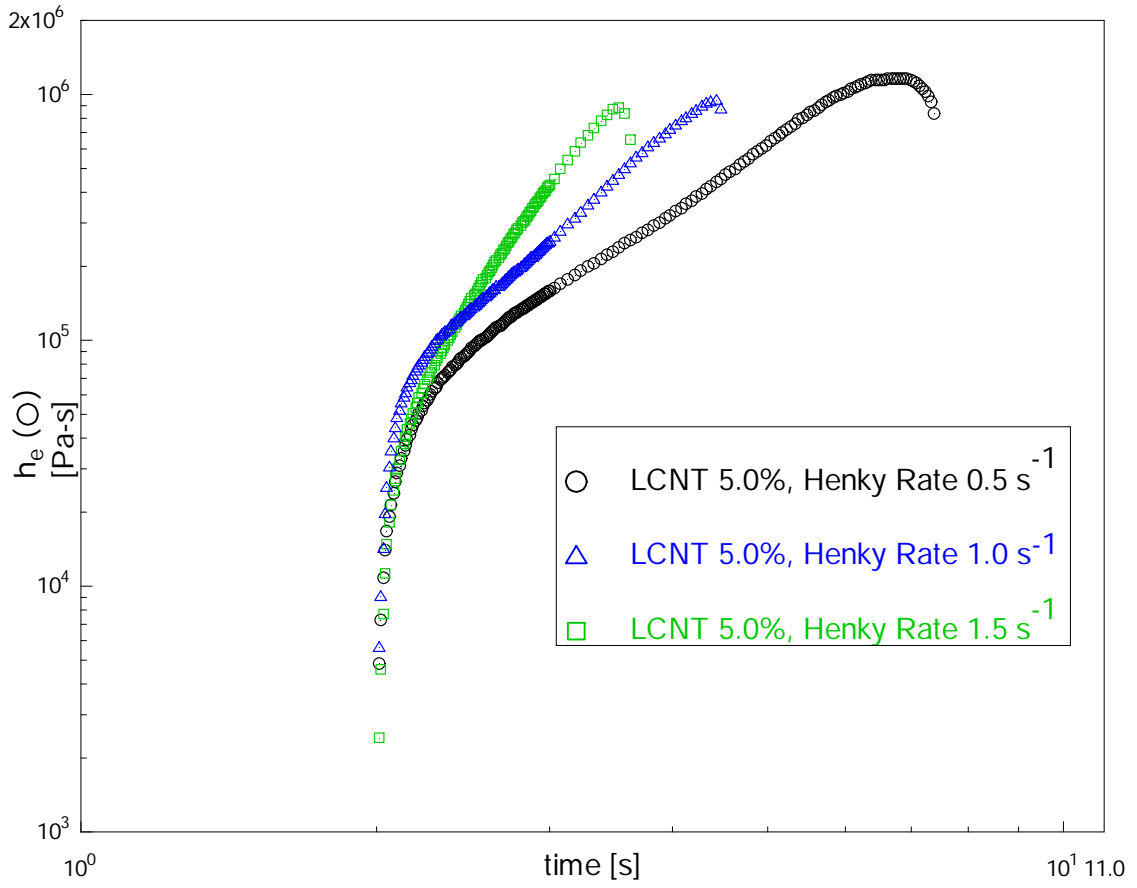


Figure 4.1.7.a. Extensional viscosity (η_e) vs time (s) for LCNT 5.0%-LDPE ($T_{\text{mix}} = 190^\circ\text{C}$, $T_{\text{test}} = 120^\circ\text{C}$).

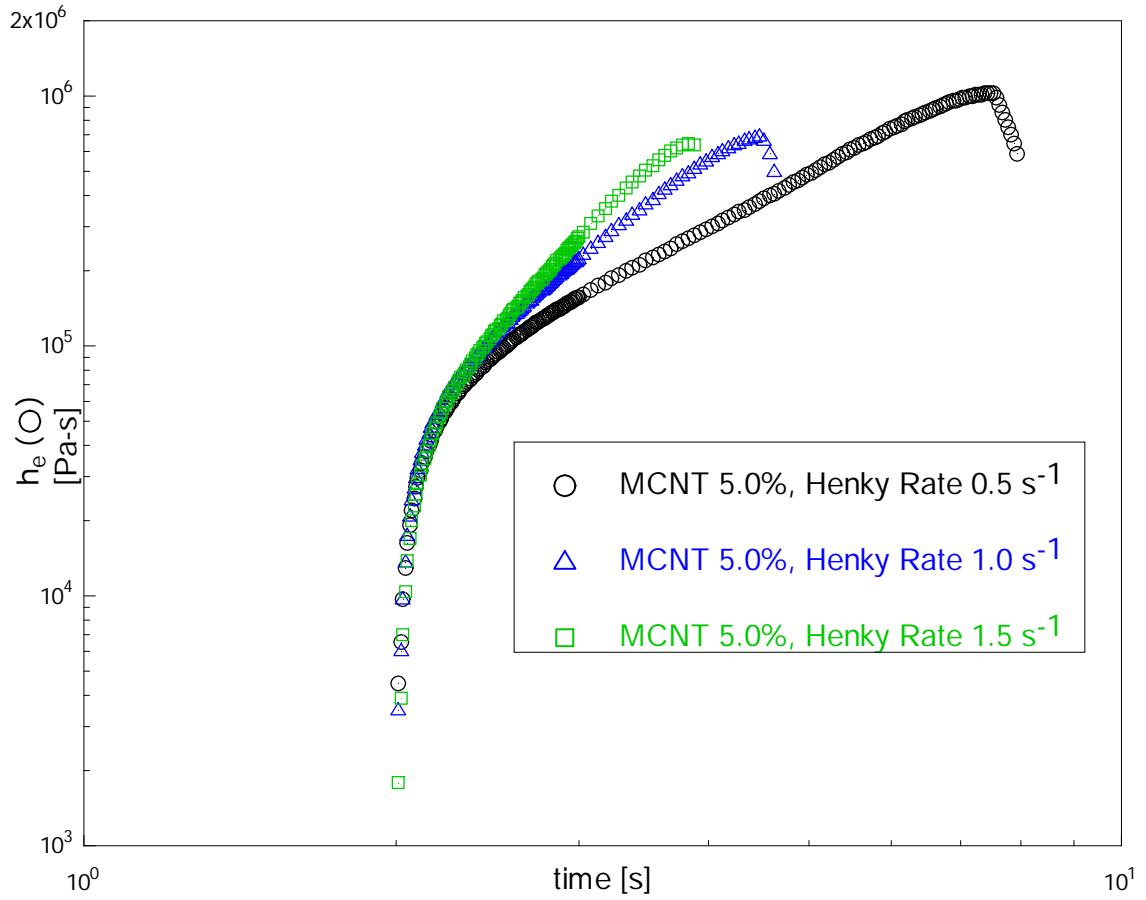


Figure 4.1.7.b. Extensional viscosity (η_e) vs time (s) for MCNT 5.0%-LDPE ($T_{\text{mix}}=190^\circ\text{C}$, $T_{\text{test}}=120^\circ\text{C}$).

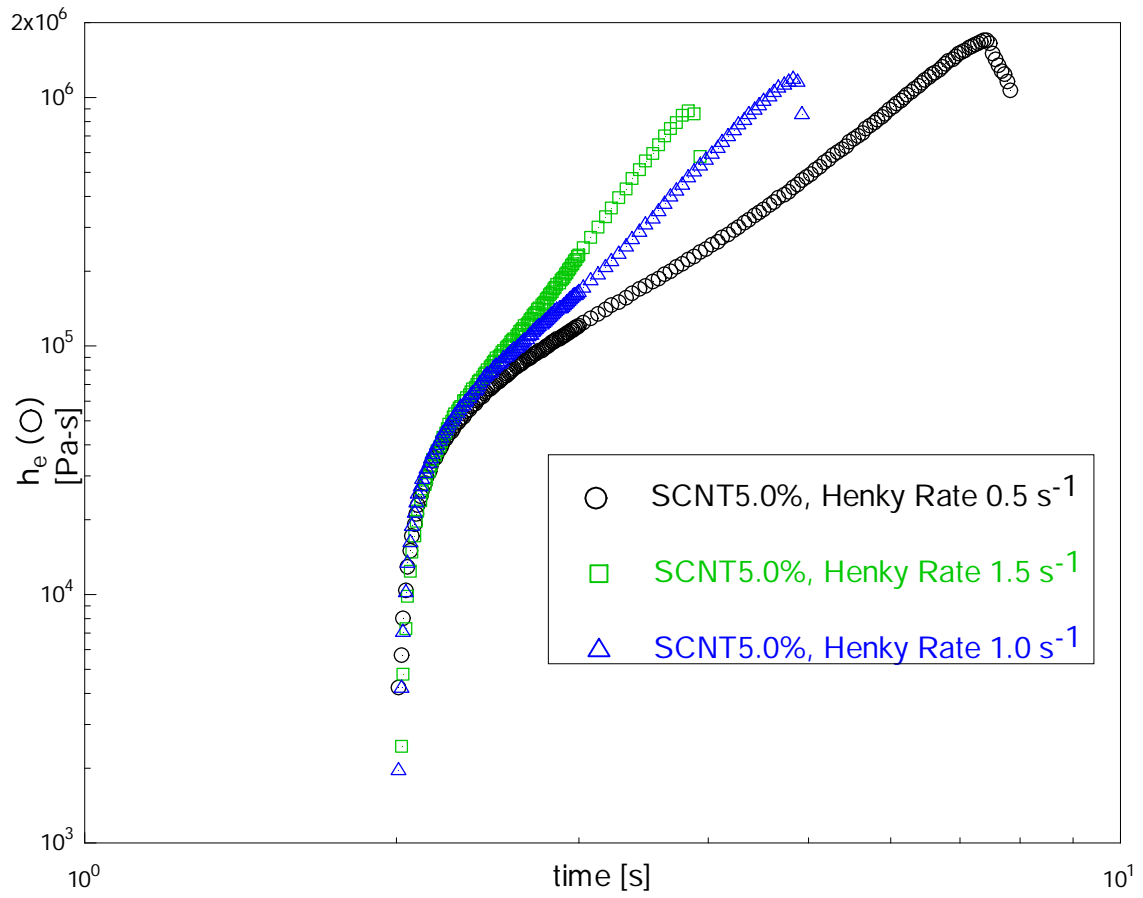


Figure 4.1.7.c. Extensional viscosity (η_e) vs time (s) for SCNT 5.0%-LDPE ($T_{\text{mix}} = 190^\circ\text{C}$, $T_{\text{test}} = 120^\circ\text{C}$).

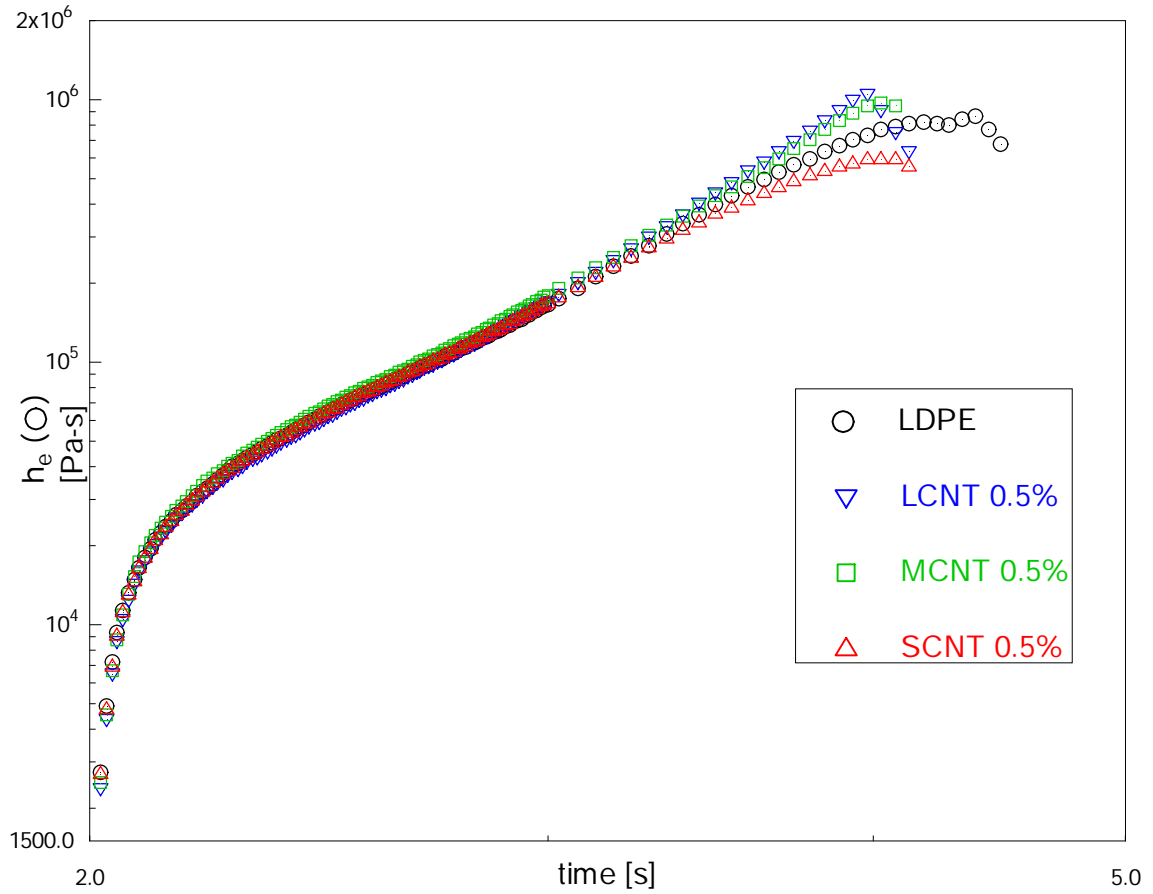


Figure 4.1.8.a. Extensional viscosity (η_e) vs time (s) for pure LDPE, Short CNT 0.5% - LDPE, Long CNT 0.5% - LDPE, Modified CNT 0.5% - LDPE ($T_{mix} = 190^\circ\text{C}$, Henky rate 1.5, $T_{test} = 120^\circ\text{C}$).

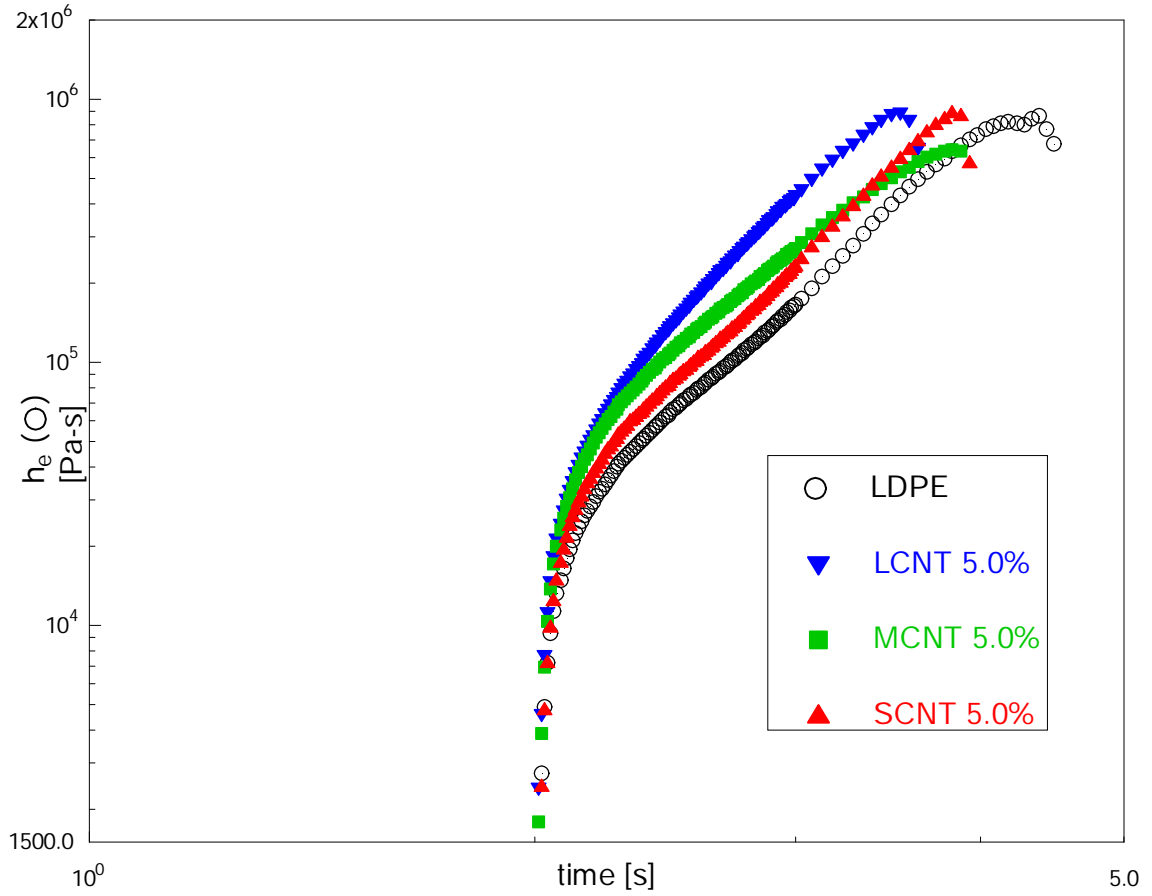


Figure 4.1.8.b. Extensional viscosity (η_e) vs time (s) for pure LDPE, Short CNT 5% - LDPE, Long CNT 5% - LDPE, Modified CNT 5%-LDPE ($T_{mix} = 190^\circ\text{C}$, Henky rate 1.5, $T_{test} = 120^\circ\text{C}$).

Table 4.1.1 shows the time of break and critical extensional stress at which the behavior of the extensional viscosity vs time changes. Time at break for all three types of nanocomposite is decreasing with increased loading and henky rate, gradually decreasing with increasing MWCNT loading and henky rate. In general, the critical extensional stress, the stress at which the strain hardening behavior of the nanocomposite changes, increases with the increase in CNT loading and henky rate for both LCNT and MCNT. But in the case of SCNT, critical extensional stress is less than that of LCNT and MCNT, at all loadings and henky rates. For SCNT nanocomposites, critical extensional stress is less sensitive to loading at high rate and more sensitive to MWCNT loading at low rates.

So, extensional viscosity shows more pronounced differences between CNTs with different aspect ratio and surface modification. LCNT showed the most strain hardening. MCNT, even though has the same aspect ratio as LCNT, showed less strain hardening. This was possibly due to surface modification where COOH has likely acted as a short branching, increasing the free volume and easing the flow hence reduced strain hardening. The time of break for the three types of nanocomposite decreases with increasing aspect ratio and henky rate. The critical extensional viscosity increased with increasing loading and henky rate for both LCNT and MCNT. However, values of SCNT were less than LCNT and MCNT at all loadings and henky rate. No drop in η_E^+ was observed at low loading up to 1.0 wt%, as has been seen for η' , η , G' , N_1 . The explanation for this is the fact that high henky rates of 0.5 to 1.5 s⁻¹ were used. If low henky rates of 0.01-0.05 were used, it would have been possible to observe this drop at low loadings of MWCNTs.

Table 4.1.1. Time at break and critical extensional stress for the various composites and 0.5 and 1.5 henky rate.

	Henky Rate	% Loading	Time at break (s)	Critical Extensional Stress (Pa)
LDPE	0.5	0	9.98	15035
	1.5	0	4.48	35365
LCNT	0.5	0.5	8.83	11920
		5	7.43	48646
	1.5	0.5	4.13	19779
		5	3.68	40674
MCNT	0.5	0.5	8.73	13749
		5	7.68	53051
	1.5	0.5	4.13	17297
		5	3.92	37978
SCNT	0.5	0.5	8.98	10991
		5	7.53	20383
	1.5	0.5	4.13	20684
		5	3.93	23844

4.1.5. Conclusion

Various nanocomposites with varying MWCNT loadings were investigated. The effect of surface modification and aspect ratio on dynamic, steady shear and extensional rheology were studied in detail. Morphology of these nanocomposites showed agglomerations present at all loadings and that these agglomerations were distributed into the LDPE matrix of LDPE. Both η' and η increased with increased CNT loading and aspect ratio at low frequency, tending towards solid-like behavior. At low loadings, both η' and η values became lower than that of pure LDPE at low frequency, a tentative explanation was suggested that MWCNTs at low loadings act as plasticizer while at high loadings they played the role of filler. A similar drop was observed in G' and N_1 . G' increased with frequency. At low loadings of upto 1 wt%, LCNT and MCNT values of G' were below that of pure LDPE. A tentative explanation was discussed earlier. The increase in G' with MWCNT loading is more prominent at low frequency. At low shear rate N_1 values for LCNT and MCNT at low loadings of 0.25 – 1.0 wt% were less than pure LDPE and higher in the range 2 to 5 wt%. As the shear rate is increased, N_1 increased but become less than that of pure LDPE for 0.25 to 2 wt% MWCNT loading. Agglomerations seem to subside faster in MCNT than LCNT and SCNT due to its surface modification even though the modification is small.

Results of extensional viscosity show more pronounced differences between the nanocomposites with different aspect ratios. LCNT nanocomposite showed the most strain hardening in the three type of nanocomposite. MCNT showed less strain hardening than LCNT, even though they have the same aspect ratio, possibly due to COOH acting

as short branching. The LCNT and MCNT have the same high aspect ratio, which enhances the orientation of polymer chains in comparison with SCNT based composites. The enhancement in orientation in high aspect ratio MWCNT nanocomposites is likely responsible for the strain hardening. The suggested increase in free volume would likely ease the flow and reduce the strain hardening. The time of break for the three types of nanocomposite decreased with the increase in aspect ratio and henky rate. The value of critical extensional stress, increased with increase in loading and henky rate for both LCNT and MCNT. However, values of SCNT were less than LCNT and MCNT at all loadings and henky rate.

In general, all rheological tools used in this study reveal a possible plasticization effect for MWCNT with high aspect ratio at low loadings (<1.0 wt%) and a filler effect at higher loadings (>1.0 wt%). The effect of COOH modification was more apparent in extensional viscosity and N_1 to some extent. Aspect ratio has influenced both viscous and elastic shear properties as well as strain hardening.

4.1.6. Acknowledgement

The authors are thankful to the Center of Research Excellence in Petroleum Refining & Petrochemicals (CoRE-PRP), established by the Ministry of Higher Education, for providing the funding for this research. KFUPM is also acknowledged for its support.

4.1.7. References

- [1] Iijima S. Helical microtubules of graphitic carbon. *Nature* 1991;354:56-58.
- [2] Deng CF, Wang DZ, Zhang XX, Li AB. Processing and Properties of Carbon Nanotubes Reinforced Aluminum Composites. *Mater Sci Eng A* 2007; 444(1-2):138-145.
- [3] Mishra S, Shimpi NG. Mechanical and flame-retarding properties of styrene-butadiene rubber filled with nano-CaCO₃ as a filler and linseed oil as an extender. *J Appl Polym Sci* 2005; 98(6):2563-2571.
- [4] Gilman JW, Jackson CL, Morgan AB, Harris RJr, Manias E, Giannelis EP, Wuthenow M, Hilton D, Phillips SH. Flammability Properties of Polymer Layered-Silicate Nanocomposites. Polypropylene and Polystyrene Nanocomposites. *Chem Mater* 2000;12(7):1866-1873.
- [5] Galgali G, Ramesh C, Lele A. A Rheological Study on the Kinetics of Hybrid Formation in Polypropylene Nanocomposites. *Macromolecules*, 2001;34(4):852-858.
- [6] Lim YT, Park OO. Rheological evidence for the microstructure of intercalated polymer/layered silicate nanocomposites. *Macromol Rapid Commun* 2000;21:231-235.
- [7] Hyun YH, Lim ST, Choi HJ, Jhon MS. Rheology of Poly(ethylene oxide)/Organoclay Nanocomposites. *Macromolecules* 2001;34(23):8084-8093.
- [8] Wu Y-P, Ma Y, Wang Y-Q, Zhang L-Q. Effects of characteristics of rubber, mixing and vulcanization on the structure and properties of rubber/clay nanocomposites by melt blending. *Macromol Mater Eng* 2004;289(10):890-894.
- [9] Mousa A, Karger-Kocsis J. Rheological and thermodynamical behavior of styrene/butadiene rubber-organoclay nanocomposites. *Macromol Mater Eng* 2001;286:260-266.
- [10] Krishnamoorti R, Ren J, Silva AS. Shear response of layered silicate nanocomposites. *J Chem Phys* 2001;114:4968-4973.
- [11] Ray SS, Bousmina M, Okamoto K. Structure and Properties of Nanocomposites Based on Poly(butylene succinate-co-adipate) and Organically Modified Montmorillonite. *Macromol Mater Eng* 2005;290(8):759-768.

- [12] Ray SS, Bousmina M. Effect of Organic Modification on the Compatibilization Efficiency of Clay in an Immiscible Polymer Blend. *Macromol Rapid Comm* 2005;26(20):1639-1646.
- [13] Ray SS, Bousmina M. Poly(butylene succinate-co-adipate)/montmorillonite nanocomposites: effect of organic modifier miscibility on structure, properties, and viscoelasticity. *Polymer* 2005;46(26):12430-12439.
- [14] Ren J, Casanueva BF, Mitchell CA, Krishnamoorti R. Disorientation Kinetics of Aligned Polymer Layered Silicate Nanocomposites. *Macromolecules* 2003;36(11):4188-4194.
- [15] Lozano K, Bonilla-Rois J, Berrera V. A study on Nanofiber-Reinforced Thermoplastic composites(II): Investigation of the mixing rheology and conduction properties. *J Appl Polym Sci* 2001;80(8):1162-1172.
- [16] Cortes P, Lozano K, Barrera EV, Bonilla-Rios J. Effect of nanofiber treatments on the properties of vapor grown carbon fiber reinforced polymer composites. *J Appl Polym Sci* 2003;89(9):2527-2534.
- [17] Lozano K, Yang S, Zeng Q. Rheological analysis of vapor grown carbon nanofiber reinforced polyethylene composites. *J Appl Polym Sci* 2004;93(1):155-162.
- [18] Lee SH, Cho E, Jeon SH, Youn JR. Rheological and electrical properties of polypropylene composites containing functionalized multi-walled carbon nanotubes and compatibilizers. *Carbon* 2007;45(14):2810-2822.
- [19] Potschke P, Fornes TD, Paul DR. Rheological behavior of multiwalled carbon nanotube/polycarbonate composites. *Polymer* 2002;43(11):3247-3255.
- [20] Moniruzzaman M, Winey KI. Polymer nanocomposites containing carbon nanotubes. *Macromolecules* 2006;39(16):5194-5205.
- [21] Xu D, Wang Z. Role of multi-wall carbon nanotube network in composites to crystallization of isotactic polypropylene matrix. *Polymer* 2008;49(1):330-338.
- [22] Micusik M, Omastova M, Krupa I, Prokes J, Pissis P, Logakis E, Pandis C, Potschke P, Pionteck J. A comparative study on the electrical and mechanical behaviour of multi-walled carbon nanotube composites prepared by diluting a masterbatch with various types of polypropylenes. *J Appl Polym Sci* 2009;113(4):2536-2551.

- [23] Ratna D, Abraham TN, Siengchin S, Karger-Kocsis J. Novel method for dispersion of multiwall carbon nanotubes in poly(ethylene oxide) matrix using dicarboxylic acid salts. *J Polym Sci Part B: Polym Phys* 2009;47(12):1156-1165.
- [24] McNally T, Potschke P, Halley P, Murphy M, Martin D, Bell SEJ, Brennan GP, Bein D, Lemoine P, Quinn JP. Polyethylene multiwalled carbon nanotube composites. *Polymer* 2005;46(19):8222-8232.
- [25] Kharchenko SB, Douglas JF, Obrzut J, Grulke EA. Flow-induced properties of nanotubes filled polymer materials. *Nat Mater* 2004;3:564-568.
- [26] Xu D-H, Wang Z-G. Influence of Carbon nanotube aspect ratio on normal stress difference in isotactic polypropylene nanocomposite melts. *Macromolecules* 2008;41(3):815-825.
- [27] Kim JA, Seong DG, Kang TJ, Youn JR. Effects of surface modification on rheological and mechanical properties of CNT/epoxy composites. *Carbon* 2006;44(10):1898-1905.
- [28] Ibnelwaleed H, Williams M. Rheological study of heterogeneities in melt blends of ZN-LLDPE and LDPE: Influence of Mw and comonomer type, and implications for miscibility. *Rheol Acta* 2004;43(6):602-614.
- [29] Prashantha K, Soulestin J, Lacrampe MF, Claes M, Dupin G, Krawczak P. Multi walled carbon nanotubes filled polypropylene nanocomposites based on materbatch route: Improvement of dispersion and mechanical properties through PP-g-MA addition. *Express Polym Lett* 2008; 2(10):735-745.
- [30] Xiao KQ, Zhang LC, Zarudi I. Mechanical and rheological properties of carbon nanotube reinforced polyethylene composites. *Compos Sci Tech* 2007;67(2):177-182.
- [31] Seo M-K, Park S-J. Electrical resistivity and rheological behaviors of carbon nanotubes-filled polypropylene composites. *Chem Phys Lett* 2004;395(1-3):44-48.
- [32] Valentino O, Sarno M, Rainone NG, Nobile MR, Ciambelli P, Neitzert HC, Simon GP. Influence of polymer structure and nanotube concentration on the conductivity and rheological properties of polyethylene / CNT composites. *Physica E* 2008;40(7):2440-2445.
- [33] Zhang Q, Lippits DR, Rastogi S. Dispersion and rheological aspects of SWNTs in ultrahigh molecular weight polyethylene. *Macromolecules* 2006;39(2):658-666.

- [34] Jain SH. Nano-scale events with macroscopic effects in polypropylene/silica nanocomposites; effect of polymer adsorption on processability and properties. Ph.D. Thesis, Technische Universiteit Eindhoven, 2005.
- [35] Mackay ME, Dao TT, Tuteja A, Ho DL, Horn BV, Kim H-C, Hawker CJ. Nanoscale effects leading to non-Einstein-like decrease in viscosity. *Nat Mater* 2003;2:762-766.
- [36] Vaia RA, Giannelis EP. Lattice model of polymer melt intercalation in organically-modified layered silicates. *Macromolecules* 1997;30(25):7990-7999.
- [37] Vaia RA, Giannelis EP. Polymer melt intercalation in organically-modified layered silicates : Model predictions and experiment. *Macromolecules* 1997;30(25):8000-8009.
- [38] A. C. Balazs, Singh C, Zhulina E. Modeling the Interactions between Polymers and Clay Surfaces through Self-Consistent Field Theory. *Macromolecules* 1998;31(23):8370-8381.
- [39] Ray SS. Rheology of Polymer/Layered Silicate Nanocomposites. *J Ind Eng Chem* 2006;12(6):811-842.

4.2. Effect of aspect ratio, surface modification & compatibilizer on the mechanical & thermal properties of LDPE-MWCNT nanocomposites.

4.2.1. Abstract

In this work, nanocomposites of low density polyethylene (LDPE) / multiwall carbon nanotubes (MWCNTs) were prepared using melt blending. The effects of aspect ratio, CNT loading, chemical modification and compatibilizer on morphology, mechanical and thermal properties were studied. Fifteen samples were prepared using different MWCNTs: long CNT (LCNT); modified CNT (MCNT) and short CNT (SCNT). FE-SEM images of produced nanocomposites show agglomeration of the MWCNTs. Addition of compatibilizer to both LCNT and MCNT nanocomposites improved their dispersion in the LDPE matrix. Yield strength and modulus increased with loading of various MWCNTs. CNTs play the role of a plasticizer at 0.5% loading and filler at 2 % loading and higher. However, ultimate strength, percent elongation and toughness reduced significantly for CNT loadings of 2% CNT and higher. The addition of maleated PE resulted in improvements of Young's modulus, yield strength and ultimate strength but no impact on elongation at break or toughness. Addition of compatibilizer did not affect the crystallinity of the produced nanocomposites. In general, the use of CNT with high aspect ratio and the addition of compatibilizer and chemical modification improved the dispersion of MWCNTs and consequently improved most of the mechanical properties except elongation at break and toughness.

4.2.2. Introduction

Carbon nanotubes (CNTs), generated a huge research activity in the field of science and engineering since 1991 [1]. They are nano-structured materials with unique mechanical, electrical and thermal properties. CNTs can range in diameter from 1 to 100 nm up into millimeters [2], with densities as low as 1.3 g/cm^3 . Their Young's moduli values have been reported 1-5 TPa [3-9], which is superior to other forms of carbon fiber 0.1-0.8 TPa [10]. Aspect ratio (length / diameter) as high as 10000 [11] and compressive strength of $\sim 150 \text{ GPa}$ [12] have been reported. However, their mechanical strength is the most amazing aspect of their properties. The measured strength for a carbon nanotube has been reported to be between 5-63 GPa [7-8, 13-15]. Even weakest type of carbon nanotubes have strengths higher than steel 0.25 GPa. For this very reason a lot of research is being devoted to producing CNT reinforced polymer composites.

The fundamental challenge that lies in achieving superior mechanical properties of polymer composites is in the dispersion of CNTs throughout the polymer matrix. Theoretical predictions suggest that the elastic modulus and tensile strength of the composite increase when either the volume fraction of the reinforcing fibers increases [16-17], or the aspect ratio of the fibers increases [17]. The aspect ratio factor is in fact related to the interfacial matrix-fiber stress transfer, where the magnitude of stress transfer is favored by increasing the high aspect ratio. Moreover, the tensile strength of the composites is strongly influenced by the magnitude of interfacial matrix-fiber stress [17-18].

Accordingly, the most important factors that affect the bulk mechanical properties of the composites are: the loading of CNT [19-22], the alignment of CNT [23-24], and the CNT-matrix stress transfer [25-29]. It is suggested that the degree of dispersion is the most critical factor that controls the bulk mechanical properties. [8, 30-39]

Ruan et al [40] demonstrated that strength and modulus are not the only parameters that can be enhanced by incorporating CNTs in a polymer matrix. In their study, they reported experimental observations on the drastically enhanced toughness in the ultrahigh molecular weight polyethylene (UHMWPE) films due to the addition of 1% multiwalled carbon nanotubes (MWCNTs). The composites were prepared by solution blending followed by film drawing. Good dispersion was observed as examined by SEM. A combination of tensile and Raman spectroscopic measurements showed that the presence of MWCNTs in the composites can lead to approximately 150% increase in strain energy in comparison with the pure UHMWPE film at similar draw ratios. This is accompanied with an increase of approximately 140% in ductility and up to 25% in tensile strength. The authors attribute the above observations to the chain mobility enhancement in UHMWPE induced by the MWCNTs. So, CNTs play the role of a plasticizer.

Bin et al. [41] prepared UHMWPE and MWCNT composites by solvent-blending method using either decalin or paraffin as solvent. SEM observations revealed that the MWCNTs within the composite prepared in decalin were covered by UHMWPE, and their diameters were much greater than those of the original MWCNTs, while the diameter of the MWCNTs within the composite prepared in paraffin was similar to the diameter of the original MWCNTs. Such different morphology was found to be due to different

crystallization. The composites prepared in decalin had high drawability. Significant increase in elastic modulus was observed.

Zou et al. [42] prepared MWCNT/HDPE composites using the method of solution blending followed by melt-blending (with the addition of PEG or SiO₂ as dispersing agents). It was found that there was a critical MWCNT concentration around 1 wt% where a fine network of MWCNT/SiO₂ was formed (and hence mechanical properties improved at this wt%). On the other hand, it is found that MWCNT could stabilize HDPE when its weight content was greater than 2 wt%. In short, the reported method does not look attractive because the dispersing agents generally decrease the mechanical properties of HDPE, and SiO₂ was found to accelerate thermo-oxidation.

McNally et al. [43] prepared composites of PE and MWCNTs by melt blending using a mini-twin screw extruder. The wt% of MWCNT was varied from 0 to 10%. They found that the yield strength increased slightly with the addition of CNT. However, they observed that the ultimate tensile strength and elongation at break decreased with addition of MWCNTs. For example, the % elongation at break decreased from 1200% for the pure PE to 700% at CNT loading of 5 wt.%, and further decreased to 300% at CNT loading of 10 wt.%. This is mainly due to the poor dispersion of CNTs. This is evident from some CNT aggregates observed by morphology tests. This led to poor stress transfer between the polymer and the filler. The authors concluded that the deterioration of mechanical properties of the nanocomposites implies that the mechanism for mechanical reinforcement for PE/MWCNT composites is filler-matrix interfacial interactions and not filler percolation.

Tang et al. [22] prepared MWCNT/HDPE composite films using the melt processing method. The composite films with CNT content varied from 0 to 5 wt.% were analyzed by SEM and TEM to observe nanotube dispersion. The mechanical properties of the films were measured by a small punch test. Results showed increases in the stiffness, peak load and work to failure for the composite films with increasing MWCNT content.

The incorporation of CNTs in a polymer generally improves the stiffness and strength of the polymer, but the ductility and toughness of the polymer are compromised in most cases [21]. Functionalization of CNT is a break-through solution to resolve this problem. Composites based on functionalized CNT are expected to have large interfacial shear strengths. Covalently grafted long-chain molecules entangle with the polymer matrix creating a very strong bond. In addition, the functional groups act to make the nanotubes more compatible with polymer hosts. This tends to dramatically improve the nanotube dispersion and hence further improve composite properties. [21, 31, 44]

Yang et al. [44] reported the mechanical reinforcement of PE using PE-g-MWCNTs. The stiffness, strength, ductility and toughness of PE are all improved by the addition of PE-g-MWCNTs. The grafting of PE onto MWNTs improves the dispersion of nanotubes in the PE matrix, hence the MWCNT/PE interfacial adhesion. The grafting was achieved by a reactive blending process through melt blending of PE containing 0.85 wt% of maleic anhydride and amine-functionalized MWCNTs. The reaction between maleic anhydride and amine groups, as evidenced by XPS and Raman spectroscopy, leads to the grafting of PE onto the nanotubes. These PE-g-MWCNTS are then incorporated into PE matrix via the common melt-blending technique. In another related study by the same

research group, Yang et. al [21] applied a similar procedure for preparing PP/PP-g-MWCNTs composites. PP was grafted onto MWCNTs by melt blending PP containing 0.6 wt% of maleic anhydride and amine-functionalized MWCNTs. The mechanical properties of PP/PP-g-MWCNTs composites were evaluated. When PP was reinforced with pristine MWCNTs, its Young's modulus and tensile strength were increased, but its ultimate strain and toughness were reduced. On the other hand, the Young's modulus, tensile strength, ultimate strain and toughness of PP were improved by 108, 141, 49 and 287%, respectively, by the addition of PP-g-MWCNTs with a MWCNTs content of 1.5 wt%. The procedure reported here is attractive from industrial point of view because of its simplicity for the following reasons: 1) PE-g-MA is available commercially at a reasonable price; 2) it is easy to functionalize CNT with amine groups; 3) melt blending is a perfect choice in polymer processing industry.

Shofner et al [45] evaluated the effect of sidewall functional group on dispersing the fluorinated single-walled carbon nanotubes (F-SWCNTs) in PE and on the mechanical properties of the F-SWCNT composites fabricated. The composites were prepared by solvent-blending followed by shear mixing. The study demonstrated that in comparison with PE composites filled with un-functionalized nanotubes, improved dispersion and interfacial and mechanical properties are achieved for F-SWCNT-loaded matrices due to chemical functionalization. Also, the observed partial removal of functional groups from the F-SWCNTs during melt processing with polyethylene by shear mixing suggests a possibility of in situ direct covalent bonding between the nanotubes and the matrix which ultimately results in mechanical reinforcement of the composite.

Zhao et al. [24] used MWCNT grafted with alkyl chain for reinforcement of PP. For achieving excellent tensile properties, the as-prepared PP/MWCNTs composites were subjected to a dynamic packing injection molding, to induce a highly oriented structure with both PP chains and MWCNTs aligned along the shear flow direction. Not only Young's modulus and tensile strength were enhanced, as expected for oriented materials, but also more importantly composites containing only 0.1-0.3 wt% MWCNTs were much ductile compared with the polymer matrix. The addition of PP-g-MMA made a drop in the elongation at break to only 15%; however, it could be improved to 80-100% after incorporation of small amount of MWCNTs. The authors attribute this enhancement in toughness to: (1) the increased mobility of both the PP chains due to the addition of MWCNTs, as they are oriented along tensile deformation direction (plasticization) and (2) the bridging effect of the oriented MWCNTs on the crack development during tensile failure.

Wang et al. [29] utilized a combination of solution blending and gel spinning methods to prepare UHMWPE-CNTs composite fibers. Functionalization of CNTs was also carried out by oxidation followed by mixing of CNT with titanate coupling agent in ethanol, to introduce COOH group. TEM, SEM, XRD, IR were used to characterize the CNTs, their dispersion in the matrix and the functional group changes on the surface of the CNTs. The results showed that there was no obvious agglomeration of CNTs in the obtained composite fibers up to 2 wt% CNT loading and consequently a good interaction between CNTs and UHMWPE matrix was established. Furthermore, it was reported that the addition of CNTs resulted in a peculiar structure, a more regular alignment of the

UHMWPE morphology. The mechanical properties of UHMWPE-CNTs were improved compared with that of pure UHMWPE fiber. However, above 2 wt% CNT the mechanical properties decreased, likely because of poor dispersion.

It can be observed from the above literature review that the effects of CNT loading and different CNT surface modifications were examined. However, the influence of aspect ratio on the mechanical and thermal properties is yet to be studied experimentally, while its impact on elastic modulus and tensile strength was stated in theoretical models [28, 46-47]. Our principal focus in this paper is to study the effect of varying the aspect ratio, surface modification, compatibilizer and MWCNT loading on the mechanical and thermal properties, primarily using the melt blending process for producing the LDPE-MWCNT composites. The choice of a film grade LDPE for this research is to assess the possibility of producing a thinner and stronger film by adding CNTs.

4.2.3. Experimental Section

4.2.3.1. Materials and Sample Preparation

MWCNTs with different aspect ratios and surface modification were supplied by Cheap Tubes Inc, USA. Table 4.2.1. shows energy dispersive x-ray spectroscopy data provided by the supplier. In Table 4.2.2, details of the three different CNTs used in the study are given. The three different types are selected to study one parameter at a time. The long and the short CNTs have the same ID and OD; however, the length of the long CNT is 12 times greater than that of the short CNTs. The aspect ratio is defined as the ratio of length / OD. Therefore a comparison of the long and short MWCNT will reveal the impact of aspect ratio. On the other hand, a comparison of MWCNT and COOH-MWCNT will

highlight the influence of chemical modification since both CNTs have the same ID, OD and length.

In all of the MWCNT used, 95% percent of the total weight is MWCNT and approximately 1.5% of the weight was ash, and the rest was by products from MWCNT production. MWCNTs used were not washed or purified. As stated by the producing company, COOH-MWCNT contains 0.7% -COOH groups. The LDPE with a melt index of 0.75 g/10 min has a weight average molecular weight of 99.5 kg/mol and a MWD of 6.5 and a total short branch content of 22 branches/1000 C as determined by GPC and NMR, respectively, as reported earlier [48]. Maleic anhydride modified polyethylene (MAPE) used in the study was acquired from Aldrich. MAPE contained ~3wt.% maleic anhydride, its viscosity is 1700-4500 cP and melt temperature is 105°C. The LDPE resin and MWCNT-LDPE composites were conditioned (or blended) in a Haake PolyDrive melt blender. The blending temperature was 190°C. The rpm was 50 and time of blending was 10 min. From here onwards the long, short, and COOH modified MWCNT will be named LCNT, SCNT, and MCNT, respectively. Carver press was used to prepare samples at 190°C. The prepared samples were then used for SEM analysis and mechanical testing.

Table 4.2.1. Elementary compositions of MWCNT used in this study.

Components	Contents (%)
C	97.34
Cl	0.21
Fe	0.56
Ni	1.87
S	0.02

Table 4.2.2. Dimensions of the multi-walled carbon nano tubes (MWCNT).

Name	OD*	ID**	Length	Aspect ratio, (L/D)
Long MWCNT 95 wt%	30-50nm	5-15nm	10-20 μ m	375
Short MWCNT 95 wt%	30-50nm	5-15nm	0.5-2.0 μ m	31
COOH-MWCNT 95 wt%	30-50nm	5-15nm	10-20 μ m	375

*outer diameter, ** inner diameter

4.2.3.2. Scanning Electron Microscopy

Samples were dipped in liquid nitrogen for approximately 5 minutes to render them brittle and then shattered to reveal the cryo-fractured surfaces. A thin layer of gold was evaporated on the exposed fracture surfaces to make them electrically conducting to avoid charge build-up during examination within SEM. Field emission scanning electron microscope (FE-SEM) Model FEI Nova Nano SEM 230 having a probe resolution of 1.0 nm (at 15 keV) and accelerating voltage range of 50 V to 30 keV was used to observe the surface morphology of samples. Backscattered electron images were obtained using a low voltage high contrast detector (VCD). The samples were placed at a working distance of approximately 6 mm and scanned with an electron beam of spot size 3 operated at an accelerating voltage of 5 keV during SEM analysis.

4.2.3.3. Mechanical Testing

The samples were tested using an Instron 5560 Mechanical Testing Machine according to ASTM test standard D-638. All tests were conducted at constant strain rate of 50 mm/min. The measured stress / strain data was used to find all the mechanical properties. Maximum of five samples were tested for each composition. The maximum standard deviation for yield strength, ultimate strength, Young's modulus, percent Elongation and toughness were 0.6, 1.7, 33.8, 1.35 and 17.6 respectively.

4.2.3.4. Differential Scanning Calorimetry

All DSC measurements were performed using a TA Q1000 instrument equipped with a liquid nitrogen cooling system and auto sampler. Nitrogen at a flow rate 50 ml/min was used to purge the instrument to prevent degradation of the samples upon thermal

treatments. The DSC was calibrated in terms of melting temperature and heat of fusion using a high purity indium standard (156.6°C and 28.45 J/g). The absolute crystallinity was calculated using the heat of fusion of a perfect polyethylene crystal of 290 J/g.

Composite samples (5–10 mg) were sliced and compressed into a non-hermetic aluminum pans. To minimize the thermal lag between the sample and the pan, samples with flat surface were used. An empty aluminum pan was used as reference. First, the baseline was calibrated using empty crimped aluminum pans. All testing was performed in the standard DSC mode. Initially the samples were heated from room temperature to 200°C at a rate of 10°C/min; followed by a hold up at 200°C for 2 min. All samples were cooled to sub ambient temperatures for complete evaluation of crystallinity. The samples were cooled from 200° to -10°C at a rate of 10°C/min. After that the sample was heated from -10°C to 200°C at 10°C/min.

4.2.4. Results & Discussion

4.2.4.1. Morphology of the LDPE/MWCNT composites

The surface morphology of SCNT-LDPE composite at 0.5% and 5.0% loading without compatibilizer (control sample) is shown in the backscattered FE-SEM images of Fig. 4.2.1.a and 4.2.1.b. Images show agglomeration of MWCNT within the matrix of LDPE. Evidence of dispersion was not found in this group of composites. Agglomeration was also observed for LCNT-LDPE composite with 0.5% and 5.0% loading, as seen in the FE-SEM image of Fig. 4.2.1.c. A higher magnification image clearly shows that the agglomerated region is composed of a large number of MCNTs present within the composite matrix (Fig. 4.2.1.d). This agglomeration was not localized at a particular

region but was seen to be distributed across the matrix of the composite, as shown in the FE-SEM images of Fig. 4.2.1.e and 4.2.1.f. Evidence of dispersion was not found in this group of composites produced without the addition of a compatibilizer.

Also, FE-SEM images show that the addition of compatibilizer to both LCNT and MCNT nanocomposites improved their dispersion, as seen in the micrographs of Fig. 4.2.2.a-d. The degree of dispersion of MCNT in LDPE matrix was seen to be higher in MCNT compared to LCNT composites. Greater improvement in dispersion within MCNT could be attributed to the synergistic effect of compatibilizer with COOH modification present within this group of composites. A similar effect was also observed by Jin et al [31] while using maleic anhydride grafted polypropylene.

It is clear that the addition of a compatibilizer and COOH modification of CNT has improved the dispersion of MCNT. In the following sections we will assess the impact of this improvement in dispersion on the mechanical and thermal properties of PE composites with low and high aspect ratio.

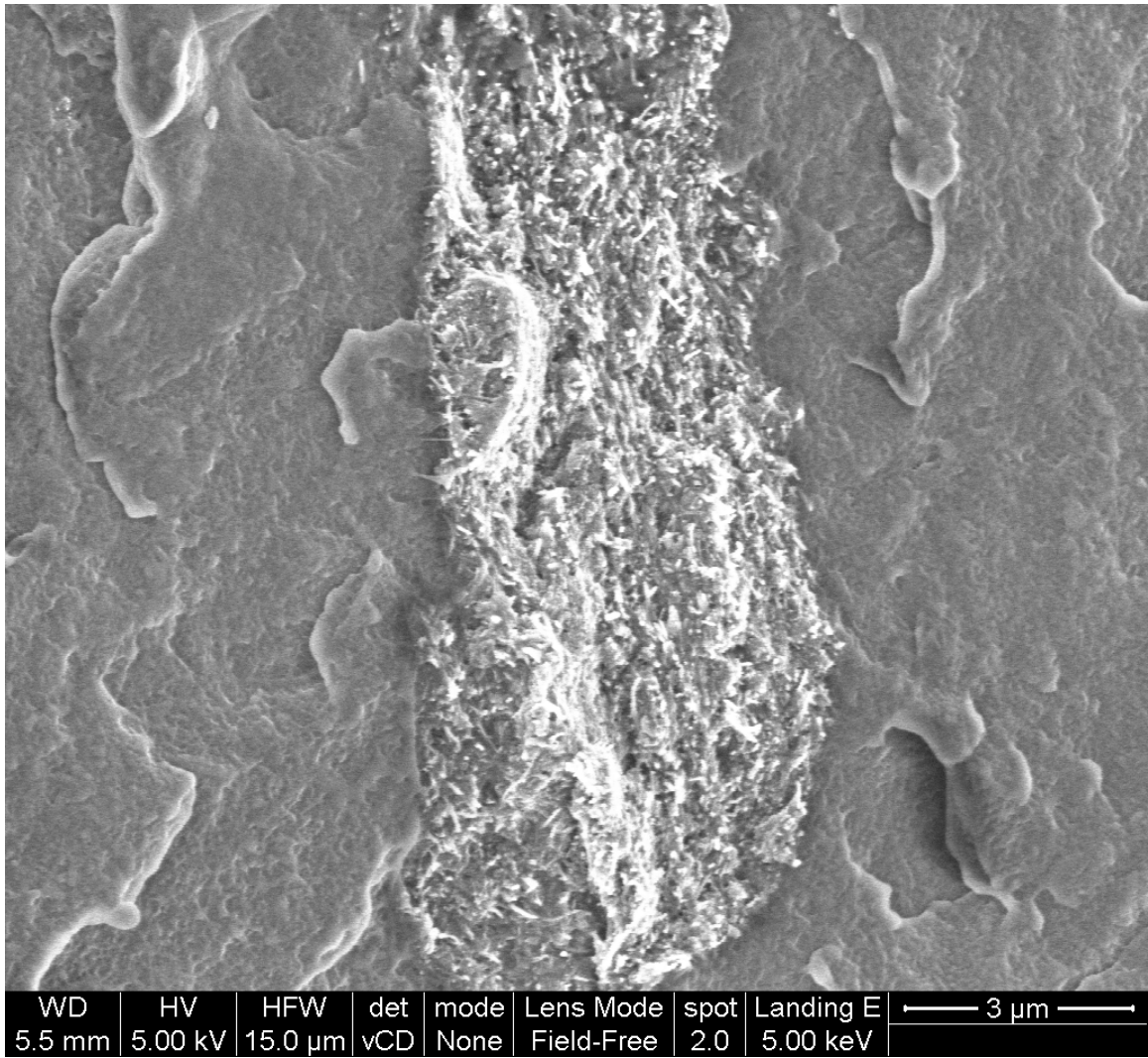


Figure 4.2.1.a. FE-SEM image of SCNT-LDPE nanocomposite with 0.5% loading.

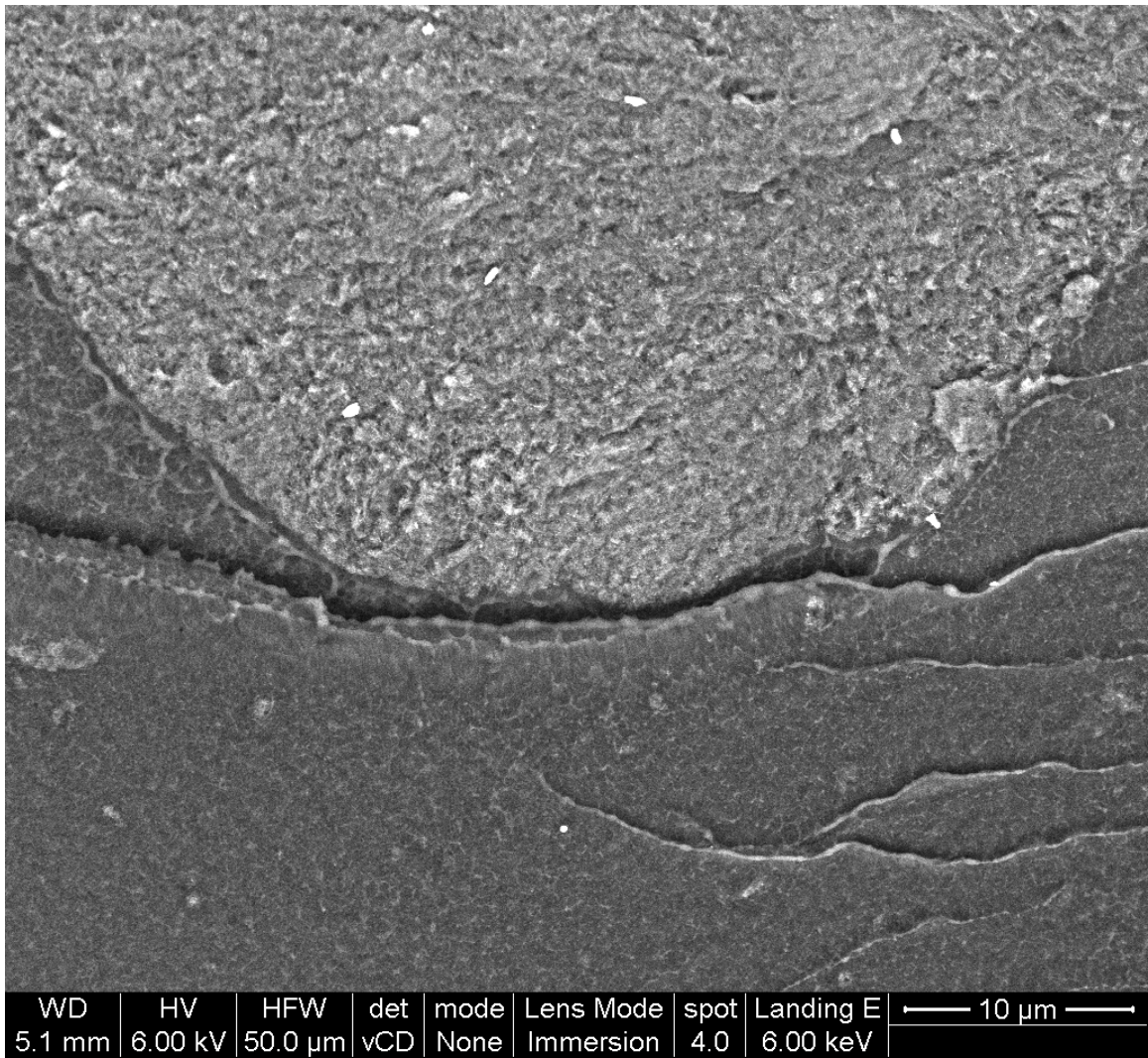


Figure 4.2.1.b. FE-SEM image of SCNT-LDPE nanocomposite with 5.0% loading.

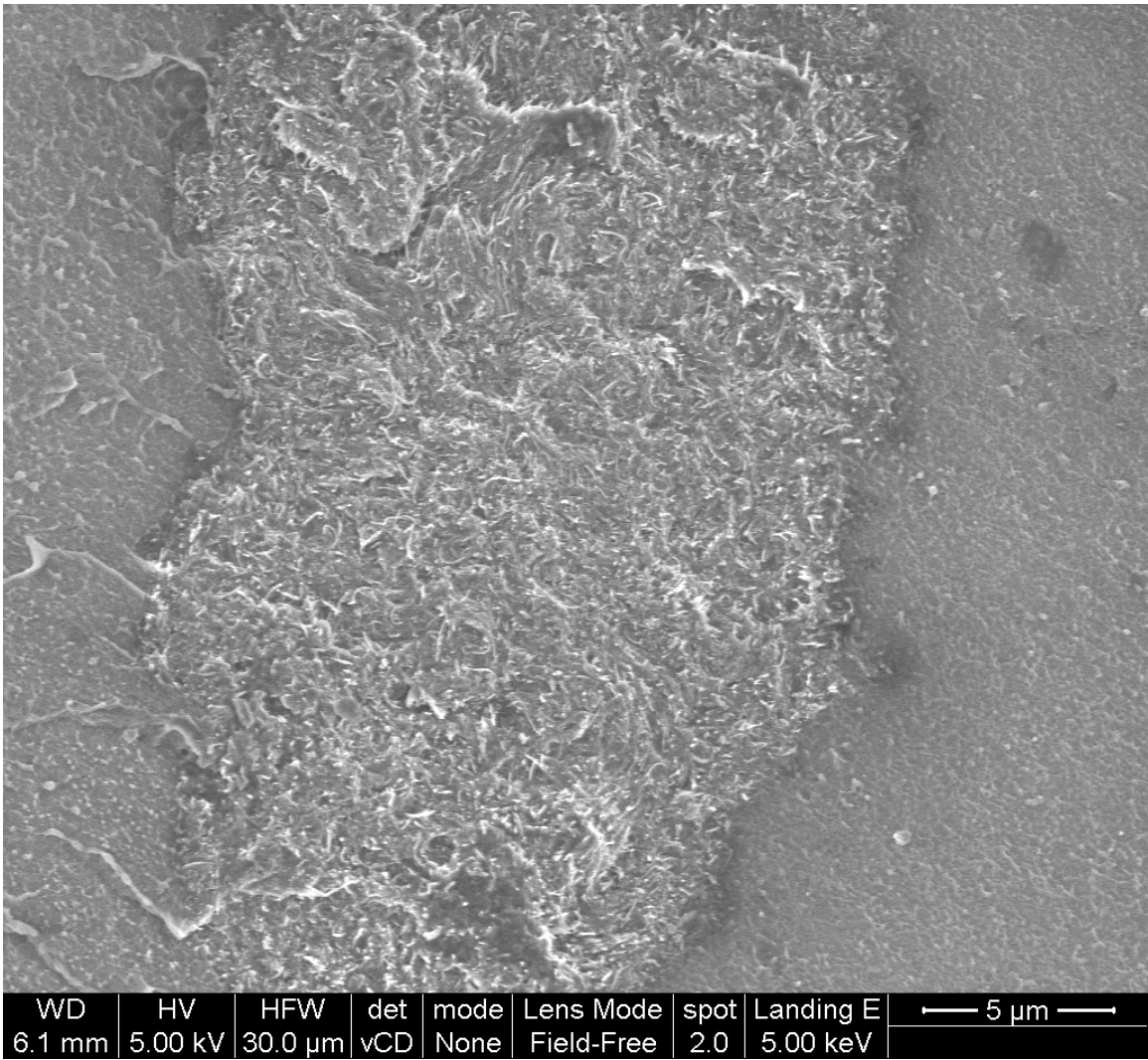


Figure 4.2.1.c. FE-SEM image of LCNT-LDPE nanocomposite with 0.5% loading.

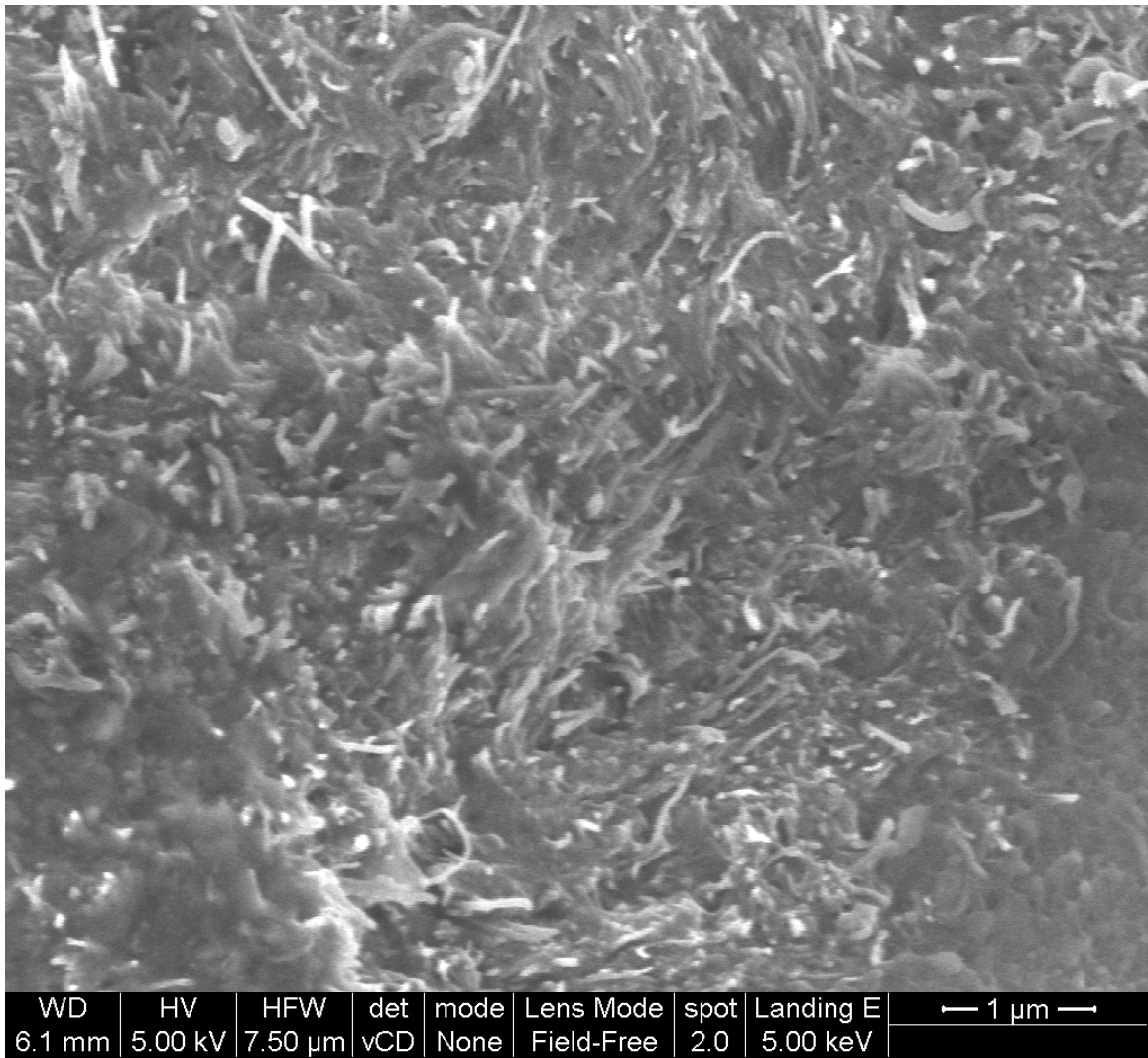


Figure 4.2.1.d. FE-SEM image of LCNT-LDPE nanocomposite with 0.5% loading.

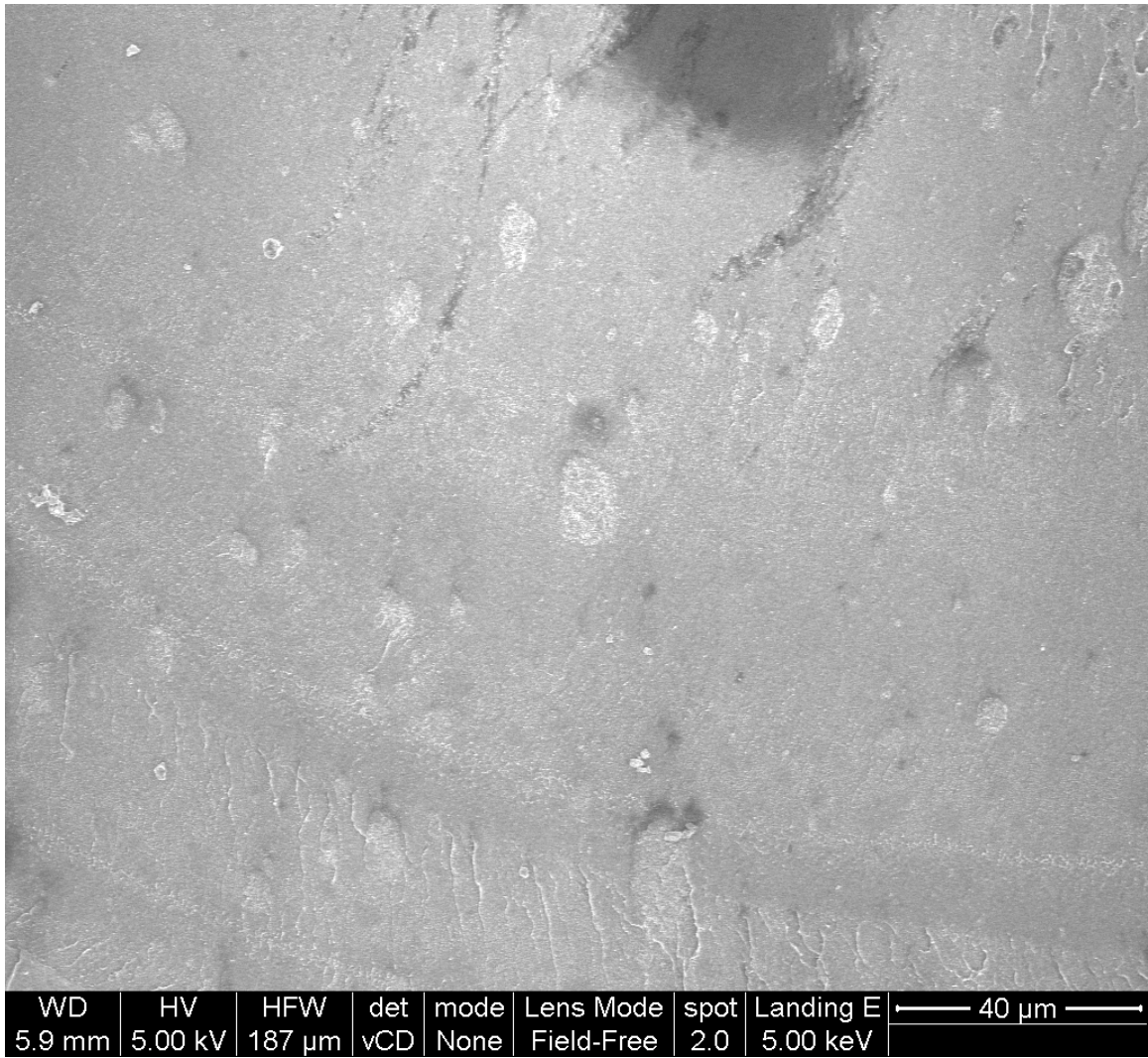


Figure 4.2.1.e. FE-SEM image of LCNT-LDPE nanocomposite with 5.0% loading.

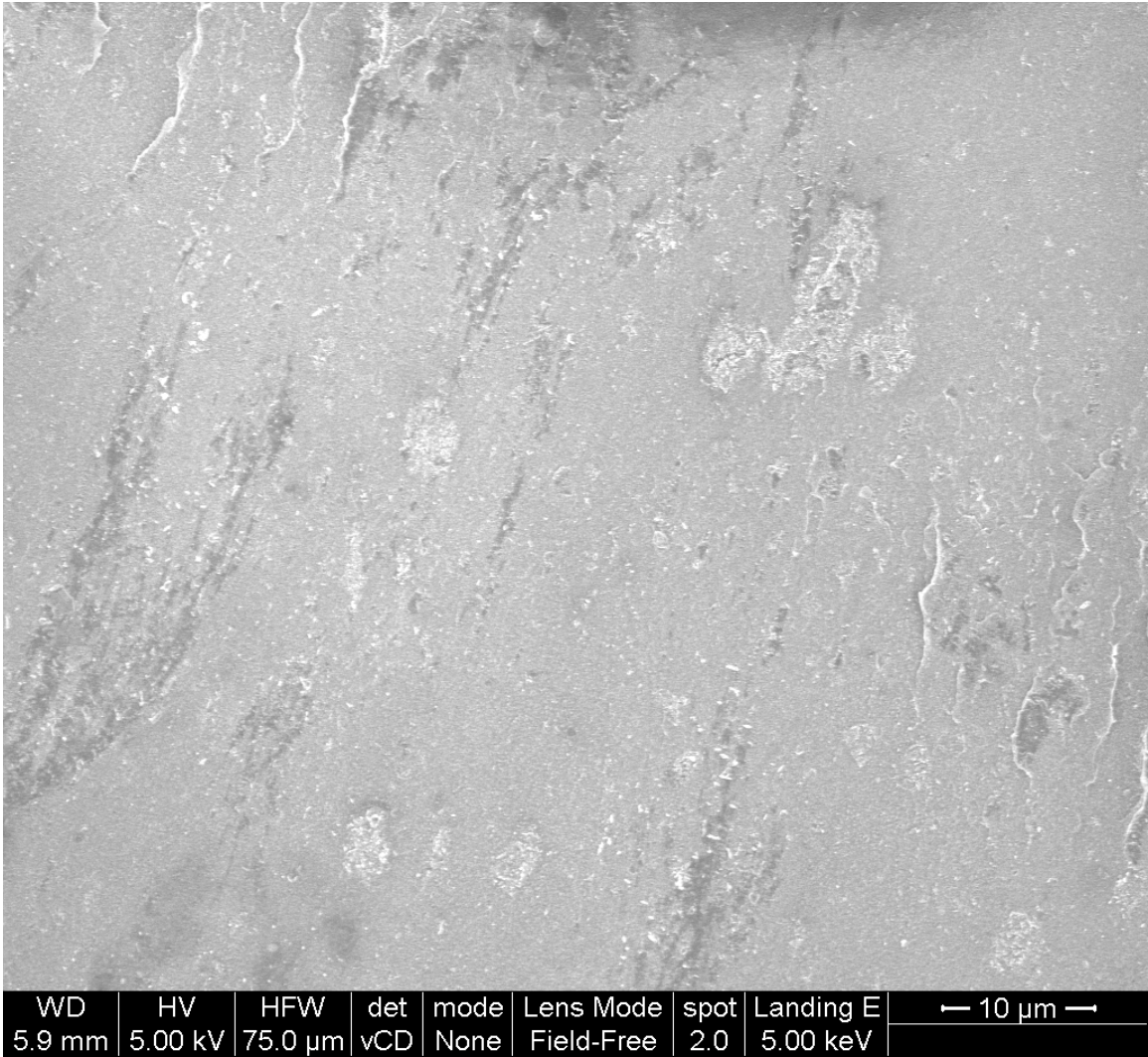


Figure 4.2.1.f. FE-SEM image of LCNT-LDPE nanocomposite with 5.0% loading.

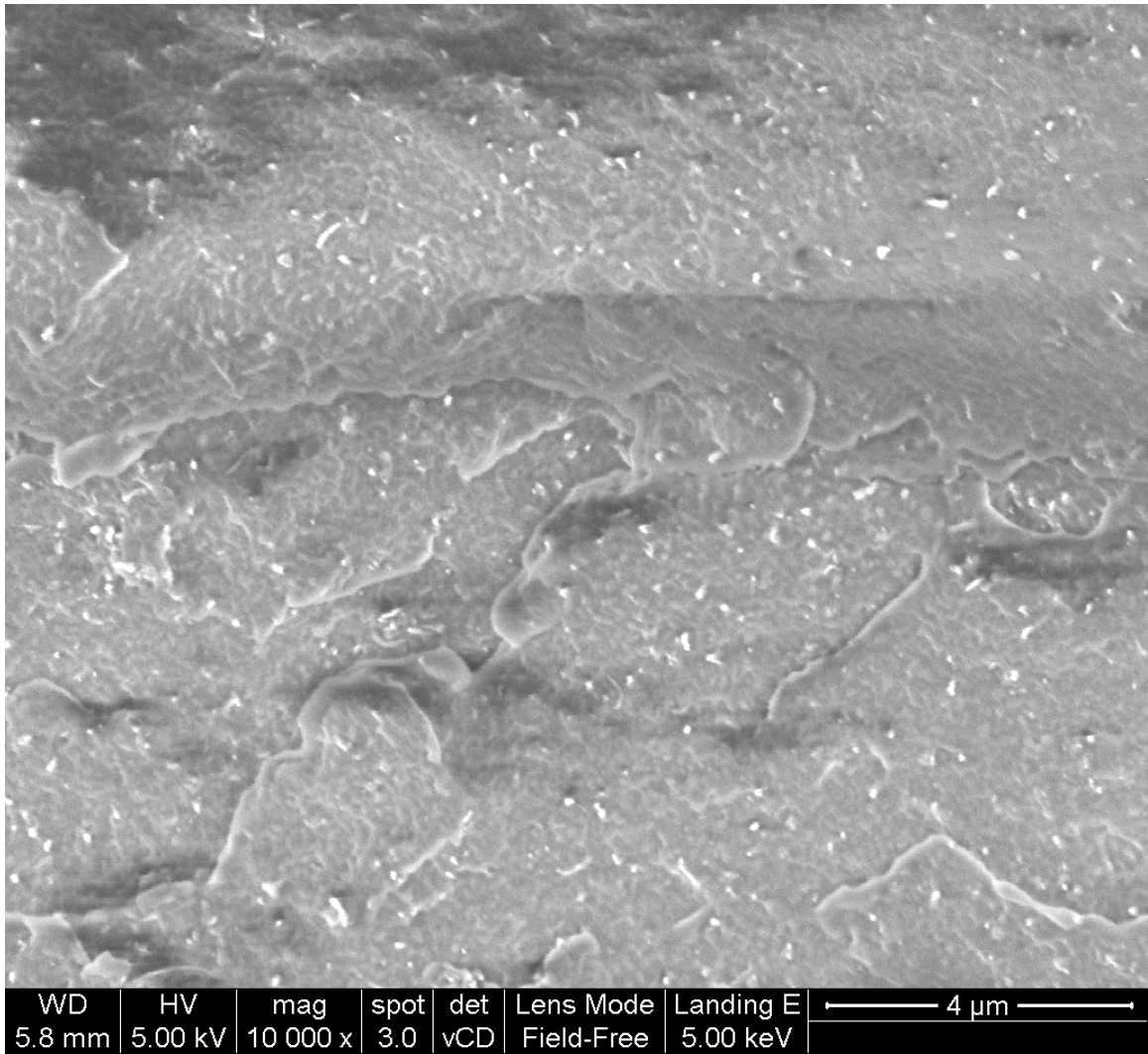


Figure 4.2.2.a. FE-SEM image of LCNT-LDPE nanocomposite with 5.0% loading coupled with 2.0% MAPE.

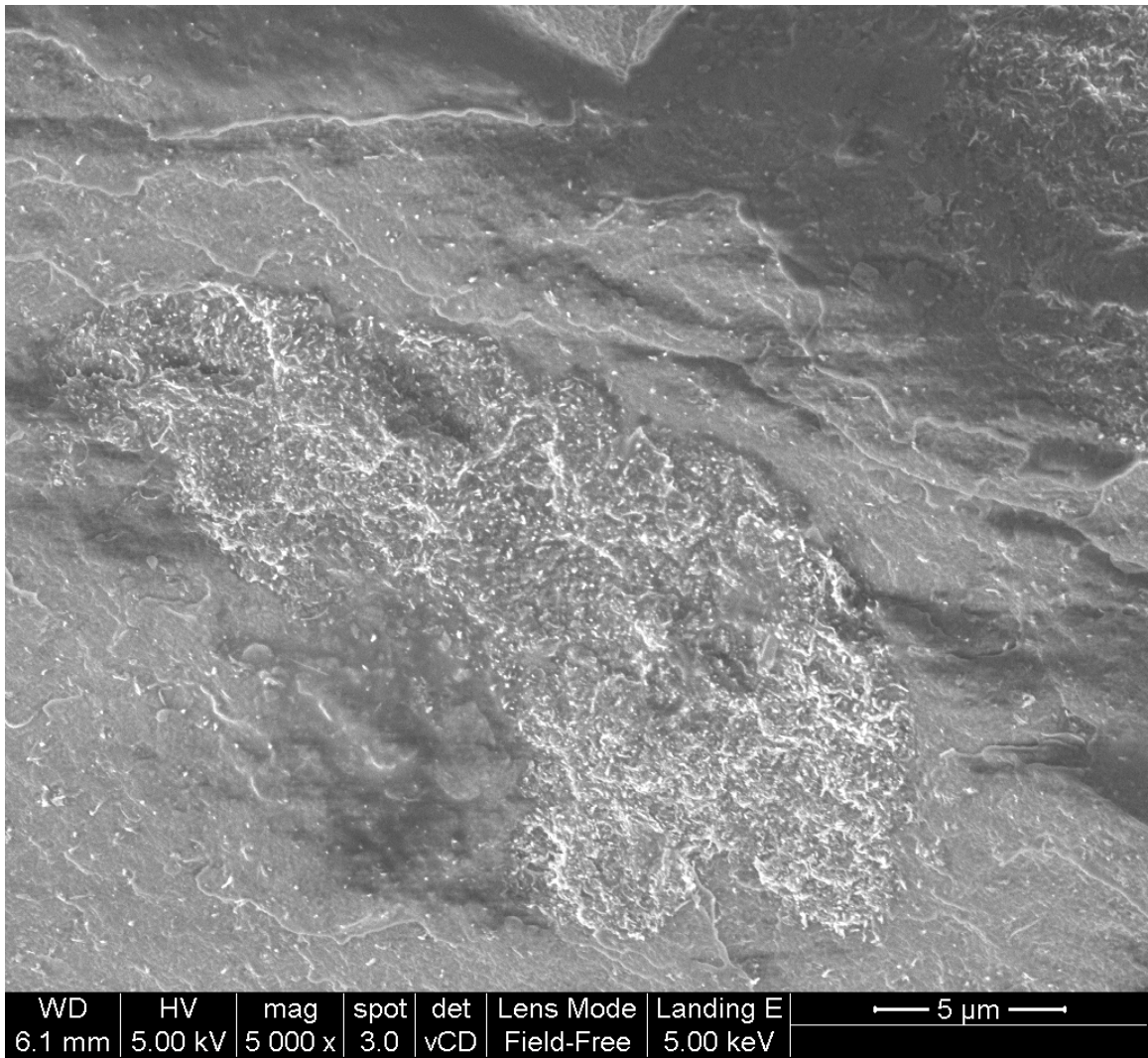


Figure 4.2.2.b. FE-SEM image of LCNT-LDPE nanocomposite with 5.0% loading coupled with 2.0% MAPE.

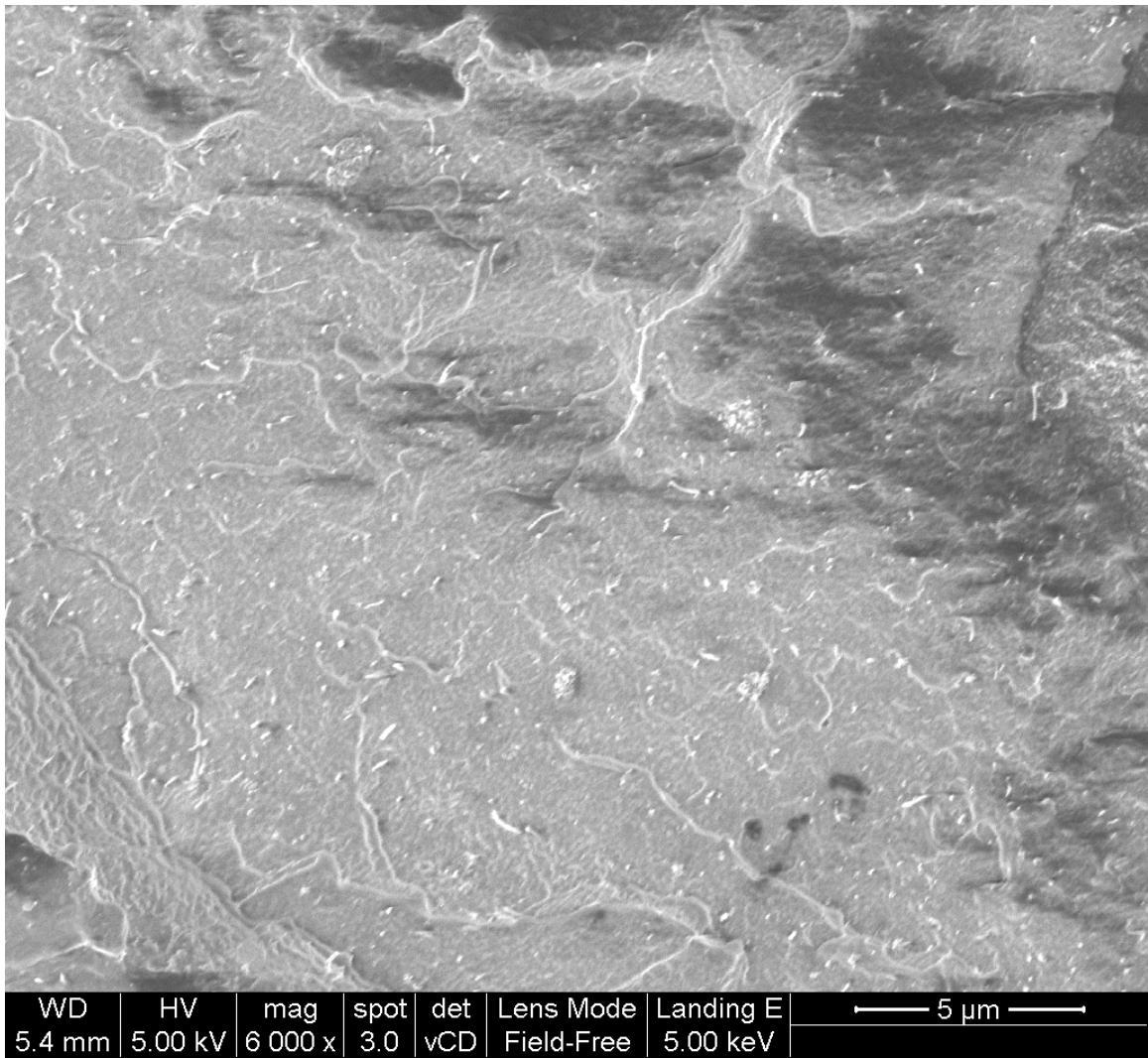


Figure 4.2.2.c. FE-SEM image of MCNT-LDPE nanocomposite with 5.0% loading coupled with 2.0% MAPE.

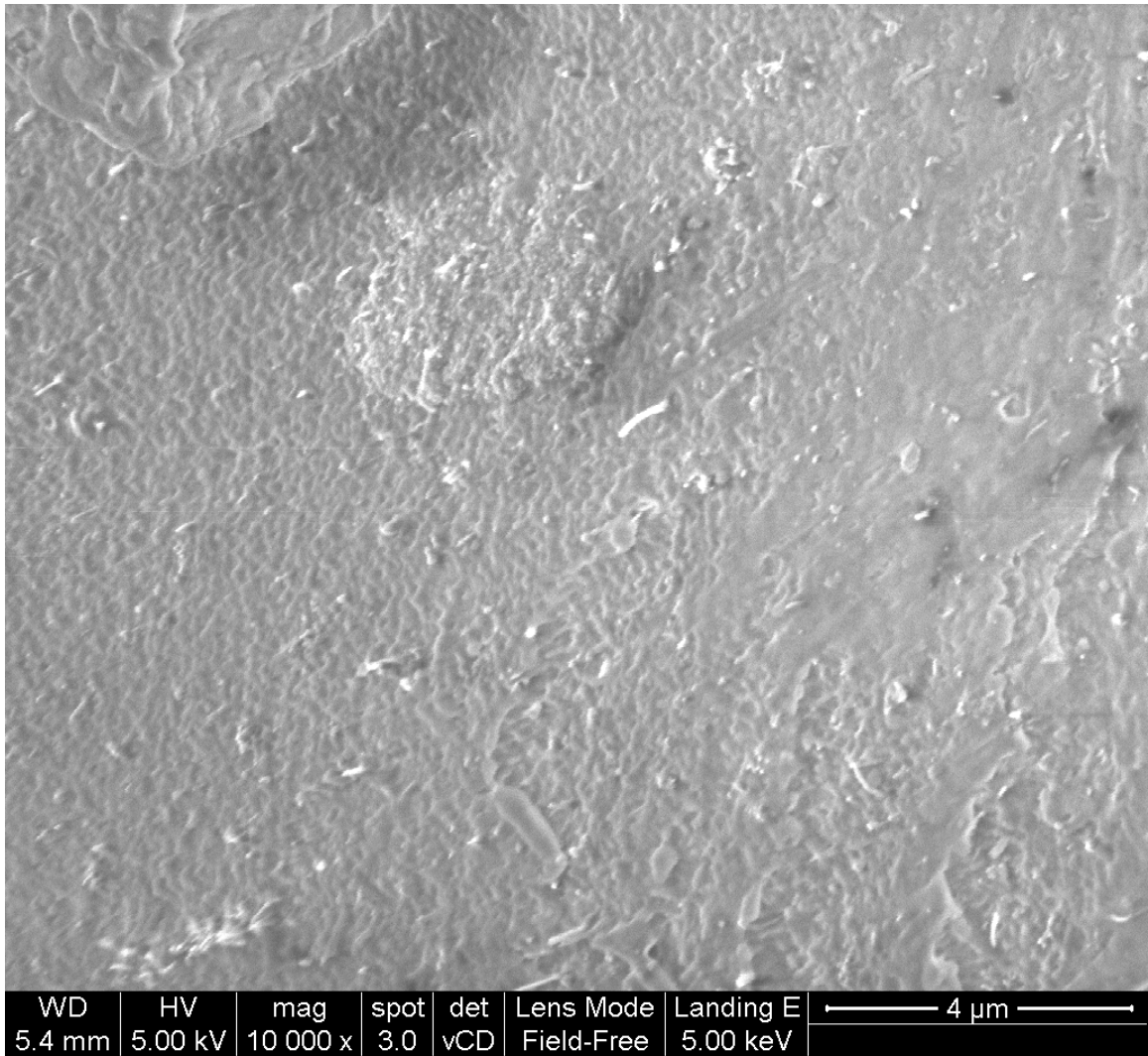


Figure 4.2.2.d. FE-SEM image of MCNT-LDPE nanocomposite with 5.0% loading coupled with 2.0% MAPE.

4.2.4.2. Mechanical Testing

Fig. 4.2.3. shows the stress-strain response for pure LDPE and LDPE nanocomposites with MCNT at various loadings. It can be observed that pure LDPE shows significant strain hardening at high elongation, which is expected. When MCNT is added at 0.5 weight %, still almost the same strain hardening effect is observed as the pure LDPE. However, as the loading is increased to 2.0 % we barely see any strain hardening and it disappears at 5.0 % loading of MCNT. A similar trend was obtained for LCNT and SCNT based composites. These results suggest that at 0.5 % loading the CNT acts as a plasticizer to increase chain mobility. These findings are in agreement with the previous reports that showed similar behavior for UHMWPE at 1 % CNT loading. Also, our results that composites with 2 % MCNT and higher concentrations show a behavior that is similar to that of fillers is in agreement with previous literature reports [49-50]. Similar trends were obtained for SCNT and LCNT.

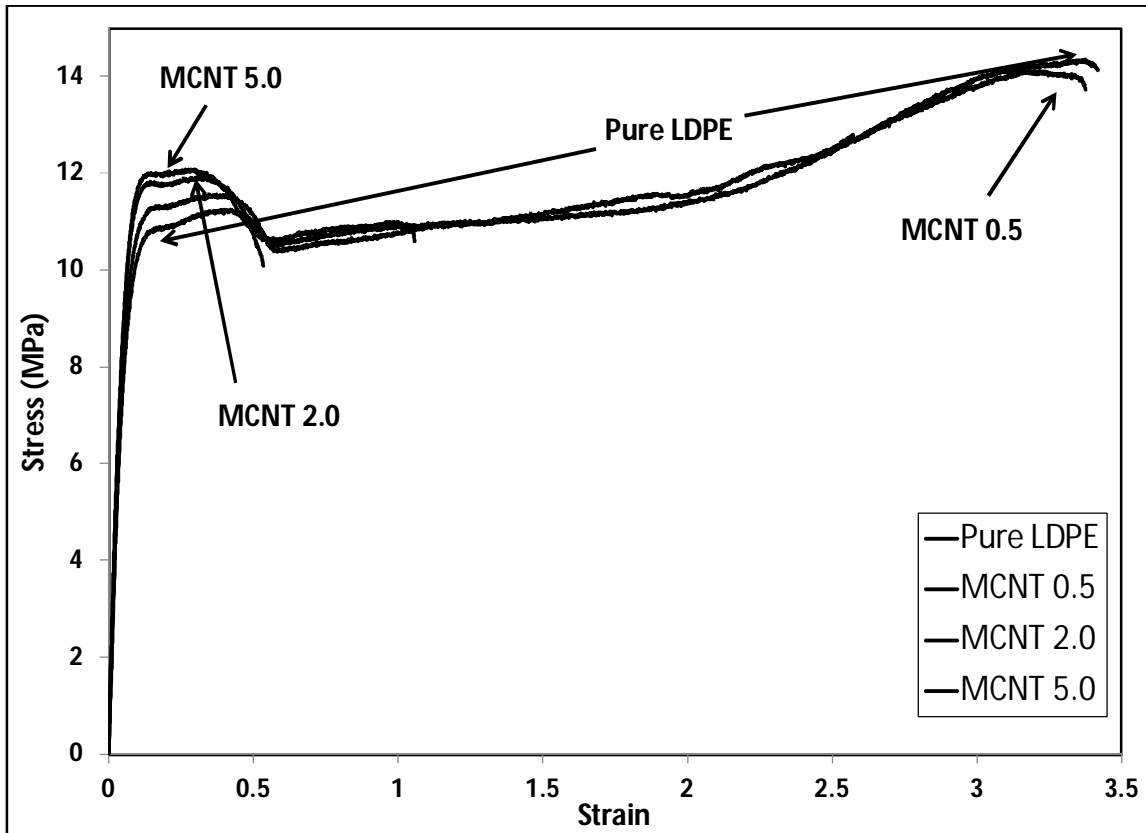


Figure 4.2.3. Tensile stress-strain diagram for Pure LDPE & various loadings of MCNT.

The results of yield strength of pure LDPE and its composites at various loadings are shown in Fig. 4.2.4.a. Fitting lines are shown for LCNT nanocomposites only and other results are left without fitting to improve clarity of the figure. First, almost all loadings produce yield strength higher than that of pure LDPE. Second, as the loading is increased the yield strength is also increased. Both LCNT and MCNT, having the same high aspect ratio, show higher values of yield strength at all loadings. MCNT produces a high yield strength of 11.9 MPa at 5.0% loading compared to 9.2 MPa for pure LDPE. So, both the high aspect ratio and chemical modification increase the yield strength. Also, MCNT at 5.0 weight % loading produces an increase of 30% in the yield strength. Despite the variation in the degree of dispersion present within different types of nanocomposites studied here, an increase in yield strength was observed for all samples with increased loading.

Addition of 2.0% MAPE resulted in an increase in yield strength for both LCNT and MCNT composites (Fig. 4.2.4.b). This increase depends on the loading of MWCNT. LCNT-MAPE composite with 5.0% loading produced a high yield strength of 13.4 MPa, which is an increase of approximately 46% compared to pure LDPE. MCNT-MAPE composite produced a maximum yield strength of 13.3 MPa. So, there is no significant difference in the yield strength obtained from composites of MCNT and LCNT with MAPE. Therefore, it can be concluded that high aspect ratio is responsible for the high yield strength at all loadings. In addition, in the presence of MAPE the effect of chemical modification is not significant. The improved distribution of MWCNT in the PE matrix is likely responsible for these improvements in the yield strength as well as the other

mechanical properties. The effect of COOH modification of MCNT, although it is of low concentration, is weak at 0.5% loadings, but some improvement was detected at 2 and 5 % loadings. However, the impact of MAPE is noticeable at all loadings. Results of MCNT vs MCNT-MAPE nanocomposites support this observation. Furthermore, addition of MAPE improved the dispersion of CNT; hence improved the yield strength at all loadings for both LCNT and MCNT composites. Improvement in dispersion was supported by the results of FE-SEM discussed earlier.

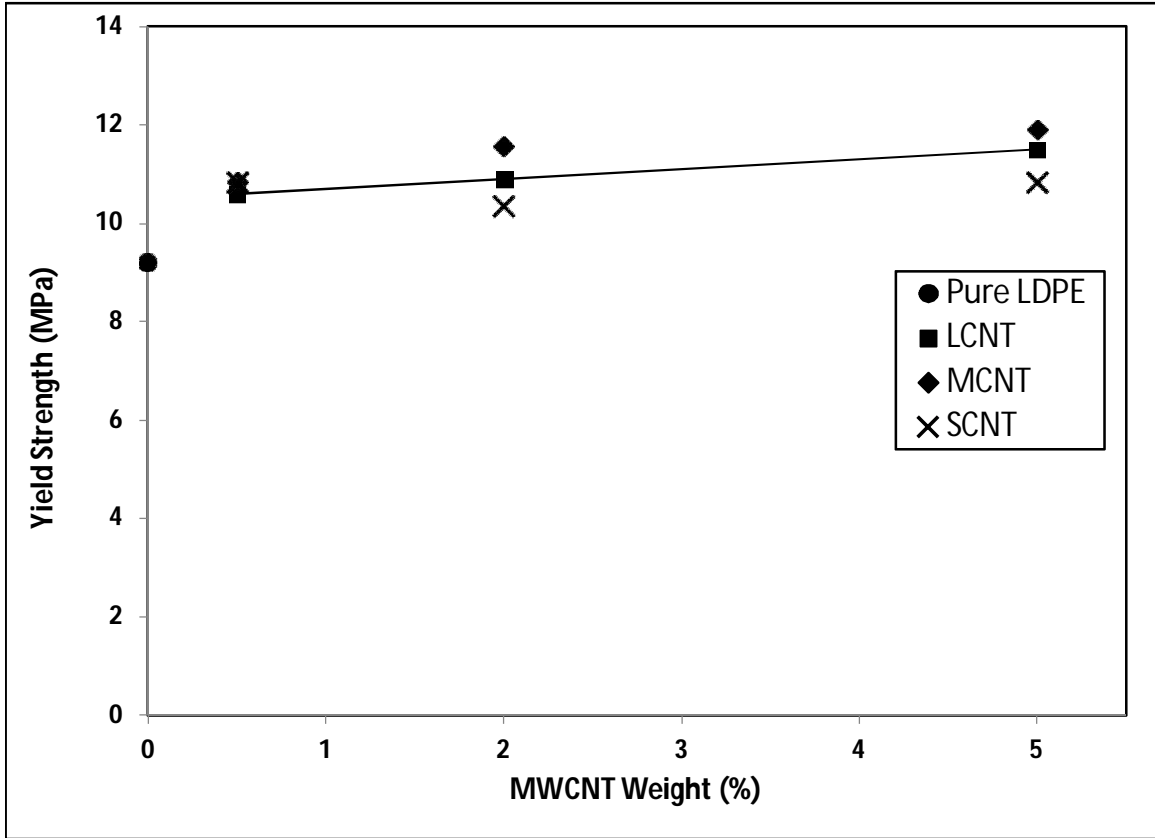


Figure 4.2.4.a. Yield strength at various loading for LDPE and its composites.

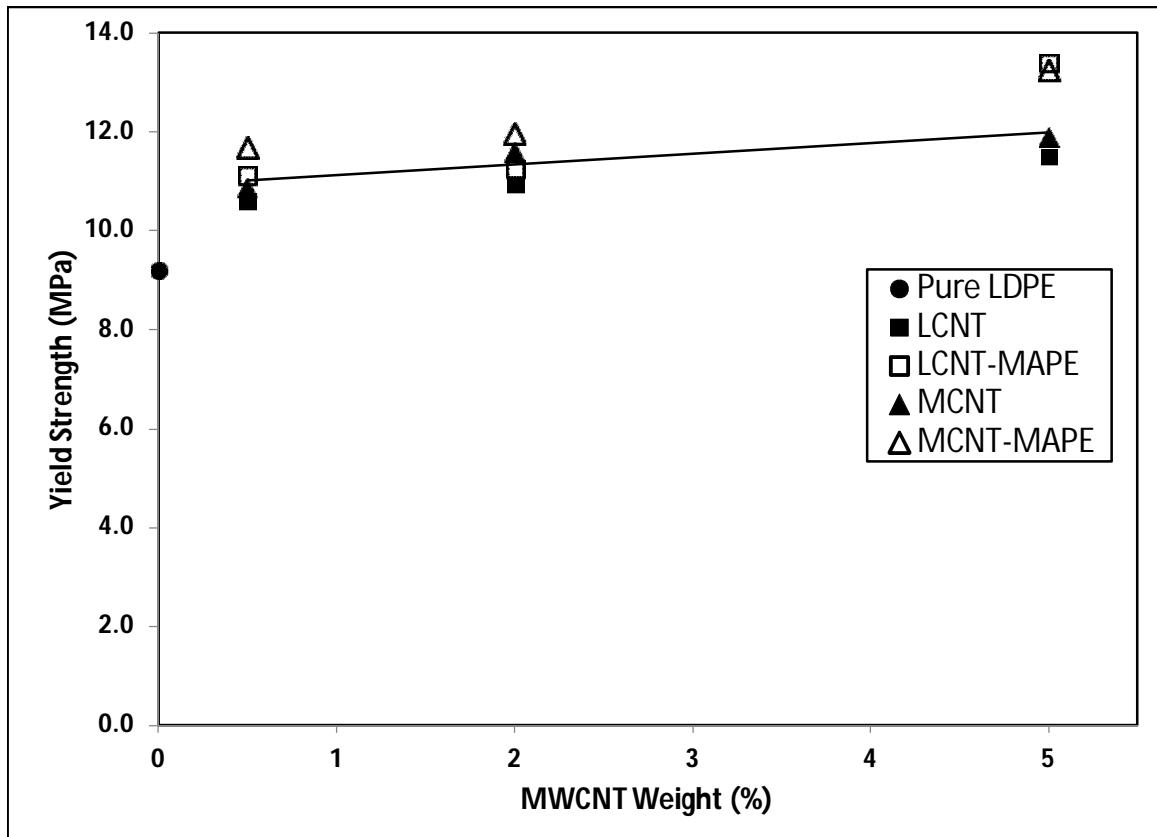


Figure 4.2.4.b. Yield strength at various loading for LDPE and its LCNT, MCNT composites with and without 2.0% MAPE.

Fig. 4.2.5.a displays the ultimate strength of pure LDPE and its nanocomposites at various loadings. Pure LDPE has the highest ultimate strength (13.9 MPa) as compared to all composites at various loadings. For 0.5 and 2.0 weight % loadings, the ultimate strength tends to drop. We know that ultimate strength is the maximum stress on the stress-strain curve. The reason for this reduction is the complete loss of strain hardening behavior from 0.5% to 2.0% loading. But, as the loading is further increased to 5.0 weight %, the maximum stress of the material is increased. Hence ultimate strength is increased for the three types of nanocomposites, however aspect ratio and MAPE tend to increase the ultimate strength.

In general, addition of 2.0% MAPE to LCNT and MCNT nanocomposites show ultimate strength that is higher than pure LDPE (Fig. 4.2.5.b). On the other hand, the ultimate strength for the same samples without MAPE is lower than that of pure LDPE. This behavior is suggested to be due to agglomeration of CNTs and weak interfacial bonding with LDPE. The trend of decreasing ultimate strength with increased loading still holds for composites with MAPE. The highest ultimate strength was 16.1 MPa and achieved for LCNT with MAPE at 2.0% loading. This represents an increase of 16% in ultimate strength over that of pure LDPE. Hence, the high aspect ratio resulted in high ultimate strength at all loadings covered in this study. Decrease in ultimate strength with increased loading holds for all aspect ratios, with and without MAPE. The use of 2% MAPE has increased the ultimate strength for LCNT and MCNT at all loadings. Again, the addition of MAPE improved the dispersion in the nanocomposite material; hence increased the ultimate strength for both LCNT and MCNT composites at all loadings.

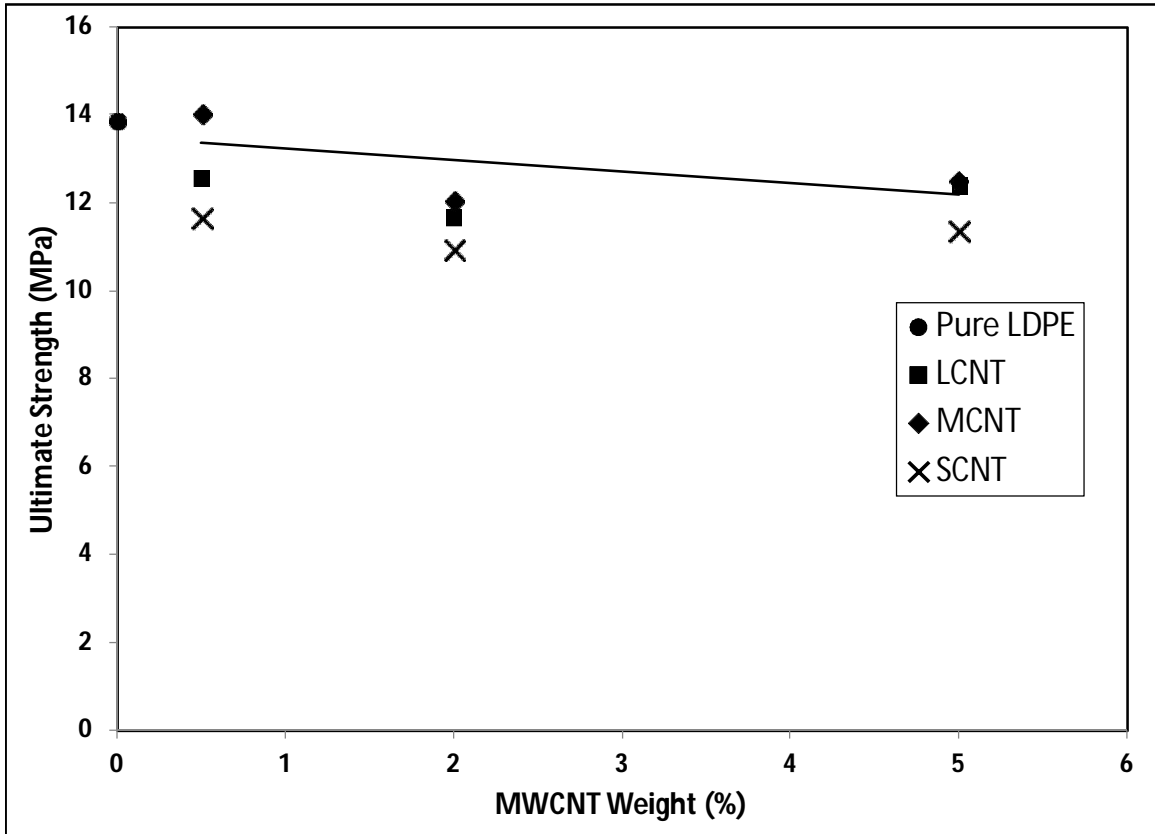


Figure 4.2.5.a. Ultimate strength for pure LDPE and its various composites.

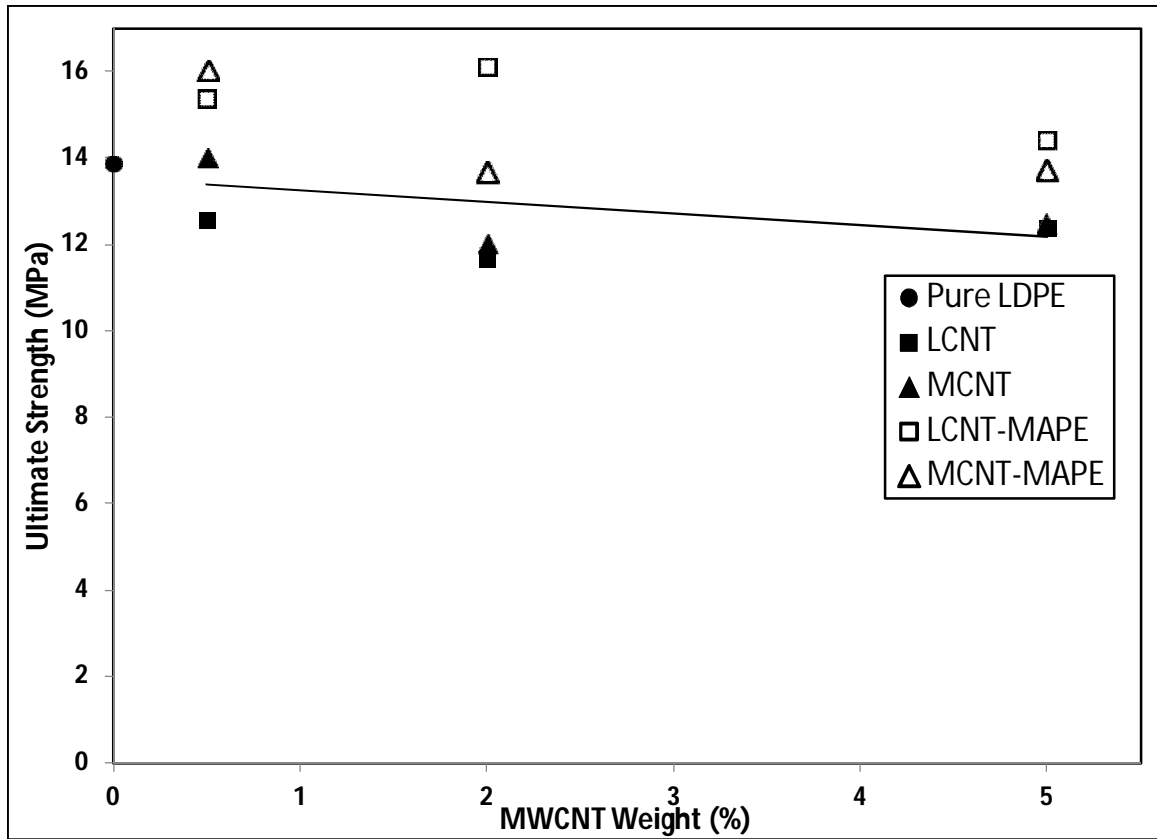


Figure 4.2.5.b. Ultimate strength for pure LDPE and various loading for LDPE and its LCNT, MCNT composites with and without 2.0% MAPE.

Results of Young's modulus for pure LDPE and its composites at various loadings are given in Fig. 4.2.6.a. Generally, as the MWCNT loading is increased, the Young's modulus is also increased. The highest modulus is observed for 5.0 weight % of MCNT. Pure LDPE has a modulus of 112 MPa while 5.0 weight % of MCNT produced a modulus of 144 MPa. This represents an increase of 28 % in modulus. Fig. 4.2.6.b shows Young's modulus for pure LDPE and its LCNT and MCNT composites at various loadings in the presence of 2.0% MAPE. Young's modulus increased with CNT loading and it increased even further with the addition of MAPE. The highest value was achieved for 5.0% loading of MCNT with 2.0% MAPE. This represents an increase of 48% when compared to pure LDPE. So, composites with high aspect ratio CNTs have high Young's moduli at all loadings. This finding is in agreement with theoretical predictions of Young's modulus by the modified form of rule of mixtures discussed in previous literature [46-47]. Addition of 2.0% of MAPE increases the Young's modulus to higher values.

Regarding the percent elongation (Fig. 4.2.7.a), the addition of unmodified MWNCT tends to reduce the percent elongation of pure LDPE. Elongation drops with the addition of 0.5% CNT from 735% for pure LDPE, to 551, 445 and 357 % for composites of MCNT, LCNT and SCNT, respectively. The elongation at break drops down to less than 100%, for all three types of composites at 5.0% loading. A comparison of the results of SCNT and LCNT at 0.5% loading suggests that high aspect ratio resulted in a higher elongation at break. This observation is in line with our previous results that showed at such low concentrations the CNT is playing the role of a plasticizer. It is evident that

CNT with high aspect ratio creates more free volume in the polymer composite. On the other hand, the chemical modification of MCNT is responsible for improving the interfacial bonding between the CNT and the polymer leading to a higher elongation at break over LCNT of the same aspect ratio. Addition of 2.0% MAPE to the nanocomposites tends to improve other properties, but in the case of elongation (Fig. 4.2.7.b), its presence did not have the same effect. LCNT and MCNT nanocomposites with and without 2.0% MAPE and at 5.0% loading tend to show elongation values between 88 and 118%. The lower aspect ratio is showing the lowest elongation at all loadings. For all different types of LCNT and MCNT, with and without the addition of 2.0% MAPE, the elongation at break decrease significantly with increased loading of the CNT. No significant influence for aspect ratio or chemical modification can be detected at high loadings.

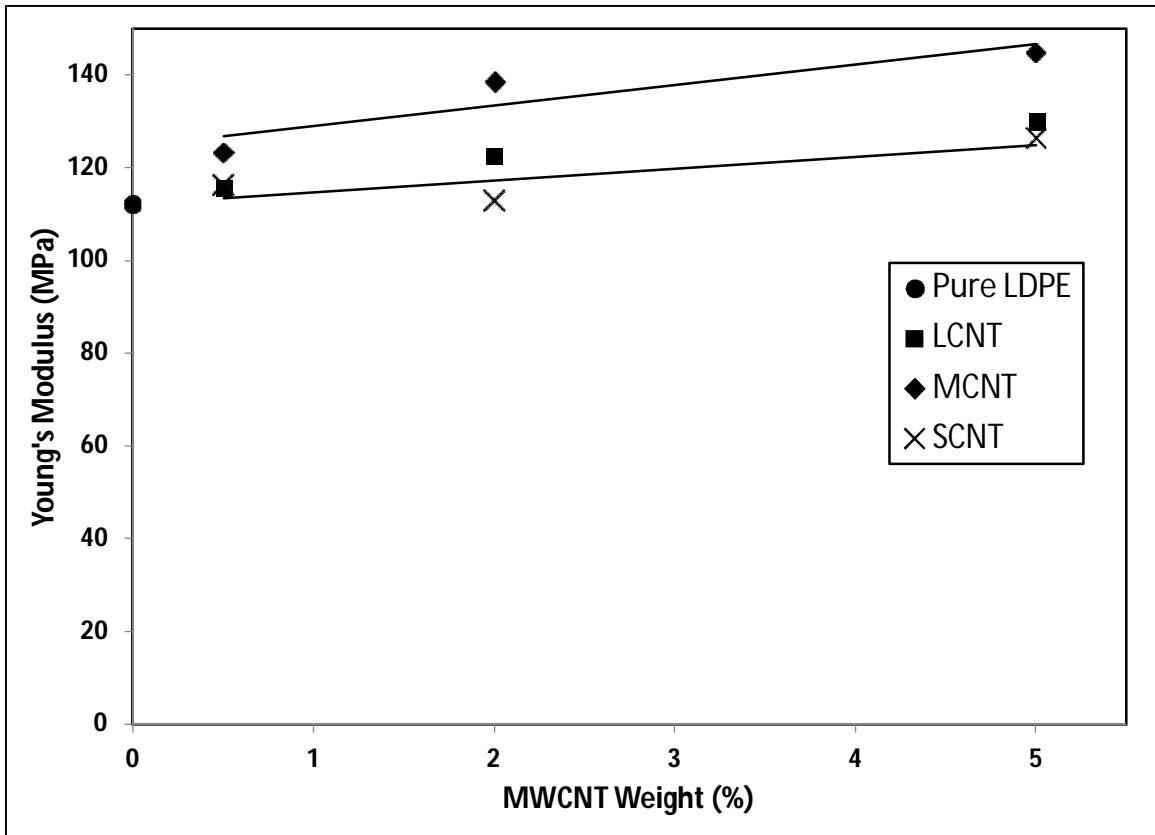


Figure 4.2.6.a. Young's Modulus for pure LDPE and its composites at various loadings.

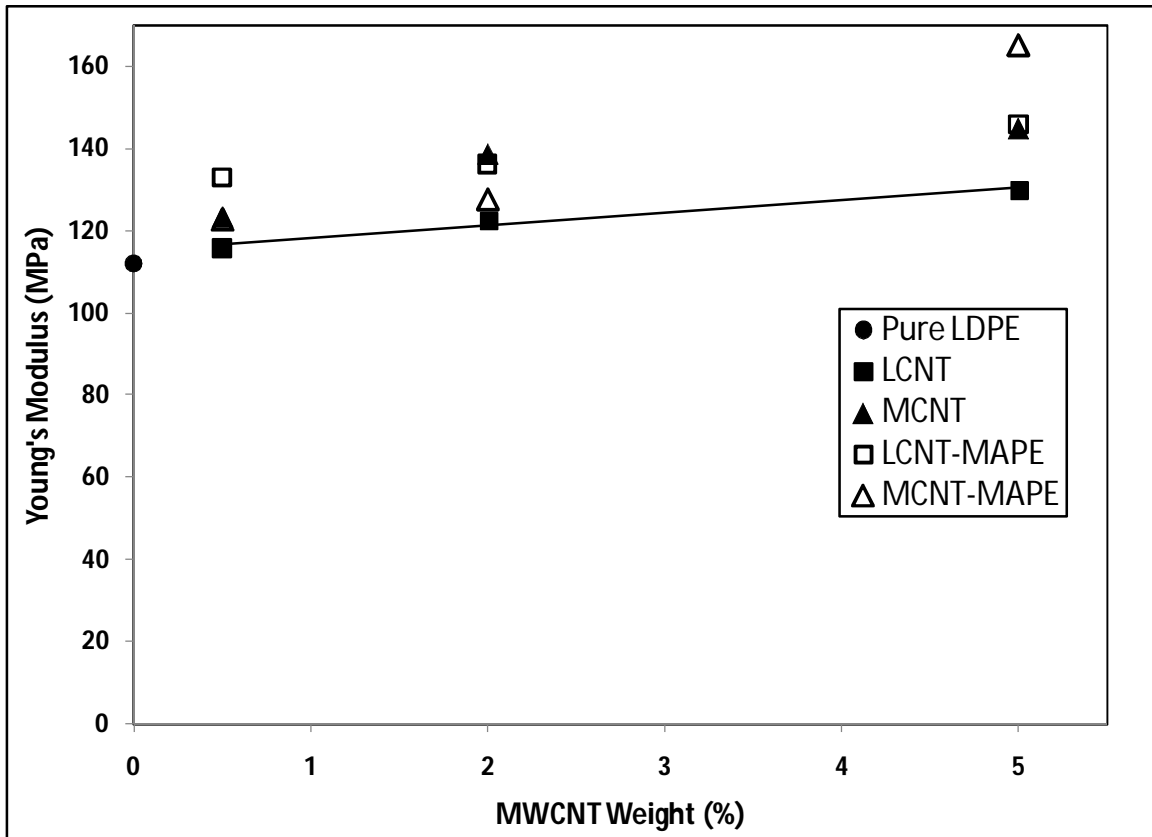


Figure 4.2.6.b. Young's Modulus for pure LDPE and its composites for LCNT, MCNT at various loadings with 2% MAPE.

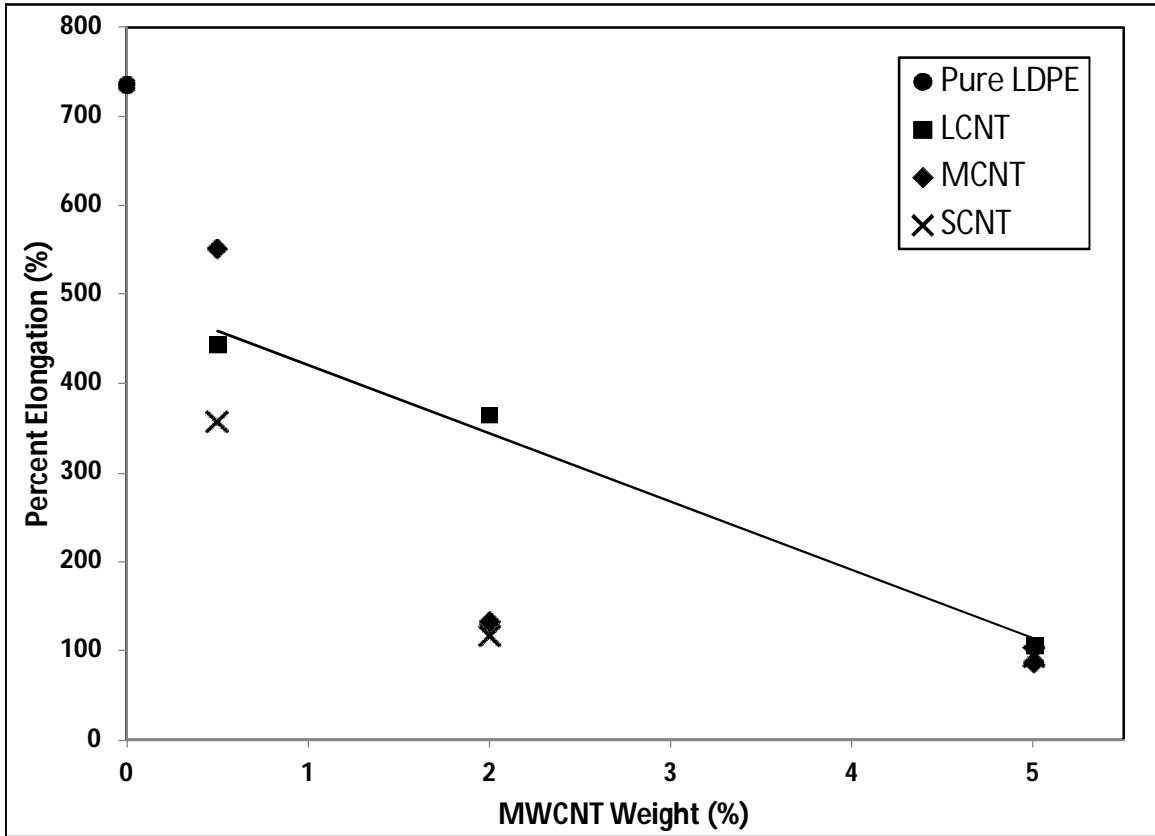


Figure 4.2.7.a. Percent elongation of pure LDPE and its composites at various loadings.

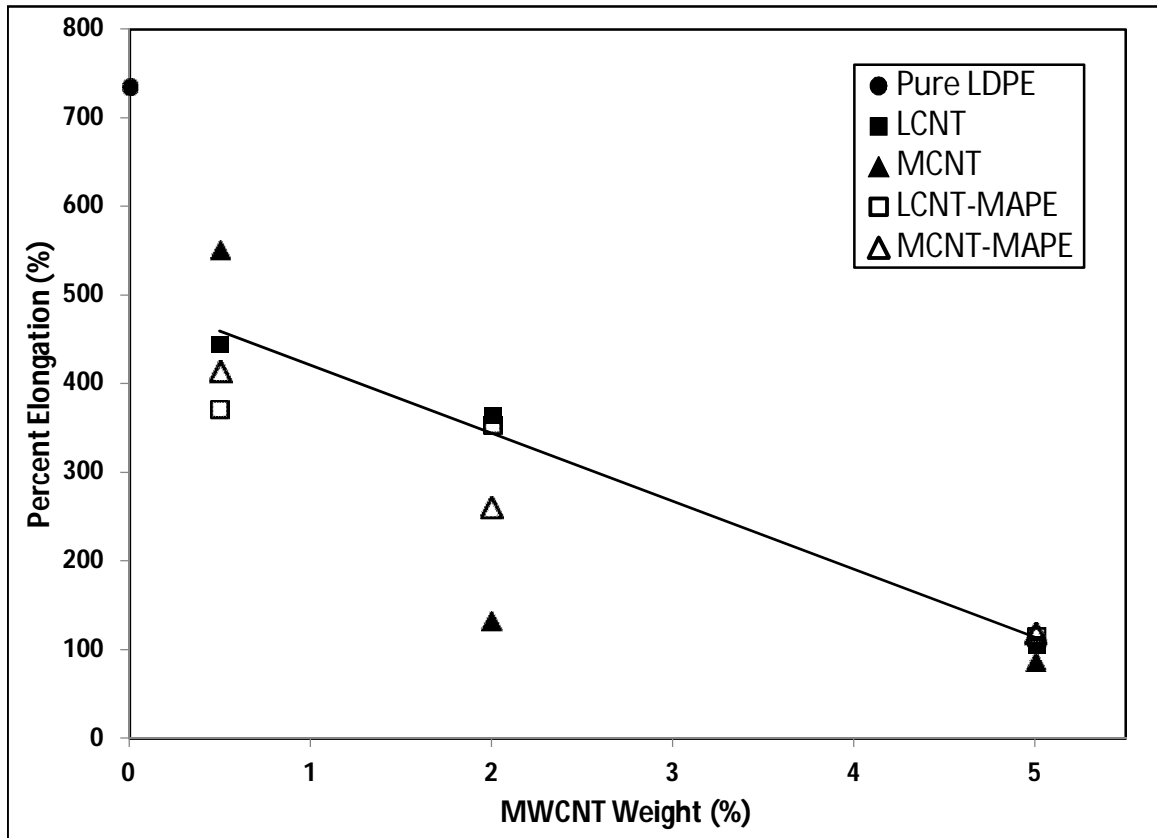


Figure 4.2.7.b. Percent elongation of pure LDPE and its composites of LCNT, MCNT at various loadings with 2.0% of MAPE.

Figure 4.2.8.a displays the toughness for pure LDPE and its nanocomposites at various loadings. Again, since the toughness is related to percent elongation of the material so we also observe that as the amount of loading for various MWCNT is increased the toughness of the produced composite is decreased. Figure 4.2.8.b shows that the addition of 2.0% MAPE did not increase the toughness of the material. All nanocomposites showed similar values of toughness at 5.0% loading, with and without MAPE.

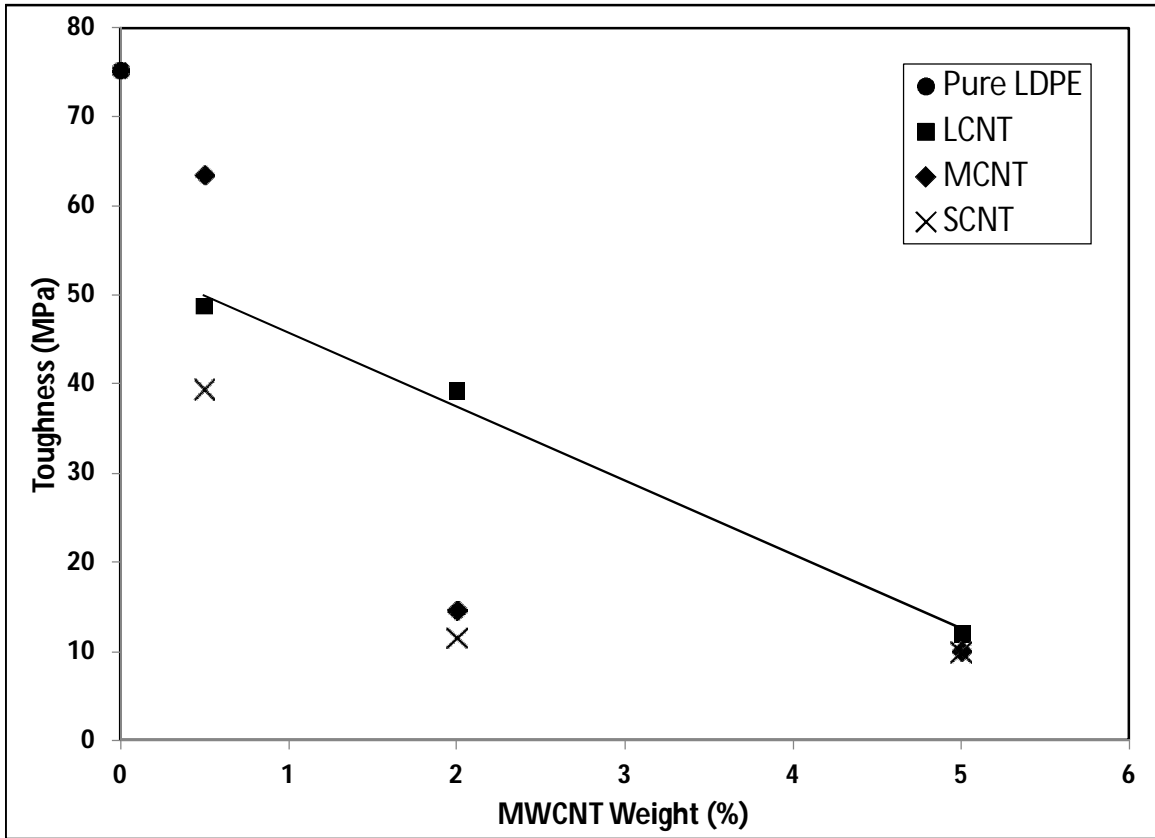


Figure 4.2.8.a. Toughness of pure LDPE and its composites at various loadings.

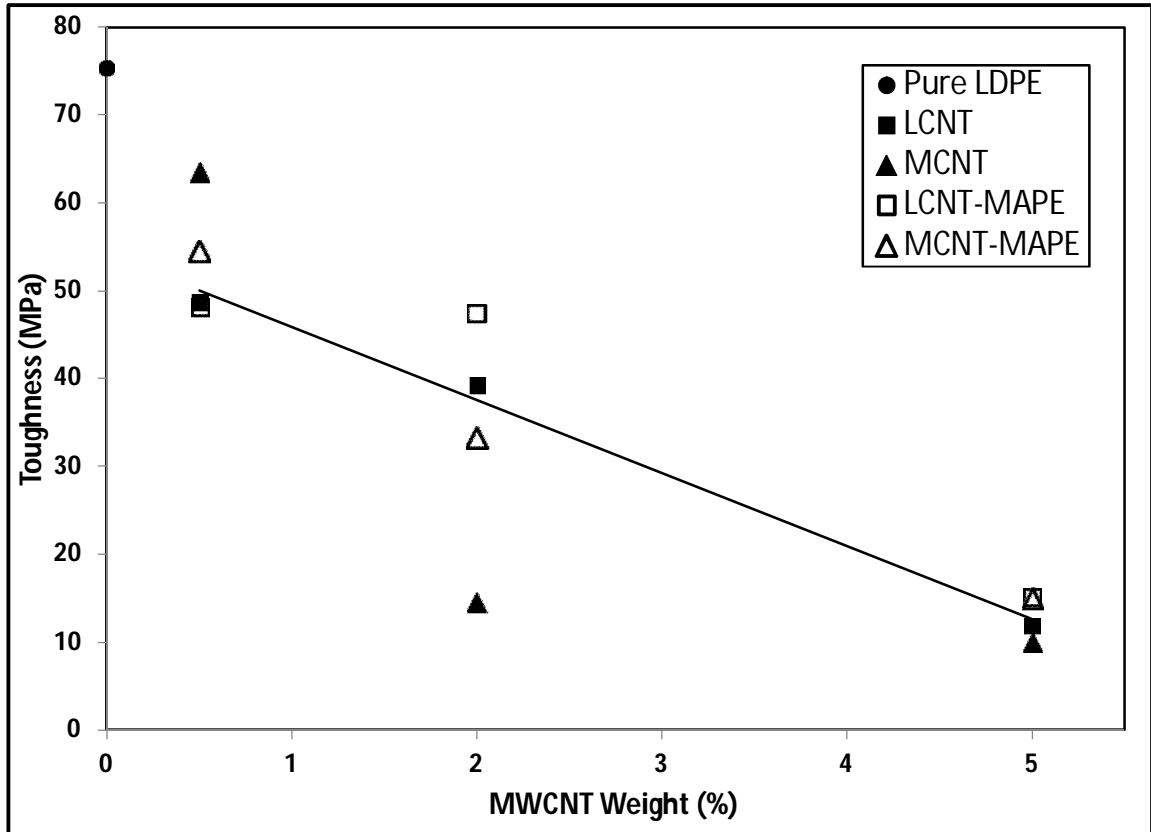


Figure 4.2.8.b. Toughness of pure LDPE and its composites at various loadings of LCNT, MCNT with and without 2.0% MAPE.

4.2.4.3. DSC Analysis

Figures 4.2.9.a and 4.2.9.b show the melting and crystallization curves for pure LDPE and its composites at various loadings. Different thermal properties of the said composites are shown in Table 4.2.3. Pure LDPE and its nanocomposites showed crystallization exotherms that were fairly similar. They showed a distinct high-temperature peak followed by a broad long tail. However, it can distinctly be observed from data in Table 4.2.3. that as the amount of MWCNT in the composite is increased, early onset of crystallization takes place. For example, for pure LDPE T_{onset} starts at 98.2°C and subsequently increases for MCNT at 0.5% to 101.5°C, at 2.0% and 5.0% it increases to 101.6°C and 103.6°C, respectively. Also, at all loadings of MCNT and in the presence of 2.0% MAPE, the onset has increased even further from 101.8°C at 0.5% MCNT loading to 104°C at 5.0% loading. However, the effect of both the aspect ratio and COOH modification is much less as given by the data shown in Table 4.2.3. For each exotherm, the peak and onset crystallization were calculated. Similarly, the influence of aspect ratio or COOH modification on T_{peak} is weak.

Also, a comparison of LCNT and MCNT (both have the same aspect ratio) and the LCNT and SCNT suggests that aspect ratio has influenced T_{onset} but not T_{peak} with weak influence of surface modification on T_{peak} as well as T_{onset} . This observation can be explained, tentatively, as follows: CNT with high aspect ratio (LCNT & MCNT) promotes nucleation due to its large surface area per tube. However, for T_{peak} the surface area of CNT is no longer a factor in enhancing crystallization since crystallization is already at its peak. Therefore, the increase in MWCNT concentration shifts T_{onset} to

higher values and promotes nucleation with almost no effect on T_{peak} . The influence of chemical modification on the onset temperature is similar to that of the aspect ratio. In both cases, higher aspect ratio and surface modification tend to improve the nucleation by increasing the surface area.

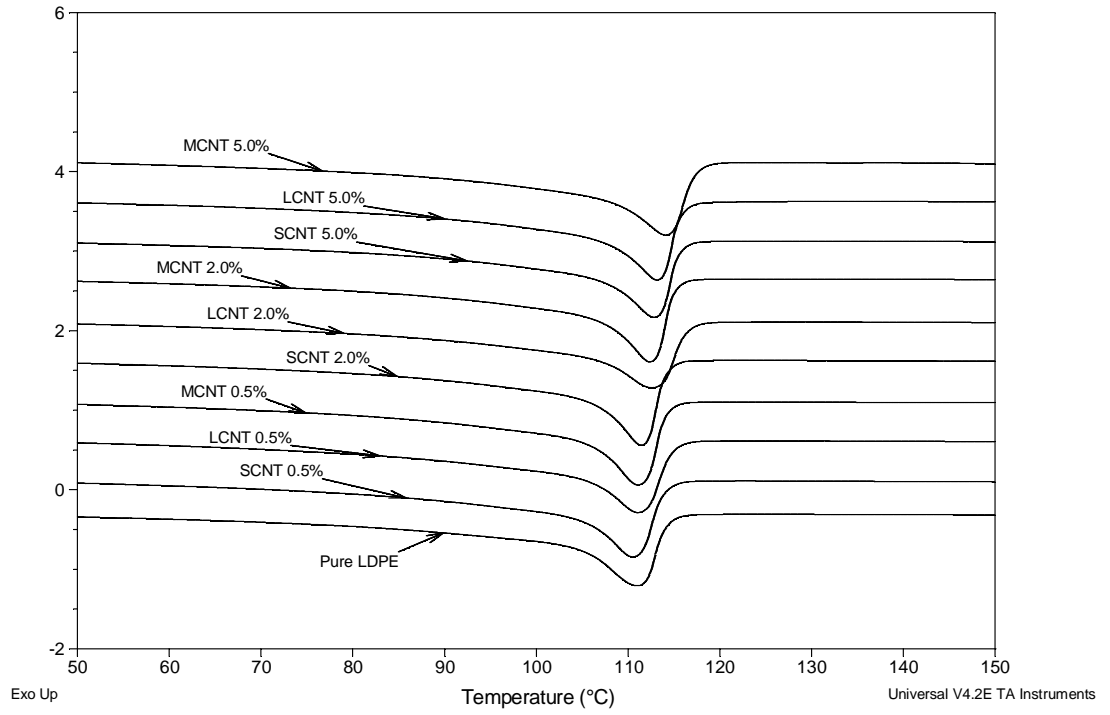


Figure 4.2.9.a. Melting curves for pure LDPE and its composites at various loadings.

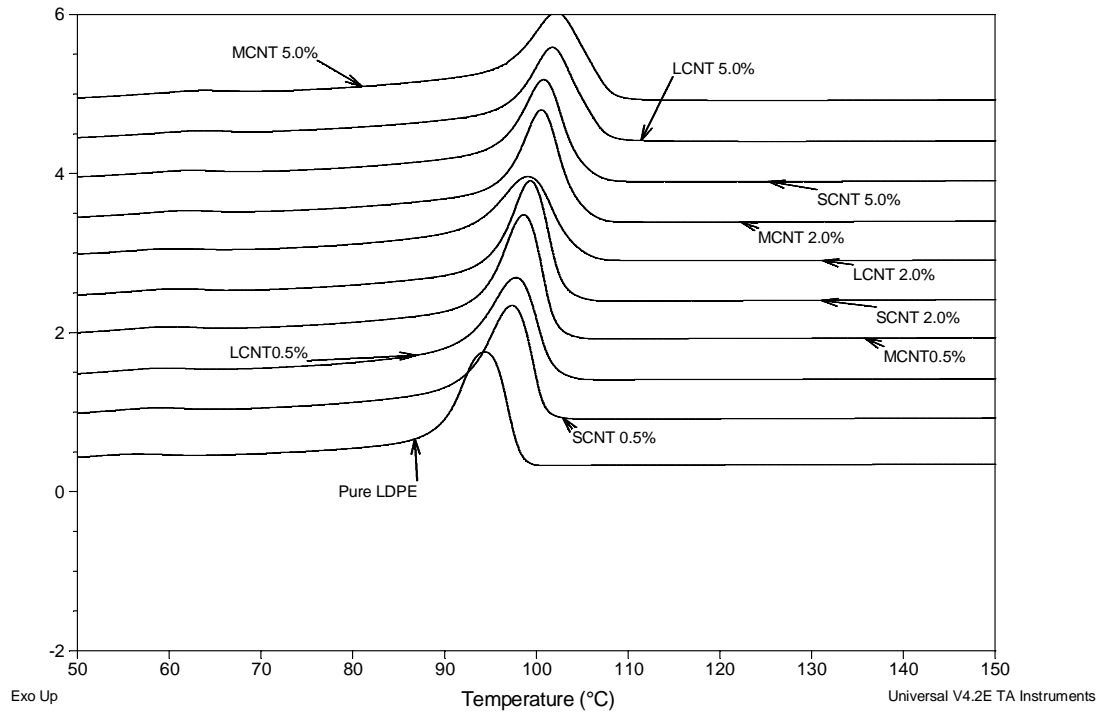


Figure 4.2.9.b. Crystallization curves for pure LDPE and its composites at various loadings.

Table 4.2.3. Various thermal properties of Pure LDPE and its composites at various loadings.

MWCNT %	MWCNT Type	T_{melting}, °C	T_{onset}, °C	T_{peak}, °C	X_c, %
Pure LDPE		111.5	98.2	94.3	35.2
0.5	Long	109.8	100.7	96.7	40.2
	Long + MAPE	109.2	103.9	98.8	40.1
	Short	110.1	100.3	96.8	38.8
	Modified	109.6	100.5	97.0	40.7
	Modified + MAPE	110.2	101.8	97.4	40.8
2.0	Long	109.2	101.6	96.8	40.7
	Long + MAPE	109.7	103.7	98.1	40.6
	Short	109.9	100.8	97.3	38.9
	Modified	109.7	101.6	97.5	40.9
	Modified + MAPE	110.1	103.0	98.3	40.8
5.0	Long	108.9	102.9	97.7	40.8
	Long + MAPE	110.47	103.7	97.3	40.9
	Short	108.9	101.3	97.3	40.1
	Modified	109.4	103.6	97.6	41.4
	Modified + MAPE	109.6	104.0	99.0	41.5

Further, we tried to assess the impact of aspect ratio and surface modification on the total crystallinity since it is an important property and it impacts mechanical properties. Table 4.2.3 shows the percent crystallinity, X_c , that was calculated using the TA Q1000 software. The initial point for the integration was chosen as 2°C above the onset temperature for each exotherm and the final point was room temperature. It is observed that both LCNT and MCNT composites show higher values of X_c in comparison with the SCNT at all loadings. It is clear that at higher concentrations, -COOH modification is not significantly influencing total crystallinity but aspect ratio is a factor with high aspect ratio yielding higher total crystallinity. These values of crystallinity correlate with Young's modulus. Both, Young's modulus and total crystallinity increase with increased loading of MWNCT, and that SCNT showed lower values of Young's modulus as compared to LCNT and MCNT at all loadings, a trend that was seen in percent crystallinity as well. Furthermore, the melting temperature is reduced with the incorporation of the MWCNTs. As the amount of MWCNT increases, the melting temperature decreases. A more detailed study of non isothermal crystallization kinetics for these nanocomposites that explains this behavior at various rates was published elsewhere [51].

4.2.5. Conclusion

LDPE / MWCNTs nanocomposites were prepared using melt blending. Samples were prepared using different MWCNT (LCNT, MCNT & SCNT). The surface morphology of SCNT-LDPE composites without the addition of a compatibilizer show agglomeration of MWCNT within the LDPE matrix. Evidence of dispersion was not found in this group of

nanocomposites. Agglomeration was also observed for LCNT-LDPE. Higher magnification shows that agglomeration was not localized at a particular region but was observed to spread across the matrix. The addition of a compatibilizer to both LCNT and MCNT nanocomposites improved the dispersion of CNTs. The degree of dispersion of MCNT in LDPE matrix was seen to be higher in MCNT when compared to LCNT nanocomposites. Greater improvement in dispersion within MCNT could be attributed to the synergistic effect of compatibilizer with COOH modification present within this group of composites. It is evident that both surface modification and the compatibilizer have a positive influence on the dispersion.

Yield strength and modulus increased with increased loading of various MWCNTs. However, ultimate strength, percent elongation and toughness were reduced for 2% loading and higher. Addition of compatibilizer improved most of the mechanical properties as compared to pure LDPE and nanocomposites without compatibilizer at all loadings studied. With the increase in properties being 46% and 48% for yield strength, Young's modulus at 5.0% loading respectively. Also, 16% increase for ultimate strength at 2.0 % loading was observed for LCNT nanocomposite in the presence of MAPE. However, percent elongation and toughness did not show any improvement, with or without the compatibilizer.

Addition of MWCNT induced early onset of crystallization. However, aspect ratio and COOH modification did not show any effect. LCNT and MCNT composites show higher values of percent crystallinity in comparison with the SCNT at all loadings. The results of crystallinity correlate to the values of Young's modulus at various loadings of the

produced nanocomposites. Addition of compatibilizer did not affect the percent crystallinity of the nanocomposites.

Finally, high aspect ratio has increased yield strength, ultimate strength, and Young's modulus, at all loadings. However it did not influence any improvement in percent elongation and toughness. The presence of MAPE improved all mechanical properties, apart from percent elongation and toughness.

4.2.6. Acknowledgement

The authors are thankful to the Center of Research Excellence in Petroleum Refining & Petrochemicals (CoRE-PRP), established by the Ministry of Higher Education, for providing the funding for this research. KFUPM is also acknowledged for its support.

4.2.7. References

- [1] Iijima S. Helical microtubules of graphitic carbon. *Nature* 1991; 354:56.
- [2] Hata K, Futaba DN, Mizuno K, Namai T, Yumura M, Iijima S. Water-assisted highly efficient synthesis of impurity-free singlewalled carbon nanotubes. *Science* 2004; 306:1362.
- [3] Wong EW, Sheehan PE, Lieber CM. Nanobeam mechanics: elasticity, strength, and toughness of nanorods and nanotubes. *Science* 1997; 277:1971.
- [4] Treacy MM, Ebbesen TW, Gibson JM. Exceptionally high Young's modulus observed for individual carbon nanotubes. *Nature* 1996; 381:678.
- [5] Zhang P, Huang Y, Geubelle PH, Klein PA, Hwang CK. The elastic modulus of single-wall carbon nanotubes: a continuum analysis incorporating interatomic potentials. *Int J Solid Struct* 2002; 39:3893.
- [6] Vodenitcharova T, Zhang LC. Effective wall thickness of a single-walled carbon nanotube. *Phys Rev B* 2003; 68:165401.

- [7] Yu F, Files BS, Arepalli S, Ruoff RS. Tensile loading of ropes of single wall carbon nanotubes and their mechanical properties. *Phys Rev Lett* 2000; 84:5552-5.
- [8] Wagner D, Lourie O, Feldman Y, Tenne R. Stress-induced fragmentation of multiwall carbon nanotubes in a polymer matrix. *Appl Phys Lett* 1998; 72:188.
- [9] Goze C, Bernier P, Henrard L, Vaccarini L, Hernandez E, Rubio A. Elastic and mechanical properties of carbon nanotubes. *Synthetic Met* 1999; 103:2500.
- [10] Peebles LH. *Carbon fibers: formation, structure and properties*. Boca Raton: CRC Press; 1995.
- [11] Hadijev VG, Iliev MN, Arepali S, Nikolaev P, Files BS. Raman scattering test of single-wall carbon nanotube composites. *Appl Phys Lett* 2001; 78:3193.
- [12] Lourie O, Cox DM, Wagner HD. Buckling and collapse of embedded carbon nanotubes. *Phys Rev Lett* 1998; 81:1638.
- [13] Yu M, Lourie O, Dyer MJ, Kelly TF, Ruoff RS. Strength and breaking mechanism of multiwalled carbon nanotubes under tensile load. *Science* 2000; 287:637.
- [14] Xie S, Li W, Pan Z, Chang B, Sun L. Mechanical and physical properties on carbon nanotube. *J Phys Chem Solids* 2000; 61:1153.
- [15] Yao Z, Zhu CC, Cheng M, Liu J. Mechanical properties of carbon nanotubes by molecular dynamic simulation. *Comput Mater Sci* 2001; 22:180.
- [16] Chow TS. Tensile strength of filled polymers. *J Polym Sci Pol Phys* 1982; 20:2103.
- [17] Wagner HD. *Encyclopedia of polymer science and technology, Reinforcement*. New York: Wiley; 2002.
- [18] Wagner HD, Vaia RA. Carbon Nanotube-Based Polymer Composites: Outstanding issues at the interface for mechanics. *Mater Today* 2004; 7:38.
- [19] Xiao KQ, Zhang LC, Zarudi I. Mechanical and rheological properties of carbon nanotube reinforced polyethylene composites. *Compos Sci Technol* 2007; 67:177.
- [20] Mierczynska A, Mayne-L'Hermite M, Boiteux G, Jeszka JK. Electrical and Mechanical Properties of Carbon nanotube / Ultra molecular Weight polyethylene composites prepared by filler prelocalization method. *J Appl Polym Sci* 2007; 105:158.

- [21] Yang B-X, Shi J-H, Pramoda KP, Goh SH. Enhancement of the mechanical properties of polypropylene using propylene grafted multiwalled carbon nanotubes. *Compos Sci Technol* 2008; 12:2490.
- [22] Tang W, Santare MH, Advani SG. Melt processing and mechanical property characterization of multi walled carbon nanotube / high density polyethylene composite film. *Carbon* 2003; 41:2779.
- [23] Mahfuz H, Adnan A, Rangari VK, Jeelani S, Jang BZ. Carbon nanoparticles/whiskers reinforced composites and their tensile properties. *Compos Part A-Appl S* 2004; 35:519.
- [24] Zhao P, Wang K, Yang H, Zhang Q, Du R, Fu Q. Excellent tensile ductility in highly oriented injection-molded bar of polypropylene / carbon nanotubes composites. *Polymer* 2007; 48:5688.
- [25] Schadler LC, Giannaris GC, Ajayan PM. Load transfer in carbon nanotube epoxy composites. *Appl Phys Lett* 1998; 73:3842.
- [26] Qian D, Liu WK, Ruoff RS. Load transfer mechanism in carbon nanotube ropes. *Compos Sci Technol*. 2003; 63:1561.
- [27] Prashantha K, Soulestin J Lacrampe MF, Claes M, Dupin G, Krawczak P. Multi walled carbon nanotubes filled polypropylene nanocomposites based on materbatch route: Improvement of dispersion and mechanical properties through PP-g-MA addition. *Express Polym Lett* 2008; 2:735.
- [28] Kangaraj S, Varanda FR, Zhil'tsova TV, Oliveira MSA, Simoes JAO. Mechanical properties of high density polyethylene / carbon nanotube composites. *Compos Sci Technol* 2007; 67:3071.
- [29] Wang Y, Cheng R, Liang L, Wang Y. Study on the preparation and characterization of ultra high molecular weight polyethylene carbon nanotubes composite fiber. *Compos Sci Technol* 2005; 65:793.
- [30] Miltner HE, Grossiord N, Lu K, Loos J, Koning CE, Mele BV. Isotactic polypropylene / carbon nanotube composites prepared by latex technology. Thermal analysis of carbon nanotube induced nucleation. *Macromolecules* 2008; 41:5753.

- [31] Jin SH, Kang CH, Yoon KH, Bang DS, Park Y. Effect of compatibilizer on morphology, thermal and rheological properties of polypropylene/functionalized multi walled carbon nanotubes composites. *J Appl Polym Sci* 2009; 111:1028.
- [32] Valentino O, Sarno M, Rainone NG, Nobile MR, Ciambelli P, Neitzert HC, Simon GP. Influence of polymer structure and nanotube concentration on the conductivity and rheological properties of polyethylene / CNT composites. *Physica E* 2008; 40:2440.
- [33] Manchado MAL, Valentini L, Biagiotti J, Kenny JM. Thermal and mechanical properties of single walled carbon nanotubes polypropylene composites prepared by melt processing. *Carbon* 2005; 43:1499.
- [34] Park C, Ounaies Z, Watson KA, Crooks RE, Smith J, Lowther SE, Connell JW, Siochi EJ, Harrison JS, St. Clair TL. Dispersion of Single Wall Carbon Nanotubes by In Situ Polymerization Under Sonication. *Chem Phys Lett* 2002; 364:303.
- [35] Cooper C A, Ravich D, Lips D, Mayer J, Wagner HD. Distribution and alignment of carbon nanotubes and nanofibrils in a polymer matrix. *Compos Sci Technol* 2002; 62:1105.
- [36] Park S-J, Cho K-S, Ryu S-K. Filler–elastomer interactions: influence of oxygen plasma treatment on surface and mechanical properties of carbon black / rubber composites. *Carbon* 2003; 41:1437.
- [37] Lee SH, Kim MW, Kim SH, Youn JR. Rheological and electrical properties of polypropylene / MWCNT composites prepared with MWCNT materbatch chips. *Eur Polym J* 2008; 44:1620.
- [38] Song YS, Youn JR. Influence of dispersion states of carbon nanotubes on physical properties of epoxy nanocomposites. *Carbon* 2005; 43:1378.
- [39] Zhang Q, Lippits DR, Rastogi S. Dispersion and rheological aspects of SWNTs in ultrahigh molecular weight polyethylene. *Macromolecules* 2006; 39:658.
- [40] Ruan SL, Gao P, Yang XG, Yu TX. Toughening high performance ultrahigh molecular weight polyethylene using multiwalled carbon nanotubes. *Polymer* 2003; 44:5643.
- [41] Bin Y, Yamanaka A, Chen Q, Xi Y, Jiang X, Matsuo M. Morphological, electrical and mechanical properties of ultrahigh molecular weight polyethylene and multi-wall carbon nanotube composites prepared in decalin and paraffin. *Polym J* 2007; 39:598.

- [42] Zou Y, Feng Y, Wang L, Liu X. Processing and properties of MWNT/HDPE composites. *Carbon* 2004; 42:271.
- [43] McNally T, Poetschke P, Halley P, Murphy M, Martin D, Bell SEJ, Brennan GP, Bein D, Lemoine P, Quinn JP. Polyethylene multiwalled carbon nanotube composites. *Polymer* 2005; 46:8222.
- [44] Yang B-X, Pramoda KP, Xu GQ, Goh SH. Mechanical reinforcement of polyethylene using polyethylene-grafted multiwalled carbon nanotubes. *Adv Funct Mater* 2007; 17:2062.
- [45] Shofner ML, Khabashesku VN, Barrera EV. Processing and Mechanical Properties of Fluorinated Single-Wall Carbon Nanotube-Polyethylene Composites. *Chem Mater* 2006; 18:906.
- [46] Coleman JN, Khan U, Blau WJ, Gun'ko HYK. Small but strong: A review of the mechanical properties of carbon nanotube-polymer composites. *Carbon* 2006; 44:1624.
- [47] Callister WD. *Materials Science & Engineering, An introduction*. New York: Wiley; 2003.
- [48] Hussein IA, Williams MC. Rheological study of heterogeneities in melt blends of ZN-LLDPE and LDPE: Influence of Mw and comonomer type, and implications for miscibility. *Rheol Acta* 2004; 43:602.
- [49] Abu-Sharkh BF, Kahraman R, Abbasi SH, Hussein, IA. Effect of epolene E-43 as a compatibilizer on the mechanical properties of palm fiber-poly(propylene) composites. *J Appl Polym Sci* 2004;92:2581.
- [50] Kahraman R, Abbasi S, Abu-Sharkh B. Influence of Epolene G-3003 as a Coupling Agent on the Mechanical Behavior of Palm Fiber-Polypropylene Composites. *Int J Polym Mater* 2005; 54:483.
- [51] Abbasi SH, Hussein IA, Pervez A. Non-isothermal crystallization kinetics study of LDPE / MWCNT nanocomposites: Effect of Aspect ratio and surface modification. In Press (*J Appl Polym Sci*).

4.3. Rheology, mechanical and thermal properties of LDPE-C₁₈-CNT nanocomposites.

4.3.1. Abstract

Nanocomposites of low density polyethylene (LDPE)/C₁₈ modified multi wall carbon nanotubes (C₁₈-CNT) were prepared by melt blending. The effect of loading and compatibilizer on the morphology, mechanical, thermal and rheological properties was studied. FE-SEM images of nanocomposites showed reduced agglomeration of the C₁₈-CNT / with LDPE in comparison with unmodified CNT. For uncompatibilized nanocomposites, yield strength and Young's modulus increased with loading of various C₁₈-CNT. Ultimate strength, showed improvement up to 2 wt% loading. However, percent elongation and toughness were reduced for C₁₈-CNT at all loadings. Apart from elongation and toughness, addition of compatibilizer improved all mechanical properties as compared to pure LDPE and nanocomposites without compatibilizer. Percent crystallinity showed a correlation with Young's modulus. Both, Young's modulus and total crystallinity increased with C₁₈-CNT loading and further increase with the incorporation of compatibilizer was observed. Results of phase angle suggest no presence of network. Also, addition of C₁₈-CNT did not increase strain hardening, maintained extensional viscosity and time of break up to 1.5 s⁻¹ henky rate. The C₁₈ modifier is viewed to act similar to a long chain branching on linear polymers. The C₁₈ modification of CNT resulted in reduced viscous and elastic properties of the composites. In turn, this is expected to lead to enhancement in the processing of these composites. Overall, the C₁₈ modification of CNT resulted in improved mechanical and rheological properties.

4.3.2. Introduction

New millennium has witnessed ever increasing research in carbon nanotubes (CNTs). This research interest is not misplaced, as CNTs show phenomenal properties. Their compressive strength has been reported as high as ~150 GPa [1]. Tensile strength and Young's moduli have been reported as 5-63 GPa [2-6] and 1-5 TPa [5-11], respectively. There has been exponential increase in polymer / CNT nanocomposite research [12], clearly indicating a growing interest among researchers around the world in this topic. The properties of polymer / CNT nanocomposite depend on several factors; the process used to produce CNTs and its effect on their purity, loading of CNT [13-16], the length of CNT, outer diameter of CNT, aspect ratio of CNT, alignment of CNT [17-18] and matrix of the polymer. Theoretical predictions point towards increase in the elastic modulus and tensile strength of the composite as either the volume fraction of the reinforcing fibers increases [19-20], or the aspect ratio of the fibers increases [20]. It is well known that tensile strength of the composites is strongly influenced by the magnitude of interfacial matrix-fiber stress [20-26].

A look at the literature available on this topic shows a wide variety of results, from very high improvements in properties to even drop in properties. There are many reasons for this discrepancy. Primary reason is inadequate dispersion of the CNTs within the polymer matrix. Dispersion of the CNTs within the matrix is considered the most critical factor in improvement of properties [27-36]. Tang et al. [22] reported increase in stiffness and peak load for the composite films with increasing multi wall carbon nanotubes (MWCNT) content in HDPE nanocomposite. Bin et al. [37] used solvent blending to

prepare ultrahigh molecular weight (UHMWPE) and MWCNT composites. Decalin and paraffin was used as solvent. SEM observations revealed that the MWCNTs within the composite prepared in decalin were covered by UHMWPE, and their diameters were much greater than those of the original MWCNTs. The composites prepared in decalin had high drawability. Significant increase in elastic modulus was observed. Ruan et al [38] demonstrated a drastic enhancement in toughness of UHMWPE films prepared by solution blending due to the addition of 1% MWCNT. Increase of approximately 140% in ductility was observed. Authors attributed this increase in ductility to the enhancement of chain mobility in UHMWPE induced by the MWCNTs. So, in our view Raun et al. [38] view CNTs as plasticizers.

McNally et al. [39] prepared composites of PE and MWCNTs by melt blending with MWCNT varied from 0 to 10%. The yield strength showed slight increase with the addition of CNT. However, ultimate tensile strength and elongation at break decreased with the addition of MWCNTs. They attributed this drop to poor dispersion of CNTs which led to poor stress transfer between the polymer and the filler. In general, two strategies were used by various researchers to improve dispersion of the CNT in the polymer matrix. One is the use of compatibilizer and the other is the functionalization of the CNT. Polypropylene (PP) grafted maleic anhydride (PP-g-MA) has been used in PP matrix with MWCNT [24, 28, 34]. The influence of various functionalized CNTs on the properties of poly(ethylene terephthalate), polyimide, polyamide 6, epoxy and poly(methyl methacrylate) were studied [40-46].

Apart from mechanical properties, rheology of polymer / CNT has been studied as well. The most peculiar result has been reported by Kharchenko et al [47] in nature materials. They observed negative normal stresses in MWCNT/PP nanocomposite, which until their work was only sometimes observed in liquid crystalline polymers. Also, Xu et al [48] measured the normal forces of MWCNT/PP composites but did not observe any negative normal forces even though they used functionalized CNT.

Lee et al [49] utilized chemically functionalized MWCNTs with PP. Acid and amine treatment were used for the functionalization and a decrease in complex viscosity (η^*) with increasing frequency was observed in dynamic shear tests. Storage modulus increased with increasing frequency. Similar trend for η^* was observed by Potschke et al. [50] for MWCNT / polycarbonate composite. However, concentrations above 2 wt% of MWCNT in the matrix tend to show a plateau behavior at low frequency. McNally et al [39] also studied the rheological properties and reported an increase in η^* with the increase of the concentration of MWCNT. The magnitude of increase is more pronounced at low ω . However, η^* decreases with increasing ω for all nanocomposites and pure PE. Also, G' for the nanocomposites showed a monotonic increase with increasing MWCNT content and approached a plateau at low ω . It was suggested that the low ω response is indicative of 'pseudo-solid-like' behavior. Lee et al [49] also studied the elongational flow properties of PP / MWCNT nanocomposite. The acid treated and heat treated MWCNT / PP nanocomposites showed elongational viscosity higher than pure PP. Amine treated MWCNT / PP showed weak strain hardening. Also, MA-g-PP has negative effects on strain hardening due to low molecular weight. However, the

literature on rheology of polyolefin / CNT is very limited, rheology of modified CNT / polyolefin is even less.

In our present study, both chemical modification of CNT and a compatibilizer were used to enhance the dispersion. The effect of C₁₈ modified CNT and maleic anhydride grafted polyethylene (PE-g-MA) on LDPE/MWCNT nanocomposite was studied. The produced nanocomposites were thoroughly characterized by analyzing mechanical, thermal and rheological properties. Film grade LDPE is used.

4.3.3. Experimental

The LDPE is supplied by ExxonMobil as pellets. This resin has weight average molecular weight of 99.5 kg/mol and a MWD of 6.5 and a melt index of 0.75 g/10 min and a total short branch content of 22 branches/1000 C as determined by GPC and NMR, respectively [51]. Maleic anhydride modified polyethylene (MAPE) used in the study was acquired from Aldrich. MAPE contained ~3 wt.% maleic anhydride, its viscosity is 1700-4500 cP and melt temperature is 105°C.

The MWCNTs was supplied by Cheap Tubes Inc, USA. MWNCTs had an outer diameter of 30-50 nm and inner diameter of 5-15 nm. The length for COOH-MWCNT (MCNT), short MWCNT (SCNT) and long MWCNT (LCNT) was 10-20 µm, 0.5-2.0 µm and 10-20 µm, respectively. As stated by the producing company, COOH-MWCNT contains 0.7% -COOH groups. MCNT was then reacted with 1-Octadecanol. Here, the Fischer esterification process was followed. This was achieved by heating 1-Octadecanol to its melting point in a reaction flask and maintaining the temperature slightly below its

boiling point (65°C). MCNT was introduced into the reaction flask containing 1-Octadecanol in a ratio of 1g: 10g of 1-Octadecanol. The mixture was stirred for few minutes before few drops of sulfuric acid were added to initiate the reaction. The reaction was left for 2 hours after which the resulting CNT was washed with toluene several times to remove any unreacted 1-octadecanol and then followed by washing with deionized water to remove any traces of acid. The resulting CNT is referred to as C₁₈-CNT. This procedure was implemented for functionalization of CNT with different functional groups [52].

The FT-IR spectrum for C₁₈-CNT is given in Figure 4.3.1. There are two new broad peaks existing at 2346.3 cm⁻¹ and 2917 cm⁻¹. The peak at 2346.3 cm⁻¹ is characteristic of long chain alkyl molecule which can be linked to the presence of the 1-Octadecanol while that at 2917 cm⁻¹ is due to the symmetric C-H stretching respectively. Traces of hydroxyl groups are also evident in C₁₈-CNT as indicated by the peaks at 3398.9 cm⁻¹.

The LDPE resin and modified and unmodified MWCNT/LDPE nanocomposites were conditioned (or blended) in a Haake PolyDrive melt blender. The temperature used was 190°C at 50 rpm and time of blending was 10 minutes. Carver press was used to prepare samples to be used in mechanical and rheological equipment.

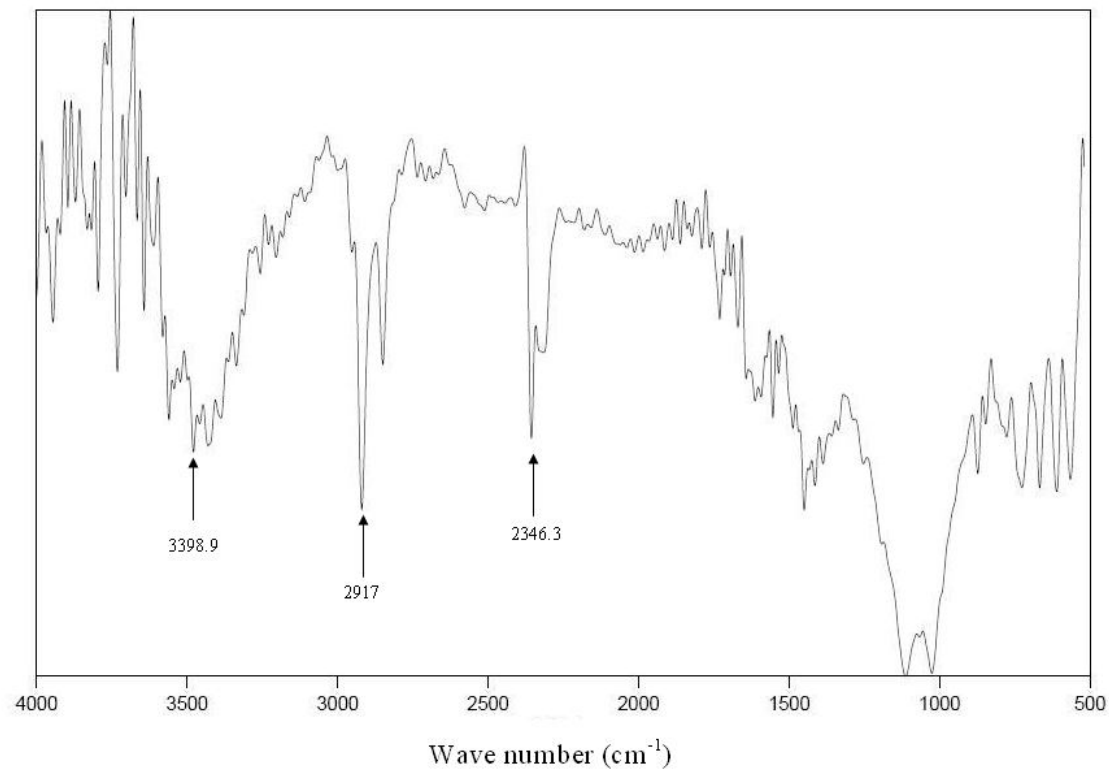


Figure 4.3.1. FTIR of C₁₈-CNT showing the evidence of long carbon alkyl chain on the MWCNT.

4.3.3.1. Mechanical Testing

The samples were tested using an Instron 5560 Mechanical Testing Machine according to ASTM test D-638. All tests were conducted at constant strain rate of 50 mm/min. The measured stress / strain data was used to calculate mechanical properties. Maximum of five samples were tested for each composition. The maximum standard deviation for yield strength, ultimate strength, Young's modulus, percent Elongation and toughness were 0.6, 1.7, 33.8, 1.35 and 17.6 respectively.

4.3.3.2. Differential Scanning Calorimetry

All DSC measurements were performed using a TA Q1000 instrument equipped with a liquid nitrogen cooling system and auto sampler. Nitrogen at a flow rate 50 ml/min was used to purge the instrument to prevent degradation of the samples upon thermal treatments. The DSC was calibrated in terms of melting temperature and heat of fusion using a high purity indium standard (156.6°C and 28.45 J/g). The absolute crystallinity was calculated using the heat of fusion of a perfect polyethylene crystal of 290 J/g.

Composite samples (5–10 mg) were sliced and compressed into a non-hermetic aluminum pans. To minimize the thermal lag between the sample and the pan, samples with flat surface were used. An empty aluminum pan was used as reference. First, the baseline was calibrated using empty crimped aluminum pans. All testing was performed in the standard DSC mode. Initially the samples were heated from room temperature to 200°C at a rate of 10°C/min; followed by a hold up at 200°C for 2 min. All samples were cooled to sub ambient temperatures for complete evaluation of crystallinity. The samples

were cooled from 200° to -10°C at a rate of 10°C/min. After that the sample was heated from -10°C to 200°C at 10°C/min.

4.3.3.3. Rheology

Rheological measurements were carried out in an ARES constant strain rheometer. Dynamic shear tests were carried out using cone-and-plate geometry of 25 mm diameter and a cone angle of 0.1 radians. A 15% strain, selected to be in the linear viscoelastic range, and a temperature of 190°C and a frequency in the range 100 rad/s to 0.01 rad/s were applied. For extensional rheology, SER Extensional viscosity fixture was used. Test temperature was 120°C. Sample dimensions were as follows: length, 17-19 mm; width, 6.5-6.7 mm and thickness, 0.48-0.62 mm. Henky rates in the range 0.5 -1.5 s⁻¹ were employed.

4.3.4. Results & Discussion

4.3.4.1. Morphology of the LDPE/C₁₈-CNT composites

The surface morphology of C₁₈ modified C₁₈-CNT/LDPE nanocomposites with and without 2% MAPE is shown in the backscattered FE-SEM images of Figure 4.3.2.a-b. Both images clearly show agglomeration of C₁₈-CNT within the matrix of LDPE. No clear evidence of these agglomerations to be well distributed in the matrix was found. However, a comparison of the agglomeration size shown in Figure 4.3.2.b for unmodified MWCNT with LDPE matrix (Figure 4.3.2.c) suggests that even without the addition of a compatibilizer the C₁₈ modification has reduced the size of agglomerations. The reduction in the size of the LCNT agglomeration due to the addition of C₁₈ is in the order of 2-3 times.

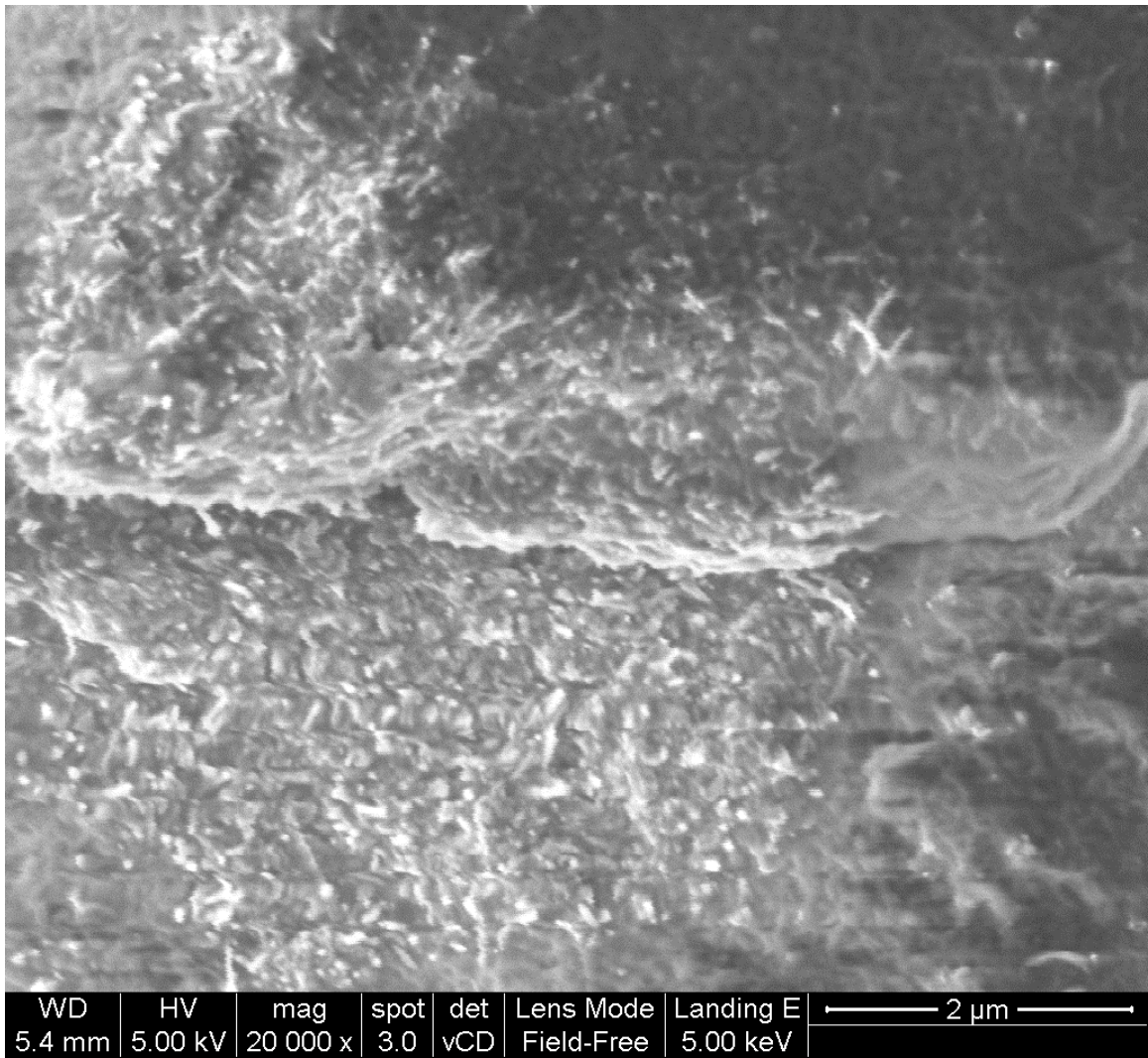


Figure 4.3.2.a. FE-SEM image of C₁₈-CNT/LDPE nanocomposite with 5.0% loading and 2.0% MAPE.

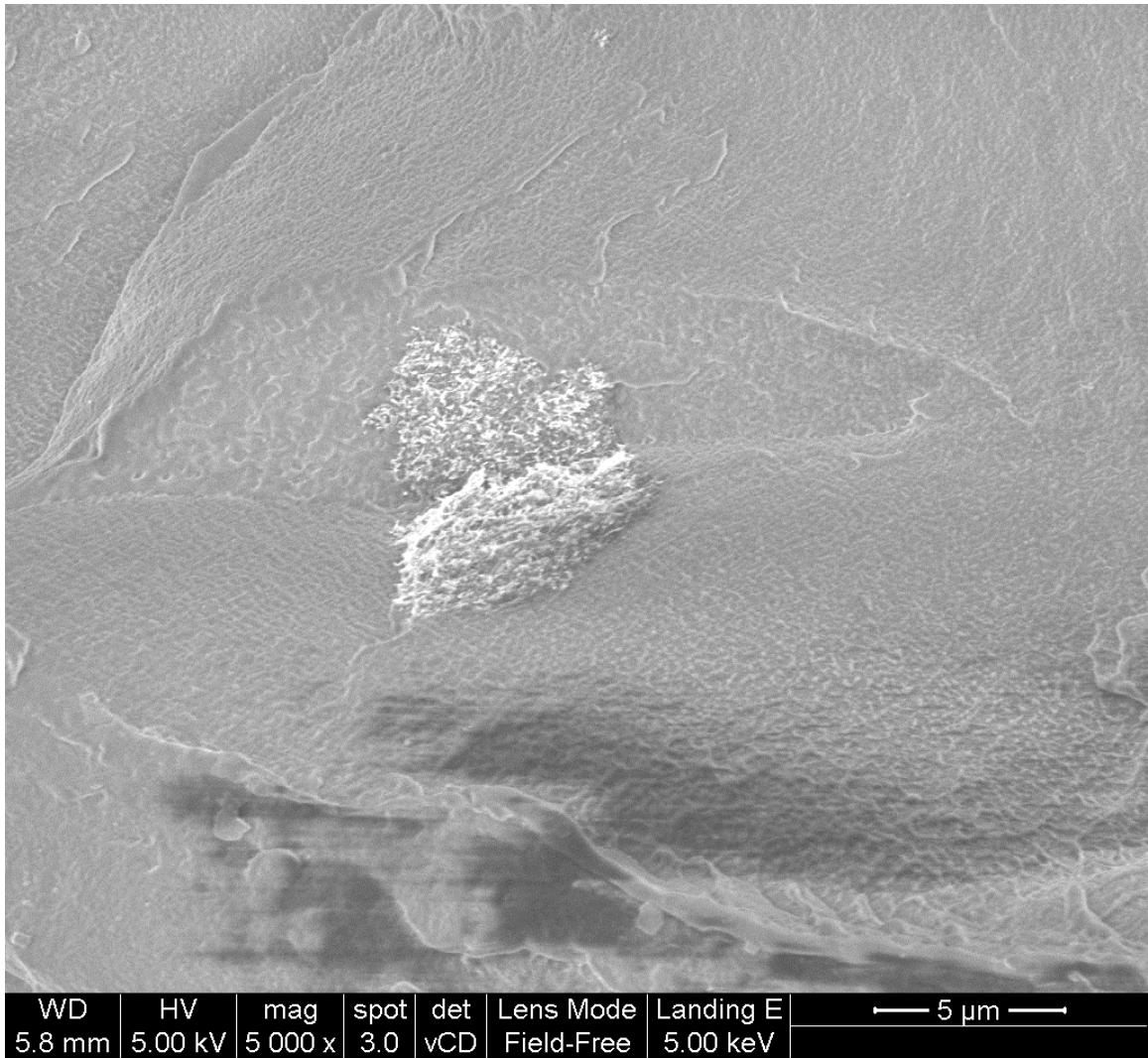


Figure 4.3.2.b. FE-SEM image of C₁₈-CNT/LDPE nanocomposite with 0.5% loading.

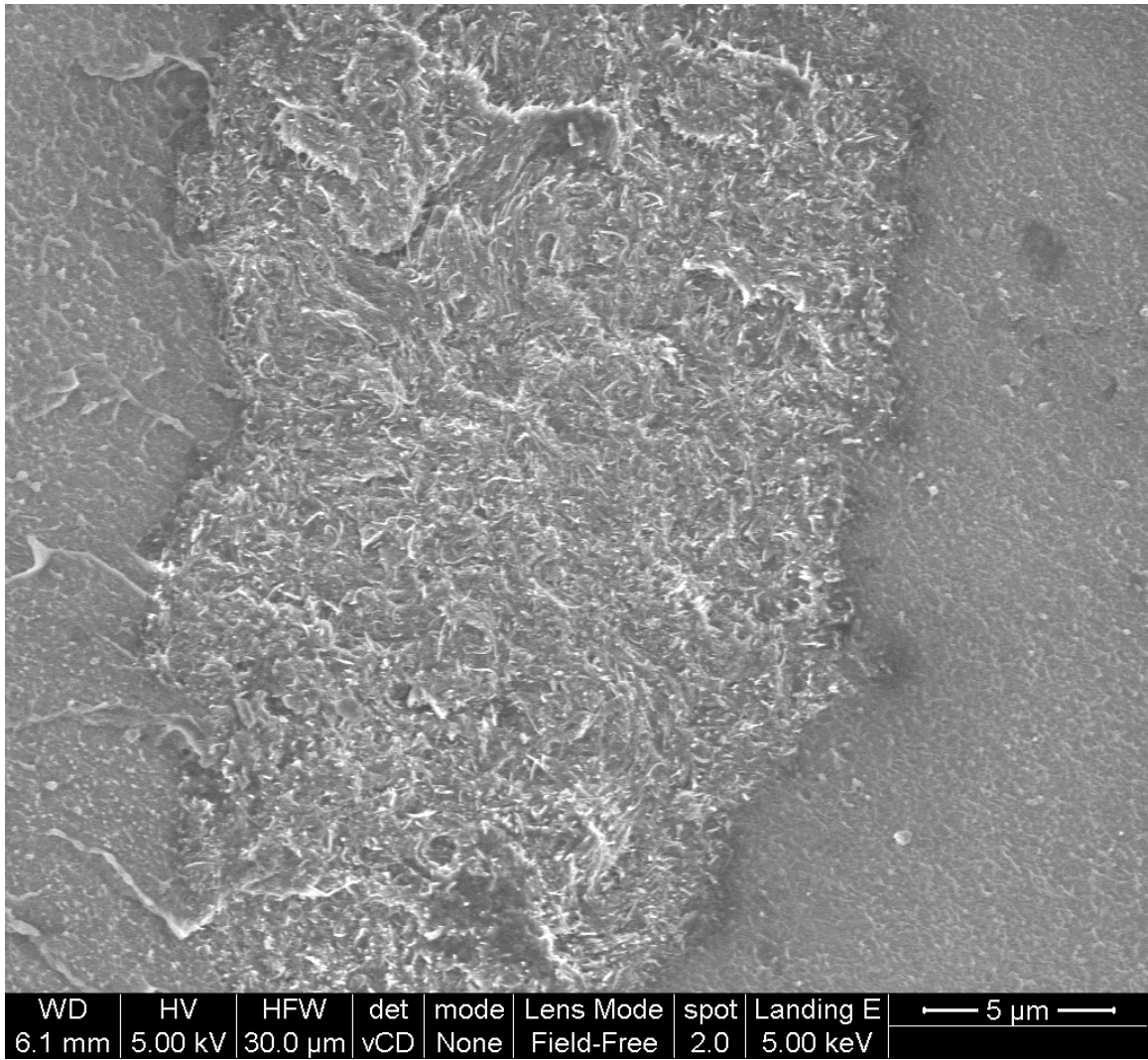


Figure 4.3.2.c. FE-SEM image of LCNT-LDPE nanocomposite with 0.5% loading.

4.3.4.2. Mechanical Testing

Mechanical properties of C₁₈-CNT/LDPE nanocomposite are shown in Table 4.3.1. Percent increase in yield strength; ultimate strength and Young's modulus are given in Figure 4.3.3.a whereas, percent decrease in elongation and toughness are presented in Figure 4.3.3.b. In general, incorporation of C₁₈-CNT at various CNT loadings with and without compatibilizer increased the yield strength of the produced nanocomposites at all loadings covered in this study. In the absence of the compatibilizer, the increase in loading of C₁₈-CNT from 0.5 to 5.0 wt% resulted in an increase in a 23-36% increase in the yield strength. The increase reaches up to 41% with the addition of 2.0% MAPE as compatibilizer at 5.0 wt% loading. This percent increase in yield strength can be attributed to the observed enhancement in dispersion with the addition of the compatibilizer. This is expected result since a 19% [39] and a 35% [13] increase in tensile strength was reported for unmodified MWCNT/PE nanocomposites. Addition of 2 wt% of compatibilizer resulted in increase in tensile strength of 50-70% for MWCNT/PP nanocomposite [24].

The ultimate strength of pure LDPE and its nanocomposites at various loadings show a different trend. Addition of 0.5 wt% of C₁₈-CNT to LDPE matrix with and without a compatibilizer results in an increase of 18 and 16%, respectively. However, further increase in C₁₈-CNT loading reduces the ultimate strength. The reason is that typical strain hardening behavior of pure LDPE, usually seen in the stress/strain curve, is still observed with the addition of 0.5 wt% C₁₈-CNT (Figure 4.3.3.c). Also, we know that ultimate strength represents the maximum value of stress at any point on the stress / strain

curve. But as the loading is increased from 0.5%, the nanocomposite subsequently loses this strain hardening behavior due to the reduction in the amorphous part [53]. Hence, with the addition of 5.0 wt% C₁₈-CNT the ultimate strength becomes less than that of pure LDPE. A 4% drop in ultimate strength of the composite was observed at 5.0 wt% loading in the presence of a compatibilizer. A drop of 38% in ultimate strength at 5.0 wt% loading has been reported in literature for PE/MWCNT system [39]. Therefore, C18 modified CNT shows much less drop in ultimate strength in comparison with published literature.

As observed before for yield strength, incorporation of C₁₈-CNT at various loadings with and without compatibilizer increases the Young's modulus of the produced nanocomposites at all loadings covered in this study. Although there is slight decrease in Young's modulus at 0.5 wt% loading. Addition of compatibilizer increases the Young's modulus from 7 % at 0.5 wt% loading up to 60% with 5.0 wt% loading of C₁₈-CNT. An increase of 40% was achieved with 5.0 wt% loading without adding any compatibilizer. So, presence of compatibilizer seems to enhance the Young's modulus even further. This enhancement is attributed to the improvement of dispersion which is supported by SEM.

With Regard to the percent elongation, the addition of C₁₈-CNT has reduced the percent elongation of C₁₈-CNT/LDPE nanocomposites, in the presence and absence of a compatibilizer. The percent decrease in the produced nanocomposites ranges from 40 to 44% at 0.5 wt% loading of C₁₈-CNT. The percent decrease goes up to 63 and 70% at 5.0 wt% C₁₈-CNT. However, this drop is not surprising as a percent drop of 96% at 5.0 wt% loading was observed previously for CNT/PP even in the presence of compatibilizer [24].

Again, the drop in elongation has improved with the addition of C₁₈ modified CNT. With increasing amount of C₁₈-CNT loading in LDPE a decreases in the toughness was observed regardless of the presence or absence of the compatibilizer. Percent drop of 64% and 53% in toughness were observed for 5.0 wt% loading of C₁₈-CNT with and without 2.0% MAPE compatibilizer. It can be concluded that the addition of C₁₈-CNT to LDPE matrix through melt blending increases the yield strength and Young's modulus. An increase in ultimate strength is also observed upto 2.0 wt% loading of C₁₈-CNT, but this improvement is lost at 5.0 wt% loading. Addition of 2.0 wt% MAPE causes further improvement in these properties. Percent elongation and toughness generally decrease with increased loading of C₁₈-CNT regardless of the presence of the compatibilizer. However, the drop in these properties has shown improvement in comparison with similar unmodified systems.

Table 4.3.1. Mechanical properties of LDPE and its nanocomposites

MWCNT, % w	Yield Strength	Ultimate Strength	Modulus	Elongation	Toughness
	MPa	MPa	MPa	(%)	MJ/m ³
0%	9.2	13.8	112.5	735	75.3
C ₁₈ -CNT 0.5%	11.3	16.1	110.5	409	53.8
C ₁₈ -CNT +2.0%	11.7	15.3	122.1	394	52.9
C ₁₈ -CNT 5.0%	12.5	13.7	161.9	268	35.4
C ₁₈ -CNT 0.5% +MAPE	11.4	16.3	120.4	440	58.2
C ₁₈ -CNT 2.0% +MAPE	12.5	15.3	134.2	356	47.8
C ₁₈ -CNT 5.0% +MAPE	13.0	13.2	179.0	220	27.0

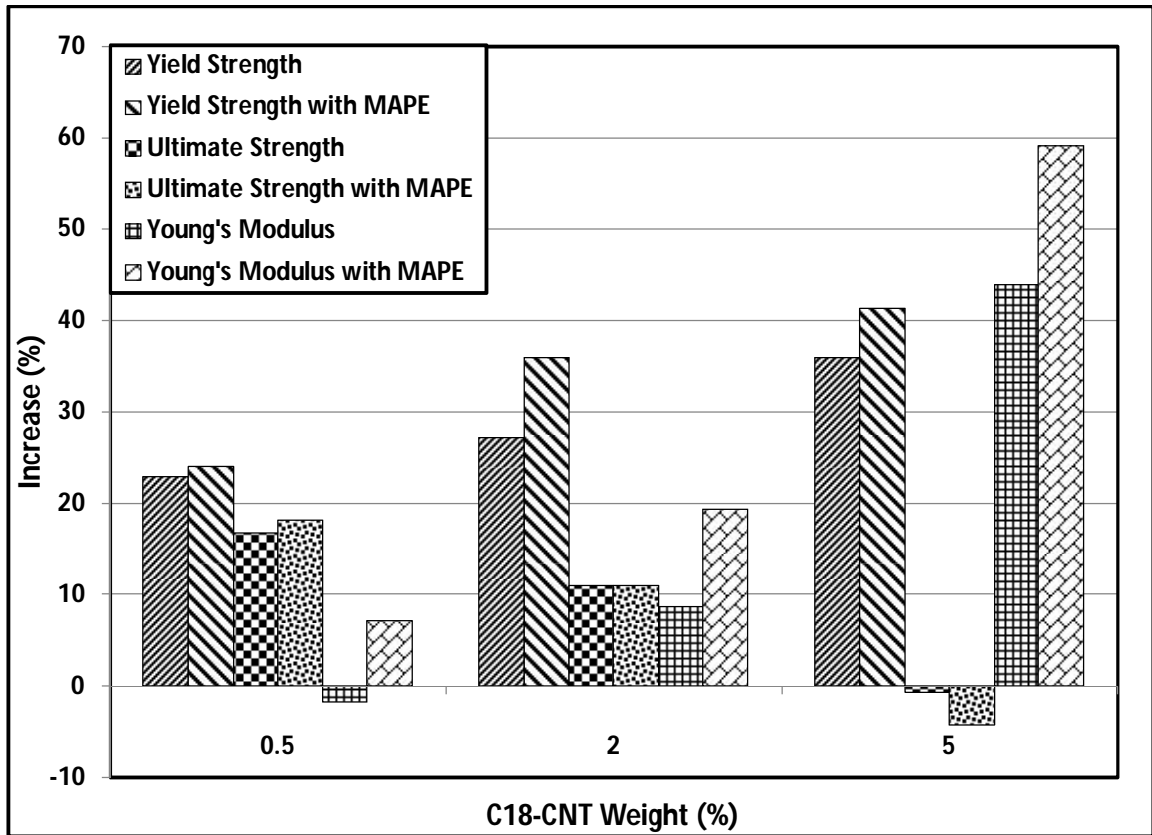


Figure 4.3.3.a. Percent increase in yield strength, ultimate strength and Young's modulus for various C₁₈CNT/LDPE nanocomposites.

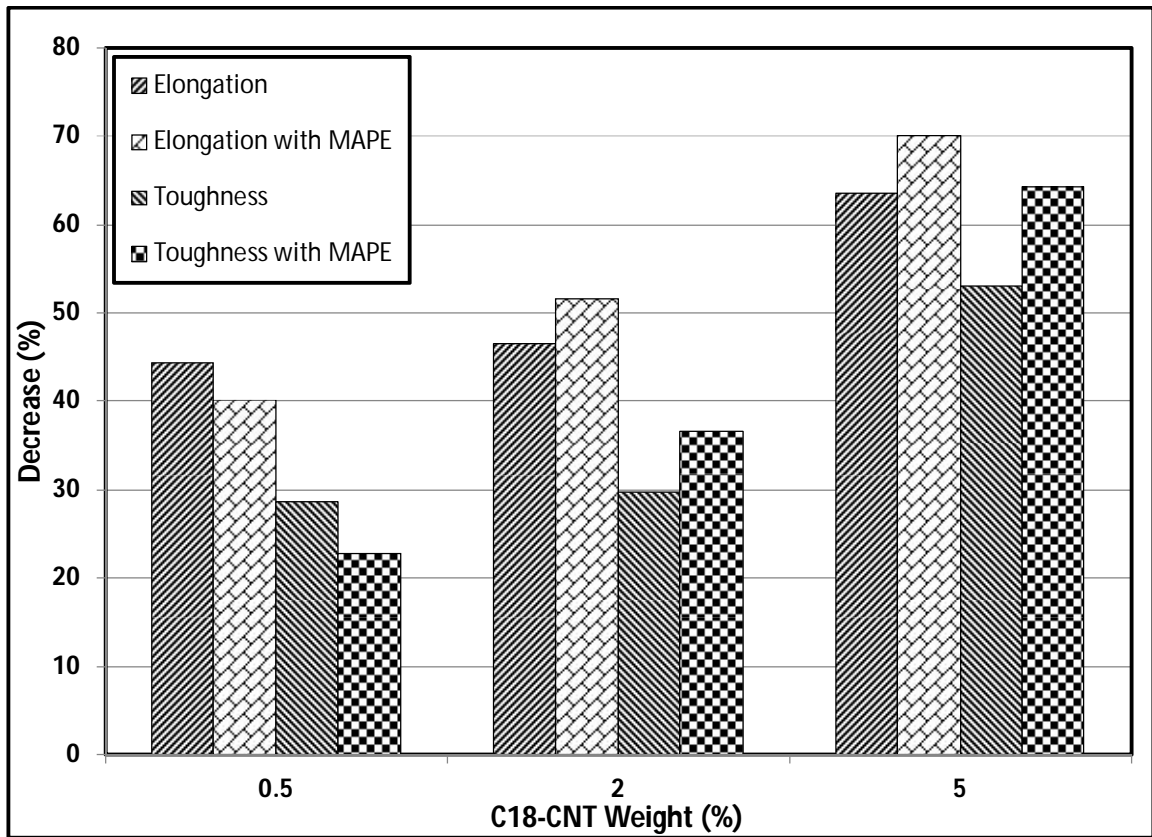


Figure 4.3.3.b. Percent decrease in elongation and toughness for various C₁₈CNT/LDPE nanocomposites.

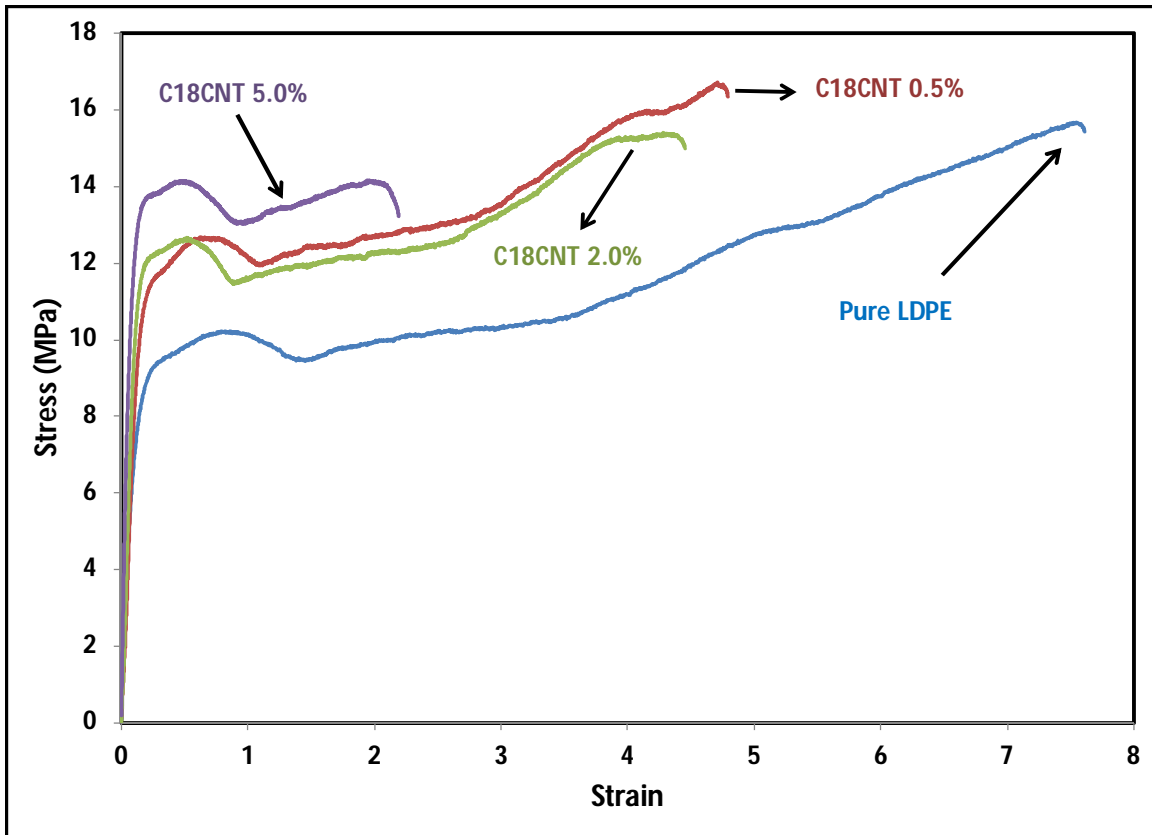


Figure 4.3.3.c. Tensile stress-strain representative curves for Pure LDPE & various loadings of C₁₈-CNT.

4.3.4.3. Thermal Characterization

Thermal properties of C₁₈-CNT composites are reported in Table 4.3.2. The addition of C₁₈-CNT shifts the onset of crystallization. As the loading of C₁₈-CNT is increased, the onset temperature (T_{onset}) increases from 98.2°C to 101.1°C and 102.3°C with the addition of 0.5 and 5.0 wt% C₁₈-CNT, respectively. A similar trend is observed when 2.0 wt% MAPE is added at all loadings, the onset temperature is slightly increased from 102.3 to 102.9°C at 5.0 wt% loading of C₁₈-CNT due to the addition of the compatibilizer. The effect of loading on peak crystallization temperature (T_{peak}) is weak since at this point the crystallization process is very fast. It initially shifts from 94.3°C to 97.7° with the addition of 0.5 wt% loading of C₁₈-CNT. Further addition of C₁₈-CNT and compatibilizer causes only limited increase to 98.0°C. The percent crystallinity, (X_c), was calculated using the Q1000 software. The initial point for the integration was chosen to be 2°C above the onset temperature for each exotherm and the final point was room temperature.

The percent crystallinity results were corrected for added weight of MWCNTs. It is observed that the increase in loading slightly increases the percent crystallinity of all nanocomposites. Addition of compatibilizer has little influence on the percent crystallinity. These values of crystallinity correlate with Young's modulus. Both, Young's modulus and total crystallinity increase with increased loading of C₁₈-CNT. The addition of compatibilizer also increases both Young's modulus and total crystallinity. Furthermore, the melting temperature (T_m) is slightly reduced with the addition of C₁₈-CNT. The melting temperature increased with the increase in the amount of C₁₈-CNT.

Table 4.3.2. Thermal properties of C₁₈-CNT/LDPE nanocomposites at various loadings.

C18CNT %	T_{melting} (°C)	T_{onset}, (°C)	T_{peak},(°C)	X_c, %
0.0	111.5	98.2	94.3	35.2
0.5	110.5	101.1	97.7	35.7
2.0	111.1	101.6	97.3	36.5
5.0	111.7	102.3	96.5	38.0
0.5 + 2.0 MAPE	110.3	102.3	98.0	36.9
2.0 + 2.0 MAPE	110.0	102.8	98.0	37.9
5.0 + 2.0 MAPE	110.7	102.9	97.8	39.0

4.3.4.4. Rheological Characterization

The dynamic viscosity (η') and storage modulus (G') vs frequency (ω) for C₁₈-CNT/LDPE nanocomposites at various loadings are shown in Figures 4.3.4.a and 4.3.4.b. The most remarkable result that stands out is the fact that the addition of C₁₈-CNT in the LDPE matrix resulted in a drop in η' which is more prominent at low ω . As the loading is increased, η' increases. Pure LDPE shows a shear thinning behavior with increasing ω ; the addition C₁₈-CNT maintains that behavior. Over the whole range of ω , η' of the nanocomposites is less or just equal to η' of pure LDPE. This trend is true for nanocomposite with and without a compatibilizer.

Figures 4.3.4.c and 4.3.4.d show the effect of compatibilizer at a fixed loading of C₁₈-CNT. For both 0.5% and 5.0% loading of C₁₈-CNT, the compatibilizer seems to have little influence on the rheology of nanocomposites unlike C₁₈-CNT. This result is very interesting because until now the majority of the published literature has reported an increase in viscosity (η) with the addition of CNT only [13, 29, 34, 39, 48, 50] and CNT with compatibilizer [49]. Only few publications have reported a drop in η with the addition of nanomaterial at low loadings of less than 1.0 wt% [54-56]. Our explanation for this behavior is that the C₁₈ modification on the CNT acts more or less like a long chain branching (LCB) on linear polymers and eases the flow. In addition, the presence of C₁₈ improves the compatibility of CNT/LDPE blends by improving the interfacial bonding with LDPE which has similar branches. Therefore, C₁₈ in CNT acts as an insitu compatibilizer. Hence, the presence of this modification has reduced the η' at all

loadings, more pronounced at low ω . It is expected that further increase in loading would eventually increase the η' beyond that of pure LDPE.

Storage modulus (G') behavior is similar to that witnessed for η' . Addition of C_{18} -CNT has reduced G' at 0.5 wt% loading. Further addition in loading increases G' but values are still below that of pure LDPE. G' increases with increasing ω but it remains below that of pure LDPE. Only at 5.0 wt% loading and high ω the value of G' becomes equal to that of pure LDPE (Figure 4.3.4.c). Plots of phase angle (δ) versus ω are used to observe the transition from liquid-like to solid-like. $\tan(\delta)$ usually becomes independent of ω once interconnected network is formed [24]. In a system without network, the value of $\tan(\delta)$ is high at low ω and decreases with increasing ω . For nanocomposites of C_{18} -CNT/LDPE (Figure 4.3.4.e) the value of $\tan(\delta)$ decreases with increasing ω . None of the loadings show network formation behavior. In addition, at all C_{18} -CNT loadings and ω , the value of $\tan(\delta)$ is higher than that of pure LDPE. This suggests that C_{18} -CNT increases the fluidity of LDPE especially at low shear. It points towards the fact that all nanocomposites show more liquid-like behavior at all loadings and ω compared to pure LDPE. This result of $\tan(\delta)$ supports the previous results of η' and G' that showed a drop in both η' and G' .

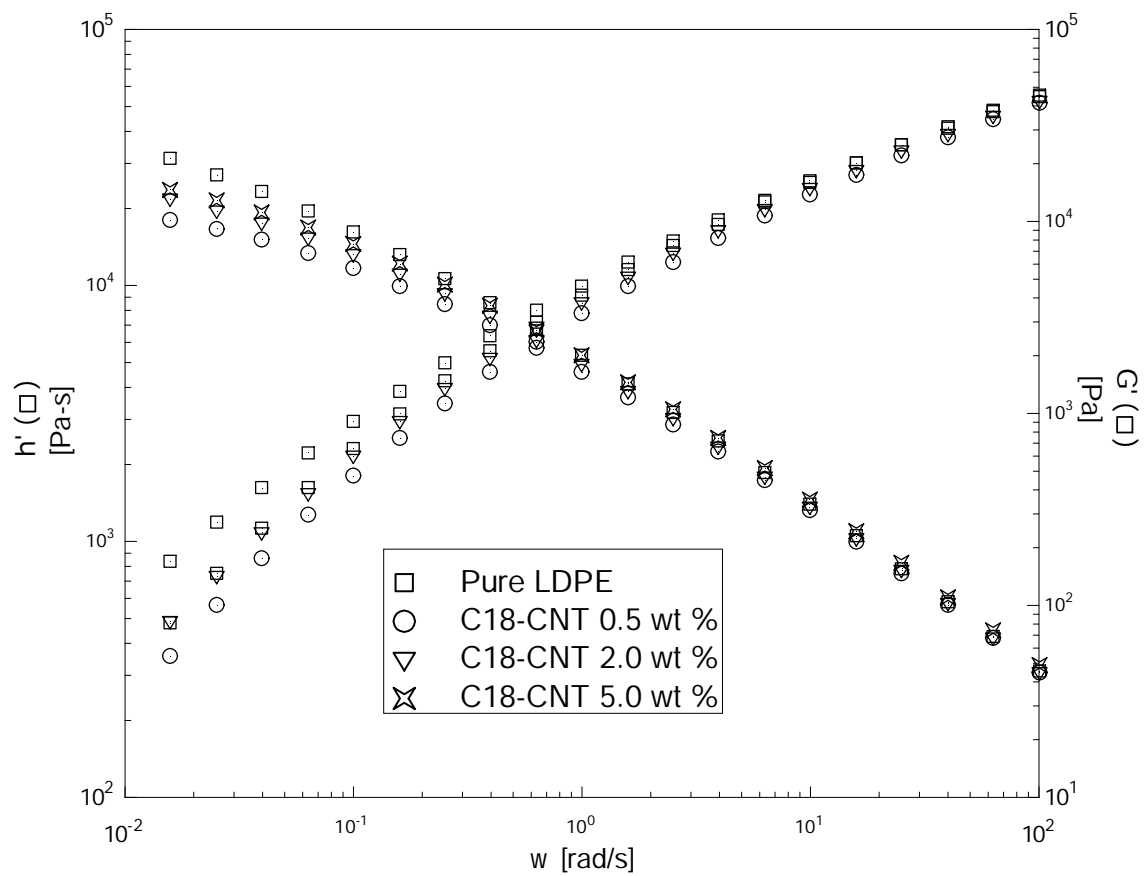


Figure 4.3.4.a. Dynamic viscosity & Storage modulus versus frequency plots for C₁₈-CNT/LDPE nanocomposites.

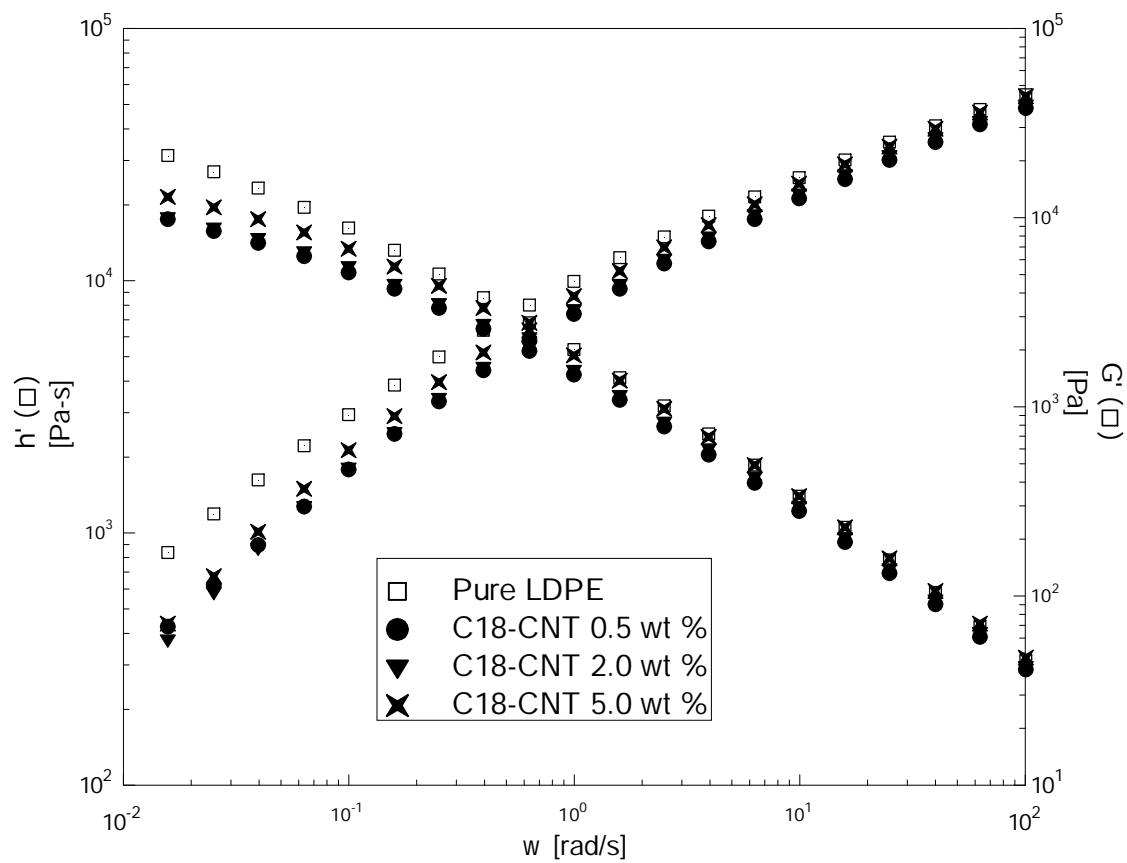


Figure 4.3.4.b. Dynamic viscosity & Storage modulus versus frequency plots for C₁₈-CNT/LDPE nanocomposites with MAPE.

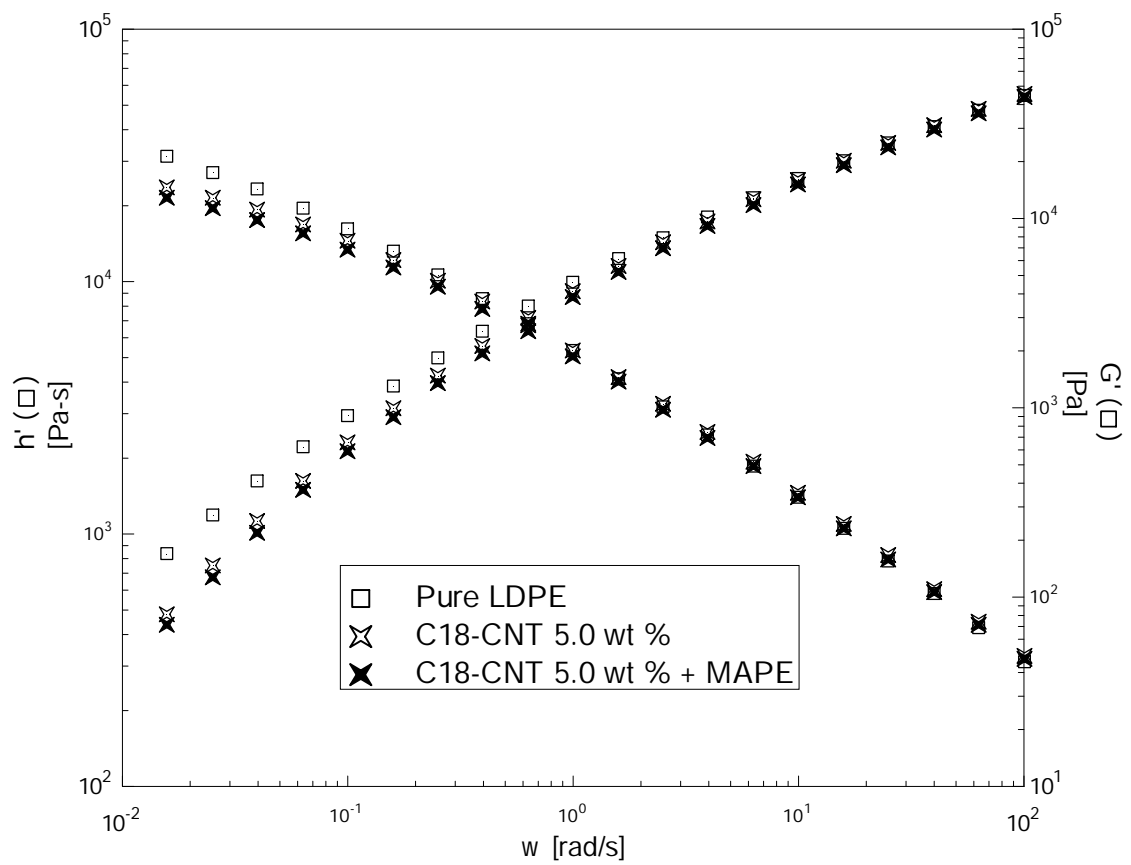


Figure 4.3.4.c. Dynamic viscosity & Storage modulus versus frequency plots for C₁₈-CNT/LDPE nanocomposites with MAPE.

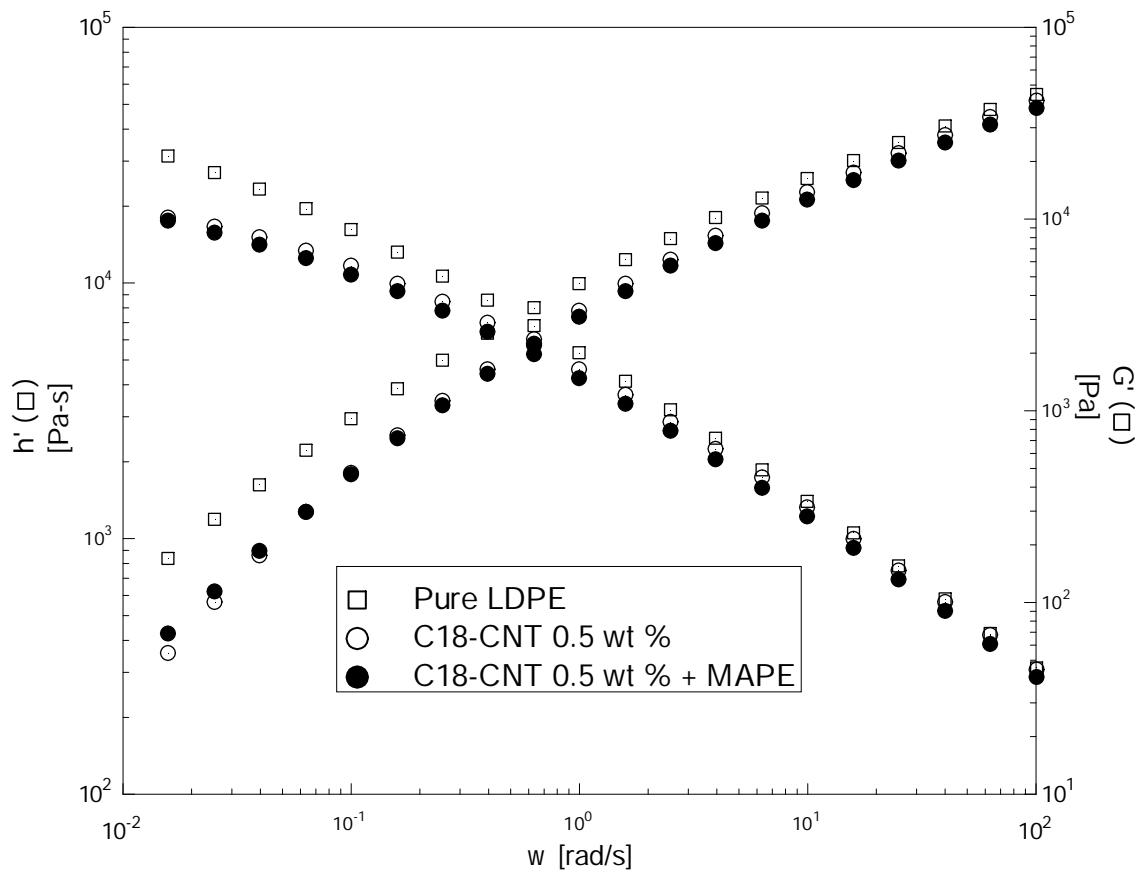


Figure 4.3.4.d. Dynamic viscosity & Storage modulus versus frequency plots for C₁₈-CNT/LDPE nanocomposites with MAPE.

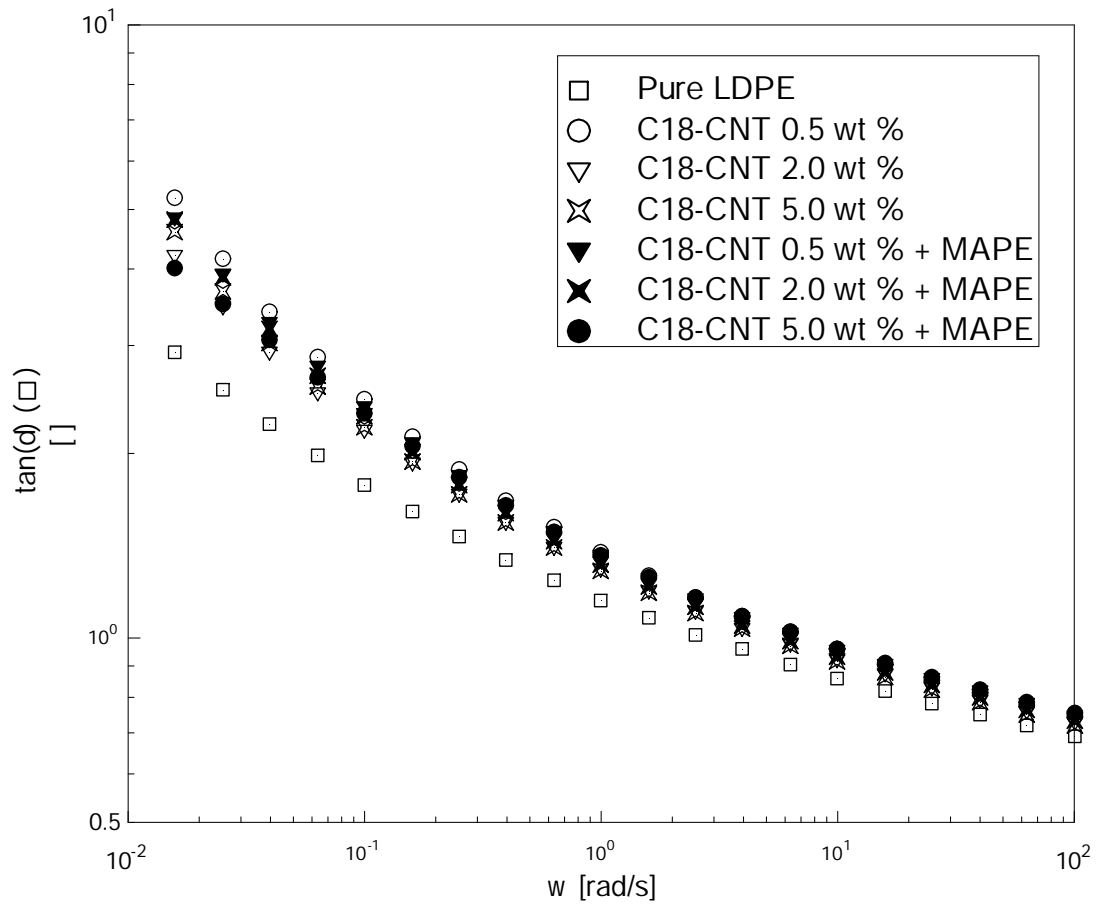


Figure 4.3.4.e. Tan (δ) versus frequency plots for C₁₈-CNT/LDPE nanocomposites with and without MAPE.

Figure 4.3.5.a shows the extensional viscosity (η_E) vs time (s) for C₁₈-CNT/LDPE nanocomposites. The loading was varied from 0.5 to 5.0 wt%. A very interesting observation is that as the loading is increased the nanocomposites showed almost the same η_E and strain hardening up to 5.0 wt% loading of C₁₈-CNT. In general, as the loading of the nanomaterial is increased the strain hardening increases and so does the η_E and time of break decreases [49]. Here, even though the loading is increased from 0.5 wt% to 5.0 wt% of C₁₈-CNT. Still the same η_E was maintained with no increase in strain hardening and without appreciable reduction in the time of break. This again can be explained by the fact that modification on the C₁₈-CNT plays the role of long chain branching. This modification is suggested to increase the free volume and helps in maintaining similar strain hardening levels up to 5.0 wt% loading of C₁₈-CNT. Interestingly, as the henky rate is increased from 0.5 s⁻¹ to 1.5 s⁻¹ (Figure 4.3.5.b), almost the same behavior of η_E as discussed above is obtained by the three nanocomposites.

So, it can be concluded from the rheological characterization that the addition of C₁₈-CNT to LDPE matrix lowers both η' and G' in the melt throughout the frequency range covered in this study. Results of phase angle suggest that all nanocomposites are more liquid-like at all frequencies and none of them have shown interconnected network behavior. For extensional viscosity the addition of up to 5.0 wt% of C₁₈-CNT did not increase strain hardening with little impact on η_E and time of break. This finding suggests that the processing of the C₁₈-CNT/LDPE would be improved due to the presence of the C₁₈ modification on the CNT.

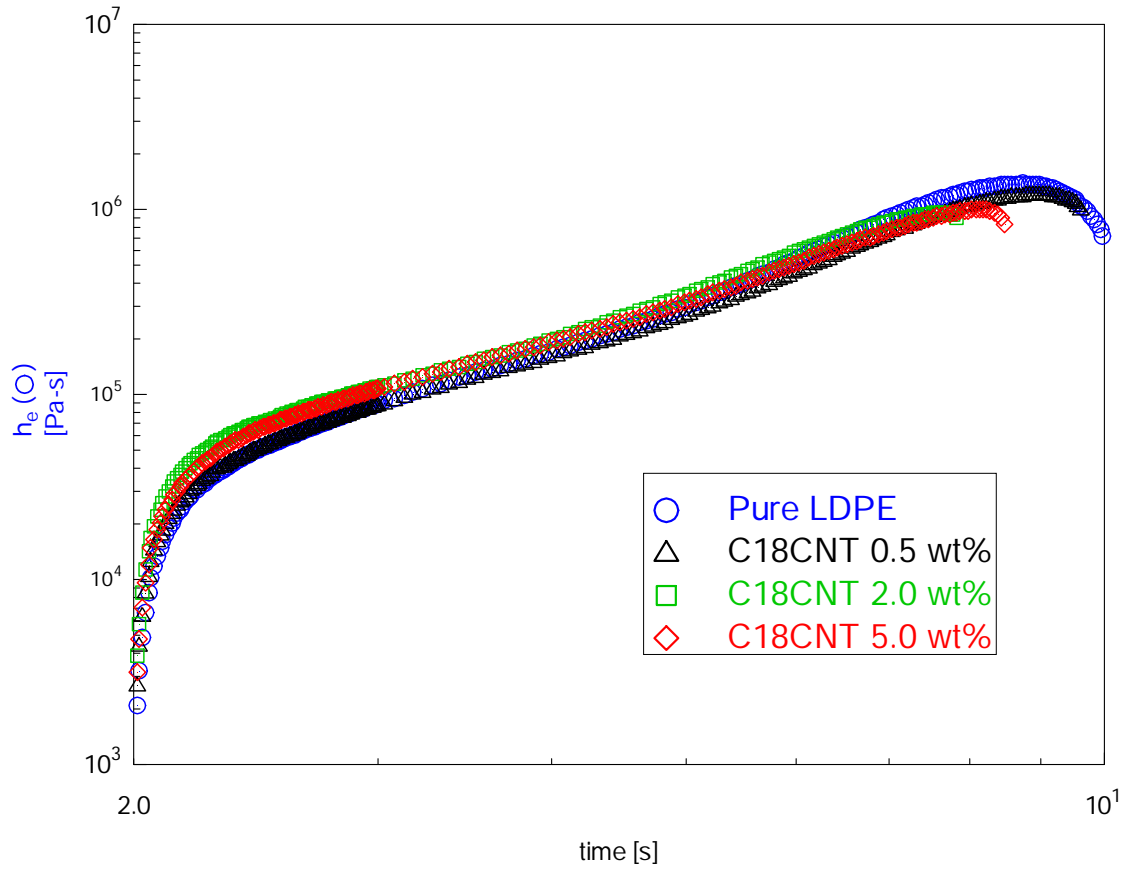


Figure 4.3.5.a. Extensional viscosity (η_E) vs time (s) for C₁₈-CNT/LDPE nanocomposites at 0.5 s⁻¹ henky rate.

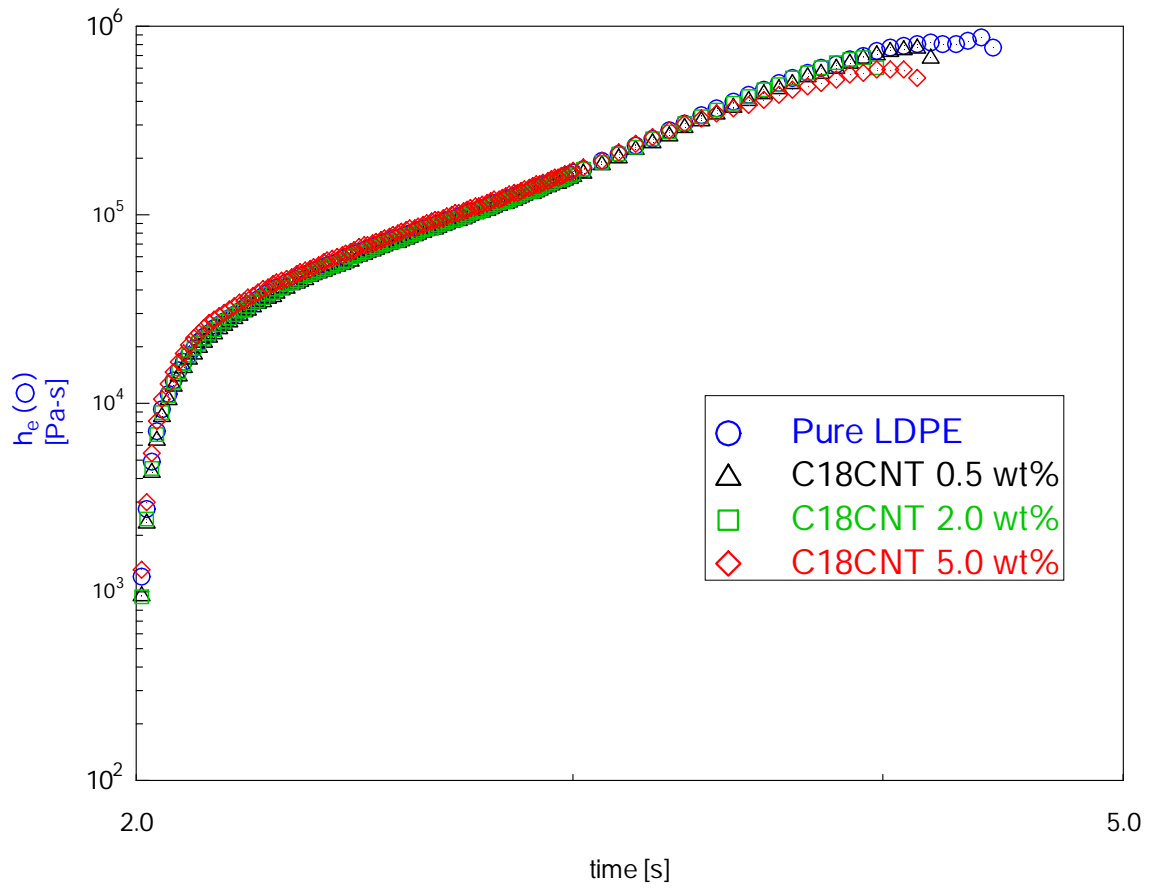


Figure 4.3.5.b. Extensional viscosity (η_E) vs time (s) for C₁₈-CNT/LDPE nanocomposites at 1.5 s⁻¹ henky rate.

4.3.5. Conclusion

Nanocomposites of C₁₈-CNT and LDPE were prepared using the melt blending process. The objective was to improve the mechanical and rheological properties. It was expected that addition of CNT would enhance the mechanical properties. CNT was chemically modified by introducing C₁₈. The addition of C₁₈-CNT to LDPE matrix improves the yield strength and Young's modulus. Ultimate strength was also improved up to 2.0 wt% loading of CNT, but a drop in ultimate strength was observed at 5.0 wt% loading of C₁₈-CNT. However, the C₁₈ modification resulted in major reduction in the drop in ultimate strength in comparison with similar systems that did not incorporate C₁₈ on CNT. Addition of 2.0 wt% MAPE into these nanocomposites further improved these properties while, percent elongation and toughness for the nanocomposite showed a decrease with increased loading. The use of MAPE did not have much effect on the two properties. The increase in C₁₈-CNT loading decreased the melt temperature. Percent crystallinity showed a correlation with Young's modulus. Both, Young's modulus and total crystallinity increased as loading of C₁₈-CNT is increased. Incorporation of compatibilizer increases both the Young's modulus and total crystallinity. Onset temperature increased with increasing loading of C₁₈-CNT in the LDPE matrix.

Usually the increase in mechanical properties tends to have adverse effect on rheological properties of the produced polymer nanocomposite. But the modification of CNT with C₁₈ proved to be useful as it effectively reduced dynamic viscosity at all frequencies and up to 5.0 wt% loadings. Storage modulus showed a similar behavior in the same range. Results of phase angle suggest no presence of network and nanocomposites that showed more liquid-like behavior in the range of 0.01-100 rad/s. Also, addition of C₁₈-CNT did

not increase strain hardening and maintained similar levels of extensional viscosity and time of break, up to henky rate of 1.5 s^{-1} . Effectively, there is an improvement in both mechanical and rheological properties. C_{18} on CNT is suggested to act as an insitu compatibilizer. It is likely that the modifier type and content play a major role on the mechanical and rheological properties of nanocomposites. This in turn opens the door for further research in this direction that takes into consideration the compatibility of the functional groups attached to CNT with the polymer matrix to improve the interfacial bonding between the CNT and the matrix.

4.3.6. Acknowledgment

The authors are thankful to the Center of Research Excellence in Petroleum Refining & Petrochemicals (CoRE-PRP), established by the Ministry of Higher Education, for providing the funding for this research. KFUPM is also acknowledged for its support.

4.3.7. References

- [1] Lourie O., Cox D. M., Wagner H. D.: Buckling and collapse of embedded carbon nanotubes. *Physics Review Letters*, **81**, 1638-1641 (1998).
- [2] Yu M., Lourie O., Dyer M. J., Kelly T. F., Ruoff R. S.: Strength and breaking mechanism of multiwalled carbon nanotubes under tensile load. *Science*, **287**, 637-640 (2000).
- [3] Xie S., Li W., Pan Z., Chang B., Sun L.: Mechanical and physical properties on carbon nanotube. *Journal of Physics and Chemistry of Solids*, **61**, 1153–1158 (2000).
- [4] Yao Z., Zhu C. C., Cheng M., Liu J.: Mechanical properties of carbon nanotubes by molecular dynamic simulation. *Computational Materials Science*, **22**, 180-184 (2001).

- [5] Yu F., Files B. S., Arepalli S., Ruoff R. S.: Tensile loading of ropes of single wall carbon nanotubes and their mechanical properties. *Physics Review Letters*, **84**, 5552-5555 (2000).
- [6] Wagner D., Lourie O., Feldman Y., Tenne R.: Stress-induced fragmentation of multiwall carbon nanotubes in a polymer matrix. *Applied Physics Letters*, **72**, 188-190 (1998).
- [7] Wong E. W., Sheehan P. E., Lieber C.M.: Nanobeam mechanics: elasticity, strength, and toughness of nanorods and nanotubes. *Science*, **277**, 1971-1975 (1997).
- [8] Treacy M. M. J., Ebbesen T. W., Gibson J. M.: Exceptionally high Young's modulus observed for individual carbon nanotubes. *Nature*, **381**, 678-680 (1996).
- [9] Zhang P., Huang Y., Geubelle P. H., Klein P. A., Hwang C. K.: The elastic modulus of single-wall carbon nanotubes: a continuum analysis incorporating interatomic potentials. *International Journal of Solids and Structures*, **39**, 3893-3906 (2002).
- [10] Vodenitcharova T., Zhang L. C.: Effective wall thickness of a single-walled carbon nanotube. *Physics Review B*, **68**, 165401-105405 (2003).
- [11] Goze C., Bernier P., Henrard L., Vaccarini L., Hernandez E., Rubio A.: Elastic and mechanical properties of carbon nanotubes. *Synthetic Metals*, **103**, 2500-2501 (1999).
- [12] Moniruzzaman M., Winey K. I.: Polymer nanocomposites containing carbon nanotubes. *Macromolecules*, **39**, 5194-5205 (2006).
- [13] Xiao K. Q., Zhang L. C., Zarudi I.: Mechanical and rheological properties of carbon nanotube reinforced polyethylene composites. *Composites Science & Technology*, **67**, 177-182 (2007).
- [14] Mierczynska A., Mayne-L'Hermite M., Boiteux G., Jeszka J. K.: Electrical and Mechanical Properties of Carbon nanotube / Ultra molecular Weight polyethylene composites prepared by filler prelocalization method. *Journal of Applied Polymer Science*, **105**, 158-168 (2007).
- [15] Yang B-X., Shi J-H., Pramoda K. P., Goh S. H.: Enhancement of the mechanical properties of polypropylene using propylene grafted multiwalled carbon nanotubes. *Composites Science & Technology*, **68**, 2490-2497 (2008).

- [16] Tang W., Santare M. H., Advani S.G.: Melt processing and mechanical property characterization of multi walled carbon nanotube / high density polyethylene composite film. *Carbon*, **41**, 2779-2785 (2003).
- [17] Mahfuz H., Adnan A., Rangari V. K., Jeelani S., Jang B. Z.: Carbon nanoparticles/whiskers reinforced composites and their tensile properties. *Composites Part A: Applied Science and Manufacturing*, **35**, 519-527 (2004).
- [18] Zhao P., Wang K., Yang H., Zhang Q., Du R., Fu Q.: Excellent tensile ductility in highly oriented injection-molded bar of polypropylene / carbon nanotubes composites. *Polymer*, **48**, 5688-5695 (2007).
- [19] Chow T.S.: Tensile strength of filled polymers. *Journal of Polymer Science Polymer Physics Part B*, **20**, 2103-2109 (1982).
- [20] Wagner H.D.: Reinforcement. in 'Encyclopedia of polymer science and technology' (ed.: Kroschwitz J. I.) Wiley-Interscience, New York, Vol 4, 94-115, (2003).
- [21] Wagner H. D., Vaia R. A.: Nanocomposites: issues at the interface. *Materials Today*, **7**, 38-42 (2004).
- [22] Schadler L. S., Giannaris G. C., Ajayan P. M.: Load transfer in carbon nanotube epoxy composites. *Applied Physics Letters*, **73**, 3842-3844 (1998).
- [23] Qian D., Liu W. K., Ruoff R. S.: Load transfer mechanism in carbon nanotube ropes. *Composites Science & Technology*, **63**, 1561-1569 (2003).
- [24] Prashantha K., Soulestin J., Lacrampe M. F., Claes M., Dupin G., Krawczak P.: Multi walled carbon nanotubes filled polypropylene nanocomposites based on materbatch route: Improvement of dispersion and mechanical properties through PP-g-MA addition. *Express Polymer Letters*, **2**, 735-745 (2008).
- [25] Kangaraj S., Varanda F. R., Zhil'tsova T. V., Oliveira M. S. A., Simoes J. A. O.: Mechanical properties of high density polyethylene / carbon nanotube composites. *Composites Science & Technology*, **67**, 3071-3077 (2007).
- [26] Wang Y., Cheng R., Liang L., Wang Y.: Study on the preparation and characterization of ultra high molecular weight polyethylene carbon nanotubes composite fiber. *Composites Science & Technology*, **65**, 793-797 (2005).

- [27] Miltner H. E., Grossiord N., Lu K., Loos J., Koning C. E., Mele B. V.: Isotactic polypropylene / carbon nanotube composites prepared by latex technology. Thermal analysis of carbon nanotube induced nucleation. *Macromolecules*, **41**, 5753-5762 (2008).
- [28] Jin S. H., Kang C. H., Yoon K. H., Bang D. S., Park Y.: Effect of compatibilizer on morphology, thermal and rheological properties of polypropylene/functionalized multi walled carbon nanotubes composites. *Journal of Applied Polymer Science*, **111**, 1028-1033 (2009).
- [29] Valentino O., Sarno M., Rainone N. G., Nobile M. R., Ciambelli P., Neitzert H. C., Simon G.P.: Influence of polymer structure and nanotube concentration on the conductivity and rheological properties of polyethylene / CNT composites. *Physica E: Low-dimensional Systems and Nanostructures*, **40**, 2440-2445 (2008).
- [30] Manchado M. A. L., Valentini L., Biagiotti J., Kenny J. M.: Thermal and mechanical properties of single walled carbon nanotubes polypropylene composites prepared by melt processing. *Carbon*, **43**, 1499-1505 (2005).
- [31] Park C., Ounaies Z., Watson K. A., Crooks R. E., Smith J., Lowther S. E., Connell J. W., Siochi E. J., Harrison J. S., St. Clair T. L.: Dispersion of Single Wall Carbon Nanotubes by In Situ Polymerization Under Sonication. *Chemical Physics Letters*, **364**, 303-308 (2002).
- [32] Cooper C. A., Ravich D., Lips D., Mayer J., Wagner H. D.: Distribution and alignment of carbon nanotubes and nanofibrils in a polymer matrix. *Composites Science & Technology*, **62**, 1105-1112 (2002).
- [33] Park S-J., Cho K-S., Ryu S-K.: Filler–elastomer interactions: influence of oxygen plasma treatment on surface and mechanical properties of carbon black / rubber composites. *Carbon*, **41**, 1437-1442 (2003).
- [34] Lee S. H., Kim M. W., Kim S. H., Youn J. R.: Rheological and electrical properties of polypropylene / MWCNT composites prepared with MWCNT materbatch chips. *European Polymer Journal*, **44**, 1620-1630 (2008).
- [35] Song Y. S., Youn J. R.: Influence of dispersion states of carbon nanotubes on physical properties of epoxy nanocomposites. *Carbon*, **43**, 1378-1385 (2005).
- [36] Zhang Q., Lippits D. R., Rastogi S.: Dispersion and rheological aspects of SWNTs in ultrahigh molecular weight polyethylene. *Macromolecules*, **39**, 658-666 (2006).

- [37] Bin Y., Yamanaka A., Chen Q., Xi Y., Jiang X., Matsuo M.: Morphological, electrical and mechanical properties of ultrahigh molecular weight polyethylene and multi-wall carbon nanotube composites prepared in decalin and paraffin. *Polymer Journal*, **39**, 598-609 (2007).
- [38] Ruan S. L., Gao P., Yang X. G., Yu T. X.: Toughening high performance ultrahigh molecular weight polyethylene using multiwalled carbon nanotubes. *Polymer*, **44**, 5643-5654 (2003).
- [39] McNally T., Poetschke P., Halley P., Murphy M., Martin D., Bell S. E. J., Brennan G. P., Bein D., Lemoine P., Quinn J. P.: Polyethylene multiwalled carbon nanotube composites. *Polymer*, **46**, 8222-8232 (2005).
- [40] Wang M., Pramoda K. P., Goh S. H.: Enhancement of interfacial adhesion and dynamic mechanical properties of poly(methyl methacrylate)/multiwalled carbon nanotube composites with amine-terminated poly(ethylene oxide). *Carbon*, **44**, 613-617 (2006).
- [41] Gojny F. H., Nastalczyk J., Roslaniec Z., Schulte K.: Surface modified multi-walled carbon nanotubes in CNT/epoxy-composites. *Chemica Physics Letters*, **370**, 820-824 (2003).
- [42] Zhao C., Hu G., Justice R., Schaefer D. W., Zhang S., Han, C. C.: Synthesis and characterization of multi-walled carbon nanotubes reinforced polyamide 6 via in situ polymerization. *Polymer*, **46**, 5125-5132 (2005).
- [43] Zhu B-K., Xie S-H., Xu Z-K., Xu Y-Y.: Preparation and properties of the polyimide/multi-walled carbon nanotubes (MWNTs) nanocomposites. *Composites Science & Technology*, **66**, 548-554 (2006).
- [44] Shin D. H., Yoon K. H., Kwon O. H., Min B. G., Hwang C. I.: Surface resistivity and rheological behaviors of carboxylated Multiwall carbon nanotube-filled PET composite film. *Journal of Applied Polymer Science*, **99**, 900-904 (2006).
- [45] Jin S. H., Park Y-B., Yoon K. H.: Rheological and mechanical properties of surface modified multi-walled carbon nanotube-filled PET composite. *Composite Science & Technology*, **67**, 3434-3441 (2007).
- [46] Jin S. H., Yoon K. H., Park Y. B., Bang D. S.: Properties of surface-modified multiwalled carbon nanotube filled poly(ethylene terephthalate) composite films. *Journal of Applied Polymer Science*, **107**, 1163-1168 (2008).

- [47] Kharchenko S. B., Douglas J. F., Obrzut J., Grulke E. A.: Flow-induced properties of nanotubes filled polymer materials. *Nature materials*, **3**, 564-568 (2004).
- [48] Xu D-H., Wang Z-G.: Influence of Carbon nanotube aspect ratio on normal stress difference in isotactic polypropylene nanocomposite melts. *Macromolecules*, **41**, 815-825 (2008).
- [49] Lee S. H., Cho E., Jeon S. H., Youn J. R.: Rheological and electrical properties of polypropylene composites containing functionalized multi-walled carbon nanotubes and compatibilizers. *Carbon*, **45**, 2810-2822 (2007).
- [50] Potschke P., Fornes T. D., Paul D. R.: Rheological behavior of multiwalled carbon nanotube/polycarbonate composites. *Polymer*, **43**, 3247-3255 (2002).
- [51] Hussein I. A., Williams M. C.: Rheological study of heterogeneities in melt blends of ZN-LLDPE and LDPE: Influence of Mw and comonomer type, and implications for miscibility. *Rheologica Acta*, **43**, 602-614 (2004).
- [52] Abuilawi F.A., Laoui T., Al-Harhi M., Atieh M.A.: Modification and functionalization of multiwalled carbon nanotubes (MWCNT) via Fischer esterification. *AJSE*, **35**, 37-47 (2010).
- [53] Ashraful Islam, Ibnelwaleed A. Hussein, "Influence of Branch Content, Comonomer Type, and Crosshead Speed on the Mechanical Properties of metallocene LLDPEs", *J. Applied Polymer Science*, 100(6), 5019-5033, 2006.
- [54] Zhang Q., Lippits D. R., Rastogi S.: Dispersion and Rheological Aspects of SWNTs in Ultrahigh Molecular Weight Polyethylene. *Macromolecules*, **39**, 658-666 (2006).
- [55] Jain S. H.: Nano-scale events with macroscopic effects in polypropylene/silica nanocomposites; effect of polymer adsorption on processability and properties. Ph.D. Thesis, Technische Universiteit Eindhoven, 2005.
- [56] Mackay M. E., Dao T. T., Tuteja A., Ho D. L., Horn B. V., Kim H-C., Hawker C. J.: Nanoscale effects leading to non-Einstein-like decrease in viscosity. *Nature Materials*, **2**, 762-766 (2003).

4.4 Non-isothermal crystallization kinetics study of LDPE / MWCNT nanocomposites: Effect of Aspect ratio and surface modification.

4.4.1. Abstract

In this paper, the effect of aspect ratio and chemical modification of multiwall carbon nanotubes (MWCNT) on the non-isothermal crystallization kinetics of LDPE/MWCNT nanocomposites was studied. Nine different samples were prepared using different MWCNT to study both effects. The cooling rate (R) was varied in the range 2–10°C/min, and it significantly affected the crystallization behavior. In this paper, the effect of CNT loading, surface modification and aspect ratio were studied. For the same MWCNT concentration, aspect ratio and -COOH modification had weak influence on both the peak crystallization temperature and the crystallization onset temperature. However, crystallization onset temperature was significantly affected by the amount of MWCNT. The rate parameters in the modified Avrami method and Mo method [F(T)] of analyses show a very good fit of data. The Vyazovkin and Sbirrazzuoli method of analysis, which is based on Hoffman–Lauritzen theory for secondary crystallization, was also used. Temperature dependency of activation energy was obtained for 30-75% relative crystallinity of the produced nanocomposites. Activation energy based on calculations of Hoffman-Lauritzen theory showed a decrease with the increase in the concentration of MWCNT and crystallization temperature. A proposed model of the form $E = a \exp(-bXT)$ which relates the activation energy, E, to relative crystallinity, X, and crystallization temperature, T, was able to fit the whole set of data. Incorporation of MWCNT in

nanocomposites lowers the activation energy; hence enhances the initial crystallization process as suggested by the different methods of data analyses.

4.4.2. Introduction

The microstructure of the polymer and nano materials play an important role in determining the polymer nanocomposite mechanical, optical, rheological, and thermal properties. In this study, the influence of structure of carbon nanotubes (CNT) and its loading on the thermal properties of polyethylene/CNT nanocomposites is investigated. The study of polymer crystallization kinetics is significant from theoretical and practical points of view [1-9]. Many researchers have investigated the crystallization behavior of different polyethylenes [10-15].

The previous research has primarily focused on the study of the influence of molecular weight (Mw), molecular weight distribution (MWD), branch type, branch content (BC), and crystallization conditions on the crystallization behavior of ethylene/ α -olefin copolymers [16-28]. Most of these studies used Ziegler–Natta linear low density polyethylenes (ZN-LLDPEs). Due to the random comonomer composition and sequence distribution, and intermolecular heterogeneity of ZN-LLDPEs, the effects of the individual factors on the crystallization phenomenon is difficult to separate. For example, increase in BC, a lamella first becomes shorter, then segmented, and eventually disintegrates into small crystallites [28]. Also, the previous studies used primarily fractions of conventional heterogeneous ZN-LLDPEs [16,18,21,25,30].

Several studies on the thermal properties and molecular structure of metallocene LLDPE (m-LLDPEs) have been reported by different authors [26,29,31-42]. Most of these studies focused on the influence of short chain branch distribution [26,31-33,37,40-42] on melting and crystallization kinetics, particularly of a single polymer and its fractions using different fractionation techniques [34,35,37-39]. Bensason et al. [29] classified homo geneous ethylene/1-octene copolymers based on comonomer content and reported the melting phenomena and crystal morphology by relating their results to the tensile and dynamic mechanical properties. Seo et al. [43] reinforced Polypropylene (PP) with multiwalled carbon nanotubes (MWCNTs), varying the weight fraction from 1 to 5%. They studied the crystallization kinetics and evaluated the isothermal crystallization parameters (n and k) for avrami. They deduced that the addition of 1% MWCNTs increases the crystallization rate by as much as an order of magnitude or higher and is attributed to enhanced nucleation, resulting from the presence of MWCNTs.

Funck et al. [44] produced PP / MWCNT composites by in situ polymerization. They studied the half time of crystallization for the produced composites using Avrami plots. They observed that crystallization rate increased with decreasing isothermal crystallization temperature and higher loadings with MWCNT for all materials that they investigated.

Vega et al. [45] produced nanocomposite samples by melt mixing a high density polyethylene (HDPE) with an in situ polymerized HDPE/MWCNT masterbatch. They also conclude that crystallization kinetics studied through DSC suggest that the MWCNTs act as nucleating agents for polymeric chains. The length of the MWCNTs

(short vs long) would likely affect the nucleation of polymeric chains. Therefore, we would like to investigate the effect of aspect ratio and chemical modification of CNT on the non isothermal crystallization kinetics which has not been reported in the literature. In this study, we will use LDPE and MWCNT to investigate these parameters. In addition, the effect of CNT loading will be studied.

4.4.3. Experimental

4.4.3.1. *Materials and Sample Preparation*

MWCNTs with different aspect ratios and surface modification were supplied by Cheap Tubes Inc, USA. Table 4.4.1. shows energy dispersive x-ray spectroscopy data provided by the supplier. In Table 4.4.2., details of the three different CNTs used in the study are given. The three different types are selected to study one parameter at a time. The long and the short CNTs have the same ID and OD; however, the length of the long CNT is 12 times higher than the short CNTs. The aspect ratio is defined as the length / OD. Therefore a comparison of the long and short MWCNT will reveal the impact of aspect ratio. On the other hand, a comparison of MWCNT and COOH-MWCNT will highlight the influence of chemical modification since both CNTs are having the same ID, OD and length.

In all of the MWCNT used, 95% percent of the total weight is MWCNT and approximately 1.5% of the weight was ash and the rest was by products from MWCNT production. MWCNT used were not washed or purified. As stated by the producing company, COOH-MWCNT contains 0.7% -COOH groups. The LDPE has a weight average molecular weight of 99.5 kg/mol and a MWD of 6.5 and a melt index of 0.75

g/10 min and a total short branch content of 22 branches/1000 C as determined by GPC and NMR, respectively Hussein and Williams [46]. The LDPE resin and MWCNT-LDPE composites were conditioned (or blended) in a Haake PolyDrive melt blender. The blending temperature used was 190°C. The rpm was 50 and time of blending was 10 minutes. From here onwards the long, short and COOH modified MWCNT will be named LCNT, SCNT and MCNT, respectively.

Table 4.4.1. Energy dispersive X-ray spectroscopy of MWCNTs.

Components	Contents (%)
C	97.34
Cl	0.21
Fe	0.56
Ni	1.87
S	0.02

Table 4.4.2. Dimensions of the multi-walled carbon nano tubes (MWCNT).

Name	OD*	ID**	Length	Aspect ratio, (L/D)
Long MWCNT 95 wt%	30-50nm	5-15nm	10-20 μ m	375
Short MWCNT 95 wt%	30-50nm	5-15nm	0.5-2.0 μ m	31
COOH-MWCNT 95 wt%	30-50nm	5-15nm	10-20 μ m	375

*outer diameter, ** inner diameter

4.4.3.2 Differential Scanning Calorimetry (DSC)

All measurements were performed using a TA Q1000 instrument equipped with a liquid nitrogen cooling system and auto sampler. Nitrogen at a flow rate 50 ml/min was used to purge the instrument to prevent degradation of the samples upon thermal treatments. The DSC was calibrated in terms of melting temperature and heat of fusion using a high purity Indium standard (156.6°C and 28.45 J/g). The absolute crystallinity was calculated using the heat of fusion of a perfect polyethylene crystal, 290 J/g [47].

Composite samples (7.5–10 mg) were sliced and compressed into a non-hermetic aluminum pans. To minimize the thermal lag between the sample and the pan, samples with flat surface were used. An empty aluminum pan was used as reference. The previous thermal effects were removed by heating the samples from room temperature to 140°C; followed by a hold up at 140°C for 5 min. All samples were cooled to sub ambient temperatures for complete evaluation of crystallization [25]. The samples were cooled from 140° to 5°C at a rate of 2 °C/min, 6°C/min and 10°C/min. First, the baseline was calibrated using empty crimped aluminum pans. All testing was performed in the standard DSC mode.

4.4.4. Theory & Calculation

4.4.4.1. *Non-isothermal crystallization kinetics*

Several analytical methods have been developed to describe the non-isothermal crystallization kinetics of polymers: (1) modified Avrami analysis, [2,48-50] (2) Ozawa analysis, [2] (3) Ziabicki analysis,[51-52] and other methods [53-54]. In this study, the modified Avrami analysis proposed by Jeziorny [3] and the Mo method suggested by Liu

et al. [55] were used to describe the non-isothermal crystallization kinetics of LDPE / MWCNT composites. Because of the variation in the range of crystallization temperatures, the Ozawa model [2] was not suitable for this study. The Avrami equation is defined as follows: [48-50]

$$1 - X_t = \exp(-k_t t^n) \quad (1)$$

where n is the Avrami crystallization exponent, which is dependent on the nucleation mechanism and growth dimensions; t is the crystallization time; k_t is the growth rate constant, which depends on nucleation and crystal growth; and X_t is the relative crystallinity [50]. X_t is defined as follows:

$$X_t = \frac{\int_{t_0}^t \left(\frac{dH_c}{dt}\right) dt}{\int_{t_0}^{t_\infty} \left(\frac{dH_c}{dt}\right) dt} \quad (2)$$

where dH_c/dt is the rate of heat evolution and t_0 and t_∞ are the onset and completion times of the crystallization process, respectively. The Avrami equation was developed on the basis of the assumption that the crystallization temperature is constant. Jeziorny [3] modified the equation to describe non-isothermal crystallization. At a chosen cooling rate (R), the relative crystallinity is a function of the crystallization temperature (T). That is, equation (2) can be formulated as

$$X_T = \frac{\int_{T_0}^{T_c} \left(\frac{dH_c}{dT}\right) dT}{\int_{T_0}^{T_\infty} \left(\frac{dH_c}{dT}\right) dT} \quad (3)$$

where X_T is the relative crystallinity as a function of crystallization temperature, T_o denotes the crystallization onset temperature, and T_c and T_∞ represent the crystallization temperatures at time t and after the completion of the crystallization process, respectively. Also, time t can be calculated from T_c using the following equation: [2,51]

$$t = \frac{T_o - T}{R} \quad (4)$$

where R is the cooling rate ($^{\circ}\text{C}/\text{min}$). The double- logarithmic form of Eq. (1) yields

$$\ln[-\ln(1 - X_t)] = \ln k_t + n \ln t \quad (5)$$

Thus, n and the crystallization rate constant (k_t) can be obtained from the slope and intercept of the plot of $\ln[-\ln(1-X_t)]$ versus $\ln t$, respectively, for each R . The physical meaning of k_t and n cannot be related to the non-isothermal case in a simple way; they provide further insight into the kinetics of non-isothermal crystallization. The rate of non-isothermal crystallization depends on R . Therefore, k_t can be corrected to obtain the corresponding primary rate constant (k_R). [2]

$$\ln k_R = \frac{\ln k_t}{R} \quad (6)$$

A method modified by Mo, which combines the Avrami equation with the Ozawa equation, was also used to describe the non-isothermal crystallization. Its final form is given as follows: [55]

$$\ln R = \ln F(T) - \alpha \ln t \quad (7)$$

where M_0 modified crystallization rate parameter $(F(T)) = [k(T)/k_0]^{1/m}$ represents the value of R and α is the ratio of n to the Ozawa exponent (m ; $\alpha=n/m$).

Furthermore, the effective activation energy (ΔE_x) was calculated theoretically with the method proposed by Vyazovkin and Sbirrazzuoli [56]. In this method, the coefficient of the growth rate (G) and the overall crystallization rate (dX/dt) are related by

$$\frac{-E}{R} = \frac{d \ln G}{dT^{-2}} = \frac{d \ln \left(\frac{dX}{dt} \right)}{dT^{-2}} \quad (8)$$

G is given as a function of T_c by the Hoffman–Lauritzen equation in the context of the Hoffman–Lauritzen secondary nucleation theory [57]. Vyazovkin and Sbirrazzuoli [56] modified the Hoffman–Lauritzen equation to calculate ΔE_x at a given conversion (X) from the following relationship:

$$\Delta E_x = U^* \frac{T^2}{(T-T_\infty)^2} + K_g R \frac{(T_m^0)^2 - T^2 - T_m^0 T}{(T_m^0 - T)^2 T} \quad (9)$$

where U^* denotes the activation energy per segment, which characterizes the molecular diffusion across the interfacial boundary between melt and crystals; T_∞ is usually set equal to $T_g - 30$ K, where T_g is the glass-transition temperature of the polymer; K_g is a nucleation constant; T_m^0 is the equilibrium melting point for the polymer, and R is the gas constant. The Vyazovkin and Sbirrazzuoli method and Hoffman–Lauritzen theory have been widely used in recent literature to calculate U^* and K_g [58-61].

4.4.5. Results & Discussion

The non-isothermal crystallization MDSC traces (non-reversing curves) of pure LDPE and its nanocomposites at low and high R values (2, 6 and 10°C/min) are shown in Figure 4.4.1.(a-c). For all the samples with varying nanocomposite amount, the DSC thermograms showed no change in the baseline above 120°C and below 30°C. So, these values are used as the initial and final values for all of the DSC calculations, if applicable. The LDPE nanocomposites crystallization exotherms were fairly similar. They showed a distinct high-temperature peak followed by a broad long tail. However, it can distinctly be observed from Figure 4.4.1. (a-c) that as the amount of MWCNT in the composite is increased, early onset of crystallization takes place. For example, at the low cooling rate (2°C/min) T_{onset} increases from an average value of 105.38 for 0.5 wt% MWCNT to 106.85°C for the 5.0 wt% MWCNT. However, the effect of both the aspect ratio and COOH modification at this low cooling rate is much less as given by the data shown in Table 4.4.3. Table 4.4.3. was prepared using the TA analysis software. For each exotherm, the peak and onset crystallization were found using the software options. Similarly, the influence of aspect ratio or COOH modification on T_{peak} is weak.

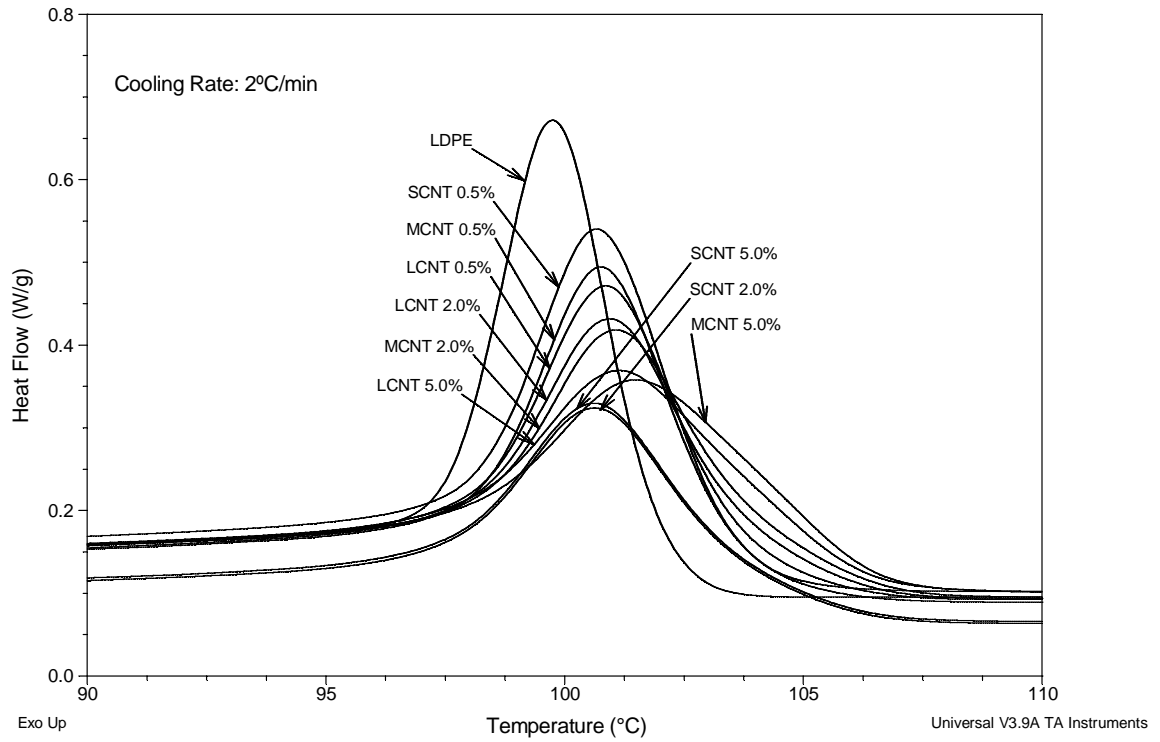


Figure 4.4.1.a. Non-isothermal crystallization exotherms of LDPE / MWCNT nanocomposites with R of 2 °C/min.

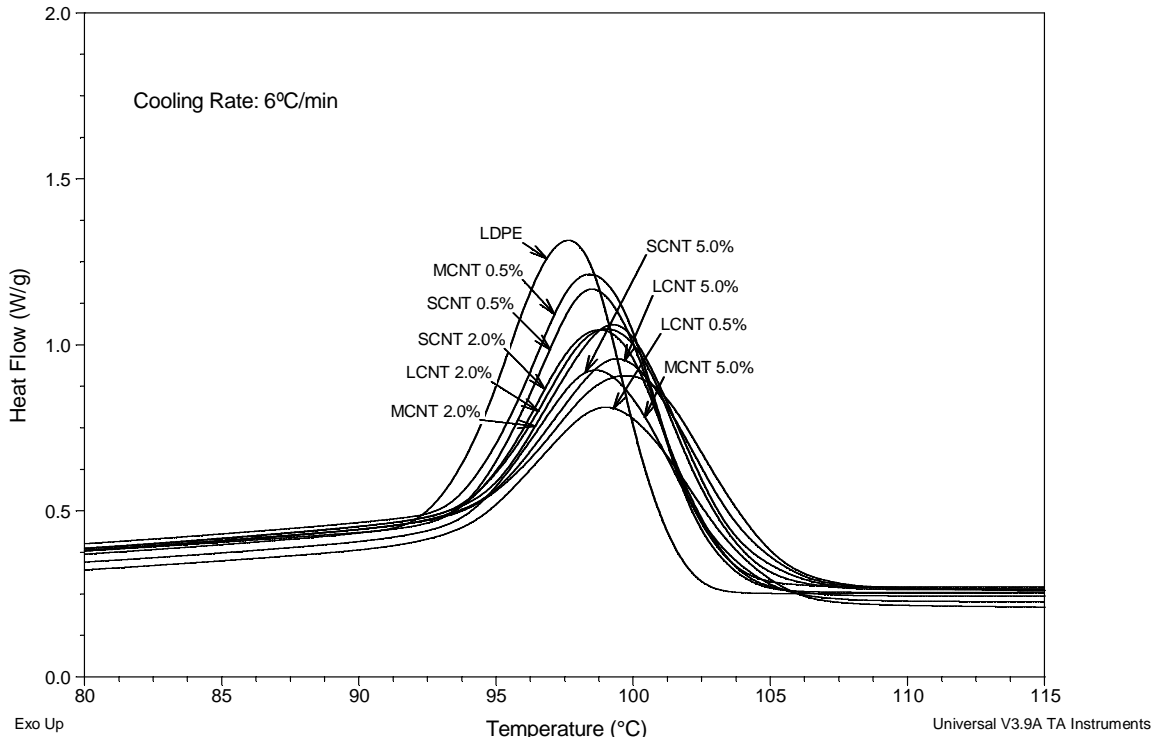


Figure 4.4.1.b. Non-isothermal crystallization exotherms of LDPE / MWCNT nanocomposites with R 6 °C/min.

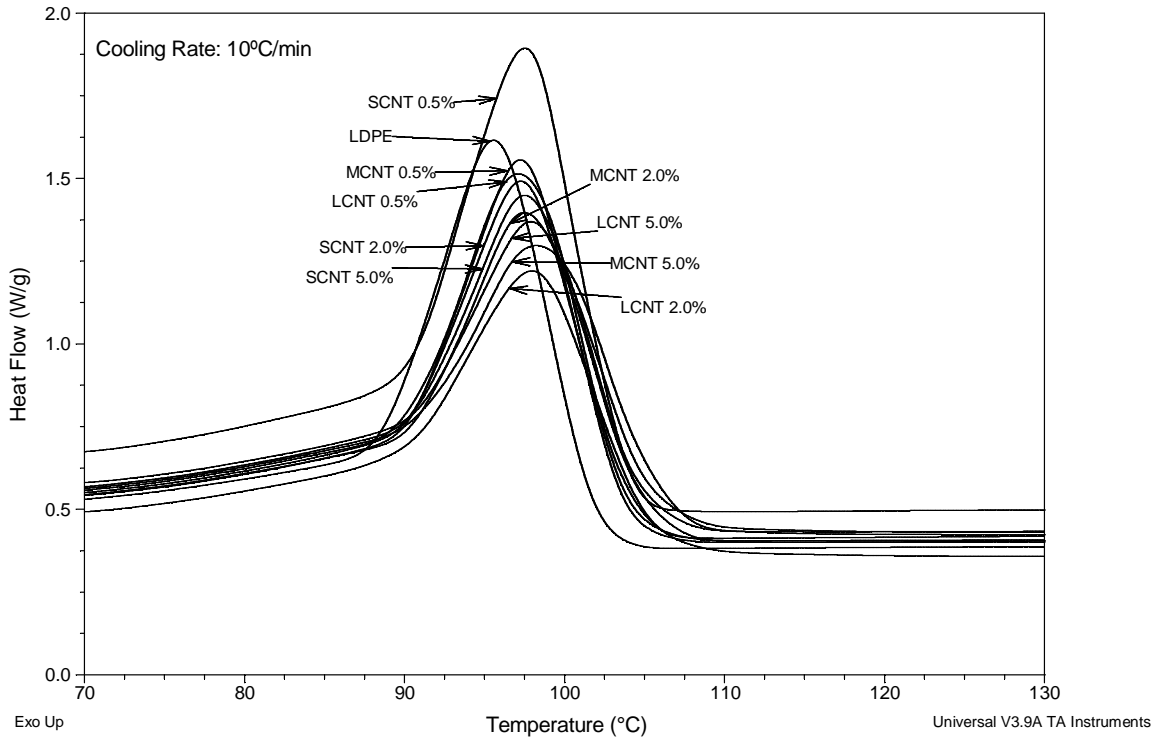


Figure 4.4.1.c. Non-isothermal crystallization exotherms of LDPE / MWCNT nanocomposites with R of 10 °C/min.

Table 4.4.3. Peak and onset crystallization temperatures for different nanocomposites.

Cooling Rate	Weight %	MWCNT Type	T_{Peak} (°C)	T_{Onset} (°C)
2°C/min	0.5	Long	100.85	105.34
		Short	100.66	105.08
		Modified	100.75	105.71
	2.0	Long	100.95	105.84
		Short	100.61	106.21
		Modified	101.05	106.08
	5.0	Long	101.14	106.82
		Short	100.61	106.88
		Modified	101.50	106.86
10°C/min	0.5	Long	97.10	105.81
		Short	97.50	104.94
		Modified	97.2	104.64
	2.0	Long	97.95	107.10
		Short	97.25	105.12
		Modified	97.45	105.94
	5.0	Long	97.90	108.01
		Short	97.50	106.69
		Modified	98.2	107.12

At high cooling rate (10°C/min), LCNT showed higher T_{onset} values that increase with MWCNT concentration. A comparison of LCNT and MCNT (both have the same aspect ratio) and the LCNT and SCNT suggests that aspect ratio has influenced T_{onset} but not T_{peak} with weak influence of surface modification on T_{peak} as well as T_{onset} . This suggests that the effect of aspect ratio on T_{onset} is cooling rate dependent and it is more pronounced at high cooling rate. On the other hand, the impact of aspect ratio or surface modification of MWCNT on T_{peak} is very weak. This observation can be explained, tentatively, as follows: CNT with high aspect ratio (LCNT) promotes nucleation due to its large surface area per tube. However, for T_{peak} the surface area of CNT is no longer a factor in enhancing crystallization since crystallization is already at its peak. Therefore, the increase in MWCNT concentration shifts T_{onset} to higher values and promotes nucleation with almost no effect on T_{peak} . Nevertheless, we observed that at low cooling rates surface modification and aspect ratio did not affect T_{onset} or T_{peak} . In general, there was a decrease in total crystallinity due to the addition of MWCNT which is a direct result of the decrease of the polymer portion in the nanocomposite.

The relative crystallinity X_T was calculated using Eq. (3) and shown in Figure 4.4.2.(a-c) for the different cooling rates. X_T was then converted into X_t using Eq. (4). X_t versus t is plotted in Figure 4.4.3.(a-c). The whole data of LDPE nanocomposites was used to fit Avrami model but it is known that it will not fit the entire crystallization range [see ref. 62 and references therein]. Avrami equation was used to fit data in the range of $X_T=0-40\%$ crystallization. But we encountered the problem getting n greater than 4 which has no physical meaning [53]. Figure 4.4.4. represents sample Avrami plots for all LDPE

nanocomposites obtained at 2°C/min. Avrami equation was used to fit data in the range of $X_T=0-40\%$. The rest of the results and extracted parameters are shown in Table 4.4.4. Table 4.4.5 shows the comparison of Avrami parameter and fit quality at 40% and 95% crystallinity.

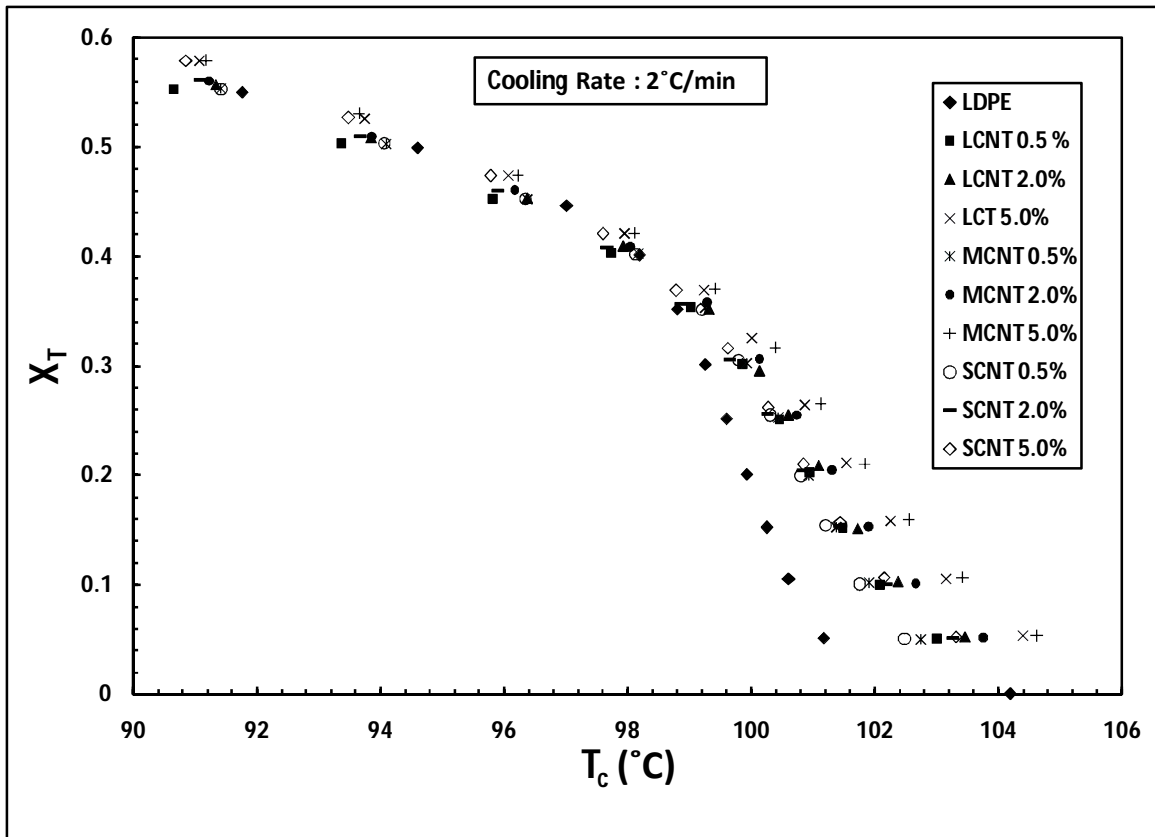


Figure 4.4.2.a. X_T vs. T_c for LDPE/MWCNT nanocomposites at cooling rate of 2 °C/min.

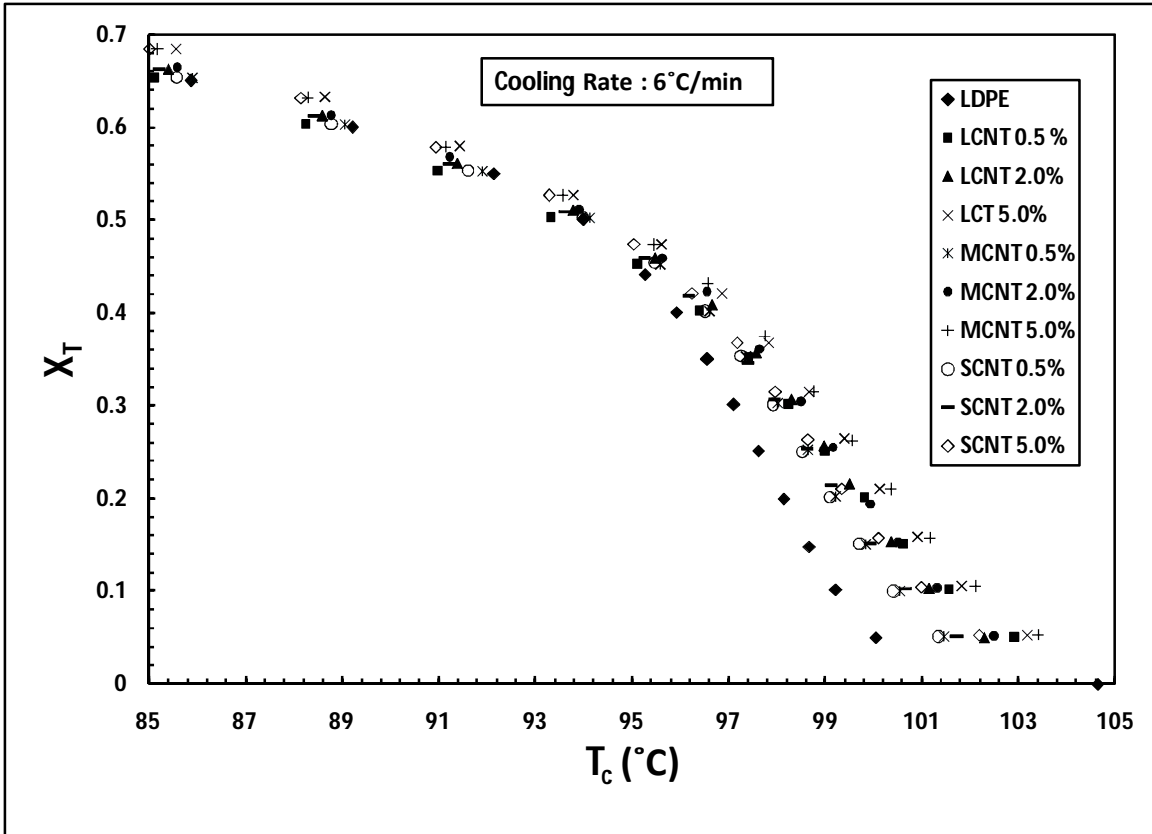


Figure 4.4.2.b. X_T vs. T_c for LDPE/MWCNT nanocomposites at cooling rate of 6 °C/min.

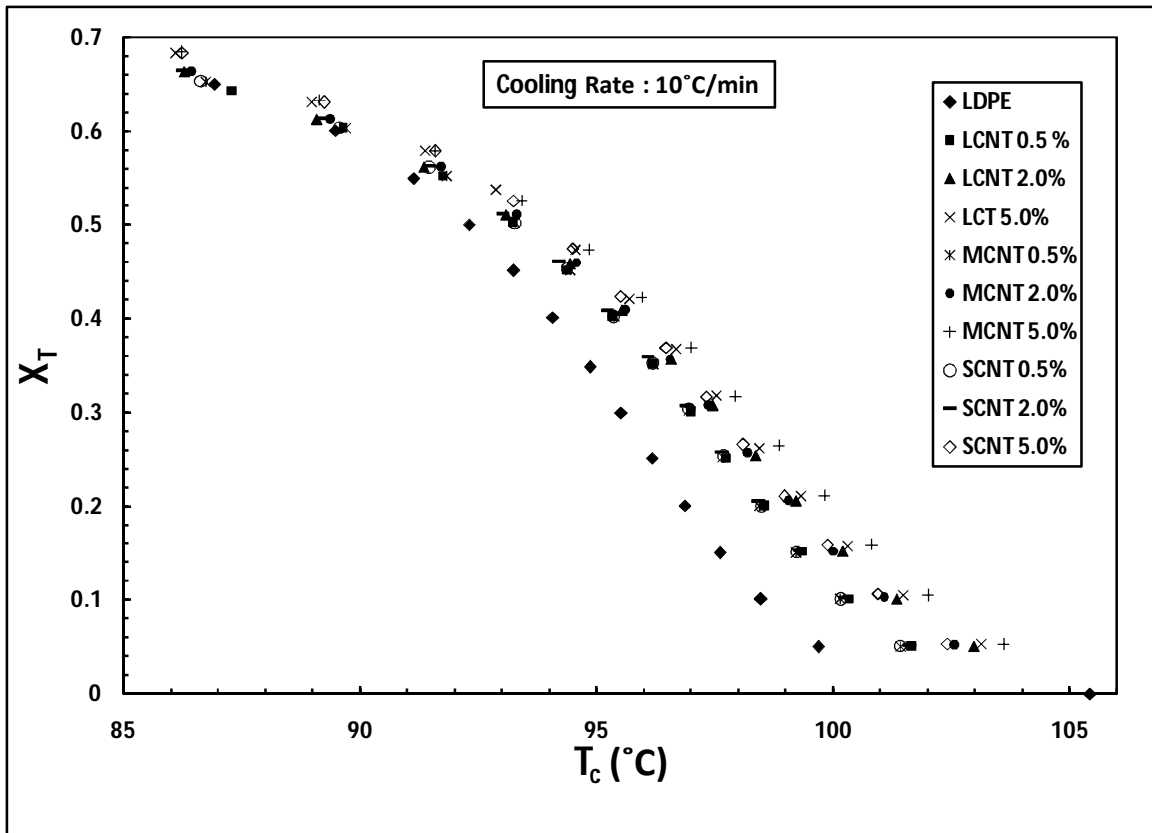


Figure 4.4.2.c. X_T vs. T_c for LDPE/MWCNT nanocomposites at cooling rate of 6 °C/min.

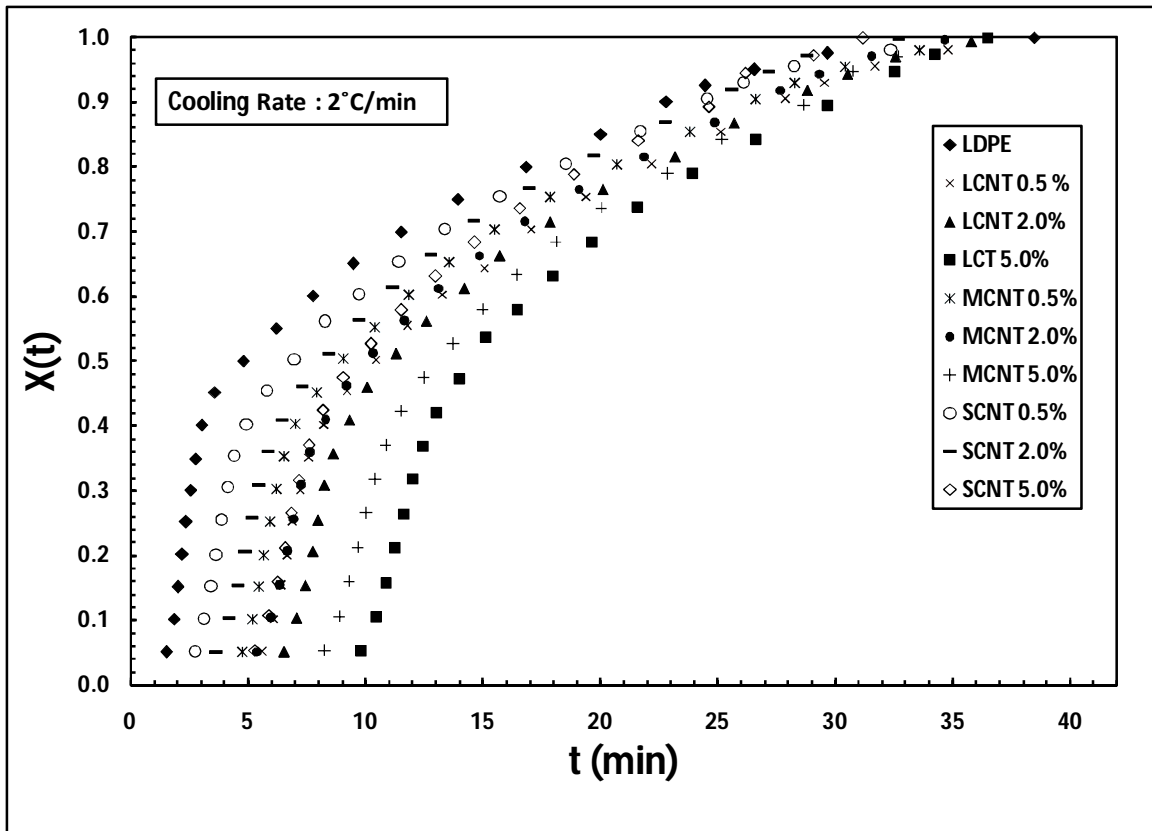


Figure 4.4.3.a. X_t vs t for LDPE/MWCNT nanocomposites at cooling rate of 2 °C/min.

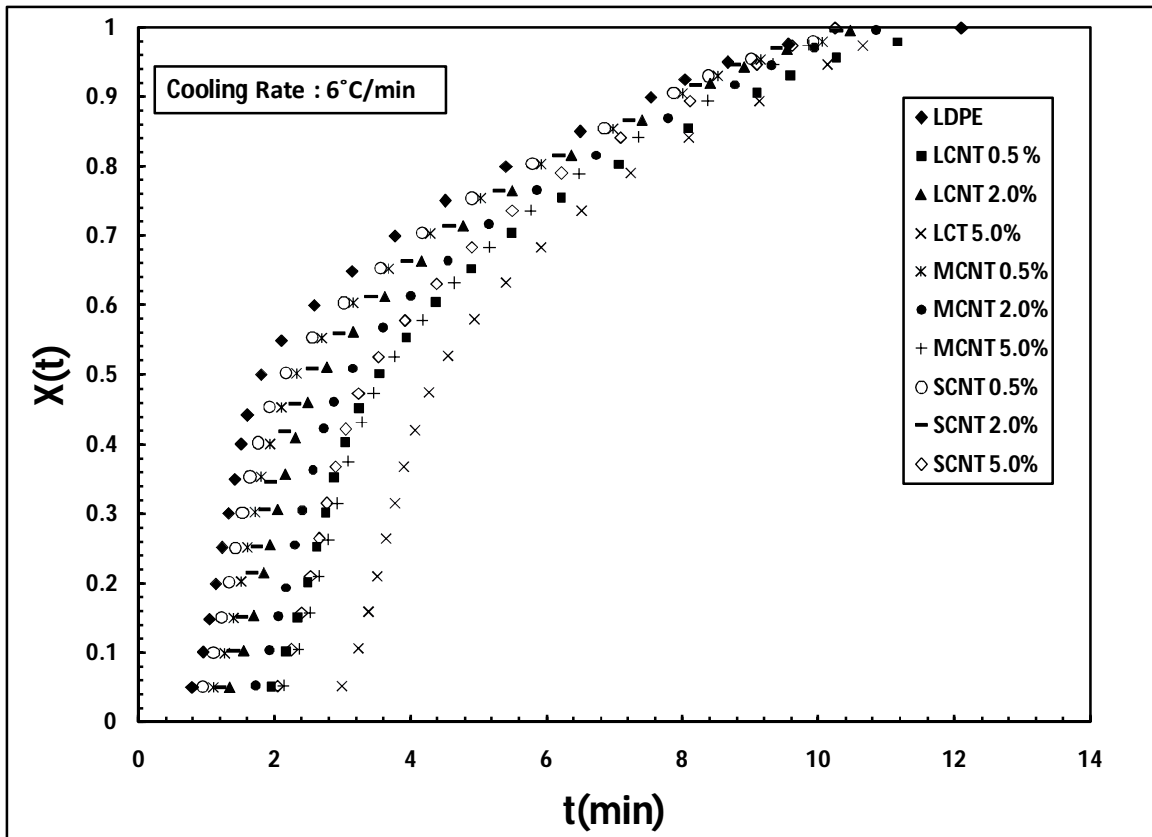


Figure 4.4.3.b. X_t vs t for LDPE/MWCNT nanocomposites at cooling rate of 6 °C/min.

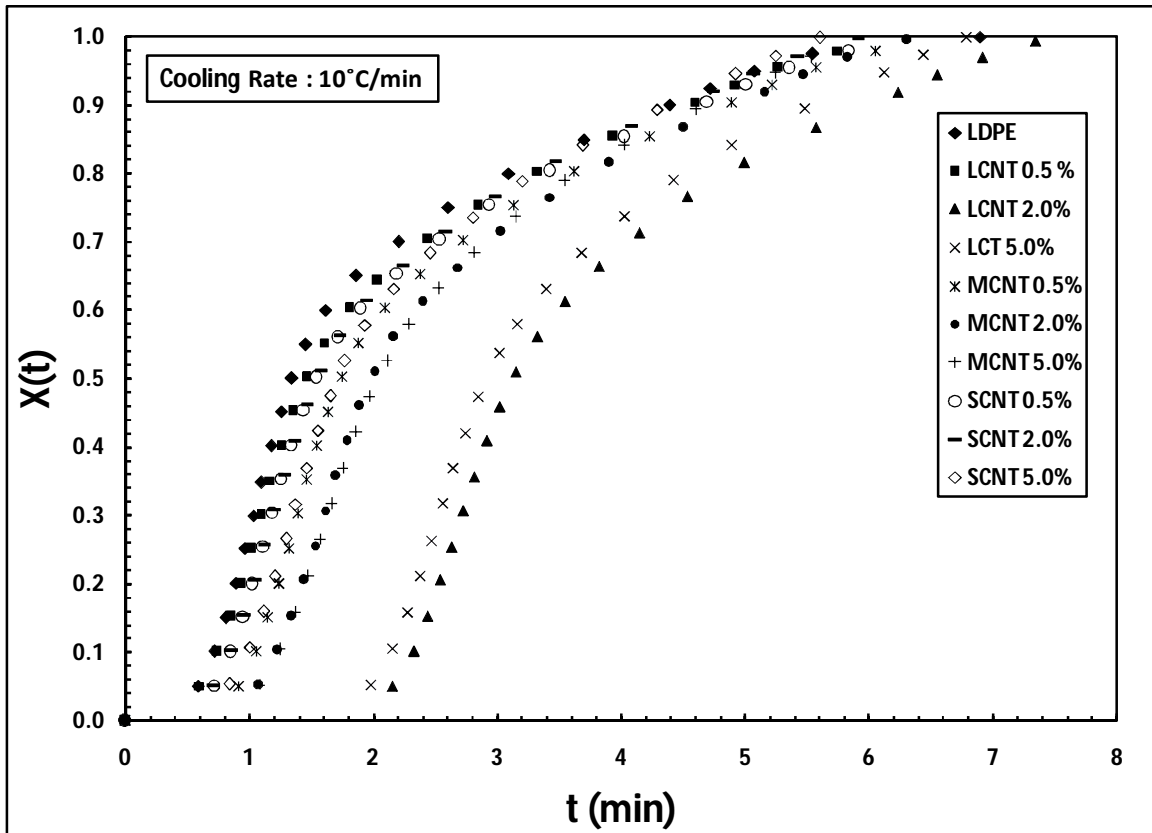


Figure 4.4.3.c. X_t vs t for LDPE/MWCNT nanocomposites at cooling rate of 10 °C/min.

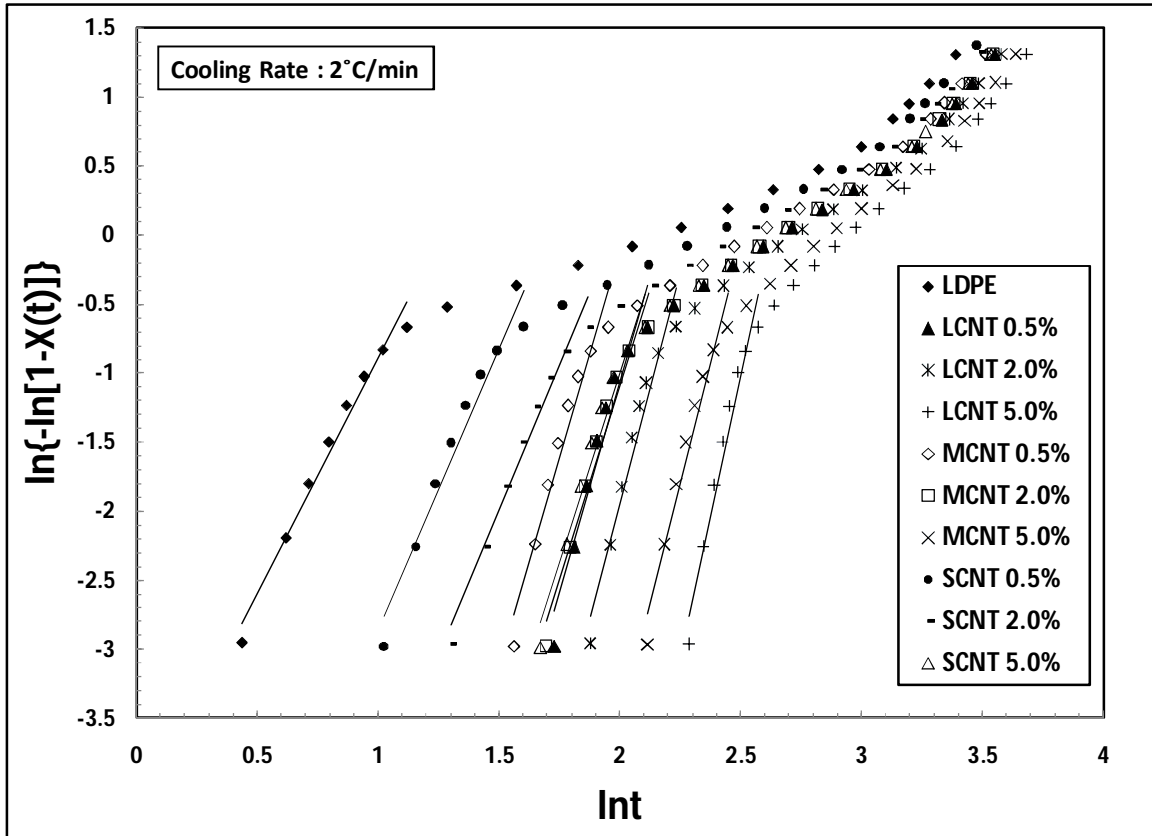


Figure 4.4.4. Avrami plot for LDPE/MWCNT nanocomposites obtained at 2°C/min.

Table 4.4.4. Avrami Parameters for LDPE / MWCNT nanocomposites.

Cooling Rate, °C/min	Sample	n_{40}	k_t	k_r	Regression Coefficient r^2
2	LDPE	3.974	0.0094	0.0971	0.998
	LCNT 0.5%	8.299	3.1E-08	0.0001	0.997
	LCNT 2.0%	8.556	5.6E-09	7.49E-05	0.999
	LCNT 5.0%	9.255	4.26E-11	6.52E-06	0.984
	MCNT 0.5%	6.846	1.34E-06	0.001159	0.982
	MCNT 2.0%	6.992	3.77E-07	0.000614	0.999
	MCNT 5.0%	8.985	3.21E-10	1.79E-05	0.995
	SCNT 0.5%	4.625	0.000499	0.022348	0.984
	SCNT 2.0%	4.988	8.12E-05	0.009014	0.999
	SCNT 5.0%	6.619	8.65E-07	0.00093	0.996
10	LDPE	3.349	0.315373	0.89101	0.997
	LCNT 0.5%	3.143	0.315373	0.89101	0.997
	LCNT 2.0%	3.663	0.266602	0.876166	0.997
	LCNT 5.0%	6.853	0.000338	0.449734	0.974
	MCNT 0.5%	7.166	0.000444	0.462088	0.99
	MCNT 2.0%	4.749	0.081268	0.778022	0.998
	MCNT 5.0%	4.805	0.038504	0.722022	0.997
	SCNT 0.5%	4.916	0.036589	0.718349	0.999
	SCNT 2.0%	3.54	0.188624	0.846369	0.991
	SCNT 5.0%	3.772	0.191666	0.847724	0.999

Table 4.4.5. Avrami Parameters for LDPE / MWCNT nanocomposites at 40 and 95 % crystallinity.

Cooling Rate, °C/min	Sample	n_{40}	Regression Coefficient r^2	n_{95}	Regression Coefficient r^2	
2	LDPE	3.974	0.998	1.063	0.903	
	LCNT 0.5%	8.299	0.997	2.007	0.901	
	LCNT 2.0%	8.556	0.999	1.977	0.897	
	LCNT 5.0%	9.255	0.984	2.584	0.876	
	MCNT 0.5%	6.846	0.982	1.632	0.887	
	MCNT 2.0%	6.992	0.999	1.846	0.903	
	MCNT 5.0%	8.985	0.995	2.355	0.886	
	SCNT 0.5%	4.625	0.984	1.341	0.907	
	SCNT 2.0%	4.988	0.999	1.596	0.921	
	SCNT 5.0%	6.619	0.996	2.007	0.901	
		Sample	n	r ²	n	r ²
	10	LDPE	3.143	0.997	1.572	0.911
LCNT 0.5%		3.663	0.997	1.595	0.93	
LCNT 2.0%		6.853	0.974	2.893	0.896	
LCNT 5.0%		7.166	0.99	3.02	0.908	
MCNT 0.5%		4.749	0.998	1.834	0.904	
MCNT 2.0%		4.805	0.997	2.059	0.92	
MCNT 5.0%		4.916	0.999	2.194	0.924	
SCNT 0.5%		3.54	0.991	1.675	0.917	
SCNT 2.0%		3.772	0.999	1.758	0.932	
SCNT 5.0%		4.053	0.999	1.999	0.934	

It is observed that if the whole data is fitted the values of Avrami parameter make sense but the data fit is very poor as reflected in the regression coefficient. But if selective fitting for upto 40% crystallization is done, the Avrami parameter loses its physical meaning. Hence, no attempt was made to discuss the results obtained by Avrami method in this paper.

The kinetic model proposed by Mo [55] was used [see eq. (7)]. Sample plots of $\ln R$ versus $\ln t$ for LDPE nanocomposite with 5 wt% MWCNT are shown in Figure 4.4.5.(a-c). Plots for the rest of nanocomposites are not shown here; however, the Mo parameters for all samples are given in Table 4.4.6. From these plots, values of α and $F(T)$ were obtained at different crystallinities in the range 20–80%. All plots were linear, as predicted by eq. (7). $F(T)$ increased with the increase in percentage crystallinity. In general, the higher the MWCNT loading, the higher the value of $F(T)$ for the same crystallinity. Also, for the same MWCNT loading $F(T)$ increases with crystallinity. This observation was valid at all levels of crystallization. These two observations suggest the increased difficulty of polymer crystallization at high crystallinity and with the addition of CNT. The results of Mo method of analysis are in agreement with the previous Avrami analysis where k_r was observed to decrease with increasing MWCNT loading. So, MWCNT promotes initial crystallization but at the expense of slower secondary crystallization process.

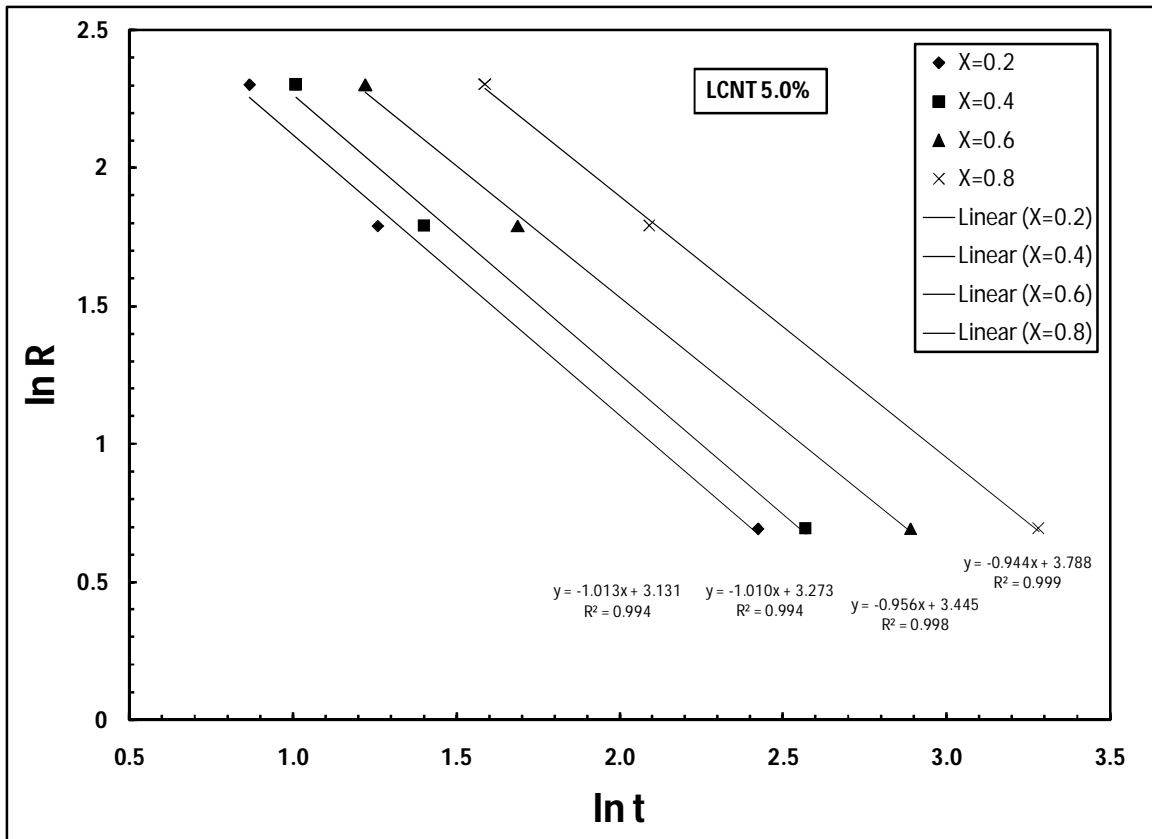


Figure 4.4.5.a. ln R versus ln t at each given relative crystallization for LCNT 5.0%.

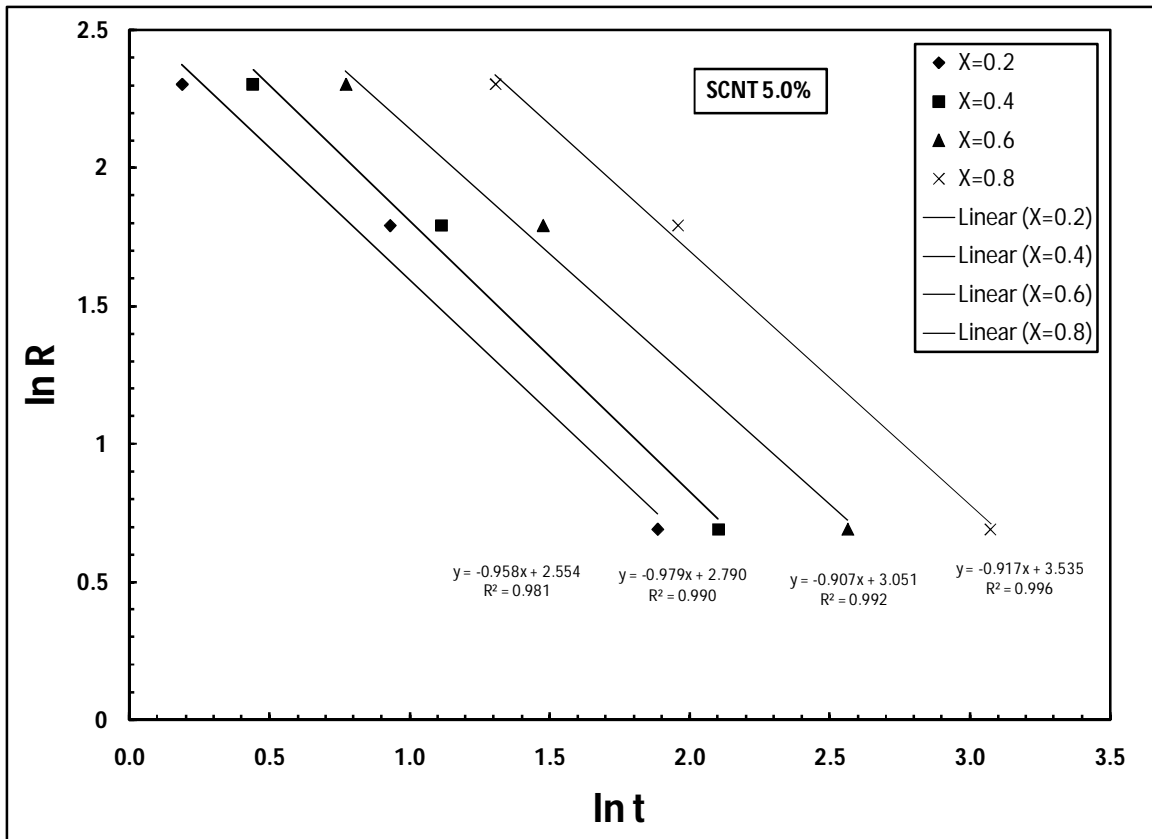


Figure 4.4.5.b. $\ln R$ versus $\ln t$ at each given relative crystallization for SCNT 5.0%.

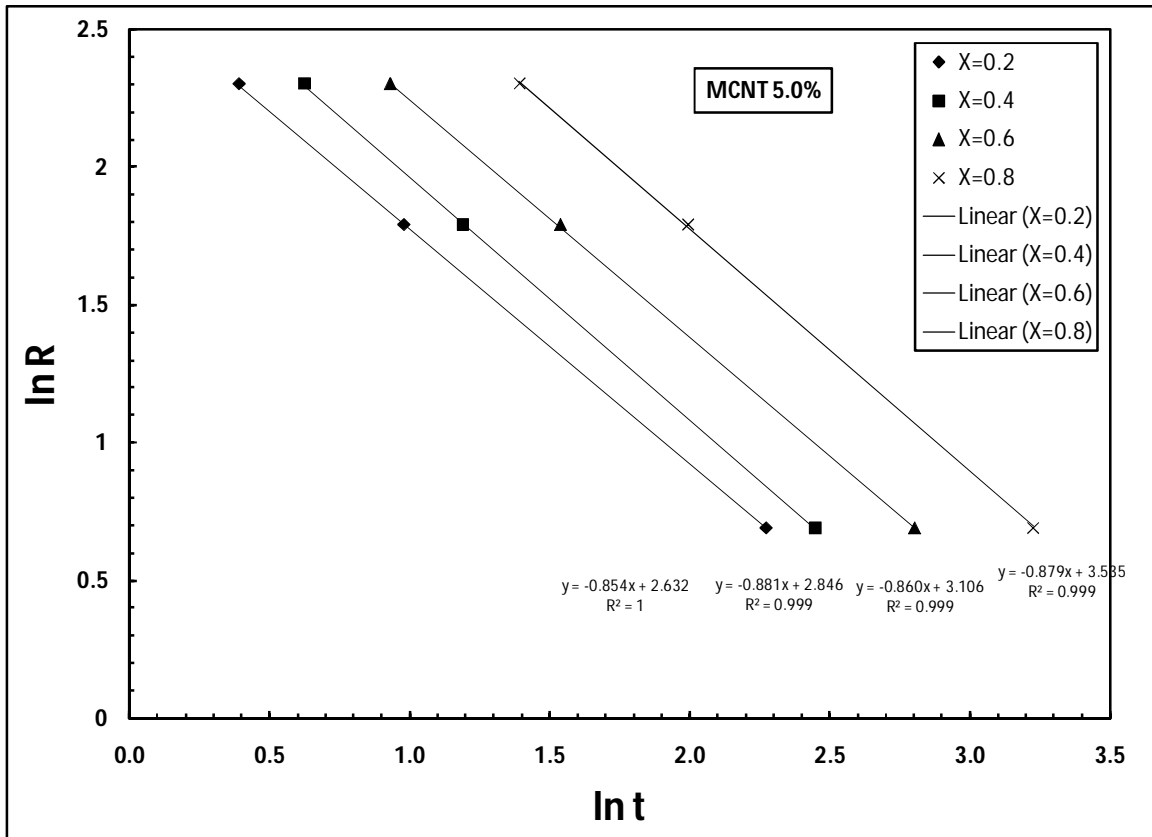


Figure 4.4.5.c. $\ln R$ versus $\ln t$ at each given relative crystallization for MCNT 5.0%.

Table 4.4.6. Values of the Mo Parameters, α and F(T), at a fixed value of the Relative Degree of Crystallinity [X(t)] for All of the LDPE/Nanocomposites.

Sample	Variable	X (t) %			
		20	40	60	80
LDPE	A	1.749	1.661	1.019	0.952
	F(T)	2.069	2.531	2.777	3.387
	r^2	0.997	0.996	0.999	0.999
LCNT 0.5	A	0.817	0.859	0.813	0.856
	F(T)	2.342	2.585	2.858	3.382
	r^2	0.959	0.97	0.979	0.992
LCNT 2.0	A	0.938	0.98	0.988	0.982
	F(T)	2.719	2.948	3.31	3.757
	r^2	0.742	0.793	0.912	0.972
LCNT 5.0	A	1.013	1.01	0.956	0.944
	F(T)	3.131	3.273	3.445	3.788
	r^2	0.994	0.994	0.998	0.999
MCNT 0.5	A	0.968	0.989	0.903	0.913
	F(T)	2.358	2.6	2.909	3.452
	r^2	0.961	0.968	0.992	0.998
MCNT 2.0	A	1.033	1.036	0.941	0.933
	F(T)	2.644	2.874	3.114	3.574
	r^2	0.997	0.998	0.999	1
MCNT 5.0	A	0.854	0.881	0.86	0.879
	F(T)	2.632	2.846	3.106	3.535
	r^2	1	0.999	0.999	0.999
SCNT 0.5	A	1.217	1.184	0.974	0.95
	F(T)	2.251	2.568	2.904	3.468
	r^2	0.985	0.986	0.998	1
SCNT 2.0	A	1.039	1.029	0.923	0.93
	F(T)	2.34	2.607	2.923	3.471
	r^2	0.999	0.999	1	0.999
SCNT 5.0	A	0.958	0.979	0.907	0.917
	F(T)	2.554	2.79	3.051	3.535
	r^2	0.981	0.99	0.992	0.996

The Vyazovkin and Sbirrazzuoli [56] method of analysis [eq. (9)], which is based on Hoffman–Lauritzen theory for secondary crystallization, [57] was used for the analysis of the activation energy data. Temperature is plotted against Activation energy for 30 to 75% relative crystallinity of the nanocomposites. We can clearly observe in Figure 4.4.6.a that the activation energy is decreasing as the amount of MWCNT is increased in the bulk from 0.5% to 5.0 % weight. This suggests that the incorporation of CNT promotes the initial crystallization process by lowering the activation energy. In Figure 4.4.6.b, Temperature is plotted against activation energy for different kinds of MWCNT at a fixed loading of 5 weight %. In general, the presence of MWCNT resulted in significant reduction in activation energy for short, long and modified MWCNT. Also, both LCNT and MCNT (both have same aspect ratio) showed similar reduction in activation energy over the whole temperature range. Nevertheless, the long CNT resulted in more drop in activation energy in comparison with short CNT. This suggests that CNT with long aspect ratio are enhancing the crystallization process as compared to CNT with short aspect ratio. However, for the same long aspect ratio the –COOH modification did not result in a reduction of the activation energy. These results are in agreement with findings from previous methods of analysis.

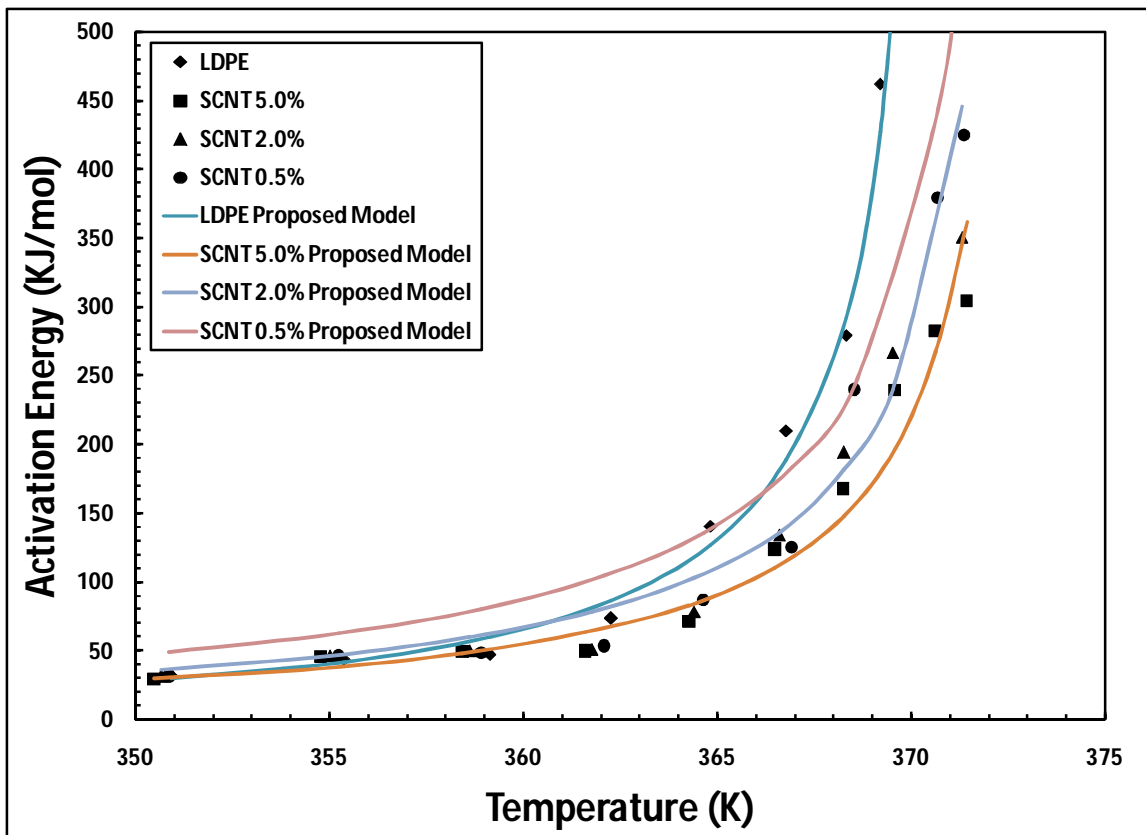


Figure 4.4.6.a. Activation energy versus crystallization temperature for LDPE with varying loadings of SCNT. Continuous lines show predictions of the proposed model.

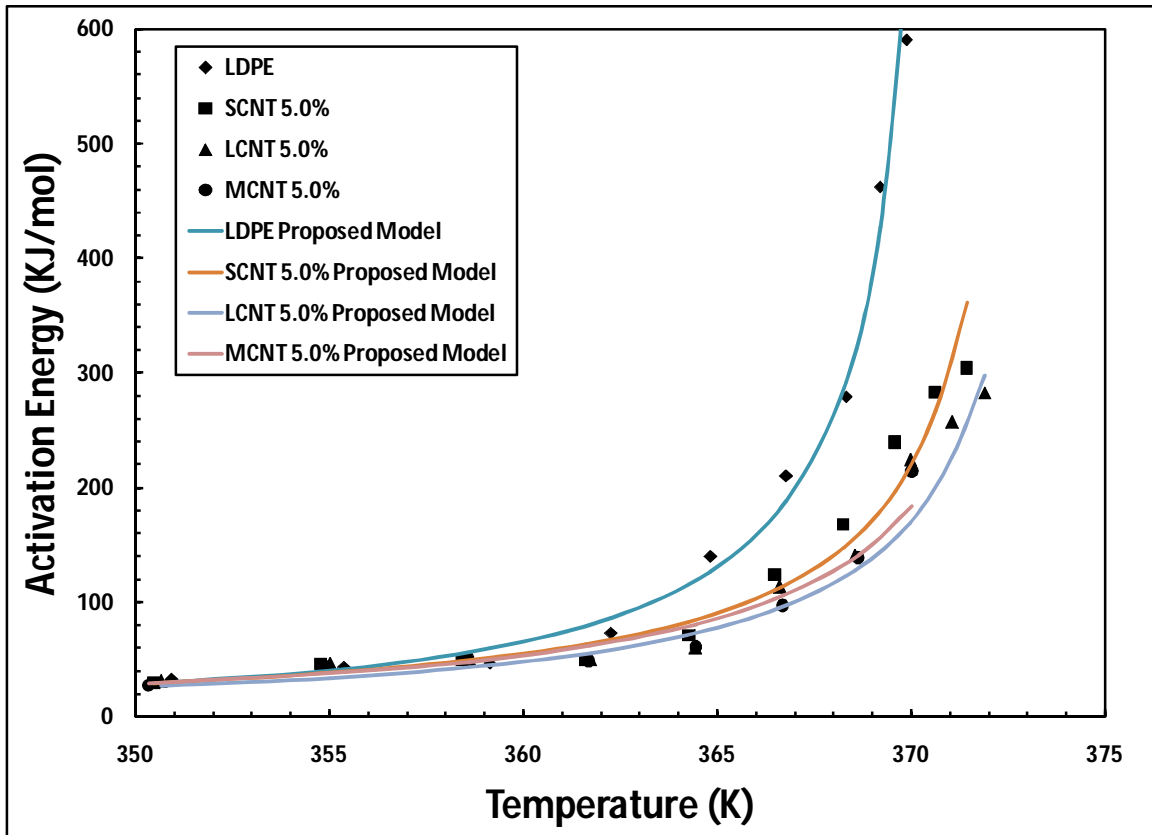


Figure 4.4.6.b. Activation energy versus crystallization temperature for LDPE with different MWCNT at 5 wt%. Continuous lines show predictions of the proposed model.

A model was proposed for fitting the above activation energy; crystallization temperature and relative crystallinity. The proposed model is given below:

$$E = a e^{-bX_t T} \quad (10)$$

where E is the activation energy, a and b are constants. X_t is relative crystallinity and T is absolute temperature. After linearization of the above equation $\ln E$ was plotted against $X_t T$ to obtain a straight line. A very good fit was obtained. Model parameters are given in Table 4.4.7. It was observed that constant b is almost independent of concentration. In fact b was in the range 0.15 to 0.18. Therefore an average value of 0.165 was used for fitting the whole data. Therefore constant b is unique and reflects the specific crystallization process. Further, the value of b is almost the same for long, short or modified MWCNT at the same MWCNT concentration. However, the constant a is concentration dependent and it decreases with increasing concentration. Therefore, the activation energy function is separable into two terms: a concentration dependent term (constant a) and a temperature dependent term (exponential term).

Table 4.4.7. Parameter values for the proposed model.

	a	b	Regression coefficient r^2
LDPE	1283	0.023	0.986
MCNT, 5.0	2008	0.016	0.940
LCNT, 5.0	1815	0.015	0.959
SCNT, 5.0	2273	0.016	0.966
SCNT, 2.0	2813	0.017	0.960
SCNT, 0.5	3782	0.018	0.970

4.4.6. Conclusion

In this paper, the effect of CNT loading surface modification and aspect ratio was studied. The presence of long MWCNT promotes initial crystallization and it impacts both the onset as well as peak crystallization temperatures. The effect is more pronounced at high cooling rates. Also, -COOH modified MWCNT behaved in a very similar fashion like unmodified MWCNT with the same length. On the other hand, the increased MWCNT loading helps in initiating the crystallization process but it slows the secondary crystallization. The surface modification with short group such as -COOH did not make any noticeable difference on the crystallization process. Three different methods of data analyses were used: The Avrami approach, Mo method and Hoffman-Lauritzen theory. However nothing was deduced from the avrami method. The other two methods agree that the addition of MWCNT promoted the initial crystallization by shifting the onset crystallization temperature to higher values. However, the crystallization process is slowed after that. For example with increasing MWCNT concentration, long crystallization tails following the peak crystallization temperature were obtained. On the other hand, $F(T)$ obtained from Mo model increased with the increase in MWCNT concentration and percent crystallinity indicating the increased difficulty in crystallization. Further, the Hoffman- Lauritzen theory showed that the activation energy decreased with the increase in MWCNT concentration which supports the observed promotion of the initial crystallization. A model was proposed to correlate the effect of MWCNT concentration, crystallization temperature and crystallinity on the activation energy ($E = \alpha e^{-0.165 X_c T}$). The model was able to fit the whole set of data obtained at different cooling rates and for short and long MWCNT.

4.4.7. Acknowledgement

The authors are thankful to the Center of Research Excellence in Petroleum Refining & Petrochemicals (CoRE-PRP), established by the Ministry of Higher Education, for providing the funding for this research. KFUPM is also acknowledged for its support.

4.4.8. References

1. Evans, U. R. *Trans Faraday Soc* 1945, 41, 365.
2. Ozawa, T. *Polymer* 1971, 12, 150.
3. Jeziorny, A. *Polymer* 1978, 19, 1142.
4. Hay, J. N.; Mills, P. J. *Polymer* 1982, 23, 1380.
5. McHugh, A. J.; Burghardt, W. R.; Holland, D. A. *Polymer* 1986, 27, 1585.
6. Jayakannan, M.; Ramakrishnan, S. *J Appl Polym Sci* 1999, 74, 59.
7. Parasnis, N. C.; Ramani, K. *J Therm Anal Calorim* 1999, 55, 709.
8. Sajkiewicz, P.; Carpaneto, L.; Wasiak, A. *Polymer* 2001, 42, 5365.
9. Qiu, Z.; Ikehara, T.; Nishi, T. *Polymer* 2003, 44, 5429.
10. Kao, Y. H.; Phillips, P. J. *Polymer* 1986, 27, 1669.
11. Phillips, P. J.; Kao, Y. H. *Polymer* 1986, 27, 1679.
12. Nordmeier, E.; Lanver, U.; Lechner, M. D. *Macromolecules* 1990, 23, 1072.
13. Sutton, S. J.; Vaughan, A. S.; Bassett, D. C. *Polymer* 1996, 37, 5735.
14. Wagner, J.; Abu-Iqyas, S.; Monar, K.; Phillips, P. J. *Polymer* 1999, 40, 4717.
15. Wagner J.; Phillips, P. J. *Polymer* 2001, 42, 8999.
16. Mandelkern L.; Maxfield, J. J. *J Polym Sci, Part B: Polym Phys Ed* 1979, 17, 1913.
17. Strobl, G. R.; Engelke, T.; Maderek, E.; Urban, G. *Polymer* 1983, 24, 1585.
18. Maderek E.; Strobl, G. R. *Colloid Polym Sci* 1983, 261, 471.
19. Alamo, R.; Domszy, R.; Mandelkern, L. *J Phys Chem* 1984, 88, 6587.
20. Mandelkern, L. *Polym J* 1985, 17, 337.
21. Usami, T.; Gotoh, Y.; Takayama, S. *Macromolecules* 1986, 19, 2722.
22. Alamo, R. G.; Mandelkern, L. *Macromolecules* 1989, 22, 1273.
23. Fatou, J. G.; Marco, C.; Mandelkern, L. *Polymer* 1990, 31, 1685.

24. Alamo, R. G.; Viers, B. D.; Mandelkern, L. *Macromolecules* 1993, 26, 5740.
25. Shanks, R. A.; Amarasinghe, G. *J Therm Anal Calorim* 2000, 59, 471.
26. Zhang, M.; Lynch, D. T.; Wanke, S. E. *Polymer* 2001, 42, 3067.
27. Rabiej, S.; Goderis, B.; Janicki, J.; Mathot, V. B. F.; Koch, M. H. J.; Groeninckx, G.; Reynaers, H.; Gelan, J.; Wlochowicz, A. *Polymer* 2004, 45, 8761.
28. Jiao, C.; Wang, Z.; Liang, X.; Hu Y., *Polym Test* 2004, 24, 71.
29. Bensason, S.; Minick, J.; Moet, A.; Chum, S.; Hiltner, A.; Baer, E. *J Polym Sci, Part B: Polym Phys* 1996, 34, 1301.
30. Voigt-Martin, I. G.; Alamo, R.; Mandelkern, L. *J Polym Sci, Part B: Polym Phys* 1986, 24, 1283.
31. Keating, M. Y.; Lee, I. H. *J Macromol Sci Phys* 1999, B38, 379.
32. Starck, P.; Lehmus, P.; Seppala, J. V. *Polym Engg Sci* 1999, 39, 1444.
33. Xu, J.; Xu, X.; Feng, L. *Eur Polym J* 1999, 36, 685.
34. Janimak, J. J.; Stevens, G. C. *Thermochim Acta* 1990, 332, 125.
35. Razavi-Nouri, M.; Hay, J. N. *Polymer* 2001, 42, 8621.
36. Fu, Q.; Chiu, F. C.; He, T.; Liu, J.; Hsieh, E. T. *Macromol Chem Phys* 2001, 202, 927.
37. Wang, C.; Chu, M. C.; Lin, T. L.; Lai, S. M.; Shih, H. H.; Yang, J. C. *Polymer* 2000, 42, 1733.
38. Chiu, F. C.; Fu, Q.; Peng, Y.; Shih, H. H.; *J Polym Sci, Part B: Polym Phys* 2002, 40, 325.
39. Starck, P.; Lofgren, B. *Eur Polym J* 2002, 38, 97.
40. Teng, H.; Shi, Y.; Jin, X. *J Polym Sci, Part B: Polym Phys* 2002, 40, 2107.
41. Hussein, I. A. *Polym Int* 2004, 53, 1327.
42. Islam, M. A.; Hussein, I. A.; Atiqullah, M. *Eur Polym J* 2007, 43, 599.
43. Seo, M. K.; Lee, J. R.; Park, S. J. *Mat Sci & Eng* 2005, A404, 79.
44. Funck, A.; Kaminsky, W. *Compos Sci & Tech* 2007, 67, 906.
45. Vega, J. F.; Martinez-Salazar, J.; Trujillo, M.; Arnal, M. L.; Muller, A. J.; Berdeau, S.; Dubios, Ph. *Macromolecules* 2009, 42, 4719.
46. Hussein, I. A., Williams, M. C.; *Macromolecules* 2000, 33, 520.

47. Turi, E. A.; Wunderlich, B. Thermal characterization of polymeric materials, vol 1, 2nd Ed., New York: Academic Press; 1997.
48. Avrami, M. J Chem Phys 1939, 7, 1103.
49. Avrami, M. J Chem Phys 1940, 8, 212.
50. Avrami, M. J Chem Phys 1941, 9, 177.
51. Ziabicki, A. Appl Polym Symp 1967, 6, 1.
52. Ziabicki, A. Colloid Polym Sci 1974, 252, 433.
53. Wunderlich, B. Macromolecular Physics, Vol. 2, New York : Academic; 1976.
54. Tanem, B. S.; Stori, A. Polymer 2001, 42, 5389.
55. Liu, T.; Mo, Z.; Wang, S.; Zhang, H. Polym Eng Sci 1997, 37, 568.
56. Vyazovkin, S.; Sbirrazzuoli, N. Macromol Rapid Commun 2004, 25, 733.
57. Hoffman, J. D.; Davis, G.T.; Lauritzen, J. I. Jr.; Hannay (Ed), N. B. Treatise on Solid State Chemistry, Vol. 3, New York: Plenum; 1976.
58. Achilias, D. S.; Papageorgiou, G. Z.; Karayannidis, G. P. Macromol Chem Phys 2005, 206, 1511.
59. Cai, J.; Li, T.; Han, Y.; Zhuang, Y.; Zhang, X. J Appl Polym Sci 2006, 100, 1479.
60. Vyazovkin, S.; Dranca, I. Macromol Chem Phys 2006, 207, 20.
61. Botines, E.; Puiggali, J. Eur Polym J 2006, 42, 1595.
62. Hussein, I. A. J Appl Polym Sci 2008, 107, 2802.

CHAPTER FIVE

CONCLUSIONS

Nanocomposites of LDPE / MWCNTs were prepared using melt blending. Samples were prepared using different MWCNT (LCNT, MCNT & SCNT). The effect of surface modification and aspect ratio on dynamic, steady shear and extensional rheology were studied. Morphology of these nanocomposites showed agglomerations present at all loadings and that these agglomerations were distributed into the LDPE matrix of LDPE. Both η' , η , G' and N_1 increased with increasing loading and aspect ratio at low frequency, tending towards solid-like behavior. At low loadings, η' , η , G' and N_1 values became lower than that of pure LDPE at low frequency, a tentative explanation was suggested that MWCNT at low loadings act as plasticizer while at high loadings they play the role of a filler.

Results of extensional viscosity show more pronounced differences between the nanocomposites with different aspect ratios. LCNT nanocomposite showed the most strain hardening. MCNT showed less strain hardening than LCNT, possibly due to COOH acting as short branching. Time of break for all three types of nanocomposite decreases with increasing aspect ratio and henky rate.

In general, the rheological tools used in this study revealed a possible plasticization effect for MWCNT with high aspect ratio at low loadings (<1.0 wt%) and a filler effect at higher loadings (>1.0 wt%). The effect COOH modification was more apparent in

extensional viscosity and N_1 to some extent. Aspect ratio has influenced both viscous and elastic shear properties as well as strain hardening.

Analysis of Mechanical properties revealed that yield strength and modulus increased with increased loading of various MWCNTs. However, ultimate strength, percent elongation and toughness were reduced for 2% loading and higher. Addition of compatibilizer improved most of the mechanical. With the increase in properties being 46% and 48% for yield strength, Young's modulus at 5.0% loading respectively. Also, 16% increase for ultimate strength at 2.0 % loading was observed for LCNT nanocomposite in the presence of MAPE. On the other hand, percent elongation and toughness did not show any improvement, with or without the compatibilizer.

Addition of MWCNT induced early onset of crystallization. However, aspect ratio and COOH modification did not show any effect. LCNT and MCNT composites show higher values of percent crystallinity in comparison with the SCNT at all loadings. High aspect ratio increased yield strength, ultimate strength, and Young's modulus, at all loadings. But it did not result in any improvement in percent elongation and toughness. The presence of MAPE improved all mechanical properties, apart from percent elongation and toughness.

MCNT was further modified to produce C_{18} -CNT. Nanocomposites of C_{18} -CNT and LDPE were prepared using the melt blending process. The addition of C_{18} -CNT to LDPE matrix improves the yield strength and Young's modulus. Ultimate strength was also improved upto 2.0 wt% loading of CNT, but a drop in ultimate strength was observed at

5.0 wt% loading of C₁₈-CNT. Addition of 2.0 wt% MAPE into these nanocomposites further improved these properties. Percent elongation and toughness showed a decrease in value with increased loading. The use of MAPE did not have much effect on the two properties. The use of C₁₈ as modification of CNT proved useful as it effectively reduced dynamic viscosity at all frequencies with the addition of C₁₈-CNT at loading up to 5.0 wt%. Storage modulus showed a similar behavior to dynamic viscosity, as its values were lower than that of pure LDPE even at 5.0 wt% loading. Results of phase angle show no presence of network and that produced nanocomposite showed liquid-like behavior. Also, addition of C₁₈-CNT did not increase strain hardening and maintained extensional viscosity and time of break, even at high henky rate of 1.5 s⁻¹. So, effectively there is an improvement in both mechanical and rheological properties and C₁₈ on CNT acts as an insitu compatibilizer. The modifier type and content play a major role on the mechanical and rheological properties of nanocomposites.

The effect of CNT loading surface modification and aspect ratio on non isothermal crystallization kinetics were then studied. The presence of long MWCNT promotes initial crystallization and it impacts both the onset as well as peak crystallization temperatures. The surface modification with short group such as -COOH did not make any noticeable difference on the crystallization process. The addition of MWCNT promoted the initial crystallization by shifting the onset crystallization temperature to higher values. The Hoffman-Lauritzen theory showed that the activation energy decreased with the increase in MWCNT concentration which supports the observed promotion of the initial crystallization. A model was proposed to correlate the effect of MWCNT concentration,

crystallization temperature, and crystallinity on the activation energy ($E = ae^{-0.165X_cT}$).

The model was able to fit the whole set of data obtained at different cooling rates and for short and long MWCNT.

In summary, the aspect ratio of MWCNT proved to influence many melt and solid-state properties of nanocomposites. This use of maleated polyethylene improved the dispersion of MWCNT and the surface modification of MWCNT with C18 showed improved mechanical and rheological properties of MWCNT/LDPE nanocomposites. Further research in this area should focus on incorporation of other selected long groups on MWCNT to enhance the properties of polymer nanocomposites.

CHAPTER SIX

RECOMMENDATIONS

The results achieved thus far are promising. A lot of research still needs to be done to fully utilize the ultimate properties of CNTs. The use of FE-SEM only made possible, the two dimensional analysis of the dispersion of the produced nanocomposite. The use of cryo sectioning machine, coupled with TEM (transmission electron microscopy) would enable three dimensional evaluation of the dispersion in the matrix of the nonmaterial. As of now, this machine is not available in Saudi Arabia.

The size of the chain length on the modified CNT should also be further studied. Particularly how changing the length of modifications of the CNTs affects both the mechanical and rheological properties in various polymer matrix. Even though CNTs are promising material, not a lot of research has been done on CNFs. CNFs have good mechanical properties and are cheaper than CNTs. So evaluation of mechanical and rheological properties using various CNFs would be an exciting avenue of research. Further the surface of the CNFs can also be modified to see how that would affect the bulk properties.

NOMENCLATURE

η^*	Complex viscosity
η'	Dynamic viscosity
η_e	Extensional viscosity
ω	Frequency
N_1	Normal Force
X_c	Percent Crystallinity
$\dot{\gamma}$	Shear rate
η	Steady shear viscosity

REFERENCES

1. Al-Kandary S.; Ali A. A. M.; Ahmad Z.; "Morphology and thermo-mechanical properties of compatibilized polyimide-silica nanocomposites", *J Appl. Polym. Sci.*, 98, 2521–2531, **2005**.
2. Andrews R, Wisenberger MC. Carbon nanotube polymer composites. *Solid State Mater Sci*, 8, 31–7, **2004**.
3. Bandyopadhyay S, Chen R, Giannelis EP. Biodegradable organic-inorganic hybrids based on poly(L-lactide). *Polym Mater Sci Eng*, 81,159–60, **1999**.
4. Iijima S. Helical microtubules of graphitic carbon. *Nature*, 354:56–8, **1991**.
5. Deng C.F., Wang D.Z., Zhang X.X., Li A.B. *Mater Sci Eng A* 444:138, **2007**.
6. Biswas M, Sinha Ray. Recent progress in synthesis and evaluation of polymer montmorillonite nanocomposites. *Adv Polym Sci*, 155,167–221, **2001**.
7. Chang JH, An YU, Cho D, Giannelis EP. Polylactide nanocomposites: comparison of their properties with montmorillonite and synthetic mica (II). *Polymer*,44, 3715–20, **2003**.
8. Chen JS, Poliks MD, Ober CK, Zhang Y, Wiesner U, Giannelis EP. Study of the interlayer expansion mechanism and thermal-mechanical properties of surface-initiated epoxy nanocomposites. *Polymer*, 43, 4895–904, **2002**.
9. Chen G. X.; Kim E. S.; Yoon J. S.; " Poly(butylene succinate)/Twice Functionalized Organoclay Nanocomposites: Preparation, Characterization, and Properties", *J. Appl. Polym. Sci.*, 98, 1727–1732, **2005**.
10. Galgali G.; Ramesh C.; Lele A. "A Rheological Study on the Kinetics of Hybrid Formation in Polypropylene Nanocomposites", *Macromolecules*, 34, 852-858, **2001**.
11. Giannelis EP. Polymer layered silicate nanocomposites. *Adv Mater*, 8, 29–35, **1996**.
12. Gopakumar T.G., Lee J.A., Kontopoulou M., Parent J.S. "Influence of clay exfoliation on the physical properties of montmorillonite/polyethylene composites", *Polymer* 43, 5483–5491, **2002**.
13. Giannelis EP, Krishnamoorti R, Manias E. Polymer–silicate nanocomposites: model systems for confined polymers and polymer brushes. *Adv Polym Sci*, 138, 107–47, **1999**.
14. Yoon P.J., Fornes T.D., Paul D.R. *Polymer* 43:6727, **2002**.
15. Grim RE. *Clay mineralogy*. New York: McGraw-Hill; **1953**.
16. Mishra S, Sonawane S, Chitodkar V *Polym Plast Technol Eng* 44:463–473, **2005**.

17. Hackett E, Manias E, Giannelis EP. Molecular dynamics simulations of organically modified layered silicates. *J Chem Phys*,108, 7410–5, **1998**.
18. Hackett E, Manias E, Giannelis EP. Computer simulation studies of PEO/layered silicate nanocomposites. *Chem Mater*,12, 2161–7, **2000**.
19. Hasegawa N.; Okamoto H.; Usuki A.; "Preparation and Properties of Ethylene Propylene Rubber (EPR)–Clay Nanocomposites Based on Maleic Anhydride-Modified EPR and Organophilic Clay", *J Appl Polym Sci* 93, 758–764, **2004**.
20. Hiroi R, Sinha Ray S, Okamoto M, Shiroy T. Organically modified layered titanate: a new nanofiller to improve the performance biodegradable polylactide. *Macromol Rapid Commun*, 25, 1359–63, **2004**.
21. Hotta S.; Paul D. R.; "Nanocomposites formed from linear low density polyethylene and organoclays", *Polymer* 45, 7639–7654, **2004**.
22. Gilman J.W., Jackson C.L., Morgan A.B., Harris R. Jr. *Chem Mater* 12:1866, **2000**.
23. Hussein IA, Implications of melt Miscibility on Thermal and Mechanical Properties of metallocene LLDPE Blends with HDPE: Influence of Comonomer Type, *Polymer International*, 54(9), 1330-1336, **2005**.
24. Hussein IA, Hameed T, "Influence of Branching Characteristics on Thermal and Mechanical Properties of Ziegler-Natta and Metallocene LLDPE blends with LDPE", *J. Applied Polymer Science*, 97(6), 2488-2498, **2005**.
25. Hussein IA and Williams MC, "Rheological Study of Heterogeneities in Melt Blends of ZN-LLDPE and LDPE: Influence of M_w and Comonomer Type, and Implications for Miscibility", *Rheologica Acta*,43(6)602-614, **2004**.
26. Hussein IA, "Implications of Melt Compatibility/Incompatibility on Thermal and Mechanical Properties of Metallocene and Ziegler-Natta LLDPE Blends with HDPE: Influence of Composition Distribution and Branch Content of LLDPE", *Polymer International*, 53(9), 1327-1335, **2004**.
27. Hussein IA and Williams MC, "Rheological Study of the influence of Branch Content on the Miscibility of octene m-LLDPE and ZN-LLDPE in LDPE", *Polym. Eng. & Sci.*, 44, 660-672, **2004**.
28. Hameed T and Hussein IA, "Effect of short chain branching of LDPE on its miscibility with linear HDPE", *Macromolecular Materials & Engineering* 289(2), 198-203, **2004**.
29. Hussein IA, Hameed T, Abu Sharkh BF, Mezghani K, "Miscibility of hexene-LLDPE and LDPE Blends: Rheological Study of the Influence of Branch Content and Composition Distribution", *Polymer*, 44(16), 4665-4672, **2003**.
30. Hyun Y. H.; Lim S. T.; Choi H. J.; Jhon M. S.; " Rheology of Poly(ethylene oxide)/Organoclay Nanocomposites", *Macromolecules*, 34, 8084-8093, **2001**.

31. Kim M. H.; Park C. I.; Choi W. M.; Lee J. W.; Lim J. G.; Park O. O.; Kim J. M.; "Synthesis and Material Properties of Syndiotactic Polystyrene/Organophilic Clay Nanocomposites", *J. Appl. Polym. Sci.*, 92, 2144–2150, **2004**.
32. Kojima Y, Usuki A, Kawasumi M, Okada A, Fukushima Y, Kurauchi T, et al. Mechanical properties of nylon 6-clay hybrid. *J Mater Res*, 8, 1185–9, **1993**.
33. Krishnamoorti R.; Ren J.; Silva A. S.; "Shear response of layered silicate nanocomposites", *J. Chem. Phys.*, 114, 4968-4973, **2001**.
34. Chen-Feng Kuan , Hsu-Chiang Kuan, Chen-Chi M. Ma, Chia-Hsun Chen, Han-Lang Wu "The preparation of carbon nanotube/linear low density polyethylene composites by a water-crosslinking reaction", *Materials Letters* 61 (2007) 2744–2748
35. Lee J. A.; Kontopoulou M.; Parent J. S.; "Synthesis and characterization of polyethylene-based ionomer Nanocomposites", *Polymer* 46, 5040–5049, **2005**.
36. Le Baron PC, Wang Z, Pinnavaia TJ. Polymer-layered silicate nanocomposites: an overview. *Appl Clay Sci*, 15, 11–29, **1999**.
37. Lee J. A.; Kontopoulou M.; Parent J. S.; "Time and shear dependent rheology of maleated polyethylene and its Nanocomposites", *Polymer*, 45, 6595–6600, **2004**.
38. Lee K.M, Han C. D., "Effect of hydrogen bonding on the rheology of polycarbonate/organoclay nanocomposites", *Polymer* 44, 4573–4588, **2003a**.
39. Lee K. M.; Han C. D.; "Rheology of Organoclay Nanocomposites: Effects of Polymer Matrix/Organoclay Compatibility and the Gallery Distance of Organoclay", *Macromolecules*, 36, 7165-7178, **2003b**.
40. Lele A.; Mackley M.; Galgali G.; Ramesh C.; "In situ rheo-x-ray investigation of flow-induced orientation in layered silicate–syndiotactic polypropylene nanocomposite melt", *J. Rheol.*, 46, 1091-1110, 2002.
41. Lim and Park "Phase morphology and rheological behavior of polymer/layered silicate nanocomposites", *Rheol Acta*, 40, 220-229, **2001**.
42. Lim Y. T.; Park O.O.; "Rheological evidence for the microstructure of intercalated polymer/layered silicate nanocomposites", *Macromol. Rapid Commun.*, 21, 231–235, **2000**.
43. Lin K. F.; Hsu C. Y.; Huang T. S.; Chiu W. Y.; Lee Y. H.; Young T.H.; " A Novel Method to Prepare Chitosan/Montmorillonite Nanocomposites", *J Appl Polym Sci*, 98, 2042–2047, **2005**.
44. Liu X.; Wu Q.; "Polyamide 66/Clay Nanocomposites via Melt Intercalation", *Macromol. Mater. Eng.*, 287, 180-186, **2002**.
45. Loo LS, Gleason KK. Fourier transforms infrared investigation of the deformation behavior of montmorillonite in nylon 6/nanoclay nanocomposites. *Macromolecules*, 36, 2587–90, **2003**.

46. Ma C. C. M.; Chen Y.J.; Kuan H. C.; " Polystyrene Nanocomposite Materials: Preparation, Morphology, and Mechanical, Electrical, and Thermal Properties", *J. Appl. Polym. Sci.*, 98, 2266–2273, **2005**.
47. Maiti P, Nam PH, Okamoto M, Hasegawa N, Usuki A. Influence of crystallization on intercalation, morphology, and mechanical properties of propylene/clay nanocomposites. *Macromolecules*, 35, 2042–9, **2002**.
48. Mishra, S, N. G. Shimpi " Mechanical and flame-retarding properties of styrene–butadiene rubber filled with nano-CaCO₃ as a filler and linseed oil as an extender", *J. Appl. Polym. Sci.*, 98, 2563–2571, **2005**.
49. Mitchell CA, Bahr JL, Arepalli S, Tour JM, Krishnamoorti R. Dispersion of functionalized carbonnanotubes in polystyrene. *Macromolecules*, 35, 8825–30, **2002**.
50. Mohanty AK, Drzal LT, Misra M. Nano-reinforcement of bio-based polymers—the hope and reality. *Polym Mater Sci Eng*, 88, 60–61, **2003a**.
51. Mohanty AK, Wibowo A, Misra M, Drzal LT. Development of renewable resource-based cellulose acetate bioplastic: effect of process engineering on the performance of cellulosic plastics. *Polym Eng Sci*, 43, 1151–61, **2003b**.
52. Mousa A.; Karger-Kocsis J.; "Rheological and thermodynamical behavior of styrene/butadiene rubber-organoclay nanocomposites", *Macromol. Mater. Eng.*, 286, 260-266, **2001**.
53. Ni P.; Wang Q.; Li J.; Suo J.; Li S.; " Novel Polyether Polyurethane/Clay Nanocomposites Synthesized with Organically Modified Montmorillonite as Chain Extenders", *J Appl Polym Sci*, 99, 6–13, **2005**.
54. R. Andrews, D. Jacques, M. Minot, T. Rantell, *Macromol Mater. Eng.* 287, 395-402, **2002**.
55. Osman M. A.; Rupp J. E. P.; "Interfacial Interactions and Properties of Polyethylene-Layered Silicate Nanocomposites", *Macromol. Rapid Commun.*, 26, 880–884, **2005**.
56. Paul M-A, Alexandre M, Degee P, Henrist C, Rulmont A, Dubois P. New nanocomposite materials based on plasticized poly(L-lactide) and organo-modified montmorillonites: thermal and morphological study. *Polymer*, 44, 443–50, **2003**.
57. Pötschke P, Bhattacharyya A, Janke A, Goering H. Melt-mixing of polycarbonate/multi-wall carbon nanotube composites. *Compos Interfaces*, 10, 389–404, **2003**.
58. Sinha-Ray S. and M. Bousmina. Nano reinforcements of Renewable Plastics: To Create the Next Generation of Value-added Novel Eco-friendly Nanocomposites. *Handbook of Biodegradable Polymeric Materials and Their Applications*. Edited by Surya Mallapragada and Balaji Narasimhan. Vol. 1, Chapter 9, Pages 1-53 (**2005a**).

59. Sinha Ray S. and M. Bousmina. Biodegradable polymers and their layered silicate nanocomposites: In greening the 21st century materials world. Progress in Materials Science. 2005, 50, 962-1079 (**2005b**).
60. Sinha Ray, S. and M. Bousmina and K. Okamoto: Structure-Property Relationship in Biobased Nanocomposites From Poly(butylene succinate-co-dipate) and Organically-Modified Layered Silicate. Macromolecular Materials and Engineering. 290, 759-768 (**2005c**).
61. Sinha Ray S and M. Bousmina. Effect of Organic Modification on the Compatibilization Efficiency of Clay in an Immiscible Polymer Blend. Macromolecular Rapid Communications 20, 1639-1646 (**2005d**).
62. Sinha Ray S and M. Bousmina, Poly(butylene succinate-co-adipate)/montmorillonite nanocomposites: effect of organic modifier miscibility on structure, properties, and viscoelasticity. Polymer, 46, 12430-12439 (**2005e**).
63. Sinha Ray, S. Pouliot, M. Bousmina and L.A. Utracki, Role of organically modified layered silicate as a compatibilizer for immiscible polystyrene/polypropylene blends. Polymer 45, 8403-8413 (**2004**).
64. Ren J.; Casanueva B. F.; Mitchell C. A.; Krishnamoorti R.; Disorientation Kinetics of Aligned Polymer Layered Silicate Nanocomposites. Macromolecules 36, 4188-4194, **2003a**.
65. Ren J.; Krishnamoorti R.; "Nonlinear Viscoelastic Properties of Layered-Silicate-Based Intercalated Nanocomposites", Macromolecules 36, 4443-4451, **2003b**.
66. Shia D, Hui CY, Burnside SD, Giannelis EP. An interface model for the prediction of Youngs modulus of layered silicate-elastomer nanocomposites. Polym Compos,19, 608-15, **1998**.
67. Sinha Ray S, Okamoto M. Polymer/layered silicate nanocomposites: a review from preparation to processing. Prog Polym Sci, 28, 1539-641, **2003**.
68. Sinha Ray S, Yamada K, Okamoto M, Ogami A, Ueda K. New polylactide/layered silicate nanocomposites. 3. High performance biodegradable materials. Chem Mater 15,1456-65, **2003a**.
69. Sinha Ray S, Yamada K, Okamoto M, Fujimoto Y, Ogami A, Ueda K. New polylactide/layered silicate nanocomposites: 5. Designing of materials with desired properties. Polymer, 44, 6633-46, **2003b**.
70. Shin S. Y. A.; Simon L. C.; Soares J. B. P.; Scholz G.; " Polyethylene-clay hybrid nanocomposites: in situ polymerization using bifunctional organic modifiers", Polymer 44, 5317-5321, **2003**.
71. Solomon M. J.; Almusallam A. S.; Seefeldt K. F.; Somwangthanaroj A.; Varadan P. ; "Rheology of Polypropylene/Clay Hybrid Materials", Macromolecules, 34, 1864-1872, **2001**.

72. Tjong S. C.; Meng Y. Z.; "Preparation and Characterization of Melt-Compounded Polyethylene/Vermiculite Nanocomposites", *J Polym Sci Part B: Polym Phys* 41, 1476–1484, **2003**.
73. A. Dufres, M. Paillet, J. L. Putaux, R. Canet, F Carmona, P. Delhaes, S. Cui, *J. Mater Sci.* 37, 3915-3923, **2002**.
74. van Zyl W. E.; García M.; Schrauwen B. A. G.; Kooi B. J.; De Hosson J. M.; Verweij H. " Hybrid Polyamide/Silica Nanocomposites: Synthesis and Mechanical Testing", *Macromol. Mater. Eng.*, 287, 106-110, **2002**.
75. Wu D.; Wang X.; Song Y.; Jin R.; "Nanocomposites of Poly(vinyl chloride) and Nanometric Calcium Carbonate Particles: Effects of Chlorinated Polyethylene on Mechanical Properties, Morphology, and Rheology", *J Appl Polym Sci*, 92, 2714–2723, **2004a**.
76. Wu Y. P.; Ma Y.; Wang Y. Q.; Zhang L. Q.; "Effects of characteristics of rubber, mixing and vulcanization on the structure and properties of rubber/clay nanocomposites by melt blending", *Macromol. Mater. Eng.*, 289, 890–894, **2004b**.
77. Wu D.; Zhou C.; Fan X.; Mao D.; Bian Z.; " Linear rheological behaviour and thermal stability of poly(butylene terephthalate)/epoxy/clay ternary nanocomposites", *Polym. Degrad. Stab.*, 87, 511-519, **2005a**.
78. Wu T. M.; Chu M. S.; "Preparation and Characterization of Thermoplastic Vulcanizate/Silica Nanocomposites", *J Appl Polym Sci*, 98, 2058–2063, **2005b**.
79. Yang F.; Zhang X.; Zhao H.; Chen B.; Huang B.; Feng Z.; " Preparation and Properties of Polyethylene/Montmorillonite Nanocomposites by In Situ Polymerization", *J. Appl. Polym. Sci.*, 89, 3680–3684, **2003**.
80. B.X. Yang, K.P. Pramoda, G.Q. Xu and S.H. Goh, "Mechanical reinforcement of polyethylene using polyethylene-grafted multiwalled carbon nanotubes", *Adv Functional Materials* 17, 2062-2069, **2007**.
81. B.X. Yang, Jia-Hua Shi, K P Pramoda, Suat Hong Goh, "Enhancement of the mechanical properties of polypropylene using polypropylene-grafted multiwalled carbon nanotubes", *Compos Sci Tech*, 68,2490-2497, **2008**.
82. Zhang J.; Jiang D. D.; Wilkie C. A.; "Polyethylene and polypropylene nanocomposites based upon an oligomerically modified clay", *Thermochimica Acta* 430, 107–113, **2005**.
83. T. Kashiwagi, E. Grulke, J. Hilding, R. Hams, W. Awad, J. Douglas, *Macromol. Rapid Commun.* 23, 761, **2002**.
84. R. H. Baughman, A. A. Zakhidov, W. A. De Heer, *Science* 297, 787 **2002**.
85. L. S. Schadler, S. C Giannaris, P. M. Ajayan, *Appl. Phy& Lett.* 73,3941, **1998**.

86. A. Thess, R. Lee, P. Nikolaev, H. Dai, P. Petit, J Robert, C. Xu, Y: H. Lee, S. G. Kim, A. G. Rinzler, D. T. Colbert, G. E. Scuseria, D. Tomanek, J. E. Fischer, R. E. Smalley, *Science* 273,483, **1996**.
87. A. Hirsch, *Angew. Chem. Int. Ed.* 41,11, **2002**.
88. S. Cui, R. Canet, A. Derre, M. Couzi, P. Delhaes, *Carbon* 41, 797, **2003**.
89. J. L. Bahr, J. M. Tour, *J. Mater. Chem.* 12,1952, **2002**.
90. C. A. Mitchell, J. L. Bahr, S. Arepalli, J. M. Tour, R. Krishnamoorti, *Macromolecules* 35, 8825, **2002**.
91. D. E. Hill, Y. Lin, A. M. Rao, L. F. Allard, Y. P. Sun, *Macromolecules*, 35, 9466, **2002**.
92. A. Al-Ostaz, G. Pal, R. Mantena, A. Cheng ; “Molecular dynamics simulation of SWCNT–polymer nanocomposite and its constituents”, *J Mater Sci* 43:164–173, **2008**.
93. S. Kanagaraj , F. R. Varanda, Tatiana V. Zhil'tsova, Monica S.A. Oliveira, Jose A.O. Simoes; “Mechanical properties of high density polyethylene/carbon nanotube composites”, *Composit Sci and Tech* 67 3071–3077, **2007**.
94. A. Mierczynska, M. Mayne-L’Hermite, G. Boiteux, J. K. Jeszka; “Electrical and Mechanical Properties of Carbon Nanotube/Ultrahigh-Molecular-Weight Polyethylene Composites prepared by a Filler Prelocalization Method”, *J Appl Polym Sci*, 105, 158–168 **2007**.
95. C. Kuan , H. Kuan, C. M. Ma , C. Chen , H. Wu; “The preparation of carbon nanotube/linear low density polyethylene composites by a water-crosslinking reaction”, *Mat Letters* 61, 2744–2748, **2007**.
96. T. Ramanathan, H. Liu, L. C. Brinson; “Functionalized SWNT/Polymer Nanocomposites for Dramatic Property Improvement”, *J Polym Sci Polym Phy* 43, 2269–2279 **2005**.
97. F. Buffa, H. Hu, and D. E. Resasco; “Side-Wall Functionalization of Single-Walled Carbon Nanotubes with 4-Hydroxymethylaniline Followed by polymerization of ϵ -Caprolactone”, *Macromolecules* 38, 8258-8263, **2005**.
98. S. Bellayer, J. W. Gilman, N. Eidelman, S. Bourbigot, X. Flambard, D. M. Fox, Hugh C. D. Long, & P. C. Trulove; “Preparation of Homogeneously Dispersed Multiwalled Carbon Nanotube/Polystyrene Nanocomposites via Melt Extrusion using Trialkyl Imidazolium Compatibilizer”, *Adv Funct Mater* 15, 910-916, **2005**.

VITA

Name	Sarfraz Haider Abbasi
Date & Place of Birth	11 August 1975, Dadu (Pakistan)
Nationality	Pakistani
Religion	Islam
Educational Qualification	B.Sc. in Applied Chemistry from University of Karachi (1995-1997) M.Sc. in Applied Chemistry from University of Karachi (1998-1999) M.S. in Chemical Engineering from King Fahd University of Petroleum & Minerals (2001-2003) Ph.D. in Chemical Engineering from King Fahd University of Petroleum & Minerals (2006-2010)
Present Address	Flat No 1825, Building No 1800, Shabab Palace, King Fahd University of Petroleum & Minerals, Dhahran, Saudi Arabia
Permanent Address	A-22, Farida Square, Block 7, Gulshan-e-Iqbal, Karachi, Pakistan
Email Address	sarfrazabbasi@gmail.com